

Alma Mater Studiorum - Università di Bologna

DOTTORATO DI RICERCA IN  
CHIMICA

Ciclo 34

**Settore Concorsuale:** 03/B1 - FONDAMENTI DELLE SCIENZE CHIMICHE E SISTEMI INORGANICI

**Settore Scientifico Disciplinare:** CHIM/03 - CHIMICA GENERALE E INORGANICA

APPLIED BIOMATERIALS FROM SUSTAINABLE SOURCES

**Presentata da:** Maria Francesca Di Filippo

**Coordinatore Dottorato**

Domenica Tonelli

**Supervisore**

Silvia Panzavolta

**Co-supervisore**

Magda Monari

**Esame finale anno 2022**



**Maria Francesca Di Filippo**  
**APPLIED BIOMATERIALS FROM SUSTAINABLE SOURCES**

## ABSTRACT

If we look back in time at the history of humanity, we can state that our generation is definitely living an era of outstanding efficiency and progress because of globalization and global competition, even if this is resulting in the rapid depletion of energy sources and raw materials. The environmental impact of non-biodegradable plastic wastes is of increasing global concern: nowadays, imagining a world without synthetic plastics seems impossible, though their large-scale production and their extensive use have only spread since the end of the World War II. In recent years, the demand for sustainable materials has increased significantly and, with a view to circular economy, research has also focused on the enhancement and subsequent reuse of waste materials produced by industrial processing, intensive farming and the agricultural sector. Indeed, giving new life to a waste material allows an intelligent use of resources, decreasing the cost of production and activating new strategies and new ideas. Plastic polymers have been the most practical and economical solution for decades due to their low cost, prompt availability, excellent optical, mechanical and barrier properties and resistance against water and grease. Biodegradable polymers, known for many decades but ignored mainly because of the low cost of synthetic polymers, could replace them in many applications, thus reducing the problems of traditional plastics disposability and the dependence on petroleum. Natural biopolymers are in fact characterized by a high biocompatibility and biodegradability and have already prompted research in the field of regenerative medicine, which to date is one of the most popular scientific fields and represents the future of life sciences, where today's new technologies and public health challenges converge.

During these three years of my PhD, I carried out my research activities in the laboratory of Materials Chemistry and Biomimetics, the science of imitating nature. My goal was to use natural polymers from sustainable sources as raw materials to produce biomaterials, which are materials designed to interface with biological systems to evaluate, support or replace any tissue, organ or function of the body. In particular, I focused on the use of the most abundant biopolymers in nature (such as cellulose, chitosan, gelatin) to produce biomaterials of different types. Biomaterials in the form of thin membranes (films), scaffolds and cements were developed, and after a complete characterization, the materials were proposed for suitable applications in different fields, from tissue engineering to cosmetics and food packaging. Some of the obtained results were published on international scientific and peer-reviewed journals.



# INDEX

<b>1. INTRODUCTION .....</b>	<b>1</b>
1.1 SUSTENABILITY AND CIRCULAR ECONOMY .....	1
1.2 BIOPOLYMERS AND RENEWABLE MATERIALS .....	4
1.3 FIELDS OF APPLICATION .....	17
1.4 BIBLIOGRAPHY .....	22
<b>2. FILMS.....</b>	<b>29</b>
2.1 INTRODUCTION.....	29
2.2 EXPERIMENTAL PART .....	33
2.2.1 Chitosan-based films with snail slime .....	33
2.2.2 Cellulose derivatives-based films with snail slime .....	34
2.2.3 Cellulose/Hyaluronate-based films with Anti-Herpes activity .....	37
2.2.4 Keratin-based films with snail slime .....	39
2.2.5 Fluconazole-loaded films based on gelatin and snail slime .....	40
2.2.6 Mucoadhesive gelatin-based films loaded with Econazole.....	45
2.2.7 Methods of Characterization .....	50
2.3 CHITOSAN-BASED FILMS WITH SNAIL SLIME .....	53
2.4 CELLULOSE DERIVATIVES-BASED FILMS WITH SNAIL SLIME .....	61
2.5 CELLULOSE/HYALURONATE-BASED FILMS WITH ANTI-HERPES ACTIVITY.....	72
2.6 KERATIN-BASED FILMS WITH SNAIL SLIME .....	79
2.7 FLUCONAZOLE-LOADED FILMS BASED ON GELATIN AND SNAIL SLIME.....	84
2.8 MUCOADHESIVE GELATIN-BASED FILMS LOADED WITH ECONAZOLE.....	97
2.9 BIBLIOGRAPHY .....	109
<b>3. SCAFFOLDS.....</b>	<b>118</b>
3.1 INTRODUCTION.....	118
3.2 EXPERIMENTAL PART .....	122
3.2.1 Gelatin-based scaffolds for bone tissue engineering.....	122
3.2.2 Chitosan and gelatin-based scaffolds for cartilage repair .....	125
3.2.2 Methods of Characterization.....	127
3.3 GELATIN-BASED SCAFFOLDS FOR BONE TISSUE ENGINEERING .....	128
3.4 CHITOSAN AND GELATIN-BASED SCAFFOLDS FOR CARTILAGE REPAIR .....	136
3.5 BIBLIOGRAPHY .....	142

<b>4. BONE CEMENTS .....</b>	<b>146</b>
4.1 INTRODUCTION.....	146
4.2 EXPERIMENTAL PART .....	149
4.2.1 Development of antibacterial calcium phosphate bone cements.....	149
4.2.2 Calcium phosphate cement enriched with self-assembling fibers.....	154
4.2.3 Methods of Characterization .....	160
4.3 DEVELOPMENT OF ANTIBACTERIAL CALCIUM PHOSPHATE BONE CEMENTS .....	162
4.4 CALCIUM PHOSPHATE CEMENT ENRICHED WITH SELF-ASSEMBLING FIBERS.....	173
4.5 BIBLIOGRAPHY .....	186
<b>5. CONCLUSIONS .....</b>	<b>190</b>
<b>APPENDIX I .....</b>	<b>193</b>
<b>APPENDIX II.....</b>	<b>194</b>



# **Chapter 1.**

## **INTRODUCTION**

### **1.1 SUSTAINABILITY AND CIRCULAR ECONOMY**

The rapid scientific and technological progress has now reached a remarkable development, bringing significant improvements in human life, but has also caused negative and sometimes even disastrous effects. Examples are the uncontrolled use of natural resources, global warming, ecological disasters, and pollution.

In particular, the environmental impact of non-biodegradable plastic material wastes is of increasing global concern. In fact, today imagining a world without plastic seems impossible, though their large-scale production and their widespread use occurred only after the end of World War II. It is estimated that between 1960 and 2005, the percentage by mass of plastics in municipal waste increased from less than 1% to over 10% in high and middle income countries <sup>1</sup>.

Most of the plastics (and therefore the waste) that we produce comes from packaging, mainly designed for immediate disposal: half of all plastics ever manufactured has been made in the last 15 years and was used only once.

In 2019 alone, plastics contributed to the emission of greenhouse gases in the equivalent of 850 million tons of CO<sub>2</sub> released into the atmosphere: if plastic production and use grow as currently planned, these emissions could reach 1.3 gigatons/year by 2030 and 56 gigatons by 2050, as much as 14% of the Earth's entire remaining carbon budget <sup>2</sup>.

The accumulation of the unused polymers in the sea or on the seaside occurs at a rate of more than 105 tons/year and causes disruption in the environmental ecosystems of fisheries and the ocean. Plastic is so abundant that traces can be found also in the glaciers and in the great sea pits, and even in the Mariana Trench: in fact, plastic has been proposed as the geological indicator for the present epoch, that of the 'Anthropocene' <sup>3</sup>.

One of the main problems of plastic accumulation is the creation of microplastics, millimeter-sized or even micrometric fragments which are also generated by photodegradation reactions, having a negative impact on the marine environment <sup>4</sup>. Microplastics can indeed act as dispersal vectors of additives, organic pollutants and provide a favorable habitat for the proliferation of a wide range of microbial organisms and communities; plastic residues are also ingested by marine species (such as sea turtles, seals, whales, but also by fish and crustaceans) and are therefore present in the human food chain. These issues also affect our country closely, especially considering the marine biodiversity of the Mediterranean Sea <sup>5</sup>.

In recent years, there has been an increase in knowledge and awareness of the negative effects that plastic has on the environment and man. Not long ago, the European Parliament has approved the Directive on disposable plastic products: from 2021, disposable plastics such as cutlery and straws has been banned, and the use of plastic products is regulated by national plans. The legislation also requires plastic bottles to contain at least 25% of recycled content by 2025 and 30% by 2030, and introduces new responsibilities for manufacturers <sup>6</sup>.

The current development model based on the linear economy (take-make-waste) is no longer sustainable, and there is the urgent need to promote a transition towards the use of renewable resources.

Circular Economy (CE) is a term that defines an economic system designed to regenerate itself, and therefore eco-sustainable. According to the definition given by the Ellen Macarthur Foundation, the CE provides tools to tackle climate change and biodiversity loss, to increase prosperity and jobs; it aims to reduce greenhouse gas emissions, waste and pollution, while addressing important social needs <sup>7</sup>. The circular economy can thus be summarized in three principles: eliminating waste and pollution, circulating products and materials and regenerating nature.

The transition to a circular economy must not only aim at restoring the negative effects of the linear economy adopted so far but must also generate economic and commercial opportunities and offer benefits to society and the environment. In fact, the recycling and reuse of waste using green technologies will limit water consumption, greenhouse gas emissions and world-wide pollution without impoverishing the environment and while saving the biodiversity of the Earth <sup>8</sup>.

The international standards ISO 14040 and 14044 defined the Life Cycle Assessment (LCA) as a method to analyze environmental aspects and impacts of product systems. LCA studies indeed the environmental aspects and potential impacts throughout a product's life from raw material acquisition through production, use and disposal <sup>9</sup>. During the early years of LCA, the methodology was mostly applied to products, but it also has the potential to act as an analysis and design tool for processes <sup>10</sup>.

Impact assessment in LCA is an important tool for authorities, industries, and individuals in environmental sciences and it generally consists of classification, characterization, normalization and valuation <sup>11</sup>. This assessment may include both quantitative and qualitative measures of improvement, such as changes in product, process and activity design, raw material use, industrial processing, consumer use and waste management.

To date, the excellent properties of plastics such as their low cost, high availability, superior optical, mechanical and barrier properties and resistance to water and grease, have made these materials the most appealing solutions for the industry, especially in the packaging sector. The plastic industry has generally used fossil-based chemicals, such as natural gas or oil, and has only recently shifted towards the use of renewable materials. In fact, while plastics have better processability and functional properties, their environmental impact has led to sharp increases in oil prices and has provided an additional economic incentive for the search for renewable alternatives.

From a circular economy point of view, the research's interest has shifted towards the development of sustainable materials capable of replacing plastics, thanks to similar or even better characteristics.

## 1.2 BIOPOLYMERS AND RENEWABLE MATERIALS

### **Polymers and Biopolymers**

The generic term 'plastics' refers to pure polymers or their mixture with polymeric resins, synthetic fibres and additives that constitute the final material, while 'polymer' refers to large chemical compounds (macromolecules) characterized by a high number of repetitive units and high molecular weight.

Depending on their nature, polymers can be synthetic or natural. The formers are obtained by means of a chemical synthesis performed in the laboratory, while the latter are those found directly in nature.

Bio-based polymers are naturally occurring polymers or natural substances that have been polymerized into high molecular weight materials by chemical and/or biological methods: they include various synthetic polymers derived from renewable resources and CO<sub>2</sub>, biopolymers, their derivatives, and their blends and composites<sup>12</sup>. Accordingly, not all biobased polymers are biodegradable.

Biopolymers are natural polymers produced by the cells of living organisms and their biological functions are associated with their complex structures. A further classification distinguishes between biopolymers of natural origin (produced directly in living biological systems such as animals, plants, fungi and bacteria) and biopolymers of synthetic origin (derived from biological raw materials and obtained by chemical processes, extraction, or by the action of micro-organisms). Biopolymers of natural origin are mainly divided into three categories: polysaccharides (linear or branched polymeric carbohydrates such as cellulose and alginate), proteins and polynucleotides (such as RNA and DNA).

Many biopolymers or biodegradable polymers can be degraded by the enzymatic action of microorganisms such as bacteria, fungi, and algae. Biodegradation allows their conversion to CO<sub>2</sub>, CH<sub>4</sub>, water, biomass and other substances, so biopolymers or biodegradable polymers can be easily recycled by means of biological processes<sup>13</sup> or by non-enzymatic reactions such as chemical hydrolysis. In Figure 1 the cyclical processes by which biodegradable polymers are synthesized and biodegraded are shown.

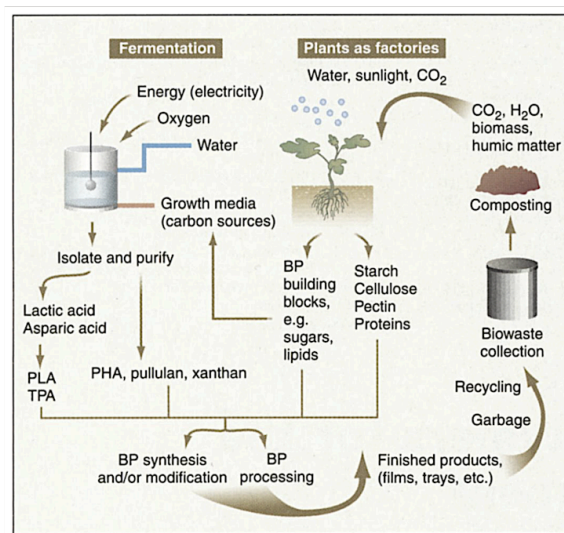


Figure 1. Cyclical processes by which biodegradable polymers (BP) and their biodegradation processes can be obtained <sup>13</sup>.

Research and development of new materials based on biopolymers and biodegradable polymers is hampered by high production costs and low mechanical and water resistance properties, which limit their industrial uptake and end-use applications.

Several approaches have been proposed to address and overcome these issues, enhancing the performances of biopolymers-based materials, and widening up their application fields. In order to improve the mechanical and barrier properties, physical, chemical and enzymatic treatments were employed as well as the introduction of natural compounds/extracts or the union of biopolymers with different chemical structures. For example, the interaction between two or more polymers through physical entanglement is one of the simplest but most effective methods to improve film properties, as reported in literature <sup>14</sup>. In particular, film formation through the combination of polyelectrolyte biomolecules with opposite charges offers advantages resulting from the strength of multiple intermolecular interactions. In fact, the mixing of biopolymers with opposite charge leads to the formation of poly-ionic compounds or complexes (polyelectrolytes), precipitates or gels that lead to the formation of supramolecular structures under specific conditions, depending on the ionic resistance, biopolymer ratio and pH <sup>15</sup>.

In the last decades new materials designed for biomedical applications in tissue engineering <sup>16–18</sup>, and as drug delivery systems in the pharmaceutical industry <sup>19,20</sup> have been developed using biodegradable polymers.

Finding solutions to increase the mechanical performance and functional properties of biopolymer-based materials is of utmost importance and would widen up their usage and application fields.

During my doctorate, I selected some of the most common and abundant biopolymers and natural polymers in nature, preferentially choosing those that can be easily found from waste sources. I used biopolymers such as chitosan, cellulose, sodium hyaluronate, keratin and gelatin, of which I report below the main characteristics and properties.

## Chitosan

Chitosan is derived from chitin, the second largest naturally occurring polysaccharide in nature after cellulose, found in the shells of living organisms such as crabs, lobsters, tortoise, shrimps and insects <sup>21</sup>. Almost 60,000–80,000 tons of shell waste is produced globally because of the consumption of seafood <sup>22</sup> and it is estimated that about 2000 tons of chitosan is produced annually from shrimp and crab shell chitin <sup>23</sup>.

Chitin consists of  $\beta$  (1-4) linked N-acetyl-2-amino-2-deoxy-D-glucose units and is synthesized by an enormous number of living organisms, when reinforcement and strength are required. Despite the high availability, its network of hydrogen bonds and high crystallinity hinder its solubilization in all usual solvents <sup>24</sup> and hence attention has been given to its derivative chitosan.

Chitosan is obtained by partial deacetylation of chitin using a chemical or biological method, or a combination of both. The term ‘chitosan’ refers to a large group of structurally different chemical entities that may have different sizes, molecular weights (MW) and degrees of deacetylation (DD) <sup>25</sup>. It is a straight-chain copolymer composed of  $\beta$ -(1-4)D-glucosamine with randomly located N-acetyl-D-glucosamine groups, based on the deacetylation degree <sup>26</sup> (Figure 2).

Even if no strict rules for defining chitosan are found, chitin with a degree of deacetylation (DD) of 70% or above is generally considered as chitosan <sup>27</sup>.

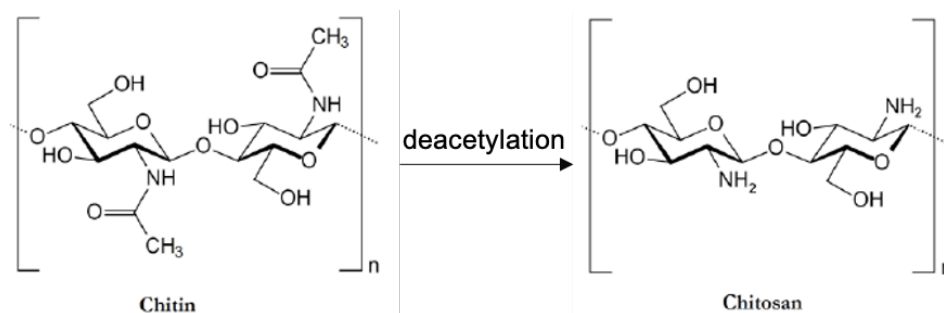


Figure 2. Structure of chitin and chitosan.

The most commercially available chitosan DD ranges within 70 and 90%; DD higher than 95% may be obtained via further deacetylation steps <sup>28</sup>, even if this may result in partial degradation

of the polymer chains and an increase in the possibility of reacylation. Thus, the lower the deacetylation, the higher the molecular weight, which provides higher chemical stability and mechanical strength, but reduces the solubility in traditional solvents<sup>29</sup>.

Due to its semi-crystalline structure with extensive hydrogen bonding, chitosan can be dissolved only in acidic media with pH lower than the pKa of amine groups (6.2–7.0). In fact, the solubilization occurs by protonation of the -NH<sub>2</sub> function on the C-2 position of the D-glucosamine repeating unit, for which the polysaccharide is converted into a polyelectrolyte in acidic media. On the other hand, as the pH increases above 6, chitosan amines undergo deprotonation, so the polymer loses its charge and becomes insoluble<sup>30</sup>.

Chitosan was approved by the FDA (Food and Drug Administration) as GRAS (generally recognized as safe), and hence can be considered suitable for many different applications, from the cosmetics, food-packaging, to the biomedical and pharmaceutical fields<sup>31,32</sup>. In particular, chitosan revealed to be a promising bioactive material for tissue engineering (bone, skin, cartilage, intervertebral disc, blood vessel, etc.), thanks to its properties of biodegradability, biocompatibility, non-toxicity and hydrophilicity, together with anti-bacterial, anti-fungal and wound-healing effects<sup>29</sup>. Moreover, the degradation of chitosan produces harmless amino sugars, which can be absorbed completely by the human body.

## **Cellulose**

Cellulose is the most abundant biopolymer in nature, and its use as a substitute for petrochemical products would therefore lead to significant reductions in CO<sub>2</sub> emissions: its total production capacity is estimated to be around 10<sup>11</sup>–10<sup>12</sup> ton/year<sup>33</sup>.

Cellulose can be extracted from various sources (for example wood and cotton) in a sustainable way: if the forests from which the wood is obtained are reforested and managed efficiently, the entire production cycle has the potential to minimize greenhouse gas production even in the long run.

Although biodegradability has been seen as an intrinsic advantage of cellulose products, on the other hand the rate of biodegradation is affected by chemical changes, such as derivatization or cross-linking<sup>34</sup>.

Cellulose is a polysaccharide in which glucose units are bound by a β 1→4 glycoside bond (Figure 3); each glucose unit contains three -OH groups.

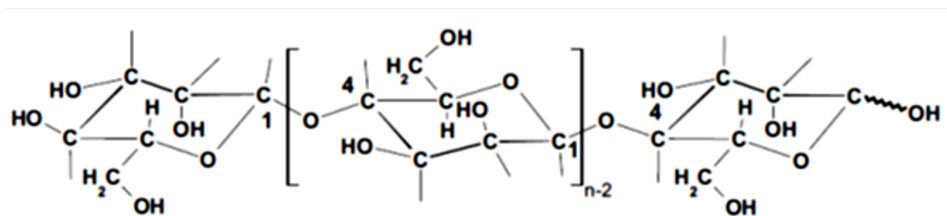


Figure 3. Structure of cellulose.

Linear polymer chains are arranged parallel to each other by hydrogen bonds, leading to the formation of fibrils difficult to solubilize. The arrangement of the fibrils is extremely regular, therefore there is the formation of hydrophobic crystalline zones. The degree of polymerisation (DP) in common wood cellulose is in the range 3000-5000<sup>35</sup>.

In woody vegetable materials, cellulose is present in combination with lignin and hemicellulose: while the latter component generally makes the material more hydrophilic<sup>36</sup>, lignin has the opposite effect<sup>37</sup>. The percentage composition of a wood typical of temperate climates shows about 40-45% of cellulose, 25-35% of hemicellulose, 20-30% of lignin and 2-5% of other components<sup>35</sup>. The relatively small amounts of other components present in the composition of cellulose can however influence the properties of the material, as they often tend to be hydrophobic<sup>38</sup>.

The processing of cellulosic materials can significantly change their chemical composition, thus giving rise to many derivatives. Among them, during my doctorate I selected hydroxypropyl methylcellulose (HPMC) and sodium carboxymethyl cellulose (CMC Na).

HPMC (Figure 4) is an easily available, non-ionic, edible cellulose derivative, with which edible, transparent, odourless, flavourless, oil-resistant, and water-soluble films can be formed. In addition, HPMC is approved for food use by the FDA (21 CFR 172.874) and the EU (EC, 1995), and its food safety has also been confirmed by the "Joint Committee of Experts on Food Additives" (ECD)<sup>39</sup>.

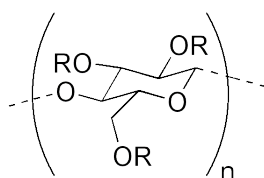


Figure 4. Structure of hydroxypropyl methylcellulose (HPMC).

Depending on the percentage content of methoxylic and hydroxypropyl groups, HPMC is divided into three families: Methocel E (HPMC 2910, USP), Methocel F (HPMC 2906, USP) and Methocel K (HPMC 2208, USP). Another HPMC classification parameter is related to the

the viscosity of 2% w/V Methocel solutions in water at 20 °C: for example, Methocel E is designated as E5, E15 or E50 because its solutions have viscosity values of 4-6 mPa·s, 12-18 mPa·s and 40-60 mPa·s, respectively. Methocel E is preferably used for film formation in aqueous solution, since the resulting films tend to have greater transparency and better properties. For my studies, I employed Methocel E 5 and 50.

Sodium carboxymethyl cellulose (CMC) is a cellulose derivative synthesized for the first time by Jansen in 1918 (E. Jansen, Ger. Patent, 332203, 1918). It is considered a GRAS polymer and it is widely used for the most diverse applications: from food, cosmetics and pharmaceuticals to products for the paper and textile industry <sup>40</sup>.

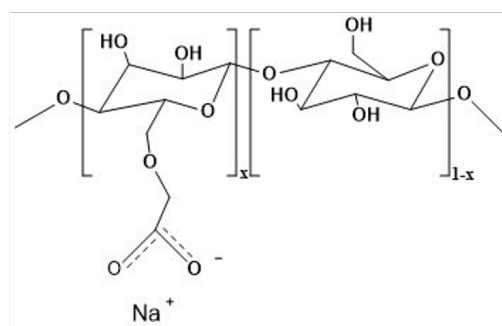


Figure 5. Structure of sodium carboxymethyl cellulose (CMC).

CMC is a typical anionic polysaccharide: more precisely, it is a copolymer of  $\beta$ -D-glucose and of  $\beta$ -D-glucopyranose 2-O-(Carboxymethyl)-monosodium salt, connected by  $\beta$ -1,4 glycosidic bonds (Figure 5). CMC contains a hydrophobic polysaccharide chain and many carboxylic and hydroxyl groups, therefore showing amphiphilic characteristics. It is also soluble in water, does not cause harmful effects on human health, and has excellent properties such as non-toxicity, biocompatibility, biodegradability, hydrophilicity and good film-forming ability: hence, it has already been widely exploited in many formulations of edible film <sup>41</sup>.

### Sodium hyaluronate

Sodium hyaluronate is the sodium salt of hyaluronic acid (or ‘hyaluronan’), the only glycosaminoglycan (GAG) member that is non-sulfated or bound to a proteoglycan core protein. It is the major component of the extracellular matrix (ECM), which plays an essential role in organogenesis, growth, function, and in many human diseases <sup>42</sup>.

Its structure (Figure 6) is composed of a linear polysaccharide chain of N-acetyl glucosamine units, sodium glucuronate (linked by  $\beta$  1–3 and  $\beta$  1–4 glycosidic bonds) and counterions <sup>43</sup>. Both individual carbohydrate residues in hyaluronan adopt the stable chair conformation.

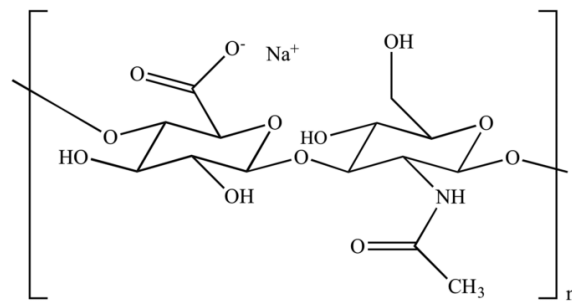


Figure 6. Structure of sodium hyaluronate. The polymer is built of alternating units of sodium glucuronate (GlcUA, left) and N-acetylglucosamine (GlcNAc, right).

Due to its strong negative charge, the polymer present an overall random coil structure in aqueous solvents, with specific stable tertiary structures <sup>44</sup>.

In contrast to other glycosaminoglycans which are synthesized in the Golgi network, hyaluronan is synthesized within a complex on the cytoplasmic surface of the plasma membrane <sup>45</sup> by hyaluronan synthase enzymes, which synthesize large, linear polymers of the repeating disaccharide  $\beta(1,4)\text{-GlcUA-}\beta(1,3)\text{-GlcNAc}$  by alternate addition of GlcUA and GlcNAc to the growing chain <sup>44,46</sup>.

The size of the polymers *in vivo* varies with the type of tissue, reaching enormous sizes in the extracellular matrix (between  $10^5$  and  $10^7$  Da). The industrial manufacturing of hyaluronan employs the extraction from animal tissues or the microbial fermentation using bacterial strains: both technologies produce high molecular weight hyaluronan with polydispersity ranging from 1.2 to 2.3.

Hyaluronan is widespread in nature, having been identified in algae, mollusks, prokaryotes and in the soft tissues of all vertebrates: high concentrations are found in the umbilical cord, in the synovial fluid between joints, skin, and in the vitreous body of the eye. It was estimated that about 15 g of hyaluronan can be found in different tissues of a person of 70 kg, of which about 50% in the skin <sup>46</sup>.

Hyaluronic acid has a wide range of biological functions, such as stimulation of cell proliferation, differentiation, migration and angiogenesis <sup>47</sup>, modulation of inflammation and of the immune cells function <sup>42,48</sup> and a high level of biocompatibility. In fact, it is extensively used in the biomedical field and in particular in viscosurgery, for the treatment of arthritis to supplement the lubrication of arthritic joints, as microcapsule for targeted drug delivery and in cosmetics as a hydrating and antiaging material <sup>49-51</sup>. Moreover, it is used in cell culture, medical devices and in pharmaceutical applications such as eye drops <sup>43</sup>. Several studies reported also the effects of hyaluronan oligosaccharides on cellular behavior that could imply the use of these molecules in cancer treatment or in wound healing <sup>52</sup>. Other applications of hyaluronic acid include its use as filler for lips, wrinkles, and other parts of the body (even if

not approved by FDA) and as topical nanocarrier for the delivery of biomacromolecules to the skin.

## Keratin

The word “keratin” first appeared in literature around 1850 to describe the material that made up hard tissues such as animal horns and hooves (keratin comes from the Greek “κέρας” meaning horn). It constitutes indeed most of the cytoskeleton structures and the epidermal appendages of animals, including hair, feathers, wool, and nails.

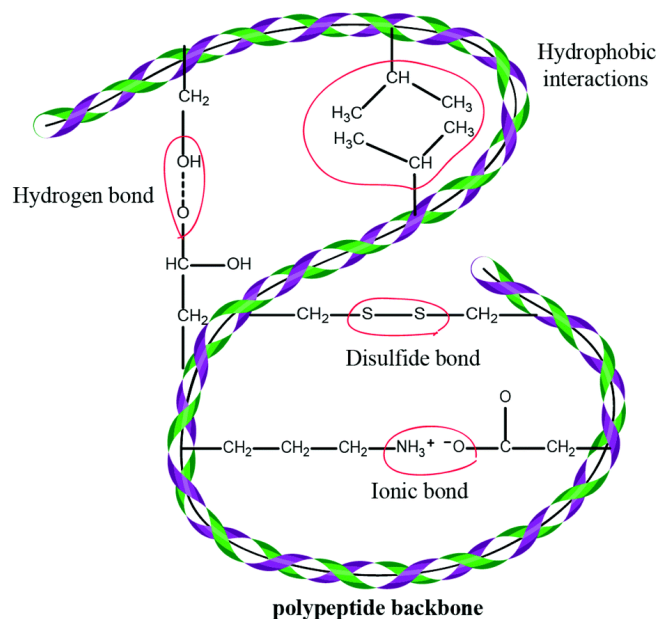


Figure 7. Interaction between keratin's functional groups<sup>53</sup>.

Keratin is a protein polymer and in particular a polypeptide made of different amino acids that have inter-molecular bonding of the disulphide cysteine amino acid and inter- and intra-molecular bonding (Figure 7) of polar and nonpolar acids<sup>53</sup>. It is often distinguished in  $\alpha$ -keratin, the primary component of wool, hairs, hooves, nails, horns, and stratum corneum and  $\beta$ -keratin, found in feathers, avian claws and beaks, reptilian claws, and scales.

$\alpha$ -Keratin is classified by the formation of a right-handed  $\alpha$ -helix structure (with a pitch of 0,51 nm), in which residues are linked by hydrogen bonds (Figure 8A). Each helix is hierarchically assembled into dimers, protofilaments, protofibrils, and intermediate filaments (Figure 8B), that are surrounded by amorphous keratin matrix and constitute the basic structural units of keratin.

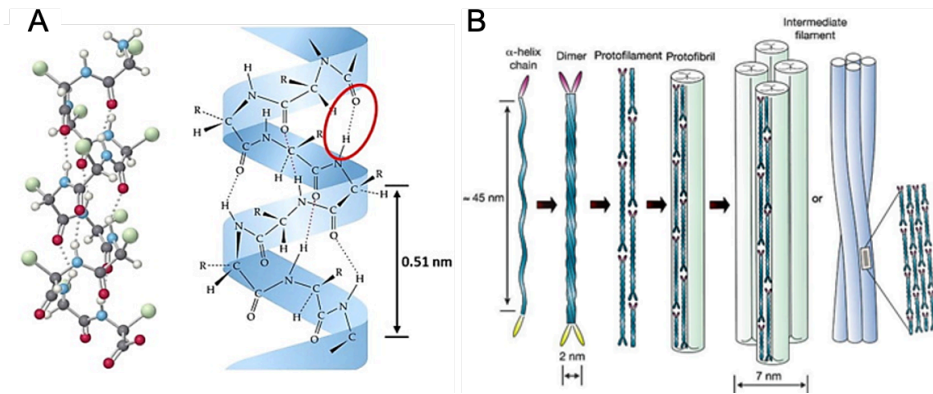


Figure 8. A. Structure of  $\alpha$ -helix<sup>54</sup> and B. Hierarchical organization of keratin within the intermediate filaments<sup>55</sup>.

The primary  $\alpha$ -helix associates with another  $\alpha$ -helix in antiparallel way, forming a coiled-coil dimer stabilized by ionic interactions of cystine residues. The  $\alpha$ -helical rod (about 45 nm in length) is located in the central zone of the dimer, while at both C- and N- terminals non-helical regions are present. Side-by-side or end-to-end aggregation of dimers by sulfur crosslinking produces protofilaments which, if tangentially connected, form protofibrils. The intermediate filaments (diameter 7 nm) consist of four protofibrils connected by a helical or circular mode<sup>55</sup>.

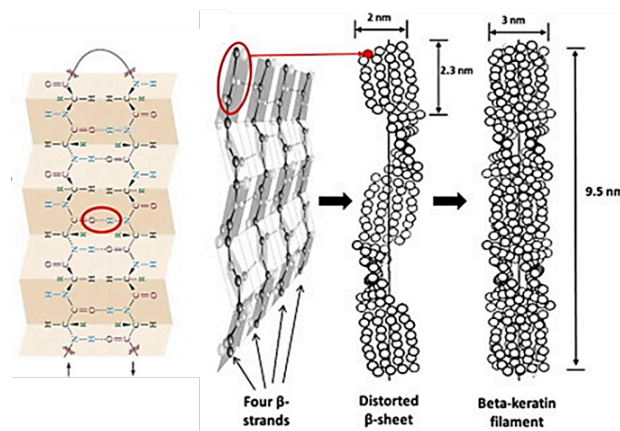


Figure 9. Structure of  $\beta$ -pleated sheet keratin<sup>54</sup>.

$\beta$  keratin has a pleated structure, with sheets composed of antiparallel chains (Figure 9). Two or more protein strands ( $\beta$  strand) are linked through hydrogen bonding, forming small rigid planar surfaces that are twisted with respect to each other, producing a pleated sheet arrangement that form a  $\beta$ -keratin filament with a diameter of 3-4 nm.

The pleated sheet structure is stabilized by two factors: the hydrogen bonds between  $\beta$ -strands, which contribute to forming a sheet, and the planarity of the peptide bond, which forces a  $\beta$ -sheet to bend. The terminal parts of the peptide chains wind around the  $\beta$ -keratin filaments and form the matrix<sup>56</sup>.

Keratins can be therefore considered as a polymer/polymer composite of crystalline filaments embedded in an amorphous matrix. These biopolymers present large variations in their properties and structure and can be also classified according to sulphur content as soft (cystine content up to 2%) and hard keratins (cystine content up to 22%).

The waste rich in keratin has been valued worldwide to be more than 5,000,000 ton/year<sup>57</sup> and, until few years ago, was heated at high temperatures along with other animal waste, requiring great costs for transportation, fuel, equipment and manpower. In recent years, with the increasing demand for sustainable materials, these by-products started to be regarded as a renewable resource worthy of a better exploitation.

The main methods used for keratin isolation and solubilization from keratin-rich materials are reduction, oxidation, microwave irradiation, alkali extraction, steam explosion, sulphitholysis and by means of ionic liquids<sup>53</sup>. The denaturation methods (such as reduction, oxidation and sulphitholysis) rely on the modification of the protein supramolecular structures by selectively breaking the inter/intra-chain disulphide covalent bonds and hydrogen bonds, while preserving the peptide bonds.

The intrinsic chemical and biological properties of this abundant and natural protein have led to the development of a variety of biotechnology and material science applications. Keratin-based materials are indeed promising candidates in the medical field due to their biodegradability, biocompatibility and their ability to support fibroblast cell growth, since keratin is also produced by the epidermal cells and plays an important role in the protective function of the skin<sup>58,59</sup>. The numerous uses of keratin based materials include drug delivery, dental implants, wound dressing and food packaging<sup>60</sup>.

## **Gelatin**

Gelatin is derived from collagen, one of the key structural proteins found in the extracellular matrices of many connective tissues in mammals, making up about 25% to 35% of the whole-body protein content<sup>61,62</sup>. Collagen is mostly found in fibrous tissues such as tendons, ligaments and skin (about one half of total body collagen), and is also abundant in corneas, cartilages, bones, blood vessels, intestinal walls, and intervertebral discs<sup>63</sup>. Collagen is synthesized by fibroblasts, and up to date 29 collagen types have been identified and described. Over 90% of the collagen in the body is of type I and is found in bones, skins, tendons, vascular, ligaments, and organs, while type II is predominant in cartilage.

The peculiarity of the amino acid sequence, where one residue every three is glycine and where proline and hydroxyproline are highly represented, accounts for the characteristic coiled coil

structure of the collagen molecule, where three distinct polypeptide chains, each of which coiled into a left-handed helix, are thrown into a right-handed superhelix stabilized through interchain hydrogen bonds and covalent crosslinks<sup>64,65</sup>. The triple helix structure forms fibres, arranged in bundles, making up the connective tissue matrix.

When subjected to acidic or alkaline hydrolysis, a mild degradative process occurs and the fibrous structure of collagen is broken down irreversibly: by destroying the triple helical structure of collagen, one, two or three chains are produced.

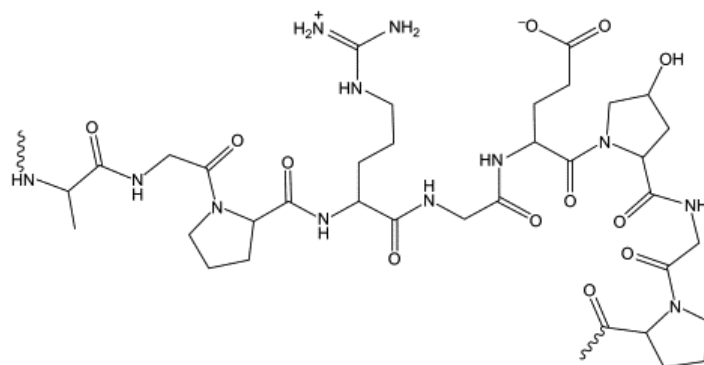


*Figure 10. Basic structure of gelatin.*

Gelatin (Figure 10) is obtained by thermal denaturation or physical and chemical degradation of collagen through the breaking of the triple-helix structure into random coils<sup>64</sup>. While collagen exists in many different forms, gelatin is mainly derived from collagen type I<sup>62</sup>.

The estimated world usage of gelatin is about 200,000 tons/year and, depending on the source from which it is extracted, two types of gelatin may be distinguished: type A gelatin, obtained by acidic hydrolysis from pig skins and characterized by an isoelectric point between 7 and 9, and type B gelatin of bovine origin, obtained by an alkaline process and characterized by an isoelectric point between 4 and 5<sup>66</sup>. The quality of gelatin is measured by the strength of the gel, also called Bloom value, which is the weight (grams) required for a specific plunger to depress the surface of a gel to a defined depth under specified conditions. Bloom values are classified as low (<150), medium (150-220) or high (220-300); commercially, high Bloom gelatin is preferred and takes a higher price<sup>67</sup>.

The different sources of gelatin and the various production techniques determine a strong variability in terms of structure, physical properties and chemical homogeneity<sup>68</sup>. The principal collagen sources for gelatin extraction include bovine and porcine skins but in the last decade other sources were explored, such as fish skins, bones and fins<sup>69</sup>, sea urchins<sup>70</sup>, jellyfish<sup>69,71</sup> and bird paws. Indeed, bovine gelatin has shown a potential risk of spreading bovine spongiform encephalopathy (BSE), widely known as ‘mad cow disease’, and it is severely

limited by religious issues (e.g., Hindus do not consume cow-related products). Similarly, Islam does not allow the consumption of pig-related products<sup>67,72</sup>. Besides, fish skin, bones and pins are the main by-products of the fish processing industry which cause waste and pollution and could therefore be a valuable and sustainable source of gelatin<sup>73,74</sup>. However, the commercial interest in fish gelatins has so far been very low, mainly due to their poor physical properties compared to those of mammalian gelatins: in particular, fish gelatins from cold water species, exhibit lower gelling and melting temperatures and low gel strength<sup>75</sup>.

Gelatin is one of the most popular biopolymers and has a wide range of applications, being generally regarded as GRAS. Firstly, it is the most widely used gelling agent in food applications due to its low antigenicity, special texture and the 'melt-in-mouth' perception<sup>76</sup>. In the food industry gelatin is also used in confections, dairy, baked goods and meat products<sup>77,78</sup>.

Gelatin is suitable for the production of biodegradable packaging materials thanks to appropriate film forming properties and good barriers against oxygen and aromas at a low/intermediate humidity<sup>79</sup>, but the low water barrier properties and the high solubility in aqueous environment make cross-linking reaction mandatory<sup>80</sup>.

Due to its nature, gelatin is biocompatible, biodegradable and it is not antigenic under physiological conditions<sup>81,82</sup>; moreover, it is completely resorbable *in vivo*. Indeed, it attracted a great interest in the pharmaceutical and medical fields, in tissue engineering, wound dressing and gene therapy<sup>81,82</sup>, being used as a matrix for implants, in injectable drug delivery microspheres, in intravenous infusions and in the manufacture of hard and soft capsules. There are also reports in which live attenuated viral vaccines used for immunization against measles, mumps, rubella, Japanese encephalitis, rabies, diphtheria, and tetanus toxin contain gelatin as a stabilizer<sup>83</sup>.

During my doctorate, I used biopolymers also in combination with snail slime, in order to evaluate the variations on the properties of the obtained materials induced by this natural extract. I report below a small section about the snail slime and snail farming, called heliciculture, which is a sustainable reality in strong growth.

### **Snail slime**

Snails' ancestors are one of the earliest known types of animals in the world. There is a huge variety encompassing over 30,000 living species, both aquatic and terrestrial: snails can be found everywhere around the world and live in a very diverse type of habitats<sup>84</sup>.

Since ancient Greece, the snails of different species were prepared in various ways, such as chopped, powdered, grilled or infused <sup>85</sup> and have been considered of medicinal value in traditional Chinese medicine.

Snail farming (heliculture) is currently a growing agricultural reality (about 9,000 professional helicicole farms in Italy) recognized by both public and institutional bodies, many of which have legislated in its favor, creating economic incentives for the spread of such production. Among the snail species living in Europe, about a dozen are edible and only four to five are commercialized. Of those, *Helix Aspersa* covers 40% of the market, *Helix Pomatia* 28%, *Helix Lucorum* 22% and *Eobania Vermiculata* 8.5%. From the above species, heliculture is possible and economically profitable only with *Helix Aspersa* <sup>86</sup>, with the aim of producing meat and eggs sold as *Escargot*. Snail slime is thus a byproduct of snail farming, and its composition depends on several variables as snail feeding and extraction method.

Slime is the mucus that covers the entire external surface of the snail, and it is secreted by salivary epidermal glands (pedal glands) to accomplish different functions. It is primarily used for locomotion due to its lubricant and adhesive properties, but it also has emollient, moisturizing, protective and even reparative abilities <sup>87</sup>.

Today, snail slimes are widely used in cosmetics and dermatological products to treat, for example, acne and scars: this products are indeed claimed to have healing, rejuvenating and protective properties <sup>88</sup> thanks to their slime content, or, more specifically, to the natural occurrence of hyaluronic acid, proteoglycans, glycoprotein enzymes and antimicrobial peptides in the slime. It is also used in the para-pharmaceutical sector to treat chronic bronchitis and for the management of skin wounds.

Different snail slime extraction methods can be used: snails can be stimulated to produce considerable quantities of slime without causing any damage to their health by means of natural methods (manual stimulation) or by using a stimulating solution inside a MullerOne machine, conditioned with ozone to preserve the final product (MullerONE method, <https://www.mullerone.com>). Although the stimulating solution has an acidic pH, it does not involve stress or dehydration to the snail, which tries to bring the pH of the epidermis back to its physiological value by producing slime. Other methods report the use of stimulating solutions with neutral pH (NaCl solution), as in the case of Colognesi farm (Ferrara) <sup>87</sup>.

### 1.3 FIELDS OF APPLICATION

The use of biopolymers and natural polymers allows to save fossil resources using biomass, which are regenerated annually contributing to the neutrality of the CO<sub>2</sub> cycle.

Thanks to increased awareness and attention to the environment and the continuous research to improve their properties, biopolymers and natural polymers have found many fields of application in recent years.

In addition, the biodegradability and the inherent biocompatibility of these materials, makes them excellent candidates for the preparation of biomaterials, that are materials designed to interface with biological systems in order to evaluate, support or replace any tissue, organ, or function of the body. Engineered biomaterials are indeed required to regenerate and ultimately reproduce the original physiological, biological, chemical, and mechanical properties. In the field of 'regenerative medicine', researchers are constantly developing new biomaterials and technologies to aid the body's natural capacity to self-repair, that is impaired with age and in cases of disease or injury <sup>89</sup>.

I carried out my PhD research activities in the laboratory of Materials Chemistry and Biomimetics, that is the science of imitating nature, and I focused on the production of biopolymer- and natural polymer-based biomaterials for tissue engineering, cosmetics, pharmaceutical and food packaging purposes.

#### **Tissue engineering**

Even if the human body has an excellent ability to repair itself, it strongly depends on the extent of tissue loss: tissues and organs can regenerate if damaged up to a threshold called 'critical size defect'. Any injury beyond that size needs an external support to heal.

Tissue engineering is an emerging discipline that combines cell biology and materials science for the *in vitro* or *in vivo* construction of tissues or organs <sup>90</sup>. The term "tissue engineering" (TE) was coined in 1988 at UCLA Symposia on Molecular and Cellular Biology by Professor Robert Nerem <sup>91,92</sup>. This interdisciplinary engineering has attracted much attention as a new therapeutic approach that can overcome the inconveniences of current artificial organs or the shortage of organ for transplants. In fact, up to now implantable materials used to fill these gaps were obtained from the patient himself (autograft) or from animals (xenograft) and corpses (allograft): this surgical treatment is limited by the availability of donors and self-donor tissues, immune rejection and by side effects of immunosuppressive drugs <sup>93,94</sup>.

To overcome these limits, tissue engineering emerged as a promising alternative in which organs and tissues can be repaired or regenerated by using artificial materials properly designed.

The concept of TE is to transplant a biofactor (cells, genes and/or proteins) within a porous degradable material known as ‘scaffold’: the key materials for TE are hence cells, growth factors and scaffolds, which can be used individually or combined. A schematic representation of the strategies applied in TE is reported in Figure 11.

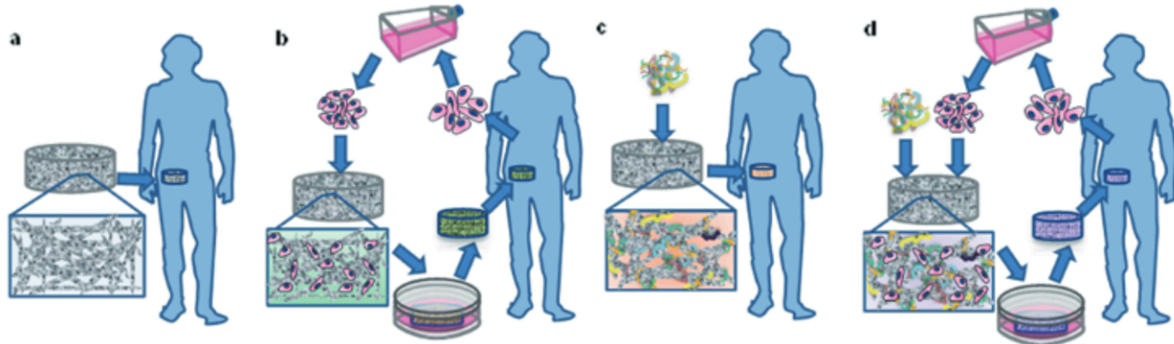


Figure 11. Overview of strategies applied in Tissue Engineering: a) Direct implantation of cell-free scaffold (gray); b) Cells are harvested, expanded and cultured on scaffolds *in vitro*, then cell-seeded constructs (green) are implanted at the defect site; c) Direct implantation of cell-free scaffold bio-activated with proteins, growth factors, genes, miRNAs or small chemical drugs (orange) for localized delivery of these external bio-stimuli; d) Cells are harvested, expanded in culture, combined with external bio-stimuli and cultured *in vitro* using scaffolds, then constructs (blue) are implanted at the defect site. Edited from <sup>89</sup>.

Scaffolds provide a suitable environment for cellular processes like spreading and proliferation, and play a significant role in preserving tissue volume, providing temporary mechanical support, and delivering bio-factors <sup>95</sup>.

A successful scaffold must mimic the tissue that is going to repair and be resorbed *in situ*, allowing the growth of new native tissue, thus avoiding a second surgery to remove the implanted devices. When selecting the materials for scaffolds fabrication, fundamental properties are required, such as biocompatibility with tissues, a biodegradability rate corresponding to the rate of new tissue formation, non-toxicity and non-immunogenicity, an optimal mechanical strength and adequate porosity and morphology for transporting cells, gases, metabolites, nutrients, and signal molecules both within and across materials and host environment <sup>29</sup>. A wide variety of materials able to stimulate the biological response of the surroundings (bioactive materials) are based on polymers, biopolymers, ceramics, and their composites.

If we refer to the regeneration of bone, materials can be classified into three types, according to the interaction that they develop with this tissue: osteoconductive, that are materials that can bond to bone tissue and stimulate its growth along the implant surface; osteopductive, that are materials that can stimulate the growth of new bone on the material away from the implant or bone interface, and are capable of bonding to soft tissue and cartilage; and osteoinductive, materials that induce the bone formation at extra-skeletal sites <sup>96</sup>.

Although both synthetic and natural polymers are used for biomaterials' fabrication, natural polymers have been the most used, thanks to their bioactivity, better overall interactions with various cell types and lack of immune response. On the other hand, synthetic polymers are less expensive and provide better functionalities, but some of them has poor biocompatibility or show toxicity resulting in inflammatory reaction or fibrous capsules formation.

Tissue-engineering has been used in the treatment of myocardial injuries <sup>97</sup>, the repair of cartilage defects <sup>98</sup>, and the treatment of bone defects <sup>99</sup>. During my doctorate, I focused on the bone and cartilage tissue engineering.

## **Cosmetics**

The global beauty market is notably acknowledged as a growing highly competitive economic sector worldwide: indeed, in the last twenty years the cosmetics industry has encountered the scenario of ever more demanding beauty standards, with a rise of 4,5% a year on average. According to the Personal Care Association, 450 millions of Europeans daily use a variety of cosmetic products such as soap, shampoo, hair conditioner, toothpaste, deodorant, shaving cream, skin care, perfume and make-up, that contain unsustainable raw materials and produce pollution both in the manufacturing stage and in the disposal of packaging and products.

The global tendency for products considered environmentally sustainable led the industry related to personal care formulations to fund the research and the development of personal care/cosmetics containing agents of natural resources and improving the use of sustainable raw materials/ingredients <sup>8</sup>. In this way, cosmetic application could be a solution to reuse byproducts discarded by several agro-industries, when they are considered not harmful, not expensive, biocompatible, biodegradable or at least compostable under specific environmental conditions, and suitable to be used in a wide range of topical preparations.

The desirable features of cosmetic ingredients are efficacy, safety, novelty, formulation stability, easy metabolism in the skin and low cost.

Since the appearance of allergies and skin irritations due to synthetic preservatives (e.g., parabens), colorants, stabilizers, etc. <sup>100</sup>, the use of biopolymers in the cosmetic field is boosted. Edible natural biopolymers are indeed widely employed as versatile constituents of personal care products as rheological modifiers, water-soluble binders, thickeners, film forming agents, conditioners, sensory and active ingredients, texturing agents, moisturizer, and hydrating agents.

## **Drug Delivery**

Drug delivery is the delivery of a substance, in a precise manner towards the area, tissue or cell, where its subsequent release will ensure the highest efficiency.

Design and synthesis of efficient drug delivery systems are of vital importance for medicine and healthcare. In particular, cancer therapy and diagnostic imaging are among the main applications where drug delivery will be able to give enormous benefits. In the first case, in fact, they will reduce the unwanted effects of chemotherapy, increasing the effectiveness of the treatment; the specific delivery of contrast fluids will also allow a more defined and precise diagnosis.

Since the first FDA approval of drug delivery system (DDS), Liposomal amphotericin B in 1990, more than 10 DDS are now commercially available to treat diverse diseases, ranging from cancer to fungal infection and to muscular degeneration <sup>101</sup>.

Using drug delivery solutions allows to decrease the doses of the drug administered, therefore reducing its possible side effects. In fact, to reduce the risk of infections, systemic antibiotic therapies (oral or parenteral) are a routine procedure, even if they can lead to antibiotic resistance, mainly caused by the inability to maintain high antibiotic concentrations.

Many different templates can be used as carriers for drug delivery purposes, such as nanocarriers, liposomes and micelles, micro- and nanoparticles, protein-based DDS, as well as biopolymer-drug conjugated DDS <sup>102-104</sup>.

In my research, I used drug delivery systems to enrich biomaterials such as films and bone cements with drugs, and thus to confer greater therapeutic properties. In particular, I designed biopolymer-based patches for topical applications able to release anti-microbial and anti-fungal drugs. Furthermore, I employed the spray congealing technique (a solvent-free technique by which a substance or a blend can be atomized and then solidified to form microparticles inside a congealing chamber) to produce antibiotic-loaded microparticles, which were then introduced in the composition of calcium phosphate bone cements, showing an effective release over time.

## **Food packaging**

Modern packaging must meet both the new stringent regulations and the demands of consumers, minimizing the impact on the environment.

Biodegradable packaging is defined by the American Society for Testing and Materials (ASTM) as one that is capable of decomposition into carbon dioxide, methane, water, inorganic compounds, and biomass, wherein the predominant mechanism of decomposition is the

enzymatic action of microorganisms, and the resulting products can be measured in a given period of time (ASTM, 2010 D996-10a) <sup>105</sup>.

While traditional food packaging concepts focused their attention only on the preservation of foodstuffs, the new food packaging systems are supposed to perform some other role than providing an inert barrier to external conditions. Many solutions involving packaging materials that can be reused, recycled or composted have been proposed so far, mainly exploiting the properties of carbohydrates and proteins <sup>106</sup>. In this way, biodegradable and edible films can be obtained, opening up new commercial opportunities for sustainable packaging materials. Indeed, edible coating offers advantages over the conventional ones, as it can be used wherever the application of conventional packaging is limited: e.g., as casing, coatings, separating layer for complex and multi-component food systems, capsules, dissolvable pre-portioned food packets, and controlled release for food additives (active packaging).

Active packaging is very appealing for the food industry and its demand increased abruptly in recent years as it can extend the food shelf-life: it acts as a carrier of additives such as flavours, colorants, nutraceuticals, antioxidant, and preservatives. The major and more promising application of this technology is addressed to the production of antimicrobial films. Films able to exhibit an effective antimicrobial activity are indeed highly desirable, as most food deterioration is caused by the growth of microorganisms. Many antimicrobial agents were incorporated into food packaging structure and among them, the preferred ones are those that provide a broad-spectrum antimicrobial protection at low concentrations, do not cause alterations in the sensory characteristics of the product, are compatible with packaging material components, and are in accordance with the applicable legislation <sup>107</sup>.

The critical step of the packaging design process relies in the biopolymer selection, since each of them has its own specific properties. With regard to degradation, some biopolymers take a few weeks, while that of traditional polymers (synthetic) takes several months or even years, depending on the type and origin of the polymer <sup>108</sup>.

In the food industry, selected biopolymers are used in the manufacture of biodegradable packaging (mono- and multi-layer), active packaging, edible films, and edible coatings for fruits, meats, and fish, among other foods, as well as food processing aids such as stabilizers and gelling agents <sup>109</sup>.

In the next chapters, the main results of my research are reported. These are grouped according to the type of biomaterial produced, namely films, scaffolds and bone cements.

## 1.4 BIBLIOGRAPHY

- (1) Jambeck, J. R.; Geyer, R.; Wilcox, C.; Siegler, T. R.; Perryman, M.; Andrady, A.; Narayan, R.; Law, K. L. Plastic Waste Inputs from Land into the Ocean. *Science (80)*. **2015**, *347* (6223), 768–771, DOI:10.1126/SCIENCE.1260352.
- (2) Center for International Environmental Law (CIEL). *Sweeping New Report on Global Environmental Impact of Plastics Reveals Severe Damage to Climate - Center for International Environmental Law*; WASHINGTON, DC , 2019.
- (3) Zalasiewicz, J.; Waters, C. N.; Ivar do Sul, J. A.; Corcoran, P. L.; Barnosky, A. D.; Cearreta, A.; Edgeworth, M.; Gałuszka, A.; Jeandel, C.; Leinfelder, R.; McNeill, J. R.; Steffen, W.; Summerhayes, C.; Waples, M.; Williams, M.; Wolfe, A. P.; Yonah, Y. The Geological Cycle of Plastics and Their Use as a Stratigraphic Indicator of the Anthropocene. *Anthropocene* **2016**, *13*, 4–17, DOI:10.1016/J.ANCENE.2016.01.002.
- (4) Andrady, A. L. *Plastics and Environmental Sustainability*; Jhon Wiley & Sons, Ed.; 2015.
- (5) Suaria, G.; Avio, C. G.; Mineo, A.; Lattin, G. L.; Magaldi, M. G.; Belmonte, G.; Moore, C. J.; Regoli, F.; Aliani, S. The Mediterranean Plastic Soup: Synthetic Polymers in Mediterranean Surface Waters. *Sci. Reports 2016 61* **2016**, *6* (1), 1–10, DOI:10.1038/srep37551.
- (6) European Parliament. Parliament seals ban on throwaway plastics by 2021 <https://www.europarl.europa.eu/news/it/press-room/20190321IPR32111/il-pe-conferma-il-divieto-d-uso-della-plastica-usa-e-getta-entro-il-2021>.
- (7) Ellen MacArthur Foundation. What is a circular economy? <https://ellenmacarthurfoundation.org/topics/circular-economy-introduction/overview>.
- (8) Mellou, F.; Varvaresou, A.; Papageorgiou, S. Renewable Sources: Applications in Personal Care Formulations. *Int. J. Cosmet. Sci.* **2019**, *41* (6), 517–525, DOI:10.1111/ics.12564.
- (9) Klöpffer, W.; Grahl, B. *Life Cycle Assessment (LCA) : A Guide to Best Practice*; John Wiley & Sons, Ed.; Wiley-VCH: Weinheim, Germany, 2014.
- (10) Jacquemin, L.; Pontalier, P. Y.; Sablayrolles, C. Life Cycle Assessment (LCA) Applied to the Process Industry: A Review. *Int. J. Life Cycle Assess.* **2012**, *17* (8), 1028–1041, DOI:10.1007/S11367-012-0432-9/FIGURES/3.
- (11) Roy, P.; Nei, D.; Orikasa, T.; Xu, Q.; Okadome, H.; Nakamura, N.; Shiina, T. A Review of Life Cycle Assessment (LCA) on Some Food Products. *J. Food Eng.* **2009**, *90* (1), 1–10, DOI:10.1016/J.JFOODENG.2008.06.016.
- (12) Sudesh, K.; Iwata, T. Sustainability of Biobased and Biodegradable Plastics. *Clean - Soil, Air, Water* **2008**, *36* (5–6), 433–442, DOI:10.1002/clen.200700183.
- (13) Richard, A. G.; Kalra, B. Biodegradable Polymers for the Environment. *Am. Assoc. Adv. Sci.* **2002**, *297* (5582), 803–807.
- (14) Rhim, J.; Wang, L. Mechanical and Water Barrier Properties of Agar/κ-Carrageenan/Konjac Glucomannan Ternary Blend Biohydrogel Films. *Carbohydr. Polym.* **2013**, *96* (1), 71–81, DOI:10.1016/J.CARBPOL.2013.03.083.
- (15) Kennedy, J. E.; Lyons, J. G.; Geever, L. M.; Higginbotham, C. L. Synthesis and Characterisation of Styrene Butadiene Styrene-g-Acrylic Acid for Potential Use in Biomedical Applications. *Mater. Sci. Eng. C* **2009**, *5* (29), 1655–1661, DOI:10.1016/J.MSEC.2009.01.015.
- (16) Jaklenec, A.; Wan, E.; Murray, M.; Mathiowitz, E. Novel Scaffolds Fabricated from Protein-Loaded Microspheres for Tissue Engineering. *Biomaterials* **2008**, *29* (2), 185–192, DOI:10.1016/J.BIOMATERIALS.2007.09.017.
- (17) Lai, J.; Lu, P.; Chen, K.; Tabata, Y.; Hsiue, G. Effect of Charge and Molecular Weight on the Functionality of Gelatin Carriers for Corneal Endothelial Cell Therapy. *Biomacromolecules* **2006**, *7* (6), 1836–1844, DOI:10.1021/BM0601575.

- (18) Skotak, M.; Leonov, A. P.; Larsen, G.; Noriega, S.; Subramanian, A. Biocompatible and Biodegradable Ultrafine Fibrillar Scaffold Materials for Tissue Engineering by Facile Grafting of L-Lactide onto Chitosan. *Biomacromolecules* **2008**, *9* (7), 1902–1908, DOI:10.1021/BM800158C.
- (19) Ghaffari, A.; Navaee, K.; Oskoui, M.; Bayati, K.; Rafiee-Tehrani, M. Preparation and Characterization of Free Mixed-Film of Pectin/Chitosan/Eudragit RS Intended for Sigmoidal Drug Delivery. *Eur. J. Pharm. Biopharm.* **2007**, *67* (1), 175–186, DOI:10.1016/J.EJPB.2007.01.013.
- (20) Ofori-Kwakye, K.; Fell, J. Leaching of Pectin from Mixed Films Containing Pectin, Chitosan and HPMC Intended for Biphasic Drug Delivery. *Int. J. Pharm.* **2003**, *250* (1), 251–257, DOI:10.1016/S0378-5173(02)00546-X.
- (21) Kumar, R.; Majeti, N. V. A Review of Chitin and Chitosan Applications. *React. Funct. Polym.* **2000**, *46* (1), 1–27, DOI:10.1016/S1381-5148(00)00038-9.
- (22) Sheth, Y.; Dharaskar, S.; Khalid, M.; Sonawane, S. An Environment Friendly Approach for Heavy Metal Removal from Industrial Wastewater Using Chitosan Based Biosorbent: A Review. *Sustain. Energy Technol. Assessments* **2021**, *43*, 100951, DOI:10.1016/J.SETA.2020.100951.
- (23) Muñoz, I.; Rodríguez, C.; Gillet, D.; M. Moerschbacher, B. Life Cycle Assessment of Chitosan Production in India and Europe. *Int. J. Life Cycle Assess.* **2018**, *23* (5), 1151–1160, DOI:10.1007/S11367-017-1290-2/FIGURES/7.
- (24) Kurita, K. Chitin and Chitosan: Functional Biopolymers from Marine Crustaceans. *Mar. Biotechnol. (NY)*. **2006**, *8* (3), 203–226, DOI:10.1007/S10126-005-0097-5.
- (25) Samuels, R. J. Solid State Characterization of the Structure of Chitosan Films.
- (26) Rahman, M. M.; Rashid, T. U.; Datta, A. Chitosan: Process and Modification. In *Encyclopedia of Biomedical Polymers and Polymeric Biomaterials*; CRC Press, Ed.; CRC Press, 2015; Vol. 11, pp 1811–1825, DOI:10.1081/E-EBPP-120050033.
- (27) Li, Q.; Dunn, E. T.; Grandmaison, E. W.; Goosen, M. F. A. Applications and Properties of Chitosan. *J. Bioact. Compat. Polym.* **1992**, *7* (4), 370–397, DOI:10.1177/088391159200700406.
- (28) Tolaimate, A.; Desbrieres, J.; Rhazi, M.; Alagui, A. Contribution to the Preparation of Chitins and Chitosans with Controlled Physico-Chemical Properties. *Polymer (Guildf)*. **2003**, *44* (26), 7939–7952, DOI:10.1016/J.POLYMER.2003.10.025.
- (29) Islam, M. M.; Shahruzzaman, M.; Biswas, S.; Nurus Sakib, M.; Rashid, T. U. Chitosan Based Bioactive Materials in Tissue Engineering Applications-A Review. *Bioact. Mater.* **2020**, *5* (1), 164–183, DOI:10.1016/J.BIOACTMAT.2020.01.012.
- (30) Pillai, C. K. S.; Paul, W.; Sharma, C. P. Chitin and Chitosan Polymers: Chemistry, Solubility and Fiber Formation. *Prog. Polym. Sci.* **2009**, *34* (7), 641–678, DOI:10.1016/j.progpolymsci.2009.04.001.
- (31) Jayakumar, R.; Prabakaran, M.; Sudheesh Kumar, P. T.; Nair, S. V.; Tamura, H. Biomaterials Based on Chitin and Chitosan in Wound Dressing Applications. *Biotechnol. Adv.* **2011**, *29* (3), 322–337, DOI:10.1016/j.biotechadv.2011.01.005.
- (32) Libio, I. C.; Demori, R.; Ferrão, M. F.; Lionzo, M. I. Z.; da Silveira, N. P. Films Based on Neutralized Chitosan Citrate as Innovative Composition for Cosmetic Application. *Mater. Sci. Eng. C* **2016**, *67*, 115–124, DOI:10.1016/j.msec.2016.05.009.
- (33) Foroughi, F.; Ghomi, E. R.; Dehaghi, F. M.; Borayek, R.; Ramakrishna, S. A Review on the Life Cycle Assessment of Cellulose: From Properties to the Potential of Making It a Low Carbon Material. *Materials (Basel)*. **2021**, *14* (4), 714, DOI:10.3390/MA14040714.
- (34) Glasser, W. G.; McCartney, B. K.; Samaranyake, G. Cellulose Derivatives with Low Degree of Substitution. 3. The Biodegradability of Cellulose Esters Using a Simple Enzyme Assay. *Biotechnol. Prog.* **1994**, *10* (2), 214–219, .
- (35) Gullichsen, J.; Paulapuro, H.; Attwood, B.; Anne, S.; Joyce, T. Chap. 1: Structure and Chemical

- Composition of Wood. In *3. Forest Products Chemistry*; Stenius, P., Ed.; Published in cooperation with the Finnish Paper Engineer's Association and TAPPI; Vol. 3, p 324.
- (36) Hubbe, M. A.; Gardner, D. J.; Shen, W. Contact Angles and Wettability of Cellulosic Surfaces: Review of Proposed Mechanism and Test Strategies. *BioResources* **2015**, *10* (4), 8657–8749, DOI:10.1039/CT9252701863.
  - (37) Obataya, E.; Shibutani, S.; Minato, K. Swelling of Acetylated Wood II: Effects of Delignification on Solvent Adsorption of Acetylated Wood. *J. Wood Sci.* **2007**, *53* (5), 408–411, DOI:10.1007/S10086-007-0876-X.
  - (38) Black, E. L.; Allen, L. H. *Pitch Control, Wood Resin and Deresination*; Black, E. L., Allen, L. H., Eds.; TAPPI press.
  - (39) Burdock, G. A. Safety Assessment of Hydroxypropyl Methylcellulose as a Food Ingredient. *Food Chem. Toxicol.* **2007**, *45* (12), 2341–2351, DOI:10.1016/j.fct.2007.07.011.
  - (40) Schmitt, C.; Sanchez, C.; Desobry-Banon, S.; Hardy, J. Structure and Technofunctional Properties of Protein-Polysaccharide Complexes: A Review. *Crit. Rev. Food Sci. Nutr.* **1998**, *38* (8), 689–753, DOI:10.1080/10408699891274354.
  - (41) Arslan, N.; Togrul, H. Modelling of Water Sorption Isotherms of Macaroni Stored in A chamber under Controlled Humidity and Thermodynamic Approach. *J. Food Eng.* **2005**, *69*, 133–145, DOI:doi:10.1016/j.jfoodeng.2004.08.004.
  - (42) Noble, P. W.; Liang, J.; Jiang, D. Hyaluronan as an Immune Regulator in Human Diseases. *Physiol. Rev.* **2011**, *91* (1), 221, DOI:10.1152/PHYSREV.00052.2009.
  - (43) Oelschlaeger, C.; Cota, M.; Coelho, P.; Willenbacher, N. Chain Flexibility and Dynamics of Polysaccharide Hyaluronan in Entangled Solutions: A High Frequency Rheology and Diffusing Wave Spectroscopy Study. *Biomacromolecules* **2013**, *14* (10), 3689–3696, DOI:10.1021/bm4010436.
  - (44) Boeriu, C. G.; Springer, J.; Kooy, F. K.; van den Broek, L. A. M.; Eggink, G. Production Methods for Hyaluronan. *Int. J. Carbohydr. Chem.* **2013**, *2013*, 1–14, DOI:10.1155/2013/624967.
  - (45) Prehm, P. Hyaluronate Is Synthesized at Plasma Membranes. *Biochem. J* **1984**, *220*, 597–600, .
  - (46) Stern, R. Devising a Pathway for Hyaluronan Catabolism: Are We There Yet? *Glycobiology* **2003**, *13* (12), 105R-115R, DOI:10.1093/glycob/cwg112.
  - (47) Nakagawa, K.; Takahashi, C.; Nishi, Y.; Jyuen, H.; Sugiyama, R.; Kuribayashi, Y.; Sugiyama, R. Hyaluronan-Enriched Transfer Medium Improves Outcome in Patients with Multiple Embryo Transfer Failures. *J. Assist. Reprod. Genet.* **2012**, *29* (7), 679, DOI:10.1007/S10815-012-9758-2.
  - (48) Tarusha, L.; Paoletti, S.; Travan, A.; Marsich, E. Alginate Membranes Loaded with Hyaluronic Acid and Silver Nanoparticles to Foster Tissue Healing and to Control Bacterial Contamination of Non-Healing Wounds. *J. Mater. Sci. Mater. Med.* **2018**, *29* (3), DOI:10.1007/s10856-018-6027-7.
  - (49) Ghosalkar, S.; Schiraldi, C.; Gatta, A. La; De Rosa, M. Biotechnological Production and Application of Hyaluronan 20 Biotechnological Production and Application of Hyaluronan. In *Biopolymers*; Elnashar, M., Ed.; InTech: Rijeka, Croatia, 2010; pp 387–412.
  - (50) Freitas, F.; Alves, V. D.; Reis, M. A. M. Advances in Bacterial Exopolysaccharides: From Production to Biotechnological Applications. *Trends Biotechnol.* **2011**, *29* (8), 388–398, DOI:10.1016/J.TIBTECH.2011.03.008.
  - (51) Ulery, B. D.; Nair, L. S.; Laurencin, C. T. Biomedical Applications of Biodegradable Polymers. *J. Polym. Sci. Part B Polym. Phys.* **2011**, *49* (12), 832–864, DOI:10.1002/POLB.22259.
  - (52) Ghatak, S.; Misra, S.; Toole, B. P. Hyaluronan Oligosaccharides Inhibit Anchorage-Independent Growth of Tumor Cells by Suppressing the Phosphoinositide 3-Kinase/Akt Cell Survival Pathway. *J. Biol. Chem.* **2002**, *277* (41), 38013–38020, DOI:10.1074/JBC.M202404200.

- (53) Shavandi, A.; Silva, T.; Bekhit, A.; Bekhit, A. Keratin: Dissolution, Extraction and Biomedical Application. *Biomater. Sci.* **2017**, *5* (9), 1699–1735, DOI:10.1039/C7BM00411G.
- (54) Wang, B.; Yang, W.; McKittrick, J.; Meyers, M. A. Keratin: Structure, Mechanical Properties, Occurrence in Biological Organisms, and Efforts at Bioinspiration. *Prog. Mater. Sci.* **2016**, *76*, 229–318, DOI:10.1016/J.PMATSCI.2015.06.001.
- (55) Feroz, S.; Muhammad, N.; Ranayake, J.; Dias, G. Keratin - Based Materials for Biomedical Applications. *Bioact. Mater.* **2020**, *5* (3), 496–509, DOI:10.1016/J.BIOACTMAT.2020.04.007.
- (56) Bruce Fraser, R. D.; Parry, D. A. D. The Structural Basis of the Filament-Matrix Texture in the Avian/Reptilian Group of Hard  $\hat{\text{I}}^2$ -Keratins. *J. Struct. Biol.* **2011**, *173* (2), 391–405, DOI:10.1016/j.jsb.2010.09.020.
- (57) Zoccola, M.; Aluigi, A.; Tonin, C. Characterisation of Keratin Biomass from Butchery and Wool Industry Wastes. *J. Mol. Struct.* **2009**, *938* (1–3), 35–40, DOI:10.1016/J.MOLSTRUC.2009.08.036.
- (58) Aluigi, A.; Zoccola, M.; Vineis, C.; Tonin, C.; Ferrero, F.; Canetti, M. Study on the Structure and Properties of Wool Keratin Regenerated from Formic Acid. *Int. J. Biol. Macromol.* **2007**, *41* (3), 266–273, DOI:10.1016/J.IJBIOMAC.2007.03.002.
- (59) Yamauchi, Y.; Yamauchi, A.; Kusunoki, T.; Kohda, A.; Konishi, Y. Preparation of Stable Aqueous Solution of Keratins, and Physicochemical and Biodegradational Properties of Films. *J. Biomed. Mater. Res.* **1996**, *31* (4), 439–444.
- (60) McLellan, J.; Thornhill, S. G.; Shelton, S.; Kumar, M. Keratin-Based Biofilms, Hydrogels, and Biofibers. In *Keratin as a Protein Biopolymer*; Springer International Publishing, Ed.; Springer International Publishing, 2019; pp 187–200, DOI:10.1007/978-3-030-02901-2\_7.
- (61) Muyonga, J. H.; Cole, C. G. B.; Duodu, K. G. Characterisation of Acid Soluble Collagen from Skins of Young and Adult Nile Perch (*Lates Niloticus*). *Food Chem.* **2004**, *85* (1), 81–89, DOI:10.1016/j.foodchem.2003.06.006.
- (62) Gorgieva, S.; Kokol, V. Collagen- vs. Gelatine-Based Biomaterials and Their Biocompatibility: Review and Perspectives. *Biomater. Appl. Nanomedicine* **2011**, 17–52, DOI:10.5772/24118.
- (63) Brinckmann, J.; Müller, P. K.; Notbohm, H. *Collagen : Primer in Structure, Processing and Assembly*, Illustrated edition.; Springer-Verlag: Berlin, 2005; Vol. 247.
- (64) Bigi, A.; Panzavolta, S.; Rubini, K. Relationship between Triple-Helix Content and Mechanical Properties of Gelatin Films. *Biomaterials* **2004**, *25* (25), 5675–5680, DOI:10.1016/J.BIOMATERIALS.2004.01.033.
- (65) Brodsky, B.; Ramshaw, J. A. M. The Collagen Triple-Helix Structure. *Matrix Biol.* **1997**, *15* (8–9), 545–554, DOI:10.1016/S0945-053X(97)90030-5.
- (66) Gómez-Guillén, M. C.; Ihl, M.; Bifani, V.; Silva, A.; Montero, P. Edible Films Made from Tuna-Fish Gelatin with Antioxidant Extracts of Two Different Murta Ecotypes Leaves (*Ugni Molinae Turcz.*). *Food Hydrocoll.* **2007**, *21* (7), 1133–1143, DOI:10.1016/J.FOODHYD.2006.08.006.
- (67) Badii, F.; Howell, N. K. Fish Gelatin: Structure, Gelling Properties and Interaction with Egg Albumen Proteins. *Food Hydrocoll.* **2006**, *20* (5), 630–640, DOI:10.1016/j.foodhyd.2005.06.006.
- (68) Hoque, M. E.; Nuge, T.; Yeow, T. K.; Nordin, N.; Prasad, R. G. S. V. Gelatin Based Scaffolds For Tissue Engineering – A Review. *Polym. Res. J.* **2015**, *9* (1), 15–32, .
- (69) Nagai, T.; Suzuki, N. Isolation of Collagen from Fish Waste Material-Skin, Bone and Fins. *Food Chem.* **2000**, *68* (3), 277–281.
- (70) Robinson, J. Comparative Biochemical Analysis of Sea Urchin Peristome and Rat Tail Tendon Collagen. *Comp. Biochem. Physiol. B. Biochem. Mol. Biol.* **1997**, *117* (2), 307–313, DOI:10.1016/S0305-0491(97)00092-8.
- (71) Hoyer, B.; Bernhardt, A.; Lode, A.; Heinemann, S.; Sewing, J.; Klinger, M.; Notbohm, H.; Gelinsky, M. Jellyfish Collagen Scaffolds for Cartilage Tissue Engineering. *Acta Biomater.*

- 2014, 10 (2), 883–892, DOI:10.1016/J.ACTBIO.2013.10.022.
- (72) Herpandi; Huda, N.; Adzitey, F. Fish Bone and Scale as a Potential Source of Halal Gelatin. *J. Fish. Aquat. Sci.* **2011**, 6 (4), 379–389, DOI:10.3923/JFAS.2011.379.389.
- (73) Kim, D.; Min, S. C. Trout Skin Gelatin-Based Edible Film Development. *J. Food Sci.* **2012**, 77 (9), E240–E246, DOI:10.1111/J.1750-3841.2012.02880.X.
- (74) Karim, A. A.; Bhat, R. Fish Gelatin: Properties, Challenges, and Prospects as an Alternative to Mammalian Gelatins. *Food Hydrocoll.* **2009**, 23 (3), 563–576, DOI:10.1016/j.foodhyd.2008.07.002.
- (75) Leuenberger, B. H. Investigation of Viscosity and Gelation Properties of Different Mammalian and Fish Gelatins. *Food Hydrocoll.* **1991**, 5 (4), 353–361, DOI:10.1016/S0268-005X(09)80047-7.
- (76) Haug, I. J.; Draget, K. I.; Smidsrød, O. Physical and Rheological Properties of Fish Gelatin Compared to Mammalian Gelatin. *Food Hydrocoll.* **2004**, 18 (2), 203–213, DOI:10.1016/S0268-005X(03)00065-1.
- (77) Johnston-Banks, F. A. Gelatine. In *Food Gels*; Harris, P., Ed.; Springer, Dordrecht, 1990; pp 233–289, DOI:10.1007/978-94-009-0755-3\_7.
- (78) Schrieber, R.; Gareis, H. *Gelatine Handbook. Theory and Industrial Practice*; Weinheim: WILEY-VCH Verlag GmbH & Co., Ed.; 2007.
- (79) Fakhreddin Hosseini, S.; Rezaei, M.; Zandi, M.; Ghavi, F. F. Preparation and Functional Properties of Fish Gelatin-Chitosan Blend Edible Films. *Food Chem.* **2013**, 136 (3–4), 1490–1495, DOI:10.1016/j.foodchem.2012.09.081.
- (80) Rault, I.; Frei, V.; Herbage, D.; Abdul-Malak, N.; Huc, A. Evaluation of Different Chemical Methods for Cross-Linking Collagen Gel, Films and Sponges. *J. Mater. Sci. Mater. Med.* **1996**, 7 (4), 215–221, DOI:10.1007/BF00119733.
- (81) Gomez-Guillen, M. C.; Gimenez, B.; Lopez-Caballero, M. E.; Montero, M. P. Functional and Bioactive Properties of Collagen and Gelatin from Alternative Sources: A Review. *Food Hydrocoll.* **2011**, 25 (8), 1813–1827, DOI:10.1016/j.foodhyd.2011.02.007.
- (82) Lien, S. M.; Ko, L. Y.; Huang, T. J. Effect of Pore Size on ECM Secretion and Cell Growth in Gelatin Scaffold for Articular Cartilage Tissue Engineering. *Acta Biomater.* **2009**, 5 (2), 670–679, DOI:10.1016/J.ACTBIO.2008.09.020.
- (83) Burke, C.; Hsu, T.; Volkin, D. Formulation, Stability, and Delivery of Live Attenuated Vaccines for Human Use. *Crit. Rev. Ther. Drug Carrier Syst.* **1999**, 16 (1), 1–83.
- (84) Snail Facts and Information <https://www.snail-world.com/>.
- (85) Bonnemain, B. Helix and Drugs: Snails for Western Health Care From Antiquity to the Present. *Evidence-based Complement. Altern. Med.* **2005**, 2 (1), 28, DOI:10.1093/ECAM/NEH057.
- (86) Conte, R. Heliciculture : Purpose and Economic Perspectives in the European Community. *J. Inst. Sci. Techonology* **2015**, No. April, 27–35.
- (87) Trapella, C.; Rizzo, R.; Gallo, S.; Alogna, A.; Bortolotti, D.; Casciano, F.; Zauli, G.; Secchiero, P.; Voltan, R. HelixComplex Snail Mucus Exhibits Pro-Survival, Proliferative and pro-Migration Effects on Mammalian Fibroblasts. *Sci. Rep.* **2018**, 8 (1), 1–10, DOI:10.1038/s41598-018-35816-3.
- (88) Chinaka, N. C.; Chuku, L. C.; George, G.; Oraezu, C.; Umahi, G.; Orinya, O. F. Snail Slime: Evaluation of Anti-Inflammatory, Phytochemical and Antioxidant Properties. *J. Complement. Altern. Med. Res.* **2021**, 13 (1), 8–13, DOI:10.9734/jocamr/2021/v13i130214.
- (89) Curtin, C. M.; Castaño, I. M.; O'Brien, F. J. Scaffold-Based MicroRNA Therapies in Regenerative Medicine and Cancer. *Adv. Healthc. Mater.* **2018**, 7 (1), 1700695, DOI:10.1002/ADHM.201700695.
- (90) Elbaz, A.; He, Z.; Gao, B.; Chi, J.; Su, E.; Zhang, D.; Liu, S.; Xu, H.; Liu, H.; Gu, Z. Recent

- Biomedical Applications of Bio-Sourced Materials. *Bio-Design Manuf.* **2018**, *1* (1), 26–44, DOI:10.1007/s42242-018-0002-5.
- (91) Eltom, A.; Zhong, G.; Muhammad, A. Scaffold Techniques and Designs in Tissue Engineering Functions and Purposes: A Review. *Adv. Mater. Sci. Eng.* **2019**, *2019*, 3429527, DOI:10.1155/2019/3429527.
- (92) Lanza, R.; Langer, R.; Vacanti, J. *Principles of Tissue Engineering - 4th Edition*, 4th ed.; Lanza, R., Langer, R., Vacanti, J., Eds.; Academic Press, 2013.
- (93) Ikada, Y. Challenges in Tissue Engineering. *J. R. Soc. Interface* **2006**, *3* (10), 589–601, DOI:10.1098/RSIF.2006.0124.
- (94) Jammalamadaka, U.; Tappa, K. Recent Advances in Biomaterials for 3D Printing and Tissue Engineering. *J. Funct. Biomater.* **2018**, *9* (1), DOI:10.3390/JFB9010022.
- (95) Hollister, S. J. Porous Scaffold Design for Tissue Engineering. **2005**.
- (96) Habibovic, P.; de Groot, K. Osteoinductive Biomaterials-Properties and Relevance in Bone Repair. *J. Tissue Eng. Regen. Med.* **2007**, *1* (1), 25–32, DOI:10.1002/TERM.5.
- (97) Gabisonia, K.; Prosdocimo, G.; Aquaro, G.; Carlucci, L.; Zentilin, L.; Secco, I.; Ali, H.; Braga, L.; Gorgodze, N.; Bernini, F.; Burchielli, S.; Collesi, C.; Zandonà, L.; Sinagra, G.; Piacenti, M.; S, Z.; R, B.; FA, R.; M, G. MicroRNA Therapy Stimulates Uncontrolled Cardiac Repair after Myocardial Infarction in Pigs. *Nature* **2019**, *569* (7756), 418–422, DOI:10.1038/S41586-019-1191-6.
- (98) Armiento, A.; Alini, M.; Stoddart, M. Articular Fibrocartilage - Why Does Hyaline Cartilage Fail to Repair? *Adv. Drug Deliv. Rev.* **2019**, *146*, 289–305, DOI:10.1016/J.ADDR.2018.12.015.
- (99) Chen, Z.; Wang, Z.; Gu, Z. Bioinspired and Biomimetic Nanomedicines. *Acc. Chem. Res.* **2019**, *52* (5), 1255–1264, DOI:10.1021/ACS.ACCOUNTS.9B00079.
- (100) Rodrigues, F.; Gaspar, C.; Palmeira-De-Oliveira, A.; Sarmento, B.; Amaral, M. H.; Oliveira, M. B. P. P. Application of Coffee Silverskin in Cosmetic Formulations: Physical/Antioxidant Stability Studies and Cytotoxicity Effects. *Drug Dev. Ind. Pharm.* **2016**, *42* (1), 99–106, DOI:10.3109/03639045.2015.1035279.
- (101) Allen, T. M.; Cullis, P. R. Drug Delivery Systems: Entering the Mainstream. *Science* (80-. ). **2004**, *303*, 2994.
- (102) Sala, M.; Diab, R.; Elaissari, A.; Fessi, H. Lipid Nanocarriers as Skin Drug Delivery Systems: Properties, Mechanisms of Skin Interactions and Medical Applications. *Int. J. Pharm.* **2018**, *535* (1–2), 1–17, DOI:10.1016/j.ijpharm.2017.10.046.
- (103) Bachhav, Y. G.; Mondon, K.; Kalia, Y. N.; Gurny, R.; Möller, M. Novel Micelle Formulations to Increase Cutaneous Bioavailability of Azole Antifungals. *J. Control. Release* **2011**, *153* (2), 126–132, DOI:10.1016/j.jconrel.2011.03.003.
- (104) Geszke-Moritz, M.; Moritz, M. Solid Lipid Nanoparticles as Attractive Drug Vehicles: Composition, Properties and Therapeutic Strategies. *Mater. Sci. Eng. C* **2016**, *68*, 982–994, DOI:10.1016/j.msec.2016.05.119.
- (105) Tang, X.; Kumar, P.; Alavi, S.; Sandeep, K. Recent Advances in Biopolymers and Biopolymer-Based Nanocomposites for Food Packaging Materials. *Crit. Rev. Food Sci. Nutr.* **2012**, *52* (5), 426–442, DOI:10.1080/10408398.2010.500508.
- (106) Kowalczyk, D.; Skrzypek, T.; Basiura-Cembala, M.; Łupina, K.; Mężyńska, M. The Effect of Potassium Sorbate on the Physicochemical Properties of Edible Films Based on Pullulan, Gelatin and Their Blends. *Food Hydrocoll.* **2020**, *105* DOI:10.1016/J.FOODHYD.2020.105837.
- (107) Dıblan, S.; Kaya, S. Antimicrobials Used in Active Packaging Films. *Food Heal.* **2018**, *4* (1), 63–79, DOI:10.3153/JFHS18007.
- (108) Shimao, M. Biodegradation of Plastics. *Curr. Opin. Biotechnol.* **2001**, *12* (3), 242–247, DOI:10.1016/S0958-1669(00)00206-8.

- (109) Avila-Sosa, R.; Ochoa-Velasco, C. E.; Navarro-Cruz, A. R.; Palou, E.; López-Malo, A. Combinational Approaches for Antimicrobial Packaging: Chitosan and Oregano Oil. In *Antimicrobial Food Packaging*; Barros-Velázquez, J., Ed.; Academic Press., 2016; pp 581–588, DOI:10.1016/B978-0-12-800723-5.00047-4.

## **Chapter 2.** **FILMS**

### **2.1 INTRODUCTION**

Films are thin membranes made of just one layer that includes all the components (polymeric matrix, plasticizer, drug, adhesive), does not require any synthetic support and can be used for many different applications. The type of polymer used and its characteristics (e.g., molecular weight, degree of substitution) play a significant role in defining the films behavior, influencing for example the solubility, the adhesive properties, the mechanical strength, the biodegradability, and hence the field of application. The interest towards more versatile films, able of performing a variety of functions with an active role, has recently speed up the research in this field.

Biopolymers and natural polymers have been widely employed for the production of films <sup>1</sup>, providing versatile matrices that can also act as carrier of a variety of biologically relevant molecules and drugs. Films can indeed be un-medicated <sup>2</sup> or intended as patches for drug delivery purposes, and hence be drug-impregnated <sup>3</sup>, providing a controlled local release of the drug at effective concentration.

When films are intended to come into contact with the body, they should be non-toxic, contain no irritant ingredients and do not provoke allergic reactions: biodegradability and an environmentally safe composition represent added values <sup>2</sup>. Moreover, based on the application, films can be designed to be soluble, hence easily washed off, or able to resist water. Similarly, they can be self-adhesive <sup>4</sup> or able to adhere to wet skin <sup>5</sup>.

These emerging platforms can have different properties, and are indeed very appealing in different fields, including biomedical <sup>6</sup>, cosmetics, packaging <sup>7</sup>, sensors and adhesives <sup>5</sup> and as drug delivery systems <sup>8</sup>. However, they generally present poor mechanical properties regarding processability and end-use applications <sup>9</sup>. Many efforts have been made to tune the composition and properties of biopolymer-based films, in order to improve their performance and widen their application fields.

In literature, films with improved properties were obtained through the incorporation of compounds and natural extracts <sup>10,11</sup> or by blending with polymers with a different chemical structure <sup>12</sup>. In particular, films exhibiting improved light barrier and extra protective shield against oxidative processes were produced by incorporation of antioxidant and/or antimicrobial agents <sup>13-15</sup>. For example, addition of propolis showed to enhance mechanical strength, antibacterial activity and antioxidant capacity of chitosan-based materials for food packaging applications <sup>16</sup>.

In my research, I employed the use of snail slime extracted from *Helix Aspersa Muller* snails in combination with a biopolymer-based matrix in order to obtain versatile films with improved properties. In fact, during my first year of PhD, my research group patented the formulation of biopolymers-based films enriched with this natural extract<sup>17</sup>. Indeed, snail slime is an attractive ingredient thanks to its emollient, moisturizing, antibacterial, and restorative properties and is receiving increasing attention, especially in the cosmetic sector: the bioactive substances that contains are responsible for its unique properties, which cannot be replicated in the laboratory with synthetic chemical compounds.

The films' preparation methods and the characterizations carried out on the different obtained compositions are reported in the following paragraphs, together with a detailed discussion of the results. Some of these studies led to the publication of scientific articles, of which I am a co-author, in international and peer-reviewed journals<sup>18-21</sup>.

Overall, the obtained films showed common characteristics of biocompatibility and biodegradability, as they were obtained through sustainable processes that use water as a solvent, and through the use of biopolymers or polymers of natural origin.

The addition of different amounts of slime to the compositions of films allowed to modulate the properties of the materials: in fact, as the amount of slime varied, also the mechanical elongation, the bioadhesion, the barrier properties and the antibacterial activity changed.

As reported in Paragraph 2.3, snail slime extracted with the MullerOne method offered a more sustainable route for the solubilization of chitosan, that is generally dissolved in acidic media such as acetic or lactic acid: it showed very good film forming ability even when dissolved directly in the slime. Moreover, increasing amount of slime added to the composition of films prepared by dissolving chitosan in acetic/lactic acid, led to increased bioadhesion properties of the resulting film towards the skin, and better elongation properties. Slime was also responsible of the antibacterial properties of the films evaluated *in vitro* against both Gram-positive and Gram-negative bacteria. Snail slime-enriched films revealed to be suitable for applications in the biomedical and cosmetic sectors as well as in the packaging field.

Mixing of snail slime with different cellulose-derivatives, leads to materials with different solubility: for example, while HPMC-based films quickly solubilize when exposed to water, CMC-based films are insoluble, thanks to different interactions established between the components (see Paragraph 2.4). The obtained films were characterized by high transparency, excellent UV barrier properties and good WVP, mandatory features for food packaging materials. Films evidenced a significant antibacterial activity, ensuring protection from possible contaminants, a good biodegradability and were printable.

In Paragraph 2.5, compositions of films based on cellulose and sodium hyaluronate in combination with snail slime HelixComplex® have been studied, revealing antiviral properties against HSV-1 virus: these transparent films have been proposed as labial patches for the treatment of cold sores (*Herpes Labialis*).

Regenerated keratin extracted by sulphitholysis was selected as sustainable raw materials for the production of films aimed at skin regeneration, exploiting the peculiar properties of keratin. Regenerated keratin is indeed biocompatible and biodegradable, and it was blended with snail slime in different proportion in order to obtain free standing films able to treat skin lesions. Even if only preliminary results have been obtained, they are listed in Paragraph 2.6.

Thanks to the collaboration with the research group of Prof. Passerini and Prof. Albertini at the FaBiT Department of the University of Bologna, I also developed biopolymer-based films for drug delivery purposes. Dermal and transdermal drug delivery, generally described as skin drug delivery, is indeed an attractive approach for the treatment of many dermatological pathologies, such as skin cancers, inflammatory disorders and cutaneous infections, known to be difficult to treat. In fact, direct and localized access to the pathological site is very promising and could offer a new channel also for the treatment of diseases not related to the skin <sup>22</sup>.

Two different formulations of gelatin-based films for drug delivery of anti-fungal drugs have been developed, of which only one included snail slime. In Paragraph 2.7, gelatin-based patches enriched with different amounts of snail slime were produced for the local administration of Fluconazole, one of the most effective broad-spectrum antifungal drugs for the treatment of cutaneous mycosis. When snail slime was present in the formulation, the drug recrystallization was prevented, and the amorphous form of the drug was stabilized over time, up to 6 months of storage. The antifungal activity measured by an *in vitro* permeation study on pig skin revealed effective action against clinical isolates of *Candida* spp.

In Paragraph 2.8, gelatin-based films loaded with Econazole Nitrate (ECN, 10% w/w compared to gelatin) for vaginal application were produced. Their composition was enriched with different polymers, such as PVP, Soluplus® and Gelucire® 50/13 to evaluate their ability to promote drug permeation. The anti-*Candida* activity results support their potential use as mucoadhesive systems for the local administration of Econazole in order to treat vaginal candidiasis with a single application per day.

Eventually, an ongoing project regards the production of carboxymethyl cellulose-based films containing a recombinant enzyme of plant origin, NAD(P)H quinone reductase, which catalyzes the reduction of oxidized quinones and other organic compounds, using a nucleotide pyridine donor (NADH or NADPH). The presence of the enzyme could therefore provide the

film with antioxidant properties, avoiding the accumulation of semiquinone radicals, and hence making the material of interest in the cosmetic field, for example for the production of beauty masks. This project is carried out in collaboration with Prof. Fermani ('G. Ciamician' Chemistry Department, Unibo) and Prof. Sparla (FaBit Department, Unibo) and so far, only first attempts have been made to incorporate the protein within the polymeric membrane, so that the activity of the protein remains effective over time: the method of drying and preservation of films plays a decisive role and the optimal parameters have not yet been found.

## 2.2 EXPERIMENTAL PART

### 2.2.1 Chitosan-based films with snail slime

#### **Materials**

Chitosan (degree of deacetylation  $\geq 93\%$ , M.W.=100 KDa) was purchased from Faravelli, Milan, Italy. Acetic acid and lactic acid were purchased from Sigma Aldrich (Milan, Italy). Snail slime from *Helix Aspersa Muller* snails was kindly offered by “I Poderi” farm (Montemerano, Italy) and stored at 4 °C in a sealed polyethylene bottle until use. The analysis of slime composition, provided by the supplier, is reported in Appendix I.

#### **Preparation of chitosan-based films with snail slime**

Chitosan films at 1% w/v were prepared by dissolving the proper amount of chitosan in acetic acid (A, 1% v/v), lactic acid (L, 1% v/v), or directly in snail slime (S). The mixture was kept under stirring at room temperature (RT) until complete dissolution of the polymer. 11 mL of this solution were poured in Petri dishes and put under laminar flow hood at RT overnight. The obtained films were labeled C\_A, C\_L and C\_S, respectively.

Furthermore, two percentages by volume (30% and 70% of the final volume) of snail slime were combined with solutions of chitosan dissolved in both lactic and acetic acid for the preparation of chitosan film dissolved in solvent blends. For the preparation of 100 mL of chitosan-S blend 70:30, 1 g of chitosan was dissolved in 70 mL of A (1% v/v) or L (1% v/v) and stirred at RT until complete dissolution of the polymer. Then, 30 mL (30% of the final volume) of snail slime were added and 11 mL of this solution were poured in each Petri dish and put under laminar hood overnight. The obtained films were labeled CA\_7030 and CL\_7030, where the first number refers to the relative volume of chitosan acidic solution and the second one to the volume of S with respect to the total volume.

In order to obtain a chitosan-based film using the slime as acidic medium, the same procedure was followed: 1 g of chitosan was dissolved in 70 (or 30) mL of S and then 30 (or 70) mL of distilled water were added, obtaining the films labeled CS\_7030 (or CS\_3070). Films were stored at RT between two sheets of plastic-coated aluminum closed inside PVC bags.

#### **Films characterization**

Films were characterized as described in ‘Thickness’, ‘Tensile tests’, ‘Structural characterization’, ‘Thermogravimetric analysis’, ‘Water vapor permeability’ and ‘Bioadhesion’ sections of Paragraph 2.2.7.

### **Cell viability bioassay**

The effect of chitosan films on non-malignant epithelial cells metabolism was assessed *in vitro* after incubation of disks ( $\varnothing = 6$  mm) in 1 mL of Eagle's Minimal Essential Medium (MEM) at 37 °C for 24 h. Then, the media were used for the analysis on African green monkey kidney cells (Vero ATCC CCL-81). Briefly, cells were cultured in MEM supplemented with 10% fetal bovine serum (Carlo Erba Reagents, Milan, Italy), 100 U/mL penicillin and 100 µg/mL streptomycin at 37 °C with 5% CO<sub>2</sub>. For experiments, cells were seeded into 96-well plates at 104 cells/well and incubated at 37 °C for 24 h. Subsequently, cell monolayer was washed with PBS and incubated with 100 µL of the different solutions, previously diluted twenty times in cell culture medium. The cell viability was assessed by a WST8-based assay according to the manufacturer's instructions (CCK-8, Cell Counting Kit-8, Dojindo Molecular Technologies, Rockville, MD, USA). After 72 h of incubation, cell monolayer was washed with PBS, and 100 µL of fresh medium containing 10 µL of CCK-8 solution were added. After 2 h at 37 °C, the absorbance was measured at 450/630 nm; results were expressed as the percentage of absorbance relative to the untreated controls. Experiment was carried out in triplicate.

### **Antibacterial activity**

The *in vitro* antibacterial activity of chitosan films was evaluated against *Staphylococcus aureus* (ATCC 25923) and *Escherichia coli* (ATCC25922), selected as controls and representative strains for Gram-positive and Gram-negative bacteria. The effectiveness of samples to inhibit the bacterial growth was assessed by a standardized Kirby-Bauer (KB) diffusion test on Mueller-Hinton agar plate and by measuring the bacterial-free zone around the disk-shaped samples ( $\varnothing = 6$  mm) after 24 h of incubation at 37 °C. All experiments were performed on duplicate in different days.

### **Statistical analysis**

Statistical analysis was performed with Graph Pad Prism 4. One-way analysis of variance (ANOVA) followed by Tukey's Multiple Comparison Test was employed to assess statistical significance of the experimental conditions for Water Vapor Permeability and Adhesive strength; statistically significant differences were determined at p values <0.05.

## **2.2.2 Cellulose derivatives-based films with snail slime**

### **Materials**

Hydroxypropyl methyl Cellulose (HPMC, Methocel E5 and E50, viscosity at 2% in water: 4–6 mPa·s and 40–60 mPa·s, respectively) were supplied by Colorcon (UK). Commercial

Carboxymethyl Cellulose sodium salt, (CMCNa, Mw: 250 KDa, viscosity at 2% in water: 850 mPa·s) was gifted by ACEF (Piacenza, Italy). These celluloses satisfy the standards of the United States Pharmacopeia and European Pharmacopeia. Snail slime (S) from *Helix Aspersa Muller* snails was supplied by “I Poderi” farm (Montemerano, GR, Italy) and stored at 4°C in a sealed polyethylene bottle until use (see Appendix I).

### Preparation of cellulose-based films with snail slime

Cellulose films were obtained with the solvent casting technique by dissolving 1 g of E5 or E50 in 20 mL of distilled water (5% w/v) or 0.4 g of CMC in 20 mL of distilled water (2% w/v) under gently stirring overnight. Then, 10.2 g of these solutions were poured in Petri dishes ( $\varnothing = 8.5$  cm) and allowed to dry under a laminar flow hood at RT overnight. The obtained films were labeled E5, E50 and CMC, respectively and stored between two sheets of plastic-coated aluminum closed inside PVC bags.

To obtain E5, E50 and CMC -based films containing different amounts of snail slime (S), the relative volume of S (30, 70 and 100% v/v) was added to the solution containing 1 g of HPMC or 0.4 g of CMC, previously dissolved in the remaining volume of water. When S is at 100%, the polymer is directly solubilized into the snail slime. After complete dissolution and disappearance of bubbles, 10.2 g of this solution were poured in Petri dishes ( $\varnothing = 8.5$  cm) and put under laminar flow hood overnight. The obtained films were labeled as reported in Table 1, according to the volume of S used.

Table 1. Films compositions and labels.

Labels	Polymer type	Polymer % (w/V)	Slime % (V/V)	Water % (V/V)
E5	HPMC E5	5	0	100
E5_S30	HPMC E5	5	30	70
E5_S70	HPMC E5	5	70	30
E5_S100	HPMC E5	5	100	0
E50	HPMC E50	5	0	100
E50_S30	HPMC E50	5	30	70
E50_S70	HPMC E50	5	70	30
E50_S100	HPMC E50	5	100	0
CMC	CMC Na	2	0	100
CMC_S30 <sup>a</sup>	CMC Na	2	30	70
CMC_S70	CMC Na	2	70	30
CMC_S100	CMC Na	2	100	0

<sup>a</sup>Due to their excessive fragility, it was not possible to characterize the films corresponding to the composition CMC\_S30.

### Films characterization

Films were characterized as described in ‘Thickness’, ‘Tensile tests’, ‘Structural characterization’, ‘Swelling’, ‘Water vapor permeability’ sections of Paragraph 2.2.7.

### **Tack test**

The adhesive strength of the films was evaluated by means of Anton Paar modular compact Rheometer MCR102 with the Rheo Compass software. Glass and aluminum supports were used for the test. Films were cut in 3 cm-diameter circles and allowed to adhere to the two different supports by wetting them with 10  $\mu$ L of distilled water and applying a gentle finger pressure. The upper plunger of the instrument was covered with double-sided tape (3 M) and was lowered until a force of 5 N was applied to the film. After 30 s, the plunger was raised up at a speed of 1 mm/s, collecting the peak detachment force and the work of adhesion of the film from the support. Each formulation was analyzed in triplicate and the mean  $\pm$  SD was reported.

### **Film solubility**

After 24 h from the swelling studies, the samples not completely dissolved were removed from water and dried until a constant weight was obtained. Solubilization as a consequence of the water uptake and dissolution of the film was calculated as follows <sup>23</sup>:

$$\text{Solubilization (\%)} = \frac{W_i - W_f}{W_i} \cdot 100 \quad 1)$$

where  $W_i$  and  $W_f$  are the weights of the sample before and after immersion in water, respectively. Solubility tests at longer times (7 and 14 days) were performed in the same way only on the samples not completely dissolved after 24 h.

### **UV-Vis spectroscopy**

In order to evaluate the barrier properties of the films against UV-Vis light, films were cut into 1 cm -wide rectangular strips and inserted into the sample holder of the Cary 60 UV-Vis spectrophotometer. Spectra were acquired in transmittance mode from 200 to 800 nm. The transparency of the films was evaluated from transmittance at 600 nm, by the following equation:

$$\text{Transparency} = \frac{-\log T(600)}{X} \quad 2)$$

where  $T_{600}$  is the fractional transmittance at 600 nm and  $X$  is the thickness of the film (mm). The analyses were performed in triplicate.

### **Antibacterial activity**

Cellulose-based films were tested *in vitro* for the evaluation of antibacterial activity by a standardized Kirby-Bauer (KB) diffusion test on Mueller-Hinton agar plate (EUCAST, 2016). For the analysis, a panel of Gram-positive and Gram-negative reference bacterial strains were selected: *Staphylococcus aureus* (ATCC 25923), *Staphylococcus epidermidis* (ATCC 12228), *Enterococcus faecalis* (ATCC 29212), *Escherichia coli* (ATCC 25922), *Pseudomonas*

*aeruginosa* (ATCC 27853), and *Klebsiella pneumoniae* (ATCC 9591). The effectiveness of the disk-shaped cellulose films ( $\text{Ø} = 6 \text{ mm}$ ) to inhibit bacterial growth was determined by measuring the diameter of the bacterial-free zone around the sample after 24 h of incubation at 37 °C. In compliance with the international guidance documents in susceptibility testing, disks containing gentamicin (GMN 10  $\mu\text{g}$ ) and/or imipenem (IPM 10  $\mu\text{g}$ ) (Oxoid SpA, Italy) were included as reference controls (CLSI, 2015). All experiments were performed in duplicate and in different days.

### **Biodegradation test**

Biodegradation tests of cellulose films were conducted in soil <sup>24</sup>. Soil was taken from the surface layer in the garden then put in a plastic tray to a thickness of around 4 cm. Films were cut into small pieces (about  $2 \times 2 \text{ cm}^2$ ), dried at 37 °C until a constant weight was raised and then buried about 2 cm beneath soil at about 25 °C. Water was sprayed once on the soil surface to maintain the moisture. The degraded samples and fragments were taken out after 2 and 4 weeks, gently cleaned from residual soil with distilled water and dried at 37 °C until a constant weight was obtained. Finally, the dried samples were weighted again, and the weight loss of the film degraded in soil was calculated.

### **Statistical analysis**

Statistical analysis was performed with Graph Pad Prism 4. One-way analysis of variance (ANOVA) followed by Tukey's Multiple Comparison Test was employed to assess statistical significance of the experimental conditions. Statistically significant differences were determined at p values < 0.05.

## **2.2.3 Cellulose/Hyaluronate-based films with anti-Herpes activity**

### **Materials**

Commercial Carboxymethyl Cellulose sodium salt, (MW: 250 KDa, viscosity at 2% in water: 850 mPa·s) was donated by ACEF (Piacenza, Italy). Sodium Hyaluronate (1650 kDa) was purchased from Acef spa, Italy. Glycerol was purchased from Fagron (Bologna, Italy). Snail slime HelixComplex® extracted from *Helix Aspersa* snails was provided by HelixPharma Company srl and stored between 0 and 4°C in a sealed polyethylene bottle until use.

### **Preparation of cellulose/hyaluronate-based films with snail slime**

Different cellulose/hyaluronate-based films were produced with the solvent casting technique. Cellulose (2% w/v) was dissolved directly into snail slime HelixComplex (or in water for

reference samples) and stirred at RT overnight. Then, different amount (0,5 and 1% w/v) of Hyaluronate were introduced and the solution was stirred until complete dissolution of the polymer. Once a homogeneous solution was obtained, glycerol as humectant was added in two different concentrations: 5 and 10% v/v. 10 mL of this solution were poured in PE petri dishes ( $\varnothing = 8.5$  cm) and allowed to dry under laminar flow hood overnight. The obtained films were labelled as reported in Table 2.

*Table 2. Compositions and labels of the obtained films.*

<b>Labels</b>	<b>Cellulose % (w/V)</b>	<b>Hyaluronate % (w/V)</b>	<b>Glycerol %(V/V)</b>	<b>Water % (V/V)</b>	<b>HelixComplex® % (V/V)</b>
<b>A</b>	2	1	5	100	0
<b>AS</b>	2	1	5	0	100
<b>B</b>	2	0.5	10	100	0
<b>BS</b>	2	0.5	10	0	100
<b>C</b>	2	0.5	5	100	0
<b>CS</b>	2	0.5	5	0	100

### **Films characterization**

Films were characterized as described in ‘Thickness’, ‘Tensile tests’, ‘Structural characterization’, ‘Thermogravimetric analysis’, ‘Water vapor permeability’ sections of Paragraph 2.2.7.

### **Bioadhesion test**

The bioadhesive properties were evaluated by using a microtensiometer (Krüss), opportunely modified. Pig ear skin obtained from a local butcher was used as substrate. It was carefully separated from underlying tissue, washed with water and soaked in PB pH 7.4 for 15 min. Then, it was fixed with acrylic glue to support before starting the analyses. Each film (3 mm<sup>2</sup>) was fixed to the plunger using double-sided tape, put in contact with skin for 15 s, then the force of adhesion, expressed as the force for cm<sup>2</sup> needed to detach the film from the skin, was recorded. At least 10 measurements were performed for each sample.

### **Cell viability bioassay**

The immortalized human keratinocyte cell line (HaCaT) was cultured in DMEM medium (Gibco), supplemented with 1% glutamine, 100 units/mL of penicillin/streptomycin and 10% FBS at 37 °C in an atmosphere of 5% CO<sub>2</sub>. The exponentially growing cells were used for the experiments.

For cell treatment, 1 cm<sup>2</sup> of biopolymer-based patch with and without HelixComplex was dissolved in 2 mL of DMEM to obtain the 100% concentrated solution. The effect on cell viability of solubilized patches was evaluated on HaCaT cells by MTT (3-(4,5-dimethylthiazol-2yl)-2,5-diphenyl tetrazolium bromide) colorimetric assay (Roche Diagnostics Corporation),

following manufacturer's instructions. Cells were treated for 24h with 100% and 50% (diluted in DMEM) solutions. Afterwards, absorbance was read at 570 nm.

### **Anti-HSV-1 activity**

The TOZGFP-HSV1 expressing GFP under the control of the ICP22 promoter was utilized. Virus stocks were prepared and titrated in Vero cells. Briefly, supernatants and infected cells approaching 100% cytopathic effect (c.p.e.) were collected and lysed by sonication. Cellular debris was pelleted by centrifugation at  $800\times g$  for 20 min at  $4^{\circ}C$ , and the supernatants were aliquoted and stored at  $-70^{\circ}C$ . For antiviral activity of biopolymer-based patches, HaCaT cells were seeded on 24-well plates at a cell density of  $5\times 10^4$  cells/well the day before treatment. A time-of-drug-addition was performed: solubilized patches at 100% and 50% were added to the cells during the infection and/or post infection with 0.01 PFU/cell (plaque forming unit) of TOZGFP-HSV1. Experiments were performed in three conditions: simultaneous addition of solubilized biomaterial and HSV-1 to the cells (during the infection step); solubilized biomaterial added immediately after the infection (post-infection) and left for 24 hours; and a combination of the previous conditions (during and post-infection). 24 hours after treatments, cells were harvested, and HSV-1 titration was performed to enumerate the infective viral particles. Viral replication was evaluated by plaque assay titration on Vero cells. The percentage of viral inhibition was calculated with respect to the untreated infected control.

## **2.2.4 Keratin-based films with snail slime**

### **Materials**

The keratin used in this project is obtained through the recovery of industrial waste materials, being extracted by sulphitholysis from raw wool by the group of Dott. A. Aluigi, PhD at CNR-ISOF of Bologna. Glycerol was purchased from Fagron (Bologna, Italy). Snail slime from *Helix Aspersa Muller* snails extracted with a natural cruelty-free method was provided by 'lumaca Madonita' (Palermo, Italy). Snail slime (pH= 7) was stored between 0 and  $4^{\circ}C$  in a sealed polyethylene bottle until use.

### **Dialysis of snail slime**

The snail slime employed for the preparation of keratin-based films was subjected to dialysis in order to remove preservatives added by the manufacturers. Membranes with a cut-off of 12-14 kDa were conditioned under stirring in distilled water for 24 h, frequently changing the water. The aliquot of snail slime was poured into the membrane and set with clips

to fix the two sides of the membrane and to avoid the leakage of the sample. The membrane was left under stirring for 24 h with frequent replacement of distilled water. The dialyzed snail slime was stored at -19 °C until use.

### **Preparation of keratin-based films with snail slime**

Keratin-based films at 10 % w/V were prepared by dissolving the proper amount of keratin in milliQ water under stirring. After the complete dissolution of the polymer, glycerol (50% v/v) was added as plasticizer. 1,5 mL of this solution were poured into square polyethylene trays (3 cm x 3 cm) and allowed to dry overnight under laminar flow hood. The obtained films were labelled K and used as control.

Keratin/snail slime films were prepared using the same procedure, but dissolving keratin directly into dialyzed snail slime. After the addition of glycerol, the solution was poured into square polyethylene trays (3 cm x 3 cm) and allowed to dry overnight under laminar flow hood. The obtained films were labelled K\_M and stored at room temperature.

### **Films characterization**

Films were characterized immediately after the preparation and after 3 months of storage inside a desiccator at 18°C, as described in ‘Thickness’, ‘Structural characterization’ and ‘Thermogravimetric analysis’ sections of Paragraph 2.2.7.

### **Film solubility**

Samples were cut in square-shaped portion of 1 cm<sup>2</sup> and immersed for 24 h in 5 mL of water at RT. Then, they were deposited on a glass watch and left overnight at 37°C until a constant weight was reached. Then, the solubility was calculated following Equation 1.

## **2.2.5 Fluconazole-loaded films based on gelatin and snail slime**

### **Materials**

Porcine gelatin (type A, 280 Bloom) was purchased from Sigma Aldrich (St. Louis, MO, USA). Snail Mucus extracted from *Helix Aspersa Muller* snails by MullerOne method was supplied by “I Poderi Farm” (Montemerano, Italy) and stored at 4 °C. Glycerol was purchased from Fagron, Bologna, Italy. Fluconazole (F) compliant with Ph. Eur specifications was purchased from Farmalabor (Assago, MI, Italy).

### **Preparation of physical mixture of Fluconazole and gelatin**

50 mg of Fluconazole and 0,5 g of gelatin were mixed in a mortar and accurately grinded. Then, X-ray diffraction patterns and FT\_IR spectra of the powders as tablets were acquired.

### **Preparation of gelatin and gelatin-slime films**

Gelatin films (5% w/V) were prepared by solvent casting technique: the weighted amount of gelatin was dissolved under gently stirring in distilled water at 38°C. After the complete dissolution of the polymer, 8.6 mL of this solution were poured in polyethylene (PE) Petri dishes ( $\varnothing= 5.5$  cm) and kept under laminar flow hood at room temperature (RT) overnight. The obtained films were labeled G and used as control samples.

Gelatin films (5% w/V) with different percentages in volume of Snail Slime (S) were produced by adding proper volumes of S (40, 50, 60 and 70% with respect to the total volume of the film forming solutions) to the gelatin aqueous solution under stirring. Before its addition, the pH of the snail slime was raised to 4.5 with few drops of concentrated NaOH. As for control samples, 8.6 mL of each solution were poured in Petri dishes and allowed to dry under laminar flow hood overnight at RT. The obtained films were labeled according to the percentage in volume of slime implied in their production: G\_S40, G\_S50, G\_S60, G\_S70, respectively.

In order to provide a better flexibility and stability over time, glycerol (30% w/w with respect to gelatin) was introduced in the composition of some selected films after the dissolution of the polymer. The obtained films were labeled by adding “\_g” to the above stated tags. All the films were stored at room temperature between plastic-coated aluminum foils inside PVC bags.

### **Preparation of gelatin and gelatin/slime films with Fluconazole**

From the results of film characterizations, the composition corresponding to G\_S70\_g was selected for encapsulation of Fluconazole (F).

50 mg of Fluconazole (5% in weight with respect to the total dry mass of gelatin and S; 10% in weight with respect to gelatin) were added to 7 mL of snail slime (adjusted to pH 4.5 with concentrate NaOH), stirred for about 2 h and then mixed with 3 mL of gelatin solution (5% m/V). After the addition of glycerol (30% w/w on gelatin weight), 8.6 mL of the mixed solution were poured in polyethylene Petri dishes ( $\varnothing= 5.5$  cm) and put under laminar hood at RT overnight. The obtained film was labeled G\_S70\_g\_F and stored at room temperature between two sheets of plastic-coated aluminum closed inside PVC bags. The compositions and labels of all the obtained films are reported in Table 3.

Table 3. Compositions and labels of the obtained samples.

Labels	Snail Mucus %(v/v)	Water %(v/v)	Glycerol %(w/w)*	Fluconazole %(w/w)**
G	0	100		
G_g	0	100	30	
G_S40	40	60		
G_S50	50	50		
G_S60	60	40		
G_S70	70	30		
G_S70_g	70	30	30	
G S70 g F	70	30	30	4.76

\* Weight of glycerol with respect to the weight of gelatin

\*\* weight of Fluconazole with respect to the dry weight of gelatin, S and Glycerol.

### **Film Characterization**

Films were characterized as described in ‘Thickness’, ‘Tensile tests’, ‘structural characterization’, ‘Thermogravimetric analysis’, ‘Swelling degree’, ‘Bioadhesive properties’ sections of Paragraph 2.2.7.

### **Solubility studies**

Solubility measurements at equilibrium of Fluconazole were performed in different media both at 25 °C (preparation of the sample solutions) and at 32 °C (permeation studies). A Fluconazole excess was added to 5 mL of phosphate buffer solution (pH 5.5) and phosphate buffer solution (pH 5.5) containing 20% w/V of ethanol. Samples were stirred for 48 h, equilibrated for 2 h, then the suspensions were centrifuged at 10000 rpm for 10 min. The supernatant was filtered through a 0.20 µm membrane nylon filter. After suitable dilutions, samples were analyzed by HPLC in triplicate.

### **Drug Content**

Films of about 45 mg were solubilized in 10 mL of a mixture of MeOH:H<sub>2</sub>O (40:60 v/v) and left under stirring for 24 h. Samples were filtered and 1 mL of each solution was centrifuged at 8000 rpm for 10 min, after which the supernatant was analyzed by HPLC. The samples were analyzed in triplicate and the results of the drug content were expressed as % w/w (weight of Fluconazole with respect to the weight of the films) and in mg/cm<sup>2</sup>.

### **Fluconazole assay**

An HPLC-UV/Vis equipped with LC-10ADvp pumps (Shimadzu), SP-10Avp UV–Vis detector (Shimadzu, 210 nm) and a SIL-20A autosampler (Shimadzu) with a C18 apolar column (Luna Phenomenex, 150 mm × 4.6 mm × 5 µm) as stationary phase was used for the quantitative analysis of Fluconazole. The mobile phase was composed of acetonitrile 25% and MQ water 75% fluxed at 1 mL/min and with an injection volume of 20 µL. The quantification of

Fluconazole was assessed by means of a calibration curve ( $R^2 = 0.9999$ ,  $n = 3$ ) made with standard solutions of known concentration in the range 0.5–50  $\mu\text{g/mL}$ . The limit of detection (LOD) was 0.18  $\mu\text{g/mL}$  while the limit of quantification (LOQ) 0.48  $\mu\text{g/mL}$ . For the permeation experiments, the same HPLC method was used, and quantification was assessed using the same calibration curve.

### ***In vitro* skin permeation and retention studies**

To determine the amount of drug able to diffuse across the skin from the formulation, *in vitro* permeation experiments were performed. Pig ear skin was selected as membrane due to its similar histological and physiological characteristics and close permeability properties to human skin<sup>25</sup>. A Franz-type static glass diffusion cell (15 mm jacketed cell with a flat ground joint and clear glass with a 12 mL receptor volume; diffusion surface area = 1.77  $\text{cm}^2$ ), equipped with a V6A Stirrer (PermeGearInc., Hellertown, PA, USA) was employed. In the donor compartment, circular films (diameter of 1.1 cm containing 4,76% w/w of F) were placed on the membrane made of pig ear skin (thickness  $1,04 \pm 0,07$  mm). The skin used was obtained from the ears of different pigs, which were kindly provided by a local slaughterhouse (Bologna, Italy). The skin was used after removing the underlying fat and subcutaneous tissues with a surgical blade and stored at  $-20$  °C until use. Each membrane was conditioned for 15 min in PB solution and then carefully placed in the interface between the donor and receptor compartments. The receiver medium contained phosphate buffer solution at pH 5.5 containing 20% (w/v) of ethanol to prevent Fluconazole precipitation and it was maintained under stirring at a constant temperature of  $32 \pm 0.5$  °C through thermostatic bath circulation. The chambers were held together tightly with a cell clamp and sealed with parafilm to limit evaporation. Aliquots of 250  $\mu\text{L}$  were collected at 15, 30, 60, 120, 180, 300 and 1440 min. Sink conditions were maintained with the replacement of the same volume of receptor medium. For comparison, a control solution (0.5 mL) containing the same amount of drug loaded into the film was prepared dissolving the drug in ethanol. Then, it was mixed with phosphate buffer solution at pH 5.5 and added to the donor chamber. All collected samples were analyzed by HPLC-UV/Vis and the results of permeation studies are shown as cumulative drug amount permeated per unit of area plotted as a function of time. Each sample was analyzed in quintuplicate, and the data are expressed as mean  $\pm$  SD. At the end of the permeation study, excess formulation was removed, and the skin surface was washed 3 times with PB. The skin samples were cut into small pieces and stored in vials containing 5 mL of methanol for 1 week. The resulting solution was filtered (0.2  $\mu\text{m}$ ), properly diluted (1:10) and the drug amount extracted from the skin was determined by HPLC. The mean of three replicates for each formulation was calculated and the

corresponding values were normalized on the average thickness of the skin used in each permeation test. The percentage of retained drug (CF) was calculated with respect to the effective drug content (C0), as follows:

$$CF = \frac{\mu g CF}{\mu g C0} \cdot 100 \quad 3)$$

### **Antimicrobial activity**

The antifungal activity of the Fluconazole-loaded films was tested *in vitro* against the reference strain *Candida albicans* ATCC 10231 (American Type Culture Collection) and 10 clinical isolates of *Candida spp.* collected at the Microbiology Unit of the St. Orsola Malpighi University Hospital, Bologna, Italy. The clinical strains were identified by standard procedures, including colony morphology on chromogenic agar (CHROMagar Candida medium, Becton Dickinson, Heidelberg, Germany) and confirmed by MALDI Biotyper System using matrix assisted laser desorption ionization–time of flight mass spectrometry (MALDI-TOF MS, Bruker Daltonik, GmbH, Germany). *Candida* strains were cultured on Sabouraud-dextrose agar. The inoculum was prepared in sterile 0.9% saline solution and adjusted at 0.5 McFarland, corresponding to 10<sup>6</sup> CFU (colony-forming units)/mL. 1 mL of the fungal suspension was added to 20 mL of Sabouraud-dextrose agar and transferred to an agar plate (Ø = 90 mm). After cooling the inoculated agar at room temperature, disks (Ø = 6 mm) of gelatin-based films were deposited on the surface of the plate. The experiments included the unloaded gelatin films (G\_g and G\_S70\_g) as negative controls, and a paper disk containing 300 µg of Fluconazole as positive control. For this purpose, the drug was solubilized in DMSO at 100 g/L, and 10 µL of a freshly diluted water solution (30 µg/µL) was loaded on the sterile paper disk. After 24 h of incubation at 37 °C, the antifungal activity was determined by measuring the microbial growth inhibition diameter around the disk.

### **Statistical analysis**

One-ways analysis of variance (ANOVA) was employed to assess statistical significance on the obtained results. The significance was performed with a NewmanKeuls Multiple Comparison test. The difference was considered statistically significant with p-value < 0.05. One-tailed t test was used to compare the two sets of measurements (inhibition zone diameters for Fluconazole-loaded gelatin film vs Fluconazole control) obtained for each *Candida spp.*

## 2.2.6 Mucoadhesive gelatin-based films loaded with Econazole

### Materials

Porcine gelatin (type A, 300 Bloom) was purchased from Sigma Aldrich (St. Louis, MO, USA). Econazole nitrate (ECN, 1-[2-(4-chlorophenyl)methoxy]-2-(2,4-dichlorophenyl)ethyl 1H-imidazole mononitrate; MW: 444.7 g/mol; Log P = 5.2; pKa 6.65)<sup>26</sup> was supplied by Erregierre S.p.A. (BG, Italy). Soluplus® (polyvinyl caprolactam-polyvinyl acetate-polyethylene acetate-polyethylene glycol graft copolymer: PCL-PVAc-PEG), Kollidon®30 (polyvinylpyrrolidone) and Kollidon®VA64 (polyvinylpyrrolidone-vinyl acetate) were supplied by BASF (Ludwigshafen am Rhein, Germany). Gelucire® 53/10 (a mixture of mono-, di- and triglycerides, mainly mono- and diesters of palmitic (C16) and stearic (C18) acids), esters of PEG 1500 and free PEG) was supplied by Gattefossè (Milan, Italy). Genipin was purchased from Wako Chemicals (Osaka, Japan) while Mucin (from porcine stomach, Type III) was purchased from Sigma Aldrich.

### Preparation of gelatin-based films with Econazole

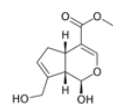
Gelatin films at 5% w/V were prepared by dissolving gelatin in distilled water at 45°C for 20 min. This solution was poured in PE petri dishes and allowed to dry at RT overnight. The produced films were labeled as G.

Films containing 10% (w/w with respect to gelatin) of ECN were prepared by mixing the drug or the solid dispersion (SD) with gelatin in a mortar. The powders were suspended in distilled water (5% w/V gelatin concentration) and the suspension was heated up at 50°C and stirred for 30 min. 5 mL of each suspension were poured in PE Petri dishes (Ø= 5.5 cm) and allowed to dry at RT overnight. The obtained films were labeled GE10, GGE10, GSE10 and GKE10, as reported in Table 4.

For the preparation of cross-linked films, genipin at 2% w/w (with respect to gelatin) was previously dissolved in 2 mL of PB pH 7.4 and added to gelatin suspension. The mixture was stirred for about 20–30 min, during which the color of the solution turned from white/transparent to a pale blue. Then, 5 mL of each suspension were poured in PE Petri dishes and allowed to dry at RT. After drying, films were rinsed with a Glycine solution (0.1 M in distilled water) to remove the excess of genipin, repeatedly washed with distilled water and air-dried at room temperature overnight. The obtained films were labeled GE10gen and GGE10gen, as indicated in Table 4. As control samples, unloaded gelatin films (G) and films containing the additives (GG, GS and GK) were prepared (Table 4). Obtained films were stored into plastic bags at room temperature.

Table 4. Gelatin (G) -based film composition.

Label	Theoretical ECN content % (w/w)	Solid Dispersion	Genipin% (w/w)
G*	-	-	-
GG*	-	-	-
GS*	-	-	-
GK*	-	-	-
GE10	10	--	--
GGE10	10	SDG	--
GSE10	10	SDS	--
GKE10	10	SDK	--
GE10gen	10	--	2
GGE10gen	10	SDG	2



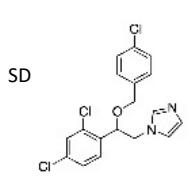
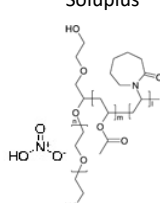
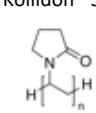
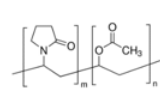
\*G, GG (G film containing Gelucire® 50/13), GS (G film containing Soluplus®) and GK (G film containing Kollidon®30 and VA64) represent the unloaded films containing the same amount of additives of the corresponding 10% drug-loaded films.

### Preparation of ECN solid dispersion

The solvent evaporation method was used to prepare solid dispersions containing Kollidon® (SDK) or Soluplus® (SDS): powders were accurately mixed in a mortar and then solubilized in ethanol. Solutions were stirred for 30 min at RT and evaporated under low vacuum using a rotary evaporator (Buchi Rotavapor R200, Flawil, Switzerland). Co-precipitate white crystals were obtained for SDS, while a slightly yellow rubbery solid was obtained for SDK.

Gelucire® SD (SDG) was prepared by adding ECN to the molten Gelucire at 60°C. The suspension was stirred for 10 min and then cooled down at -20°C for 10 min. All the obtained SD were stored at 4°C and characterized in terms of solubility and drug-carrier interactions. The labels and compositions of each formulation are reported in Table 5.

Table 5. Composition of the solid dispersions: drug to polymer weight ratio (w/w).

	ECN	Polymers			
		Soluplus®	Kollidon® 30	Kollidon® VA64	Gelucire® 50/13*
SD					
SDS	1	2	-	-	-
SDK	1	-	2	0.5	-
SDG	1	-	-	-	2

\*Mixture of PEG-32 esters, free PEG, mono-, di- and triglycerides (mainly composed of stearic and palmitic acids).

## **Solid dispersions characterization**

### **ECN analysis**

The HPLC system consisted of two mobile phase delivery pumps (LC-10ADvp, Shimadzu, Japan), an UV–Vis detector (SPD-10Avp, Shimadzu, Japan) and an autosampler (SIL-20A, Shimadzu, Japan). The stationary phase was a Luna C18 column (150 mm × 4.60 mm × 5 μm, Phenomenex, Bologna, Italy). The mobile phase comprised of methanol and ammonium phosphate buffer 20 mM pH 2.5 (75:25 V/V). The flow rate was 1 mL/min, and the detection wavelength was set at 230 nm. The retention time of ECN was about 5.4 min, while the run time was set at 10 min. The injected volume was 20 μL and the quantitation was carried out using the linear calibration curve of ECN, obtained in the range of 0.5–40 μg/mL ( $R^2 = 0.9999$ ). In particular, six standard solutions were prepared by solubilizing the suitable amount of ECN in 10 mL of ethanol containing 150 μL of DMSO. Then, the solutions were diluted with PB pH 4.5 to have the following concentrations: 0.5, 1, 5, 10, 20 and 40 μg/mL. A fresh ECN standard solution of 10 μg/mL was injected every day as control.

### **Solubility studies**

An excess of ECN (or of each SD) was added to 10 mL of PB pH 4.5 under stirring at 37 °C for 72 h. Then, the suspensions were centrifuged twice at 8000 rpm for 10 min and the supernatant analyzed by HPLC-UV/Vis. Measurements were performed in triplicate for each sample and the mean ± S.D. was reported.

### **Differential scanning calorimetry**

Differential scanning calorimetry (DSC) measurements were performed using a PerkinElmer DSC 6 (PerkinElmer, Beaconsfield, UK). The instrument was calibrated with indium and lead for temperature, and with indium for the measurement of the enthalpy. The samples, weighing 10–12 mg, were placed into the DSC under a nitrogen flux (20 mL/min) and heated from 25 °C to 250 °C at a scanning rate of 10 °C/min. The same procedure was used for the raw materials.

### **Films characterization**

Films were characterized as described in ‘Thickness’, ‘Tensile tests’, ‘Structural characterization’, ‘Swelling degree’, ‘Scanning electron microscopy’ sections of Paragraph 2.2.7.

### **Drug content analysis**

The ECN content within the film formulations was assayed by the same HPLC method described in the above section ‘ECN analysis’. Briefly, 50 mg of each film were dissolved in 10 mL of pure ethanol and stirred for 60 min. Then, 15 mL of an acidic solution composed of

NaCl and HCl (pH 1.5) were added. The solution was stirred at 8000 rpm for 10 min and assayed by HPLC. Each formulation was analyzed at least in triplicate and the results are expressed as the mean of recovered drug (%)  $\pm$  SD.

### ***In vitro* release studies**

The drug release from the films through cellulose acetate membranes (pore size: 0.45  $\mu$ m; thickness: 150  $\mu$ m) was performed using six modified Franz type diffusion cells. Films of 1 cm<sup>2</sup> (containing about 1.7 mg of drug) were allocated in the donor compartment, while the receptor compartment phase was filled with 12 mL of PB pH 4.5 and maintained at 37 °C by circulating water through the jacket of the lower compartment and constantly stirred at 100 rpm during the experiments. An aliquot of 0.8 mL was withdrawn at predefined time and analyzed by HPLC. The results are expressed as cumulative percentage of drug released and for each sample the mean of six replicates  $\pm$  SD was reported.

### **Mucoadhesive properties**

The mucoadhesive properties were evaluated by using a micro-tensiometer. Vaginal tissue, obtained from a local slaughterhouse (CLAI, Faenza, Italy), was transported to the laboratory and used within 2 h. The tissue was suitably cut, washed and hydrated with PB pH 4.5 containing 1.5% (w/v) of mucin at 37 °C for 15 min and then fixed with acrylic glue to the top of the homemade cell before starting the analyses. Each film (3 mm<sup>2</sup>) was fixed at the top plate using double-sided tape. Film and mucosa were put in contact for 30 s after which the top plate was moved up at a speed of 30 mm/min until their complete separation. The force was recorded as a dyne/cm<sup>2</sup> and was expressed as the force for cm<sup>2</sup> needed to detach the film from the mucosa. The results were then reported as mean values  $\pm$  S.D. and at least 10 replicate measurements were performed for each sample.

### ***In vitro* antifungal susceptibility testing**

*Candida albicans* ATCC 10231 (American Type Culture Collection) and six isolates of *Candida albicans* recovered from urine specimens and genital swabs (collected at the Microbiology Unit, St. Orsola-Malpighi University Hospital, Bologna, Italy) were used for the analysis. The clinical strains were identified by standard procedures, including colony morphology on chromogenic agar (CHROMagar Candida medium, Becton Dickinson, Heidelberg, Germany) and confirmed by MALDI Biotyper System using matrix-assisted laser desorption ionization–time of flight mass spectrometry (MALDI-TOF MS, Bruker Daltonik, GmbH, Germany). The effectiveness of the sample films to inhibit fungal growth was determined by means of disk diffusion assay performed on Sabouraud dextrose agar (SDA,

Becton Dickinson, Heidelberg, Germany) plate. Briefly, the SDA surface was inoculated with a yeast suspension adjusted at 0.5 McFarland and prepared in sterile 0.9% saline solution, and disk-shaped films ( $\varnothing = 6.0$  mm) were laid down on the agar plate, perfectly adhering to the surface. As reference controls, sterile disks containing ECN 300  $\mu\text{g}$  were included in each test. After 24 h at 37 °C, the diameter of inhibition zone, corresponding to the fungal-free zone around the sample, was measured and expressed in millimeters. All experiments were performed in duplicate and in different days.

### **Cell viability and cell damage assays**

The human cervix adenocarcinoma cell line HeLa (ATCC CCL-2) were used for *in vitro* cytotoxicity testing. Cells were routinely grown in Eagle's Minimal Essential Medium (EMEM) supplemented with 10% fetal bovine serum (Carlo Erba Reagents, Milan, Italy), 100 U/mL penicillin and 100  $\mu\text{g}/\text{mL}$  streptomycin at 37 °C with 5%  $\text{CO}_2$ . The safety profile of the film formulations was quantitatively evaluated by measuring cell viability and lactate dehydrogenase enzyme (LDH) release from damaged plasma membranes after treatment with some selected gelatin-based films. In detail, disk shaped samples were dissolved in 6 mL of culture medium for 24 h at 37 °C. The pH of the tested solutions was 6.8–7.0, therefore suitable for cellular investigations. The cell viability was evaluated by using the CCK-8, Cell Counting Kit-8 (Dojindo Molecular Technologies, Rockville, MD, USA), that is a WST-8 [2-(2-methoxy-4-nitrophenyl)-3-(4-nitrophenyl)-5-(2,4-disulfophenyl)-2H-tetrazolium, monosodium salt]-based assay. WST-8 reagent is reduced by dehydrogenases in cells to formazan dye, which is soluble in the tissue culture medium. The amount of the formazan dye generated by dehydrogenases in cells is directly proportional to the number of viable cells. The LDH released was determined by the Cytotoxicity LDH Assay Kit-WST (Dojindo Molecular Technologies). For experiments, HeLa cells were seeded in a transparent 96-well plate at a density of 104 cells/well, grown for 24 h, and treated with 200  $\mu\text{L}$  of solution in which the disks were dissolved. The following controls were included: untreated cells (control cells incubated with 200  $\mu\text{L}$  of culture medium) and cells treated with the Lysis Buffer supplied by the LDH Assay kit (lysed cells). After 48 h, the culture medium was collected from each well, cell monolayer was washed with PB (pH 7.4) and 200  $\mu\text{L}$  of fresh medium containing 20  $\mu\text{L}$  of CCK-8 solution were added. After 2 h at 37 °C, the absorbance was measured at 450/630 nm; results were expressed as the percentage of absorbance relative to the control cells. In parallel, the collected cell-free supernatants were assayed for LDH release by adding a volume of the working reagent and allowing the reaction to proceed for 30 min at RT in the dark. Then, the

stop solution was added, and the absorbance was measured at 490 nm. Data were expressed by the following equation:

$$\text{Cytotoxicity (\%)} = \frac{A-C}{B-C} \times 100 \quad 4)$$

where A is the absorbance of the test solution, and B and C are the absorbances of lysed cells and control cells, respectively. Experiments were carried out in triplicate, and in two independent assays.

### **Statistical analysis**

One-way analysis of variance (ANOVA) was employed to assess statistical significance on the obtained results. The significance was performed with Tukey's multiple comparison test. Differences were considered statistically significant with p values < 0.05.

## **2.2.7 Methods of Characterization**

### **Thickness**

The thickness of the samples was determined using a hand-held digital micrometer (Mitutoyo, Japan) to an accuracy of 0.001 mm. At least ten samples were measured for each composition.

### **Tensile tests**

Tensile tests were performed on films immediately after drying using a 4465 Instron dynamometer equipped with a 100 N load cell and the Series IX software package and stress-strain curves were collected. The Young's modulus (E), the maximum stress ( $\sigma_m$ ) and the strain at break ( $\epsilon_b$ ) were evaluated. The test was performed at a crosshead speed of 5 mm/min on strip-shaped samples. At least 6 specimens were tested for each composition.

### **Structural characterization**

FTIR spectra were recorded in ATR mode using a Thermo Scientific Nicolet iS10 FTIR spectrometer. Spectra were acquired at room temperature with a resolution of  $2 \text{ cm}^{-1}$  from 4000 to  $800 \text{ cm}^{-1}$ .

XRD patterns were recorded in the  $2\theta$  range from  $4^\circ$  to  $40^\circ$  with a step size of  $0,067^\circ$  and time/step of 40 s by means of a Philips X'Celerator diffractometer equipped with a graphite monochromator in the diffracted beam.  $\text{CuK}\alpha$  radiation at 40 mA and 40 kV was used.

### **Thermogravimetric analysis**

Thermogravimetric analysis (TGA) was carried out using a Perkin-Elmer TGA7. Heating was performed in a platinum crucible in air flow (20 mL/min) at a rate of 10 °C/min up to 800 °C. Samples weights were in the range of 5–10 mg.

### **Swelling degree**

Square-shaped (1 cm × 1 cm) air-dried films were weighted and immersed in 5 mL of Phosphate Buffer solution (PB) pH 4.5. After set periods of time samples were removed from the solution, wiped with filter paper to remove the excess of liquid and then reweighted. The amount of adsorbed water was calculated as follows:

$$\text{Swelling (\%)} = \frac{W_w - W_d}{W_d} \cdot 100 \quad 5)$$

where  $W_w$  and  $W_d$  are the weights of the wet and the air-dried sample, respectively.

### **Water vapor permeability**

Water vapor permeability (WVP) is the water vapor transmission rate through a flat film area induced by a vapor pressure between two surfaces under specific conditions of moisture and temperature. It was measured slightly modifying the ASTM E 96–93 method<sup>27</sup>. Films disks ( $\varnothing = 2$  cm) were glued with silicon on the opening of glass vials containing 2 g of anhydrous  $\text{CaCl}_2$ . Weighted vials were placed in a glass desiccator containing saturated  $\text{Mg}(\text{NO}_3)_2 \cdot 6\text{H}_2\text{O}$  solution (75% RH at 25 °C). The vials were weighted every day until constant weights were achieved. WVP was calculated as follows:

$$\text{WVP (gs}^{-1}\text{m}^{-1}\text{Pa}^{-1}\text{)} = \frac{\Delta W \chi}{\Delta t A \Delta P} \quad 6)$$

where  $\Delta W/\Delta t$  is the amount of water gained per unit time of transfer,  $A$  is the exposed area of the samples (0.00020 m<sup>2</sup>),  $\Delta P$  is the water vapor pressure difference between both sides of the film (1670 Pa at 25 °C, table value) and  $\chi$  is the film thickness. Samples were tested in triplicate.

### **Bioadhesive properties**

The bioadhesive properties of the obtained films were evaluated by means of an AntonPaar modular compact rheometer MCR102 and the RheoCompass Software. Pig's ear skin, bought in a local butcher's shop, was carefully separated from the underlying tissue and repeatedly washed with water. Then, disks of 2.5 cm of diameter were cut and glued on the disposable support of the instrument. The film was allowed to adhere on the skin by wetting it with water and applying a gentle finger pressure. Subsequently, the upper plunger, coated with double-sided tape (3 M), was lowered until a force of 5 Newton (N) was applied to the film for 30 sec. Then, the plunger was raised at a speed of 1 mm/s, and the force required to detach the film

from the skin was measured and expressed in Newton (N). Tests were carried out in triplicate for each composition.

### **Scanning Electron Microscopy**

The samples were fixed on the sample holder with double-sided adhesive tape, sputter coated with Au under argon atmosphere by using a vacuum evaporator (Edwards, Crawley UK). Then, films were examined by means of a scanning electron microscope (SEM, Philips XL-20) operating at 15 kV accelerating voltage.

## 2.3 CHITOSAN-BASED FILMS WITH SNAIL SLIME

### Introduction

Chitosan has been proposed as an eligible material with potential applications in many fields, including medicine, agriculture, food, textile, environment, and bioengineering, due to its excellent properties of nontoxicity, biocompatibility, biodegradability, chelating capability<sup>28-31</sup>. In particular, chitosan ability to form films has been widely exploited for food packaging<sup>32</sup>, wound dressing and drug delivery applications<sup>33-36</sup>. Chitosan is soluble in acid solutions due to the protonation of the NH<sub>2</sub> groups on the C-2 position of the D-glucosamine repeat unit: as a consequence, the polysaccharide is converted to a polyelectrolyte in acidic media. Hence, molecular weight and distribution of the acetyl groups along the main chain are determinant factors in chitosan properties<sup>37-39</sup>. In particular, the positive charge of the amino groups at acidic pH is considered responsible for the antimicrobial activity of chitosan, through the interaction with the negatively charged cell membranes of microorganisms<sup>33</sup>. Several studies have been focused to modify composition and properties of chitosan-based films in order to improve their performance and widen their application fields. In this study I investigated the modifications of the properties of chitosan-based films induced by snail slime (S) obtained by MullerOne extraction method. To this aim, different amounts of snail extract were added to chitosan previously solubilized in acetic acid or in lactic acid. Moreover, the acidic character of the slime allowed the preparation of a further series of films obtained by solubilizing chitosan directly into the slime. Films were then fully characterized for their solid-state properties, cell viability and antibacterial activity.

### Results and discussion

Films-forming solutions of chitosan in lactic or acetic acid are extensively reported in literature<sup>40,41</sup>. However, this is the first attempt to prepare chitosan films with the addition of snail slime obtained by MullerOne extraction. This method of extraction provides an acidic solution suitable for the solubilization of chitosan, which needs pH values below 6 to dissolve. It follows that the use of the slime allows direct solubilization of chitosan through a 'green' procedure and provides materials where the good characteristics of chitosan are enriched by the peculiar properties of snail slime.

All the chitosan-based films appeared transparent, with color gradually turning to yellow on increasing the amount of slime, as shown in Figure 12.

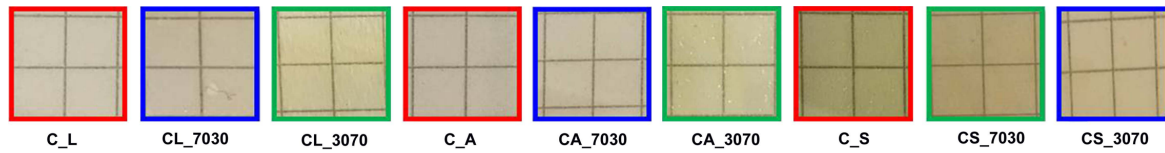


Figure 12. Appearance of the prepared films.

The SEM images of some chitosan films containing or not snail slime revealed a smooth surface without uneven areas. As a general consideration, the flexibility of the films and their adhesiveness increased with S volume, making difficult to detach them from Petri dishes.

Table 6. Effect on thicknesses and mechanical properties of snail slime incorporation into chitosan-based films

Samples	Thickness (mm)	$\sigma_b$ (MPa)*	$\epsilon_b$ (%)*	E (MPa)*
C_L	$0.076 \pm 0.009$	$32 \pm 4$	$4.0 \pm 0.8$	$1200 \pm 100$
CL_7030	$0.100 \pm 0.006$	$7 \pm 2$	$23 \pm 8$	$170 \pm 20$
CL_3070	$0.156 \pm 0.007$	$1.4 \pm 0.2$	$50 \pm 10$	$46 \pm 12$
C_A	$0.052 \pm 0.020$	$40 \pm 3$	$10 \pm 3$	$1760 \pm 300$
CA_7030	$0.096 \pm 0.019$	$15 \pm 4$	$13 \pm 6$	$270 \pm 100$
CA_3070	$0.118 \pm 0.007$	$0.9 \pm 0.1$	$138 \pm 10$	$0.8 \pm 0.1$
C_S	$0.199 \pm 0.005$	$0.43 \pm 0.2$	$163 \pm 30$	$0.38 \pm 0.05$
CS_7030	$0.168 \pm 0.021$	$1.1 \pm 0.19$	$88 \pm 7$	$1.4 \pm 0.22$
CS_3070	$0.158 \pm 0.010$	$8.6 \pm 1.5$	$12 \pm 4$	$301 \pm 44$

\*Each value is the mean of ten determinations, and it is reported with its standard deviation.

As reported in Table 6, films thickness was significantly affected by the acid used for chitosan dissolution: the thickness increase from acetic to lactic acid films can be ascribed to the increasing dimensions of the counterion<sup>42</sup>. A significantly greater augmentation of the values of thickness occurred on increasing the S content, most likely because of the increasing amount of dry matter (dry matter content of S after lyophilization: 5% m/v, as reported in Appendix I). The influence of the nature and composition of the film forming solution on thickness is clearly shown by the results obtained for the C\_S samples, where water addition did not significantly affect the values of thickness<sup>43</sup>.

The results of mechanical characterization are summarized in Table 6. Both C\_L and C\_A films were rigid and brittle with high values of elastic modulus (E) and stress at break ( $\sigma_b$ ), whereas C\_S films exhibited a relatively high extensibility ( $\epsilon_b$ ) and low values of E and  $\sigma_b$ . In agreement, slime addition to C\_L and C\_A compositions greatly influenced the mechanical properties of the films, as clearly shown in Figure 13:  $\epsilon_b$  increased with S content while  $\sigma_b$  and E decreased. The same trend was observed ongoing from CS\_3070 to C\_S, in agreement with the increase of S content. The effect produced by S addition is similar to that obtained by the introduction of plasticizers into the composition of chitosan films<sup>44-46</sup>.

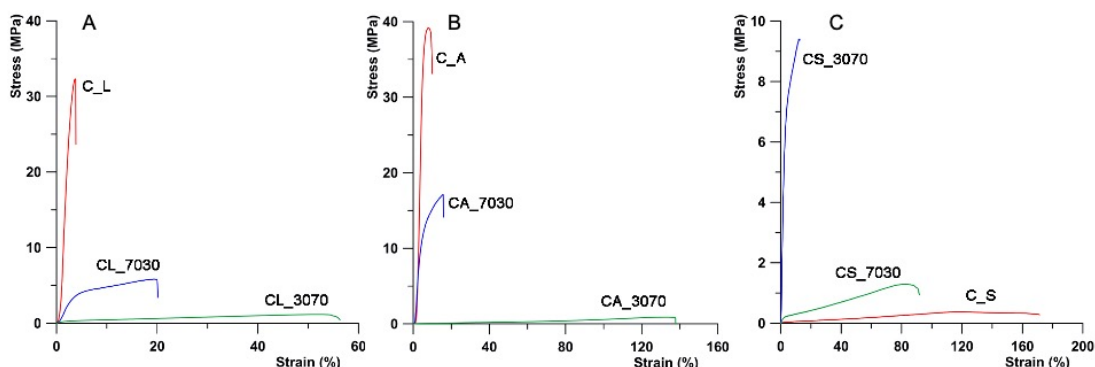


Figure 13. Stress-strain curves recorded on chitosan films prepared in: A) lactic acid; B) acetic acid; C) snail slime.

The increased extensibility of the films at higher S concentration can be attributed to snail slime–polymer interactions, which reduced the intermolecular interactions between polymer chains, facilitating their sliding and mobility and improving the overall extensibility. The increased mobility of the polymer chains usually promotes also water vapor permeability (WVP) <sup>46</sup>, that is the ease of moisture for penetrating and passing through the hydrophilic portion of film. However, in our samples we found a peculiar trend as a function of composition (Figure 14A): CA\_7030 and CL\_7030 exhibited WVP values significantly smaller than the other films of the series. Interestingly, C\_S films exhibited lower permeability than C\_L and C\_A films ( $*p < 0.05$ ) and their WVP values were not significantly affected by water addition.

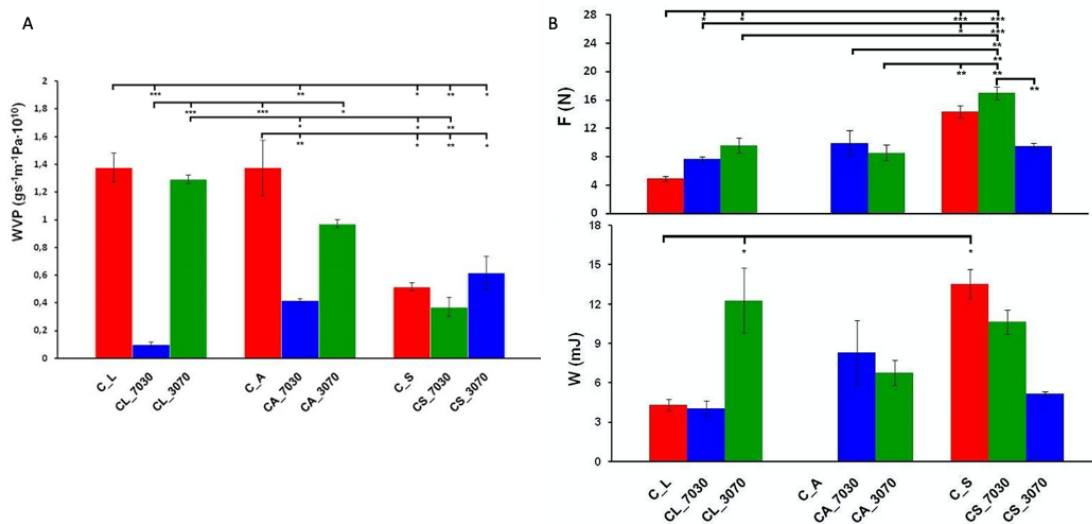


Figure 14. A) Water vapor permeability ( $***p < 0.001$ ,  $**p < 0.01$ ,  $*p < 0.05$ ) and B) Adhesive properties of chitosan-based films ( $***p < 0.001$ ,  $**p < 0.01$ ,  $*p < 0.05$ ).

As described in Paragraph 2.2.7, bioadhesion tests were performed using pretreated pig rind and applying a preloading to the film. As stated previously, the films became sticky after addition of S: the adhesive properties, expressed in terms of force needed for film detachment (F) and work of adhesion (W), are reported in Figure 14B. C\_A films did not exhibit any adhesive performance; however, the addition of S enhanced the adhesiveness, requiring a force

up to about 10 N (CA\_3070) to detach the films. A similar trend was observed for films prepared in lactic acid: C\_L exhibited an appreciable adhesive behavior, which was further enhanced by S addition. As expected, the highest adhesive properties were recorded for films prepared by direct solubilization of chitosan into the slime. In fact, the presence of polar groups into the snail slime, most probably belonging to glycolic acid, allantoin and proteins naturally present in the extract, increases the interactions with the skin and thus the bioadhesive properties.

### Structural characterization

According to the literature, several crystalline polymorphs are known for chitosan; the most represented ones are an anhydrous form indicated as “annealed polymorph” and two different hydrated forms named “tendon” and “Type II”<sup>47,48</sup>. The variety of polymorphs is due to the presence of water molecules, which play an important role in the packing, conformation, and mechanical properties of chitosan-based films. In hydrated forms, the chitosan structure can be stabilized by several hydrogen bonds between -N-H groups and water molecules. In addition, the crystalline structure of chitosan is strongly dependent on its processing treatment, as well as on its origin and molecular composition, such as degree of deacetylation and molecular weight<sup>49</sup>.

The X-ray diffraction patterns collected from chitosan films are reported in Figure 15: films obtained in acetic acid (C\_A) showed two prominent reflections at about 9.2° and 12°/2 $\theta$ , together with a sharp peak at 19°/2 $\theta$ , attributed to type II hydrated polymorph of chitosan acetate<sup>50</sup>.

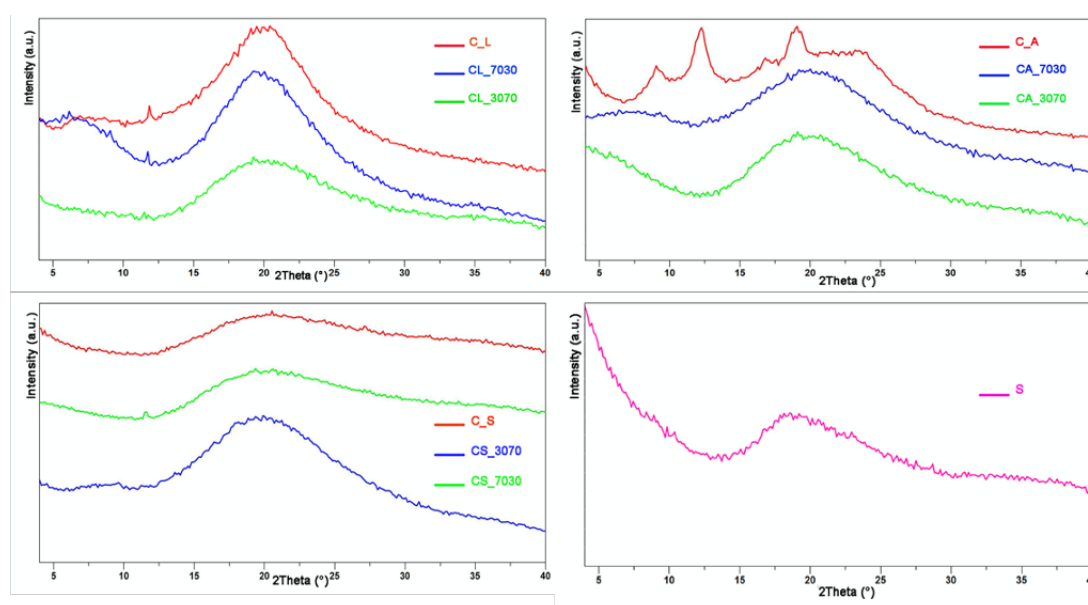


Figure 15. X-Rays diffraction patterns of chitosan-based films and lyophilized snail slime.

Snail mucus is a complex mixture of active ingredients, and it is not easy to discriminate the effectiveness and the interaction of each component with the chitosan functionalities. However, the comparison of the patterns collected from snail slime-containing samples puts into evidence that the material becomes less crystalline on increasing the S content. In fact, CA\_7030 films showed only two broad halos, centered at about  $8^\circ$  and  $20^\circ/2\theta$ , while only a broad halo centered at  $20^\circ$  of  $2\theta$  could be detected when the samples contained a greater amount of slime (CA\_3070). The X-ray pattern of the chitosan films obtained in lactic acid (C\_L), reported in Figure 15, evidences a poorly crystalline structure, with two broad reflections at about  $6^\circ$  and at about  $20^\circ/2\theta$ . S addition provoked an overall decrease of the intensity of the diffraction patterns. It can be hypothesized that, on S addition, the chitosan-slime interactions outweighed the chitosan-chitosan interactions, leading to loss of structural order and, consequently, to the observed significant reduction in crystallinity. In agreement, the XRD patterns of all the samples of the C\_S series displayed just a very broad halo centered at about  $20^\circ/2\theta$ .

In agreement with the X-rays patterns, the infrared absorption spectrum of C\_A films displayed a number of bands which can be ascribed to the hydrated polymorph of chitosan<sup>51</sup>. In particular, the absorption band at about  $1640\text{ cm}^{-1}$  can be assigned to the C=O stretching (amide I), whereas those centered at about  $1540$  and  $1390\text{ cm}^{-1}$  can be attributed to N-H bending (amide II) and C-N stretching, respectively<sup>52</sup>.

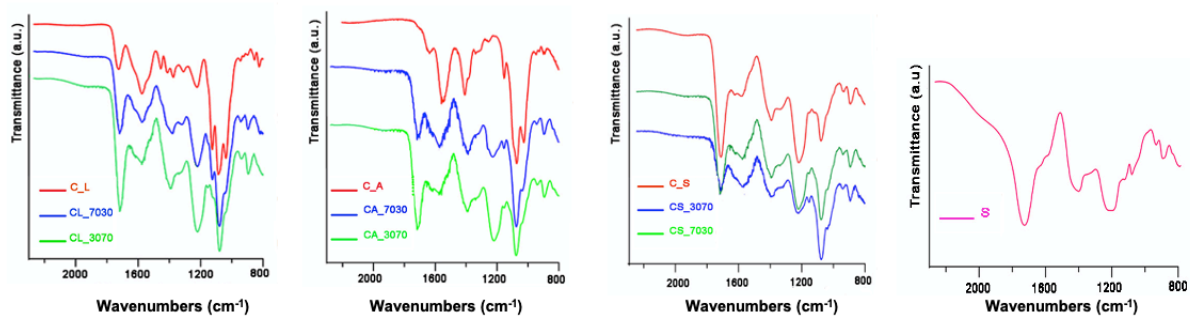


Figure 16. FT-IR spectra of chitosan-based films and lyophilized snail slime.

Addition of S provoked a general broadening of the spectra, which assumed the characteristic features of the spectrum of S powder (see Figure 16): an intense absorption peak appears at around  $1712\text{ cm}^{-1}$  and is probably due to the high content of allantoin and glycolic acid in the snail slime (see Appendix I). This absorption band can also be found in the spectra of composite films, with an intensity that increases on increasing S content. The resolution of the absorption bands centered at about  $1072\text{ cm}^{-1}$ , associated to C-O stretching, decreased on increasing S content, suggesting interactions between the hydroxyl groups of chitosan and polar groups of S through hydrogen bonds<sup>52</sup>. By comparing IR spectrum of S with that reported in literature<sup>53</sup>, it is clear that snail slime obtained by MullerOne method contains a minor amount of proteins

with respect to that obtained by a different method of extraction. We hypothesize that the use of ozone during snail stimulation could induce a partial protein degradation, thus lowering the proteic component of the final extract. In agreement with XRD results, the infrared absorption spectrum of C\_L films was quite different and resembled those reported in literature for chitosan films prepared in lactic acid<sup>54</sup>. Addition of S to C\_L films had a similar effect to that observed on C\_A films, and the spectra were similar to those recorded for the C\_S series.

The thermal stability of chitosan films was assessed by TGA analysis in air. Results obtained for the different films are reported in Figure 17, together with the thermal behavior of lyophilized S.

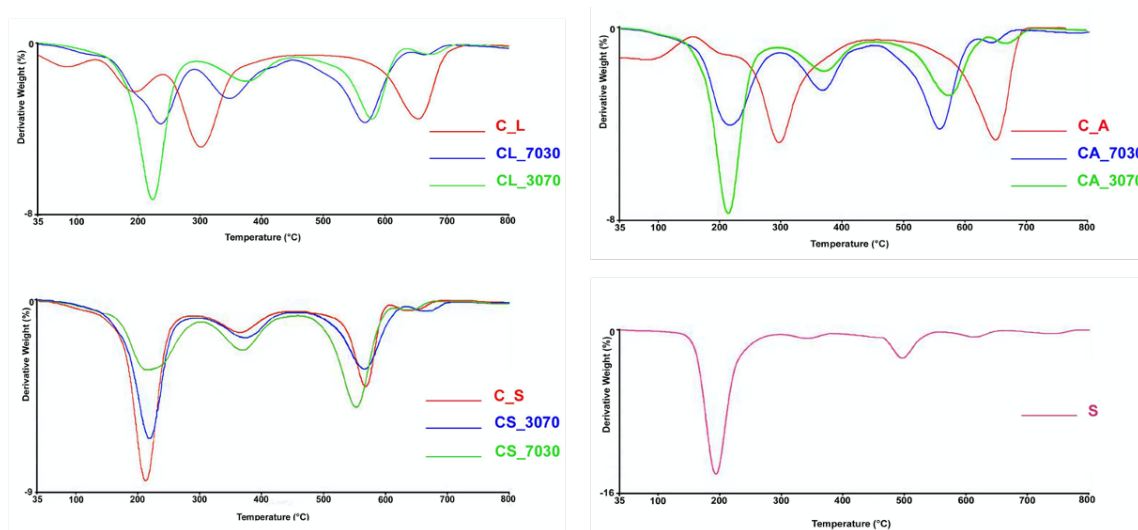


Figure 17. DTG plots recorded on films in L, films in A, films in S and lyophilized S.

C\_A films displayed three steps of thermo-oxidative degradation<sup>55</sup>. The first one, in the temperature range 35–160 °C, is attributed to the loss of absorbed water. The second one, between 160 °C and 460 °C and centered around 310 °C, corresponds to the chemical degradation and deacetylation of chitosan<sup>56</sup>, while the third step, in the temperature range 460–700 °C, can be associated with the oxidative degradation of the carbonaceous residue formed during the second step. The thermogravimetric plot of C\_L differs from that of C\_A in the first region, which shows two distinct weight losses in the range 37–240 °C, in agreement with the different structures evidenced by XRD and FT-IR data. The derivative plot of TGA (DTG) of freeze-dried S (Figure 17) displays a weight loss centered at 190 °C, which accounts for about 70% w/w of weight loss, and further degradation steps between 300 and 800 °C, probably due to the degradation of residues. A very similar thermogravimetric plot is that of sample C\_S, with just some shift of the degradation steps to higher temperatures. Water addition (CS\_7030 and CS\_3070) caused just a reduction of the relative amount of the first weight loss. When S was added to the composition of C\_A and C\_L, all the films displayed similar thermogravimetric plots to that of C\_S series: in particular, the thermal degradation started at a

temperature lower than that of pure chitosan films. Moreover, the first mass loss, determined between 37 °C and 300 °C, accounts for about 35% and 48% w/w for the 7030 and 3070 compositions, respectively. Moreover, no water loss was observed between 35 °C and 160 °C.

### Biological properties

In our experimental conditions, C\_L and C\_A films did not interfere with Vero cells metabolism after 72 h of incubation (93.7% and 103.3%, respectively, and relative to untreated control cells), as shown in Figure 18.

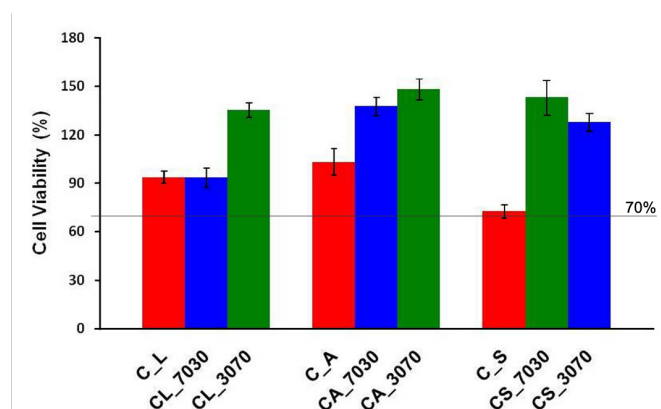


Figure 18. Vero cells viability after 48 h of incubation with the media containing film components following disks dissolution. Data (mean values  $\pm$  SD) are relative to the untreated control (set to 100%).

Addition of snail mucus to these films induced an improvement in cell viability, especially for the samples of C\_A series. These samples exhibited a dose dependent increase in Vero viability as a function of S content. The lowest cell viability was detected for C\_S films (72.7%); nevertheless, as a material is considered cytotoxic when its viability is <70% in comparison to untreated controls<sup>57</sup>, all samples displayed a promising safety profile.

The antibacterial properties of the different chitosan films were evaluated *in vitro* by means of a disk agar diffusion method where inhibition of bacterial growth is demonstrated by the clear bacterial-free zone around sample disks following a 24 h-incubation. Results are reported in Table 7.

Table 7. Ranges of the inhibition zone diameters (mm) measured for the chitosan films.

Sample	<i>S. aureus</i> (ATCC 25923)	<i>E. coli</i> (ATCC 25922)
C_L	NA*	NA
CL_7030	NA	NA
CL_3070	NA	NA
C_A	NA	NA
CA_7030	NA	NA
CA_3070	12-13	11-12
C_S	15-22	11-14
CS_7030	15-16	12-13
CS_3070	NA	NA
GMN 10 mg	18-19	18-19

\*NA; not appearing.

There was no difference between the antibacterial effects on the different microbial species. Although it is generally recognized that chitosan solutions have strong antibacterial activities<sup>58</sup>, chitosan films did not inhibit bacterial growth in agar diffusion tests because chitosan in a film form is unable to diffuse through the surrounding agar media<sup>59</sup>. The present results confirm this feature since both C\_A and C\_L samples did not inhibit bacterial growth. As a consequence, the bacterial-free zones observed for S-containing films could be definitely ascribed to snail slime addition. Chitosan films prepared in acetic acid and directly in S showed antibacterial activity at the highest S content (CA\_3070, C\_S and CS\_7030) confirming the inhibitory role of slime. On the contrary, films prepared in lactic acid did not display antibacterial properties irrespective to S content.

### **Conclusion**

New and highly versatile films containing different amounts of snail slime, extracted with the MullerOne method, and chitosan were obtained by simple solvent casting. The results of this work show that snail slime can be added to chitosan previously solubilized in acetic or lactic acid, or it can also be used to directly dissolve chitosan through a greener route. Tensile tests revealed that composite films can be stretched up more than ten times with respect to chitosan films, demonstrating that S addition displays a plasticizing effect on the films. Moreover, snail mucus also enhanced water barrier properties and bioadhesion. Structural characterizations indicated that the interactions between snail mucus and chitosan chains involve hydrogen bonds between the hydroxyl groups of chitosan and polar groups of S, even if the complexity of the extract composition requires more detailed analysis. Thanks to the presence of S, composite films displayed enhanced cytocompatibility and significant antibacterial activity towards both Gram-positive and Gram-negative bacteria. These results demonstrate that variations in composition can be utilized to modulate the properties of these materials for a wide range of possible applications including those in the biomedical field. However, due to the influence of the extraction methods on the snail extract properties, composite films made with different snail extract should be useful to get more information about the interactions between the components and to highlight the peculiar extract effect.

## 2.4 CELLULOSE DERIVATIVES-BASED FILMS WITH SNAIL SLIME

### Introduction

Following the evidence that snail slime addition to chitosan films not only provides them with antimicrobial activity, but also remarkably improves their water barrier and bioadhesion properties (see Paragraph 2.3), in this study I further explored the influence of snail slime on the properties of cellulose derivatives-based films. Cellulose was chosen because it is the most abundant renewable polymer <sup>60</sup>, it is biodegradable and non-toxic <sup>61</sup>. Indeed, cellulose-based materials are very good candidates for applications in the packaging field <sup>62</sup> and herein different cellulose-derivatives were employed for film preparation.

Hydroxypropyl-methylcellulose (HPMC) was selected since is a renewable, largely available, and non-ionic vegetable derivative. Moreover, it is very attractive because it is edible, transparent, odorless, tasteless, and able to form oil-resistant and water-soluble films. Its use is approved as food additive by the FDA (21 CFR 172.874) and by the EU <sup>63</sup> and it is also proposed for the preparation of packaging materials <sup>64</sup>, although it exhibits a high moisture absorption <sup>65</sup>.

The highly crystalline derivative sodium carboxymethyl cellulose (CMC) is a GRAS (Generally Recognized As Safe) polymer and it is also widely used for film formulations <sup>66</sup> and as a food stabilizer thanks to its non-toxicity, biocompatibility, biodegradability and hydrophilicity.

The preliminary results obtained on cellulose-based materials in combination with snail slime were very promising: films were biodegradable, showed excellent barrier properties, a suitable mechanical behavior and were provided with antibacterial activity, which are very appealing features in the food packaging sector. In fact, the research on antimicrobial food packaging films has attracted great attention in recent years <sup>67</sup>, since they can act as effective physical barriers against bacteria invasion and prolong the food shelf life <sup>68</sup>. In literature, the studies aimed to imbue these materials with antibacterial activity are based on the use of essential oils as additives <sup>69,70</sup> since the introduction of natural extract is considered to be safe and friendly to human and environment <sup>11</sup> compared with the nano-antibacterial agents prepared by different inorganic materials.

Further food preservation analyses were carried out, suggesting that these biocomposite films are good candidates to be employed in the packaging sector.

### Results and discussion

The barrier properties of a polymeric film are crucial features to predict the behavior of the material as well as the shelf-life of the product when used as a food packaging <sup>71</sup> and they derive

mainly from the permeability of the film to gases and vapors, that are noxious to the quality of the product <sup>72</sup>. The thickness measurements of the films are reported in Table 8: thickness ranged from 29 to 171  $\mu\text{m}$ .

Table 8. Thicknesses and transparency values of the obtained cellulose-based films.

Labels	Thickness ( $\mu\text{m}$ )	T <sub>600/100</sub>	Transparency Values
E5	84	0.90	0.545
E5_S30	113	0.87	0.535
E5_S70	158	0.85	0.447
E5_S100	171	0.84	0.443
E50	59	0.90	0.776
E50_S30	85	0.76	1.402
E50_S70	126	0.65	1.485
E50_S100	137	0.50	2.197
CMC	29	0.92	1.249
CMC_S70	60	0.77	1.892
CMC_S100	91	0.40	4.373

For every type of cellulose, the thickness increased on increasing the snail slime amount. As all the films were prepared by casting the same amount of solution into Petri dishes (8.5 cm in diameter), the observed trend could be due to the increasing of the dry matter. In fact, the snail extract contains approximately a 5% w/v of dry matter, and so, on increasing the S content the total amount of dry matter also increases and the thickness become greater. As thickness influences mechanical and barrier properties, all the values are normalized with respect to thickness.

### UV barrier, light transmittance, and transparency value

Transparency of films for food packaging applications is one of the main requirements in the packaging industry <sup>73</sup>, as well as the UV barrier properties are a key feature to prevent chemical reactions induced by UV light in food <sup>74</sup>. In fact, the UV-radiations are responsible for the activation of reactions such as lipid oxidation, vitamins oxidation or loss of color which result in a loss of the quality of packaged foods <sup>75</sup>. However, the mechanisms that allow films to acquire the UV light barrier properties can affect their transparency.

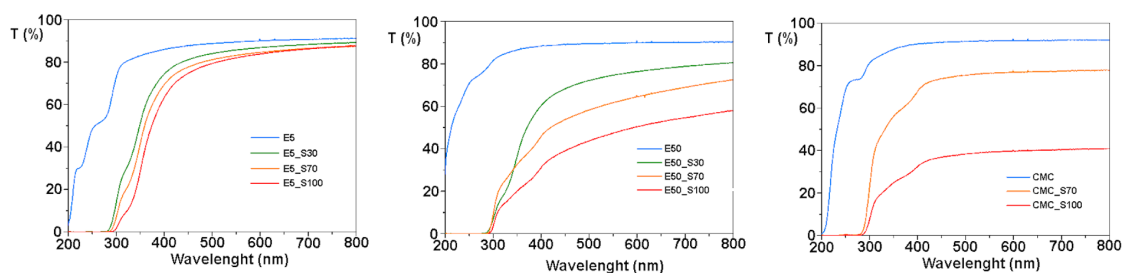


Figure 19. UV-Vis spectra collected on cellulose-based films containing different amount of S (from left to right): E5-, E50- and CMC-based films.

The UV–Vis spectra acquired on the cellulose-based films are shown in Figure 19. In the UV region (200–280 nm) samples E5, E50 and CMC showed high transmittance values, which rapidly fell to zero after S addition. As reported in literature <sup>76</sup>, a transmittance value below 10% at 280 nm indicates that the films have effective UV barrier properties. It can be concluded that S addition confers excellent UV barrier properties both to HPMC and CMC based films, regardless of the snail slime content.

By comparing the spectra, it is worth of note that S-containing films also showed a lower transmittance in the visible range (400–800 nm) compared to the control films, indicating that the incorporation of snail extract into the film composition had a strong effect on the barrier properties also against visible light. A quantitative evaluation of this important feature is obtained by using Equation 2 and the obtained transparency values are reported in Table 8. According to this value, the greater is the transparency value, the lower is the transparency of the film <sup>75,77,78</sup>. For E50- and CMC- based films, the transparency decreased on increasing the amount of S, while S addition had a minor effect on E5-based films. Anyway, all the transparency values were lower than 5, and hence the films can be considered transparent, as reported in literature. The mechanism of action of the snail slime could be due to the combination of two elements: the absorption of UV rays thanks to the presence of proteins containing aromatic amino acids, and the decrease in transparency that prevents the visible light passing through the films <sup>79</sup>. This decrease can be attributed to the effect of the macromolecular components of the snail slime dispersed into the biopolymer's matrix, which could change the optical properties of the material. This effect was more pronounced for E50 and CMC-based films, probably because of the higher viscosity of these solutions.

### **Water vapor permeability**

Prevention of moisture transfer between food and the surrounding atmosphere or between two different food products is a main requirement of packaging films <sup>80</sup>. Water vapor permeability (WVP) was used to test whether moisture can easily penetrate and pass through a substance and the results for the different film compositions are reported in Figure 20.

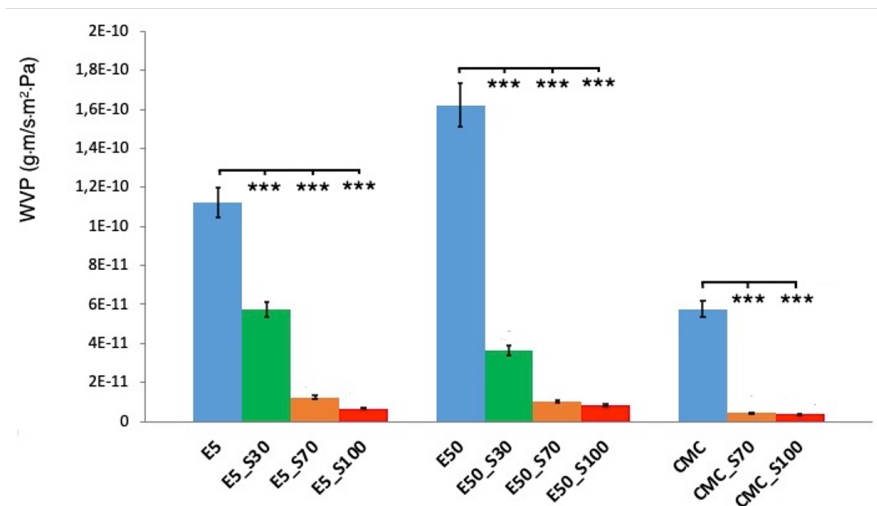


Figure 20. Water Vapor Permeability of cellulose-based films (\*\*\*) $p < 0.001$ ).

Data show that the introduction of snail extract into film composition strongly influenced the WVP, which decreased by one or two orders of magnitude as a function of S content: for example, the WVP values vary from  $1.3 \cdot 10^{-10}$  to  $6.5 \cdot 10^{-12}$  g·m/s·m<sup>2</sup>·Pa when measured on E5 and E5\_S100, respectively. This trend could be explained by the formation of a polymeric network within the films: the different internal structure could lead to the creation of fewer empty spaces, preventing or hindering the diffusion of water molecules through the films. Greater S contents (S70 and S100) provoked a greater barrier effect, independently from the HPMC molecular weight (E5 and E50). In addition, the decrease in WVP of CMC-based films could also be due to a decrease in the hydrophilicity and solubility of the films as the slime content increases <sup>70</sup>.

### Film solubility and swelling degree

Solubilization and swelling degree measurements are of particular relevance in order to evaluate the films stability in aqueous solutions: in fact, a good resistance is needed when films are proposed for applications such as food packaging <sup>61</sup>. The results of water solubility test showed that HPMC-based films are highly soluble and their solubilization in water is immediate, whatever their composition. CMC-based films displayed a different and more interesting trend: while in absence of snail extract the films solubilized in few minutes, CMC\_S70 and CMC\_S100 films preserved their structure for more than two weeks. In fact, after 24 h their solubilization (calculated from Eq. 1) accounted for 30% and 45%, respectively, and these values were unchanged even after 7 and 14 days, suggesting a good resistance of the films in aqueous solution. Moreover, both samples reached a degree of swelling of 100% after 4 h, with no further significant variation up to 24 h. These results suggest that the interactions between HPMC and snail slime are not strong enough to build a network resisting to water permeation, which resulted in an increase of the free volume in the material structure <sup>81</sup>. On the

contrary, the significant decrease of the dissolution of the CMC-based films with the addition of S leads to hypothesize that the protonation of the COO<sup>-</sup> groups into COOH could occur due to acidic pH, as reported in literature <sup>82</sup>.

### Structural characterization

The infrared spectra collected from E5 and E50 are reported in Figure 21a,b. The characteristic absorption bands of HPMC, in accordance with those reported in literature <sup>83</sup>, can be detected: in particular, the absorption bands at 3500 cm<sup>-1</sup>, 1060 cm<sup>-1</sup> and around 2915 cm<sup>-1</sup> are due to O–H, C–O and C–H stretching vibration, respectively, whereas the absorption band around 1457 cm<sup>-1</sup> is characteristic of the CH<sub>3</sub> asymmetric bending vibrations. S addition provoked the appearance of new bands, centered at 1717, 1390 and 1224 cm<sup>-1</sup>, which can be attributed to the high amount of allantoin and glycolic acid contained into snail slime (see Appendix I). In the FTIR spectra collected from CMC-based films (Figure 21c) the bands belonging to the functional groups of CMC are well recognizable: the O–H stretching and bending vibrations occur at 3385 cm<sup>-1</sup> and 1324 cm<sup>-1</sup>, respectively, while antisymmetric and symmetric vibrations bands of –COO– are at 1600 and 1413 cm<sup>-1</sup>. The absorption band at 1059 cm<sup>-1</sup> is associated with the asymmetric stretching of glycosidic bridge C–O–C. The low intensity band centered at around 900 cm<sup>-1</sup> could be attributed to the β-glycosidic linkages between sugar units <sup>84</sup>. As observed for HPMC-based films, introduction of snail extract into CMC-based films strongly modified the IR spectra, which also displayed an impressive broadening. Figure 21c shows the strong reduction of the intensity of the band at 1593 cm<sup>-1</sup> (attributable to the asymmetric stretching vibration of free carboxyl groups in the salt form), and the appearance of two bands at 1717 and 1224 cm<sup>-1</sup> as a consequence of slime addition. The band at 1717 cm<sup>-1</sup> could be due both to S addition (as stated above) and to the formation of COOH groups on the side chain of CMC, as a consequence of pH lowering. The reduction of the charge on the side chains supports the strong effect observed on the swelling properties and on the water uptake ability of CMC\_S70 and CMC\_S100, as well as the decrease in solubility.

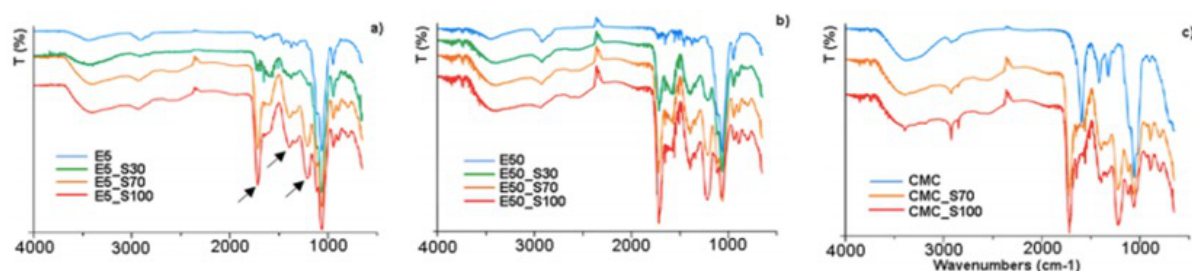


Figure 21. FT-IR spectra of cellulose-based films: a) E5-based films, b) E50-based films and c) CMC-based films. The arrows indicate the most intense bands due to S.

The X-ray patterns recorded on cellulose-based films are reported in Figure 22. It is known that crystallinity of cellulose is associated with strong hydrogen bonding interaction of cellulose (intermolecular and intramolecular) and Van der Waals forces between adjacent molecules.

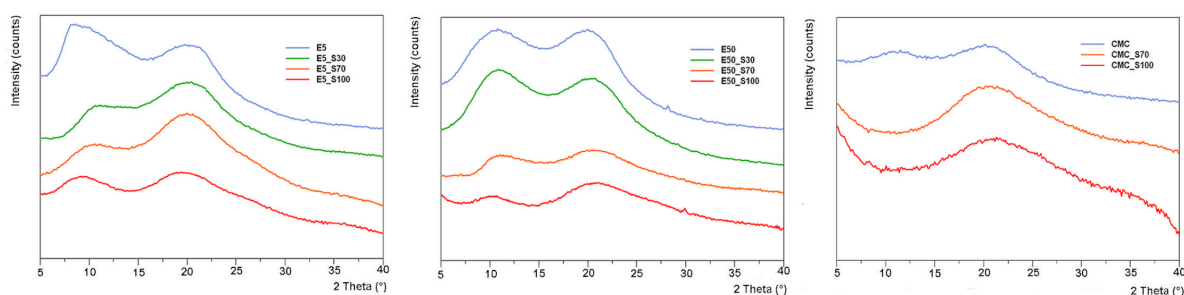


Figure 22. XRD patterns of E5-, E50- and CMC-based films.

During the processing of cellulose, reactions of methylation and carboxymethylation result in the extending the distance between cellulose molecules, thus disrupting hydrogen bonds and hence lowering the crystallinity of the polymers<sup>85</sup>. As a matter of fact, reference films showed the characteristic diffraction patterns of a poorly crystalline material, with two broad reflections at  $9.5\text{--}12^\circ/2\theta$  and  $20.0\text{--}21.5^\circ/2\theta$  characteristic of cellulose II<sup>86</sup>, which is obtained by means of chemical and physical treatments of cellulose I, the most abundant form found in nature<sup>87,88</sup>. The broadness of the reflections increases on increasing slime content, in agreement with a decrease of crystallinity. This effect, even more evident in the patterns of CMC films where the signal between  $9.5$  and  $12^\circ/2\theta$  is no longer appreciable, might be attributable to the presence of S interlaid between the polymer chains.

### Mechanical properties

The tensile strength at break ( $\sigma_b$ ), the elastic modulus (E) and the deformation at break ( $\epsilon_b$ ) are reported in Table 9, while the stress-strain curves are shown in Figure 23.

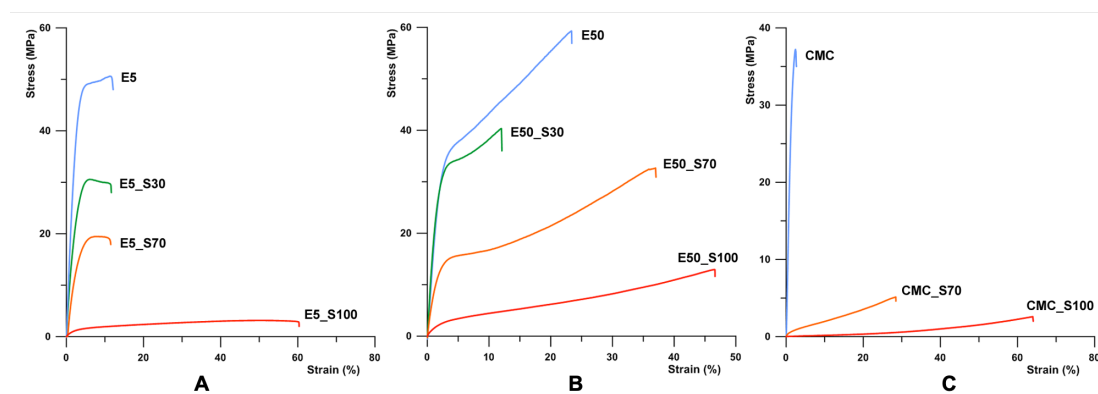


Figure 23. Stress-strain curves of a) E5, b) E50 and c) CMC films.

Both HPMC and CMC films exhibited high stress at break, and they could be extended only by a few percentage units. Enrichment of the formulation by S addition greatly enhanced films

extensibility, whereas it reduced the stress at break and the elastic modulus. Furthermore, the different series of films displayed different mechanical behavior upon S addition, as shown by the stress-strain curves reported in Figure 23: in particular, while E50\_S100 and CMC\_S100 showed an elastic behavior, E5\_S100 seemed to display a plastic behavior. The effect produced by S addition to cellulose-based films is like to that obtained on slime-containing chitosan films (see Paragraph 2.3): probably, as a consequence of the interactions between S and the polymer chains, the intermolecular interactions between the cellulose molecules are reduced, thus facilitating their sliding and improving their mobility. According to conventional standard<sup>89,90</sup>, the tensile strength of packaging films must be higher than 3.5 MPa: all the prepared films, except E5\_S100 and CMC\_S100, met this requirement.

*Table 9. Effect of S incorporation on the tensile properties of cellulose-based films. Each value is the mean of ten determinations and is reported with its standard deviation. (\* $p < 0,05$ , \*\* $p < 0,01$  and \*\*\* $p < 0,001$  compared to the control).*

<b>Labels</b>	<b><math>\sigma_b</math> (MPa)</b>	<b><math>\epsilon_b</math> (%)</b>	<b><math>E</math> (MPa)</b>
E5	50 ± 6	16 ± 8	1760 ± 400
E5_S30	31 ± 3**	13 ± 5	1220 ± 90
E5_S70	18 ± 1***	11 ± 3	720 ± 100**
E5_S100	3 ± 1***	61 ± 8***	72 ± 10***
E50	54 ± 10	22 ± 7	2020 ± 140
E50_S30	49 ± 10	16 ± 7	1920 ± 430
E50_S70	31 ± 3*	34 ± 5	860 ± 80**
E50_S100	13 ± 1***	46 ± 1**	140 ± 20***
CMC	32 ± 4	2 ± 1	2750 ± 600
CMC_S70	5 ± 1***	29 ± 3***	44 ± 14***
CMC_S100	2.7 ± 0.3***	67 ± 6***	2 ± 1***

### **Adhesion studies**

As found for chitosan-based films, also cellulose-based films became sticky after the snail slime addition: the adhesive properties, expressed in terms of force needed for film detachment (F), are reported in Figure 24.

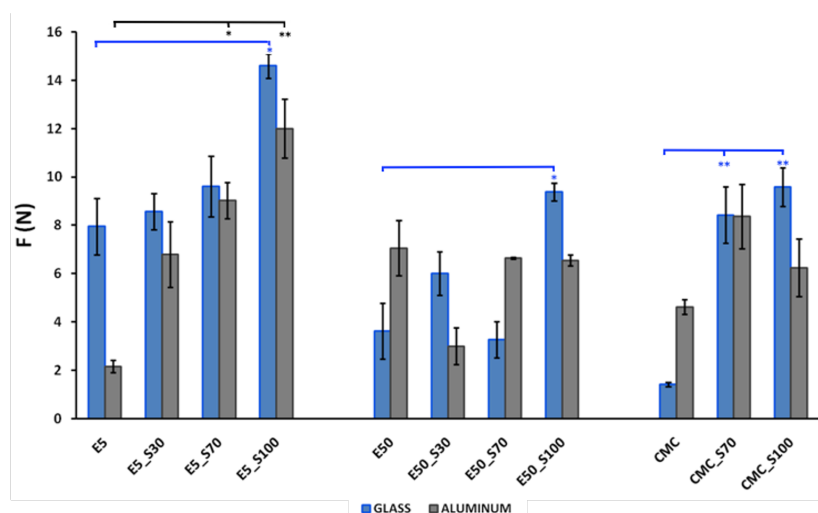


Figure 24. Detachment forces (N) of films from glass (blue) and aluminum (grey) supports (\* $p < 0.05$ ; \*\* $p < 0.01$ ).

In order to evaluate a possible application of our films in the field of food packaging, adhesive studies were conducted by using aluminum and glass as supports: these materials are in fact very used as domestic food container. Cellulose-based films exhibited good adhesive performances on both the substrates, even if some differences should be remarked. In particular, the adhesion force on glass support showed a fairly linear trend on increasing the amount of S. Furthermore, films based on HPMC E5 were stickier than the others even without S, although its addition considerably increased this property. On the other hand, CMC based films were not very sticky on glass, but the addition of S surprisingly increased the adhesiveness of almost 10 times.

### Preservation of food

The effectiveness of the obtained films to preserve the freshness of food and to remain attached to the container for a desirable period of time was qualitatively assessed using a fresh apple purchased in a local shop at commercial maturity and immediately used, following a method reported in literature and suitably modified<sup>91</sup>. The apple was cut into cubes of regular dimensions (side about 1 cm) and arranged into a glass container. The container was covered with the film CMC, as shown in Figure 25A, and then placed in the refrigerator at 4 °C. As a control, apples cubes were maintained in the refrigerator without any coverage. Digital photos were acquired at time zero and after ten days of storage. After ten days of storage at 4 °C, the uncovered apple cubes became dried and darker while those covered with the film showed an excellent state of preservation, allowing only a slight enzymatic browning on their surface (see Figure 25A) thus demonstrating the efficacy of CMC\_S70 in the preservation of food. Moreover, it is important to underline that the film immediately adheres to the glass container and remains attached to it for the whole time of storage.

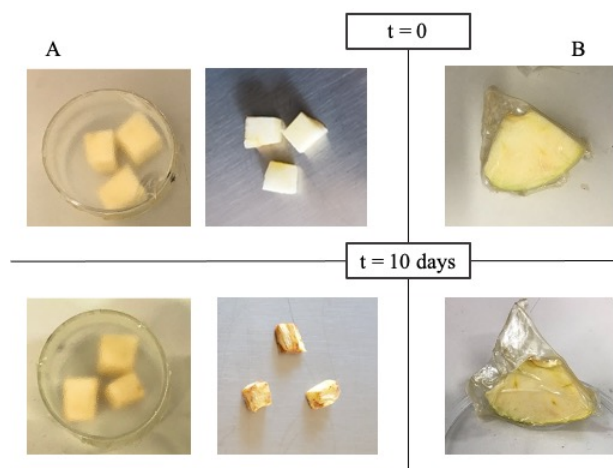


Figure 25. A) Apple cubes covered with the film CMC\_S70 (left) and uncovered (right) at time 0 (top) and after 10 days (bottom) of storage at 4 °C; B) Apple slice wrapped with the CMC\_S70 film immediately after cutting (top) and after 10 days (bottom) of storage.

A further investigation was made by cutting a small slice of apple and wrapping it with the CMC\_S70 film in order to check its appearance after ten days of storage in the refrigerator at 4 °C.

The adhesiveness of the CMC\_S70 film on itself and on the surface of an apple, together with its effectiveness in food preservation, was evaluated from a qualitative point of view. In fact, from the comparison of the digital photos of the apple slice wrapped with CMC\_S70 taken at time zero and after ten days of storage in the refrigerator at 4 °C (Figure 25B), it can be inferred that no significant oxidative processes have damaged the state of apple conservation.

### Antibacterial tests

The antibacterial activity of the different cellulose-based films was assessed *in vitro* by means of a disk agar diffusion method against both Gram-positive and Gram-negative bacteria. Results are reported in Figure 26.

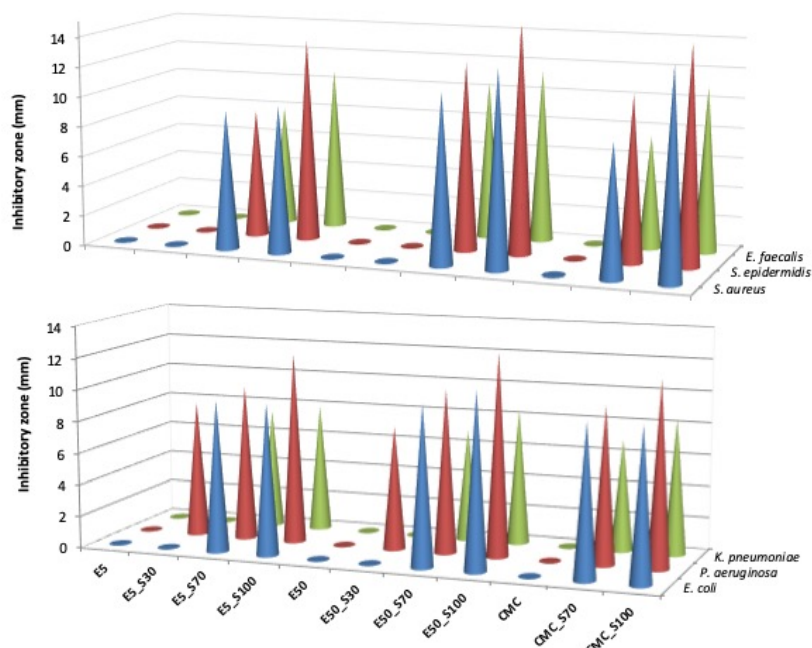


Figure 26. Antibacterial activity of cellulose-based disks against a) Gram-positive bacteria; b) Gram-negative bacteria. Data are the mean value of the diameter (in mm) of the clear bacterial free zone measured around the disk samples.

All cellulose films without snail slime did not show any inhibition on the tested bacteria. Instead, the antimicrobial activity of S-containing films on contact surface around the discs was evident, indicating the antibacterial effect of snail slime. This is further confirmed by the increased diameter of the bacterial-free zone for the samples at the highest slime content. Disks used for antibacterial assay were weighted and the S content of each composition was determined, considering that they contain about 6% w/w of residual water. Considering the weight of the cellulose-based films, and the amount of snail mucus on the different 6 mm-diameter disks, it is evident that the inhibitory activity of the samples was strictly related to S content. Of note, even the cellulose-based disks containing S at 30% displayed a significant inhibitory zone for *Pseudomonas aeruginosa*, one of the most versatile pathogens present in a variety of environments, including soil and water, and intrinsically resistant to numerous antibacterial agents. It is an opportunistic pathogen responsible for a broad spectrum of infections as respiratory tract and urinary infections, primary skin infections, ear and eye infections.

### Biodegradability test

Biodegradation tests were conducted in soil, as described in the Experimental Part (Paragraph 2.2.7). After 2 weeks, only fragments of the sample CMC\_S70 were still present: a weight loss of 54% was calculated. After 4 weeks, sample CMC\_S70 was fully biodegraded. The biodegradation data meet very well to the results reported in literature<sup>24</sup> and represent an added value of the snail-containing cellulose films.

## **Conclusions**

The results of this work demonstrate that the use of snail slime in the preparation of cellulose derivatives-based films provides materials characterized by high transparency, excellent UV barrier properties and very good WVP. Addition of the snail slime results in an increase of the extensibility, together with a decrease of the stress at break and of the elastic modulus, in all the three different types of cellulose (HPCM E5, HPCM E50 and CMC) films. Moreover, all the films prepared in the presence of the slime displayed enhanced adhesion towards glass and aluminum and a significant antibacterial activity against both Gram-positive and Gram-negative bacteria. However, the structural characterization evidenced that the snail extract establishes different interactions with the internal structures of the different types of cellulose. In fact, while immersion in water causes immediate solubilization of all HCPM-based films, the addition of high amounts of S to the composition of CMC-based films makes them insoluble for more than a week, thus allowing their use for food packaging. In addition, all the prepared films were fully biodegradable in few weeks and printable. On the basis of these results, it can be inferred that snail-enriched CMC-based films might find potential applications that require direct contact with food as edible antimicrobial packaging, hence they are good candidates to replace synthetic polymers in the packaging industry.

## 2.5 CELLULOSE/HYALURONATE-BASED FILMS WITH ANTI-HERPES ACTIVITY

### Introduction

In Europe, more than 200 million women (69%) and 187 million men (61%) suffer from cold sores, a widespread and annoying disease caused by the Herpes Simplex Virus type 1 (HSV-1). Cold sore (*Herpes labialis*) is very contagious and spreads from person to person through close contact. Generally, herpes is a rash of the skin and mucous membranes (in particular, the lips) and is characterized by the erythema of the affected area followed by the formation of vesicles<sup>92</sup>, which can burst and form scabs. HSV-1 hides inside the nerve cells, where it lies latent throughout the individual's lifetime, so it has never completely healed: it cannot therefore be cured, but it is possible to manage the symptoms. Stimuli such as fever, menstruation, sunlight, and upper respiratory infections can reactivate the virus, after which it returns to the epithelial cells via the sensory nerve. Tacking action at the early stage is the most effective way to contain the virus and promote fast healing.

In order to stop the replication of the virus and to avoid the use of antiviral drugs, administered in the form of pills or creams, transparent patches are a widespread remedy, as they make cold sores less visible and also act as an antiviral shield, reducing the risk of infection.

In this context, the aim of this work was to evaluate the ability of snail slime HelixComplex® to confer anti-viral activity against HSV-1 to biopolymer-based films in order to act as biodegradable and bio-adhesive labial patches.

The slime used for this purpose was extracted from *Helix Aspersa* snails by the HelixPharma Company srl with a natural and cruelty-free patented method, which allows to obtain the extract at a neutral pH (between 6.5 and 7). Carboxymethyl cellulose (CMC) and sodium hyaluronate were selected as biopolymers and films were prepared by solvent casting, dissolving the polymers directly into snail slime or in water for reference samples. Different patch formulations were prepared varying the relative amounts of hyaluronate and glycerol, which was introduced as humectant.

All samples were characterized for their ability to remain attached to the skin without the use of glue and then tested against HSV-1, evaluating their efficacy pre- infection, post-infection and both pre- and post- infection. Only the labial patches enriched with HelixComplex® were able to reduce the infection, suggesting that its use could be very effective in the prevention and in the reduction of the disease, avoiding the infection of neighboring cells. In conclusion, these films represent a sustainable alternative to the commercial plastic patches. Thanks to their adhesiveness and biocompatibility, films enriched with snail mucus extract demonstrated to be very good candidates to act as a labial patch for the treatment of *Herpes labialis*.

## Results and discussion

Since *Herpes labialis* is composed of small blisters filled with fluid that accumulate on the lips or around the mouth, this can be very annoying but also embarrassing. Recent data report the use of essential oils to treat cold sores: it has been shown that Tea Tree oil has the ability to fight the HSV-1 and both peppermint oil and lemon balm oil inhibit its activity; however, their misuse could cause allergic reactions. A lip patch is a suitable and widespread remedy as it creates a protective barrier against potential external triggers, reducing the risk of infection and preventing worsening symptoms. The patches can be applied at any stage of the infection; however, it is better to apply them as soon as possible to contain the infection.

Biodegradable active films were obtained by solvent casting incorporating different amount of hyaluronate and glycerol into cellulose matrix films, as reported in the Experimental Part (Paragraph 2.2.7). All the obtained films appeared homogenous and transparent, as shown in Figure 27.



Figure 27. Appearance of some obtained films inside petri dishes (left) and adhered on lips (right).

## Bioadhesion

Bioadhesion tests of films to the skin were carried out as described in Paragraph 223, and the results are shown in Figure 28.

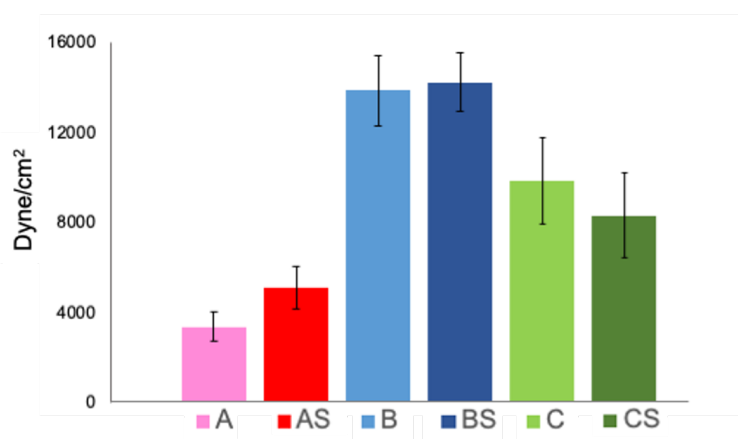


Figure 28. Bioadhesion strength values of the obtained films.

The lowest adhesion force values were obtained from films A and AS, the compositions with the highest sodium hyaluronate content (1% w/v) and with glycerol at 5% v/v. Halving the sodium hyaluronate content led to a significant increase in bioadhesion strength: in fact, C films

(glycerol v/v=5%) showed values higher than those of A films by about 2.9 times, while B films by about 4 times. The highest bioadhesion strength values were obtained from films B and BS, the compositions with the highest glycerol content (10% v/v), while presence of snail slime had no significant influence compared to the corresponding reference samples.

### Tensile tests

Tensile tests were performed on films immediately after drying using a dynamometer. Stress-strain curves were collected and the maximum stress (MPa) and the deformation at break (%) were evaluated and reported in Figure 29.

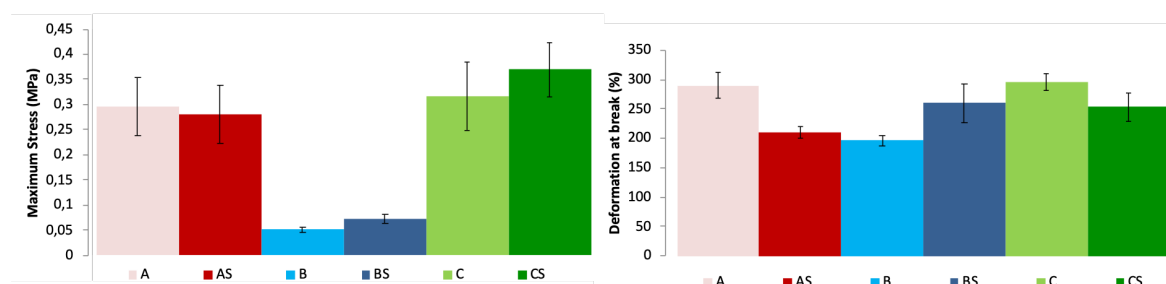


Figure 29. Maximum stress (left) and deformation at break (left) values of the obtained patches.

All films showed suitable mechanical properties, with deformation at break values exceeding 200% for all compositions. As expected, tensile strength was lower for samples B and BS, due to the high glycerol content in their formulation, which added free volume between the polymers' chains<sup>93</sup>.

### Structural characterization

The XRD patterns collected on the air-dried cellulose/hyaluronate-based films are reported in Figure 30, left: only a broad reflection at 20.0–21.5°/2θ, characteristic of cellulose II<sup>86</sup>, was detected.

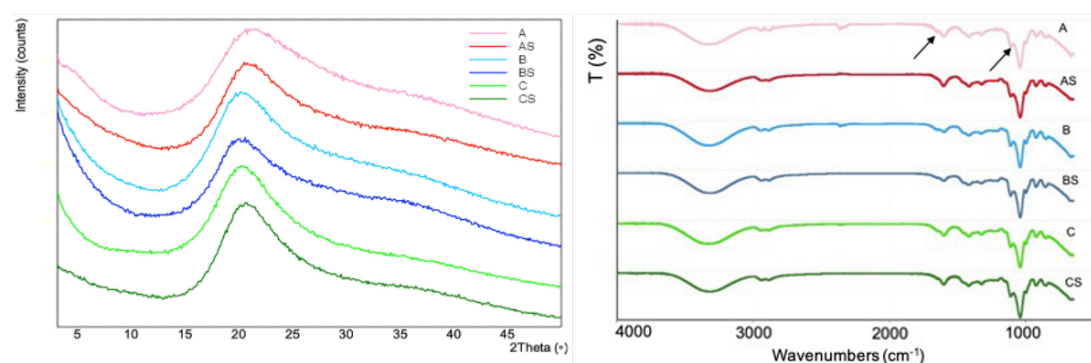


Figure 30. XRD patterns (left) and FT-IR spectra (right) of the obtained films.

The FT-IR curves (Figure 30) show the characteristic bands of cellulose at 1600 and 1413 cm<sup>-1</sup>, related to the –COO- antisymmetric and symmetric vibrations, respectively. O-H stretching band can be found at 3318 cm<sup>-1</sup>, while bands related to hyaluronate can be found at 2875 cm<sup>-1</sup>,

due to the aliphatic C-H stretching and at  $1616\text{ cm}^{-1}$ . Bands centered at  $1565$  and  $1556\text{ cm}^{-1}$  are related to the  $-\text{NH}_2$  bending while that at  $1318\text{ cm}^{-1}$  is associated to the amide I. Absorption peak at  $1151\text{ cm}^{-1}$  is related to the antisymmetric stretching of the C-O-C bridge while those at  $1072$  and  $1040\text{ cm}^{-1}$  (skeletal vibrations involving the CO stretching) are due to the saccharide structure <sup>94</sup>.

### Thermogravimetric analysis

By thermogravimetric analysis, the thermal behavior of all the film was monitored and reported in Figure 31.

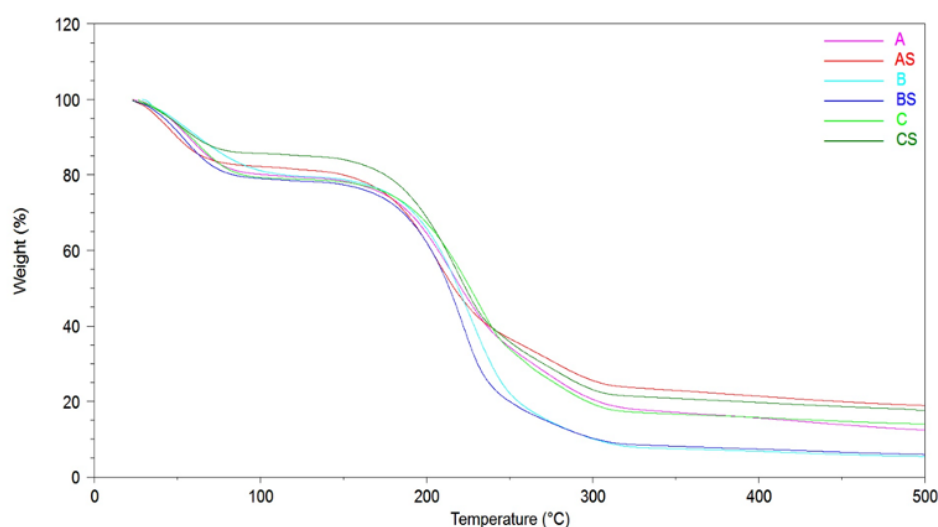


Figure 31. TGA curves of the obtained films.

All the compositions showed a similar behavior: the first weight change occurred between  $50$  and  $120^\circ\text{C}$  and it is due to the water loss. At higher temperature, between  $150$  and  $400^\circ\text{C}$ , the weight loss is mainly due to the biopolymer's degradation. The amount of loss water during the first weight change was calculated for each film and no significative difference was found among them: all the compositions had on average a percentage of water loss around  $20\%$ , which could be useful in maintaining a damp place in the area of infection and hence to avoid the formation of unwanted crusts.

### Water vapor permeability

Water vapor permeability (WVP) was calculated using Equation 7 and was used to test whether moisture can easily penetrate and pass through the patches. Allowing the passage of moisture through the film is indeed useful to avoid the dryness of the skin and the formation of crusts.

The films showed good permeability to water vapor, with WVP values ranging between  $3$  and  $4,5 \times 10^{-10}$ . No significant difference was found between the samples, suggesting that the presence of snail slime did not affect the permeability of the compositions.

## Evaluation of biopolymer-based patches biocompatibility

The toxicity of the biopolymer-based patches was evaluated on HaCat cells using two working concentrations (100% and 50%) of medium-solubilized patches. After 24 h of incubation at 37 °C, MTT assay was performed, and viability was calculated as percentage in comparison to not-treated cells.

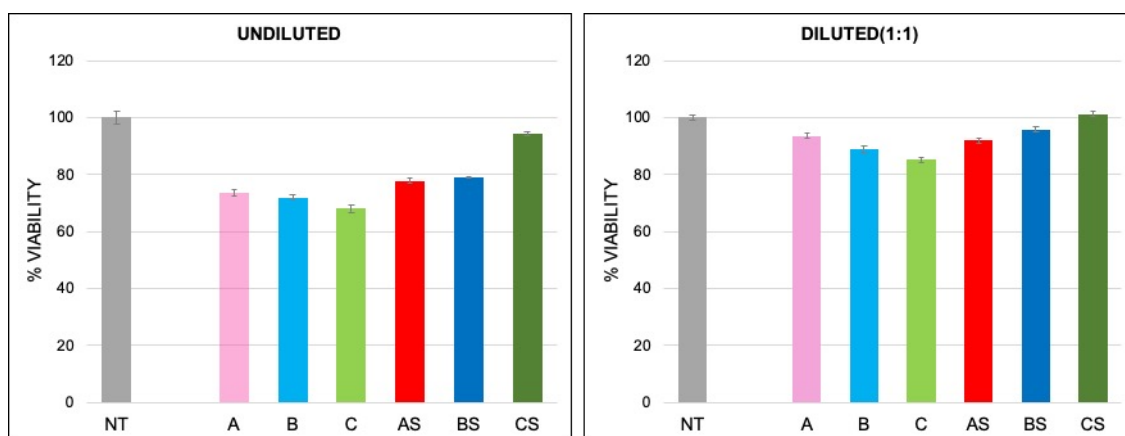


Figure 32. Evaluation of biopolymer-based patches cytotoxicity. HaCat cells were exposed to 100% (left) and 50% (right) concentrations of solubilized biomaterials for 24 h. Cell viability was calculated as percentage with respect to the untreated control.

As shown in Figure 32, no sign of cytotoxic effect was found for the samples. Cells exposed to undiluted solubilized patches without HelixComplex® exhibited viability values around 70% compared to the untreated cells, while those enriched with HelixComplex® revealed viability values over 80%, indicating that the presence of the snail slime inside the biomaterials increased their cells viability. After 1:1 dilution of the solubilized biomaterials, the cell viability reached values of viability around 89% and 96% from patches with and without HelixComplex®, respectively.

## Anti-HSV-1 activity of biomaterial

In order to evaluate if the biopolymer-based patches had an antiviral potential, the inhibition of HSV-1 replication in HaCaT cells was tested in presence of the solubilized biomaterial at 100 (undiluted) and 50% (diluted 1:1) concentrations. The time-of-drug-addiction allowed to investigate in which stage of the viral infection the biomaterial could act. Therefore, experiments were performed in three conditions: simultaneous addition of solubilized biomaterial and HSV-1 to the cells (during the infection step); solubilized biomaterial added to the cells immediately after the infection (post-infection) and left for 24 hours; and a combination of the previous conditions (during and post-infection). 24 hours after treatments, cells were harvested, and HSV-1 titration was performed to enumerate the infective viral particles. The percentage of viral inhibition was calculated with respect to the untreated

infected control. The results of viral load reduction (%) are summarized in Table 10, together with the logarithmic reduction (LR).

*Table 10. Percentages of viral load reduction of obtained patches at 100% (undiluted) and at 50% (diluted with respect to untreated control cells).*

Sample	undiluted		diluted		Sample	undiluted		diluted		Sample	undiluted		diluted	
	% reduction	LR	% reduction	LR		% reduction	LR	% reduction	LR		% reduction	LR	% reduction	LR
<b>A during</b>	68,9%	0,51	39,8%	0,22	<b>B during</b>	66,3%	0,47	40,4%	0,23	<b>C during</b>	57,9%	0,38	29,7%	0,15
<b>AS during</b>	82,5%	0,76	67,9%	0,49	<b>BS during</b>	81,3%	0,73	72,4%	0,56	<b>CS during</b>	95,6%	1,4	93,7%	1,2
<b>A post</b>	79,8%	0,69	56,2%	0,36	<b>B post</b>	78,8%	0,68	60,8%	0,41	<b>C post</b>	73,7%	0,58	44,9%	0,26
<b>AS post</b>	86,4%	0,87	74,0%	0,59	<b>BS post</b>	85,6%	0,84	72,9%	0,57	<b>CS post</b>	97,8%	1,6	96,6%	1,5
<b>A during + post</b>	77,6%	0,65	57,4%	0,37	<b>B during + post</b>	77,5%	0,64	58,9	0,39	<b>C during + post</b>	70,1%	0,52	45,4%	0,26
<b>AS during + post</b>	99,7%	2,5	99,1%	2,0	<b>BS during + post</b>	100%	4,3	99,8%	2,6	<b>CS during + post</b>	99,6%	2,3	99,3%	2,2

LR= Logarithmic Reduction.

The 100% concentrated solubilized reference patches (A, B and C) were able to decrease the viral replication when tested during the infection (68.9, 66.3 and 57.9%, respectively), post infection (79.8, 78.8 and 73.7%, respectively), and during and post-infection (77.6, 77.5 and 70.1%, respectively), compared to the not-treated infected cells. When the biomaterials were diluted (50%), the values of viral inhibition dropped to values on average around 37% in the during infection administration and around 54% in the ‘post-infection’ administration and in the during and post-infection application. The biomaterial formulated with HelixComplex® showed a significantly higher inhibition of HSV-1 replication with respect to the untreated infected cells, especially for CS samples. The treatment of cells with AS, BS and CS was able to reduce the viral load by more than 80% for each application condition, reaching even values of 99% in the ‘during and post-infection’ administration. The percentages of reduction of viral replication were significantly higher during infection and in the combined administration (during and post-infection) for biomaterial with snail slime compared to the same administration of reference samples ( $p=0.0221$  and  $p=0.0099$ , respectively). When diluted AS, BS and CS samples were added, the values of viral inhibition suffered a slight decrease, but were significantly higher than the viral inhibition reached by biomaterial without HelixComplex® ( $p=0,0216$ ;  $p=0,05$ ;  $p=0,00869$ , during infection, post-infection, and combined, respectively). The results suggest a dose-dependent activity of biomaterial: all the formulations are more active if used at full concentration in comparison to 50%. Moreover, the presence of HelixComplex® in the biopolymer patches increased the antiviral activity of the product at all steps of the viral infection (entry, release of new virions) in comparison to patches without snail mucus. The time-of-drug-addiction revealed also that the treatment of infected

cells during the infection and post-infection, acts synergistically to reach the highest viral inhibition (99.74%) suggesting that the biopolymer-based patches with HelixComplex® might interfere both with the viral entry, and the new viral particles release.

## **Conclusions**

*Herpes labialis* is a common self-limited ailment and approximately one-third of all infected patients suffer relapses. Prompt treatment can shorten the duration of eruptions and, in some cases, pain symptoms, even if it cannot be definitely healed.

Herein, a transparent labial patch for the treatment of *Herpes labialis* was produced by combining cellulose and hyaluronate with the snail slime HelixComplex®, extracted from *Helix Aspersa* snails. All the obtained films were transparent and easy to handle, without superficial defect and biodegradable. All the formulations had suitable mechanical properties and were soluble, allowing it to be disposed of in compost or washed away. Once adhered to the skin, the films remained attached for hours without drying out or detaching from the edges, important features for a labial patch. In vitro cytotoxicity assay displayed a promising safety profile, which was further confirmed by anti-HSV tests. All samples enriched with HelixComplex® were able to reduce the infection when tested against HSV-1, suggesting that their use could be very effective in the prevention and in the reduction of the disease, avoiding the infection of neighboring cells.

## 2.6 KERATIN-BASED FILMS WITH SNAIL SLIME

### Introduction

Waste from intensive farming (wool, hair, feathers, hooves, horns) is very abundant in Europe and is highly rich in keratin, but only in recent years it has been considered a renewable resource worthy of better exploitation rather than mere by-products. In fact, keratin is one of the most promising natural biopolymers for applications in several fields, ranging from cosmetics, to pharmaceuticals, to biomedical thanks to its unique molecular structure and its biological properties: indeed, it is biodegradable, biocompatible, and suitable to support cell growth, since it is also produced by epidermal cells and plays a key role in the protective function of the skin. Keratin represents one of the toughest biological materials, serving as an effective protective integument (surface layer), although it is purely composed of proteins. The inadequate knowledge of the protein' structure after interacting with other components and the poor mechanical properties of keratin-based materials, still limit their application. Usually, the use of crosslinking agents (such as formaldehyde or epoxy resins) to improve its processing and the final mechanical properties is required; however, most of the cross-linking agents are toxic and cause environmental problems. As an alternative, keratin is often mixed with different polymers, both of natural or synthetic source, since blending is one of the most feasible options improving mechanical properties and stability of keratin-based films, preserving its excellent biological activity.

Since snail slime addition strongly influenced the mechanical and structural behavior of cellulose derivatives- and chitosan- based films, the aim of this project concerns the use of regenerated keratin for the production of biodegradable, sustainable and antibacterial membranes for skin regeneration, as keratin has demonstrated to play a key role in wound healing. Indeed, an effective and rapid regeneration of skin wounds, such as burns or ulcers, continue to create incredible frustrations and expenses for the health system. While many advancements have been made in products currently on the market, there remains a need for better wound care interventions that could make wound healing more efficient and effective<sup>95</sup>. The keratin used in this project is obtained through the recovery of industrial waste materials and is extracted by sulphitholysis from raw wool by the group of Dott. A. Aluigi at CNR-ISOF of Bologna. Moreover, since proteins form brittle films without the addition of plasticizing compounds, glycerol was introduced in the patch formulation, being the best plasticizers that can be used in protein films<sup>96,97</sup>.

At present, this research is still going on and further data will be collected in order to characterize the obtained materials and to evaluate their use for wound dressing applications.

## Results and discussion

Keratin-based films were obtained by dissolving regenerated keratin in both distilled water and snail slime, using glycerol as a plasticizer. So far, only preliminary results have been obtained, including the structural characterization of keratin in powder, lyophilized snail slime and of the obtained keratin-based films. In addition, the thermogravimetric analysis of the obtained films was performed.

### Structural characterization

The XRD diffractogram of the lyophilized Madonita snail slime (Figure 33, red) showed a high number of reflections, probably due to the presence of added substances as preservatives.

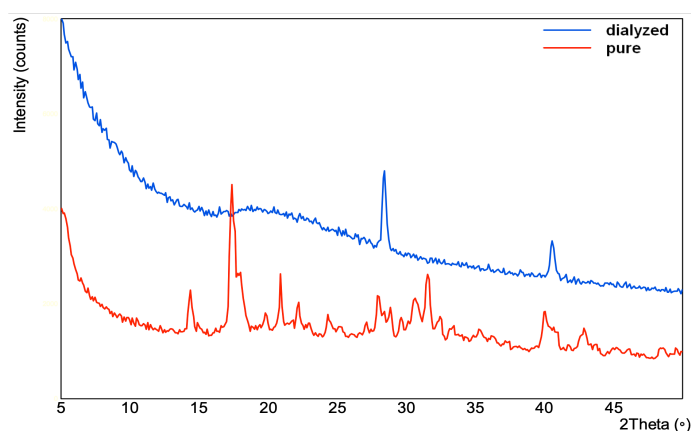


Figure 33. XRD patterns of the snail slime as received (red) and after dialysis (blue).

A dialysis was performed to remove all added substances, and the resulting XRD pattern (Figure 33, blue line) revealed the disappearance of most peaks: only a band centered around  $20^\circ/2\theta$  and two reflections at  $28^\circ$  and  $40^\circ/2\theta$  were observed. Hence, for the preparation of the films I only used dialyzed slime.

The XRD pattern of the films obtained by dissolving keratin in water and in dialyzed snail slime are reported in Figure 34.

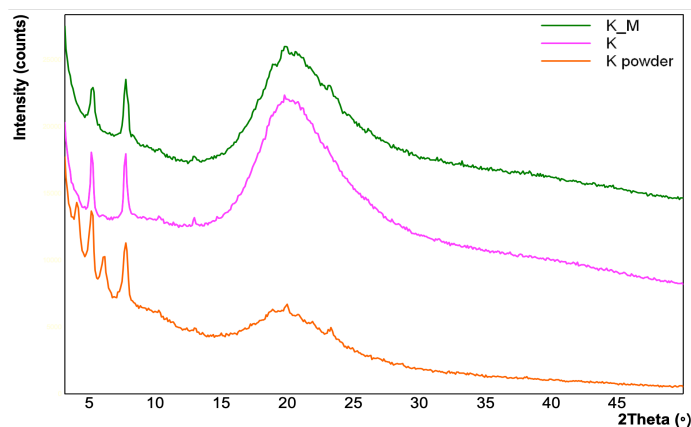


Figure 34. XRD patterns of keratin in powder (orange), keratin-based film in water (pink) and keratin-based film in dialyzed slime (green).

The diffractogram of the films obtained in water and in dialyzed snail slime are very similar, showing a broad band centered around  $20^\circ/2\theta$  and two sharp reflections at  $5^\circ$  and  $8^\circ/2\theta$ . Keratin in powder showed two additional reflections, one centered around  $4^\circ/2\theta$  and the other at about  $6^\circ/2\theta$ .

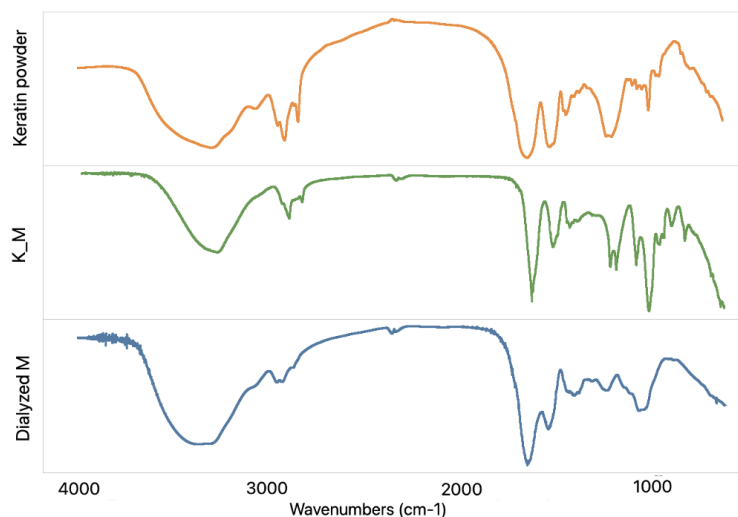


Figure 35. FT-IR spectra of keratin in powder (orange), keratin-based film in dialyzed slime (green) and of dialyzed snail slime (blue).

Infrared absorption spectrum of keratin powder (Figure 35, orange) shows characteristic absorption bands assigned mainly to the peptide bonds (-CONH): vibrations in the peptide bonds originate bands known as amide A, amide I, II and III. The amide A band at  $3288\text{ cm}^{-1}$  relates to the stretching vibration of N-H bonds; the amide I band is connected mainly with the C=O stretching vibration and occurs in the range of  $1700\text{--}1600\text{ cm}^{-1}$ , while the amide II (centered at  $1542\text{ cm}^{-1}$ ) is related to N-H bending and C-H stretching vibrations. The amide III band occurs in the range of  $1220\text{--}1300\text{ cm}^{-1}$  as result of in phase combination of C-N stretching and N-H in-plane bending, with some contributions from C-C stretching and C-O bending vibrations. Peaks at  $1195$  and  $1021\text{ cm}^{-1}$  are associated with the asymmetric and symmetric S-O stretching vibrations of the Bunte salts residues, respectively. In addition, a low intensity peak at  $2918\text{ cm}^{-1}$  relative to methylene stretching is visible.

In the FTIR spectrum of the film obtained by dissolving keratin in dialyzed slime (Figure 35, green) it is possible to appreciate an increase in intensity of the characteristic band of the slime around  $1720\text{ cm}^{-1}$  (Figure 35, blue), together with the main bands of glycerol in the region between  $800$  and  $1150\text{ cm}^{-1}$ , that are related to the vibrations of C-C and C-O bonds<sup>98,99</sup>.

### Thermogravimetric analysis

Keratin-based films were heated at  $10\text{ }^\circ\text{C}/\text{min}$  up to  $800\text{ }^\circ\text{C}$  and the derivative of weight (%) as a function of temperature is reported in Figure 36.

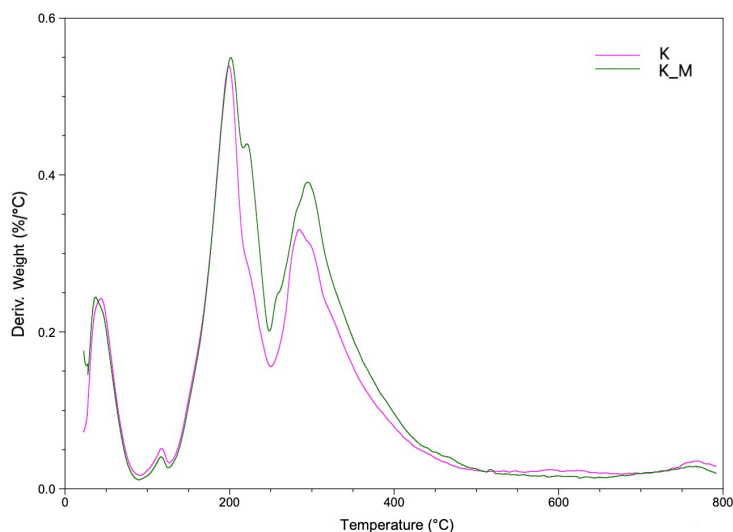


Figure 36. DTG plots of the obtained keratin-based films.

Keratin-based films prepared by dissolving both keratin in water and in slime showed similar thermal behavior, with four main thermo-oxidative degradation peaks. The first weight loss occurred in the temperature range 30–100 °C and is attributed to the loss of absorbed water, while the second and very small one, between 100 °C and 150 °C, is related to the loss of structural water. The most intense weight loss occurring around 200°C is attributable to the degradation of glycerol and it overlaps to the weight loss of keratin, which starts over 250 °C and is complete above 400°C.

### Film solubility

As reported in Paragraph 2.2.4, film solubility tests were performed by immersing 1 cm<sup>2</sup> of samples in 5 mL of distilled water at room temperature.

Both films K and K\_M were very soluble in water and dissolved within minutes. In literature, low solubility (30%) was found for keratin-based films without the addition of plasticizers, which increased up to 51% when 0.09 g of glycerol/g keratin were added<sup>100</sup>. Hence, the addition of glycerol could be used to tune the film's solubility in water; however, its presence in the film composition is required, since too fragile films are obtained without its plasticizing effect, as found in literature<sup>101</sup>.

Interestingly, when keratin-based films were immersed in CaCl<sub>2</sub> 0.1M solutions prepared both in distilled water and in HCl (pH= 4,5) they became white and insoluble for more than 1 week. Probably, the precipitation of some salts on the film's surface occurred, and XRD patterns of film after solubility tests must be acquired to confirm this hypothesis.

## **Conclusions**

Further tests shall be carried out for a complete assessment of the properties of the obtained films. In particular, the mechanical properties of the materials will be evaluated together with their bioadhesion, necessary for application as patch. A better understanding of the protein's structure may be obtained by deconvolution of IR spectra, which could also provide information on the relative content of keratin  $\alpha$  or  $\beta$  in films. Moreover, the patches' biocompatibility and their possible antibacterial activity against Gram-negative and Gram-positive strains will be assessed. In addition, wound healing tests will be carried out thanks to the collaboration with the team of Prof. Giordano of the Engineering Department (Unibo): the effectiveness of patches to promote the closure of the flaps of an open wound will be evaluated.

## 2.7 FLUCONAZOLE-LOADED FILMS BASED ON GELATIN AND SNAIL SLIME

### Introduction

In the last decades, thin polymeric films have been proposed as an alternative approach to conventional pharmaceutical forms such as creams, ointments and gels for the local delivery of drugs, both to mucosal tissue and to skin<sup>102</sup>. Topical formulations for the local delivery of drugs must provide an effective concentration and a controlled release to avoid multiple applications per day. Unlike common topical patches (medicated plasters), films do not need of an appropriate support, usually made of synthetic material, and can be designed either to be easily washed off or to resist water and to be self-adhesive<sup>4</sup> or to adhere to wet skin<sup>5</sup>.

Herein, gelatin-based films enriched with snail slime are developed, aimed to act as a biodegradable and naturally bioadhesive patches for cutaneous drug delivery.

Fluconazole, a broad-spectrum bis-triazole approved in 1990 by the Food and Drug Administration (US FDA), was selected thanks to its high antifungal activity, which make it one of the most commonly treatment option for virtually all forms of *Candida* infections in both immune competent and immune compromised hosts. The administration of Fluconazole directly on the skin provides an effective alternative to oral administration and hypodermic injection and reduces the risk of systemic side effects<sup>26,103</sup>.

In the case of fungal skin infections, an effective drug concentration must penetrate the stratum corneum, which is responsible for low drug permeability. Fluconazole is less lipophilic when compared to other antifungal imidazole-derivatives, due to the presence of two triazole rings, and presents high affinity for keratin prolonging its retention in the skin<sup>104</sup>. Therefore, the main obstacle facing the efficiency of topical Fluconazole delivery is the stratum corneum permeation<sup>105</sup>. Films prepared by mixing gelatin and snail slime were obtained through solvent casting and then characterized by means of FTIR, X-ray spectroscopy and optical and electronic microscopy. Additionally, their tensile strength, swelling properties and adhesion to skin were evaluated (See Paragraph 2.2.7). Finally, the ability of promoting the percutaneous absorption of Fluconazole and the antifungal properties of the novel patch-like platform were assessed.

### Results and discussion

The main hurdle facing the efficiency of topical antifungal drugs is their ability to penetrate the skin efficiently. Different formulation strategies have been studied to improve the Fluconazole cutaneous permeation, including microemulsion-based hydrogel, micelles and solid lipid nanoparticles<sup>26,105–107</sup>.

In this study, I investigated the characteristics of a novel film-forming patch formulation, designed starting from biomaterials as porcine gelatin and snail slime at different volume ratio,

and I evaluated its ability of promoting the percutaneous absorption of Fluconazole and its effective antifungal properties. Gelatin-based films were prepared by mixing the gelatin solution with different amounts of S (see Table 3 of Paragraph 2.2.5). Films properties were highly modified by the snail slime addition: in fact, films became more flexible, stretchable and adhesive on increasing the slime content. Therefore, Fluconazole was added to the composition containing the highest amount of slime, G\_S70. All the obtained films were transparent with a color turning more and more yellowish on increasing S content, as it can be observed by comparing the appearance of films G (Figure 37a) and G\_S70 (Figure 37b).

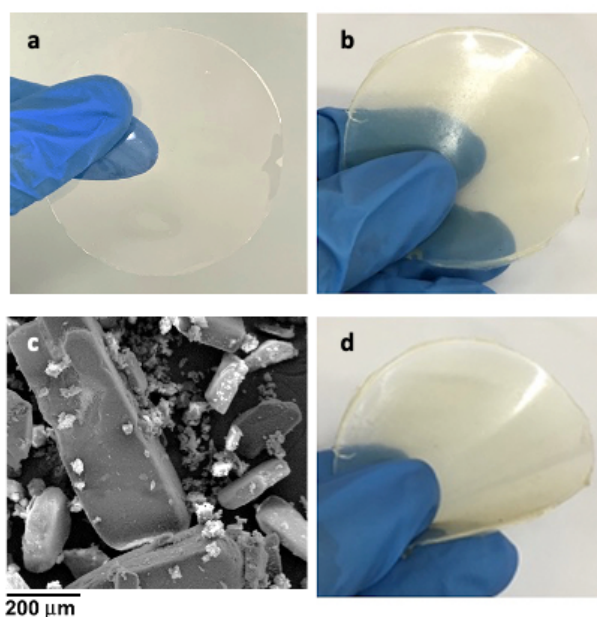


Figure 37. Digital pictures of a) G; b) G\_S70 and f) G\_S70\_g\_F; e) Scanning electron image of F crystals.

Fluconazole is a white crystalline powder having a columnar form with length between 200 and 400  $\mu\text{m}$ , as shown in Figure 37c: however, this crystalline form was no longer observed in the film formulation G\_S70\_g\_F. In fact, the drug completely solubilized in the film forming solution, giving transparent and homogeneous films in which the presence of drug crystals could not be detected (Figure 26d), suggesting the formation of an amorphous solid dispersion after the solvent evaporation. The films surfaces appeared smooth with no flaws or defects.

### Structural characterization

Literature reports the existence of at least nine different polymorphs of Fluconazole, the main ones being forms I, II, III and a hydrated form <sup>108</sup>.

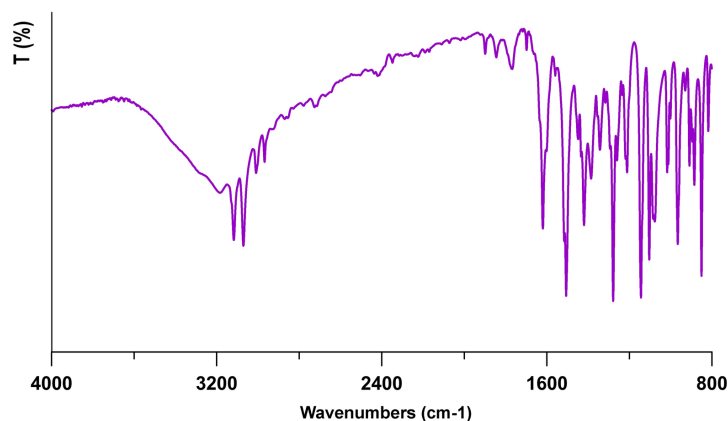


Figure 38. FT-IR spectrum of commercial F powder.

The FTIR spectrum of F (Figure 38) shows a broad band around  $3200\text{ cm}^{-1}$  due to hydrogen bonded hydroxyl group stretching vibrations, together with sharp bands between  $3100$  and  $3070\text{ cm}^{-1}$  arising from aromatic C-H stretching vibrations. Further sharp bands are also detectable: in the fingerprint region, the bands at about  $1620$ ,  $1600$  and  $1510\text{ cm}^{-1}$  are associated with the stretching of the C=C and C=N bonds present in triazole, whereas those at  $1220$  and  $1150\text{ cm}^{-1}$  arise from the stretching vibrations of aromatic C-F and from C-O belonging to a tertiary alcohol, respectively. Bands centered at  $1900$ ,  $1845$  and  $1770\text{ cm}^{-1}$  are described as overtone and combination bands consistent with 1,2,4 tri-substitution of phenyl group <sup>108</sup>.

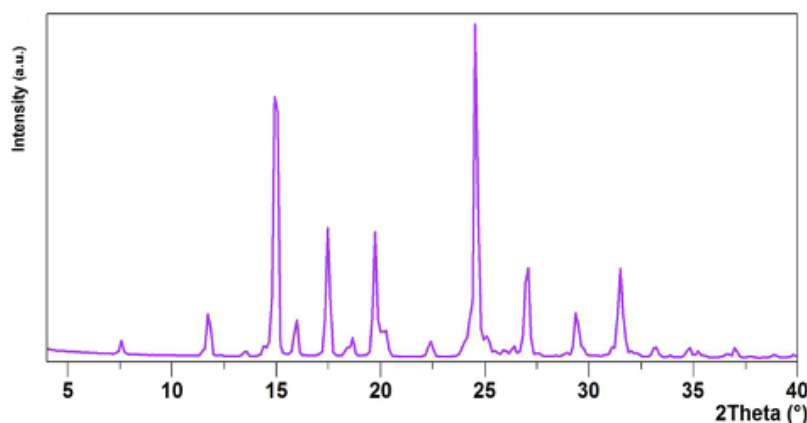


Figure 39. X-Ray diffraction pattern of commercial F powder.

Figure 39 displays the X-ray diffraction pattern of Fluconazole: the positions and relative intensities of the XRD peaks, as well as those of the infrared absorption bands, are typical of form III polymorph <sup>108</sup>.

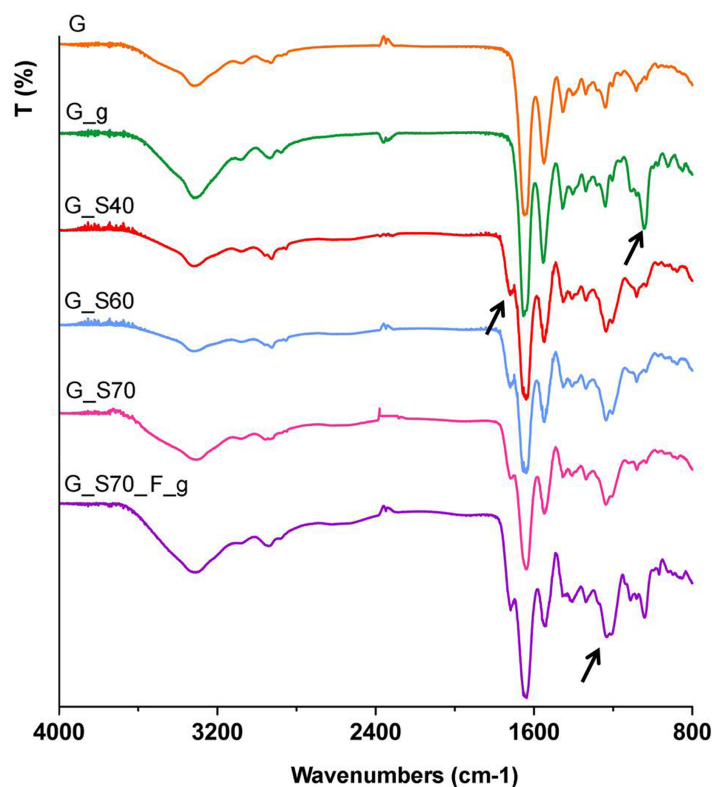


Figure 40. FT-IR spectra collected on gelatin/snail slime -based films. Arrows indicate the most prominent bands attributed to glycerol and snail slime.

In Figure 40 the FT-IR spectra of the composite films are shown, and the characteristic bands of the gelatin structure are clearly visible. In particular, the peak at  $1653\text{ cm}^{-1}$  can be ascribed to the C=O stretching of amide I, that centered at  $1550\text{ cm}^{-1}$  is associated to the NH bending of amide II, while at  $1238\text{ cm}^{-1}$  the CN stretching of amide III can be found <sup>11</sup>. The broad band above  $3000\text{ cm}^{-1}$  corresponds to the free and bound hydroxyl and amino groups, whereas the absorption band at about  $1330\text{ cm}^{-1}$  is assigned to the wagging of the CH<sub>2</sub> groups of the prolines <sup>109</sup>. The main absorption bands of glycerol appear in the  $800\text{--}1150\text{ cm}^{-1}$  region and are related to the vibrations of C-C and C-O bonds (compare G and G\_g spectra) <sup>98,99</sup>. IR spectra of the films containing different amount of snail slime are very similar to each other and show, in addition to the bands belonging to gelatin, two characteristics bands at about  $1230\text{ cm}^{-1}$  and at  $1719\text{ cm}^{-1}$  ascribable to the presence of allantoin and glycolic acid in the slime extract <sup>18</sup>. Surprisingly, addition of F did not modify the IR spectrum and the presence of the drug was not revealed by infrared spectroscopy (see G\_S70\_g\_F): this pattern differs from that recorded on G\_S70 only for the presence of the bands belonging to glycerol.

Infrared spectroscopy and X-rays diffraction were carried out also on a physical mixture of gelatin and Fluconazole, in the same relative amounts used for the films, to verify the detection limits of these techniques: obtained spectra confirmed the presence of polymorph III of Fluconazole (data not shown).

In order to confirm the drug solid state into G\_S70\_g\_F film, a structural characterization by means of X-ray diffraction was carried out and reported in Figure 41.

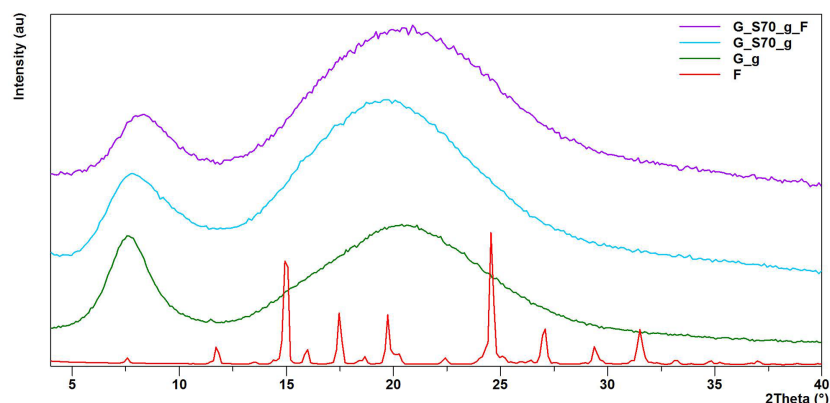


Figure 41. XRD patterns of Fluconazole and of composite films G\_g, G\_S70\_g and G\_S70\_g\_F.

Type A gelatin is characterized by a large reflection at about  $8^\circ/2\theta$  and a broad halo centered at  $21^\circ/2\theta$ <sup>110</sup>. It is known that the peak at  $\sim 8^\circ/2\theta$  is related to the diameter of the triple helix whereas the halo, corresponding to a periodicity of about 0.45 nm, is related to the distance between adjacent polypeptide strands<sup>111</sup>. Following the addition of snail extract in the film composition (G\_S70\_g), the reflection centered at about  $8^\circ/2\theta$  slightly decreased its intensity, suggesting that the reconstitution of the triple helix structure of gelatin was partially destroyed because of its interaction with the natural extract<sup>112</sup>. This leads to the hypothesis that the presence of the slime can outweigh the polymer-polymer interactions, leading to loss of structural order and, consequently, to the observed reduction in crystallinity, thus indicating the plasticizing effect of the snail slime. The diffraction pattern of G\_S70\_g\_F did not exhibit the characteristic reflections of the drug, thus supporting the hypothesis of the formation of an amorphous phase after solvent casting. Amorphous forms exhibit high level of supersaturation due to the lack of ordered crystals with high lattice energy state. However, due to their thermodynamical instability, amorphous forms show the tendency of recrystallize, thus negating the solubility enhancement and compromising the therapeutic action. It is reported<sup>113</sup> that solid dispersion of Fluconazole with selected polymers can stabilize the amorphous form of the drug, hindering its recrystallization process during storage. In order to investigate the role of gelatin, glycerol and snail slime on the solid-state transformations of Fluconazole, some parallel experiments were conducted. We found that the contemporary presence of glycerol and gelatin enhanced the drug dissolution inside the film-forming solution, which appeared clear and without evidence of residual Fluconazole crystals. However, just after solvent evaporation, films clearly showed the presence of tiny crystals grown inside gelatin layers, as it can be appreciated in Figure 42b-d.

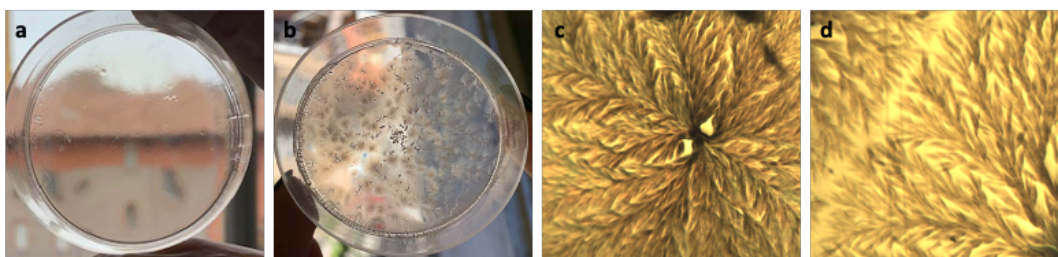


Figure 42. Digital images of films a) *G\_S70\_g\_F* and b) *G\_g\_F*; c,d) optical microscope images of crystals grown inside the film *G\_g\_F*.

The structural characterization revealed that Fluconazole recrystallized as a hydrate polymorph<sup>108</sup>, the same solid form which was obtained by solvent evaporation of the solution obtained by solubilizing the drug in acidic water (pH 4.5). These findings are very interesting because they highlight the central role of snail slime in stabilizing the amorphous form of the drug. Noteworthy, this effect lasts over time: as a matter of fact, X-rays diffraction and infrared spectroscopy performed on films *G\_S70\_g\_F* stored for 3 and 6 months at 25 °C and 50% RH (Figure 43), clearly demonstrated that the drug is still present in the amorphous solid state and the film kept its appearance and transparency.

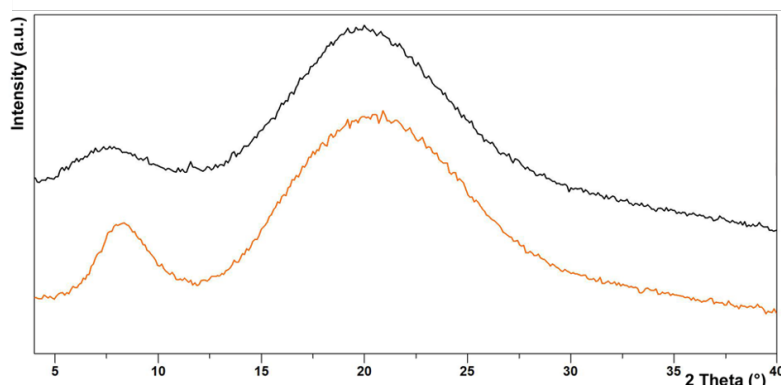


Figure 43. X-ray diffraction patterns of *G\_S70\_g\_F* after 3 (orange line) and 6 (black line) months of storage.

This phenomenon could be explained by the interactions that gelatin and the snail extract (which is a heterogeneous aqueous mixture containing proteins, collagen, allantoin, mucopolysaccharides and glycolic acid) form with the drug, acting as “amorphous polymer carriers”. In fact, according to the literature, amorphous solid dispersions of polymers such as PVP, PVP-VA, HPMC, chitosan and gelatin may increase the solubility and/or the dissolution rate of poorly water-soluble drugs, maintaining a sufficient level of supersaturation over storage<sup>114–116</sup>.

### Thermogravimetric analysis

The amount of moisture in the film could be crucial as it affects the mechanical strength, adhesive properties and friability of film. TGA analyses were performed on *G*, *G\_g*, *G\_S70\_g*

and G\_S70\_g\_F, and the amount of adsorbed water was evaluated from the first loss up to 130 °C. G films contained up to 15% w/w of water, while those added with glycerol retained a lower content, 11% w/w, which decreased to 8% when glycerol and S were both present into the formulation. Films containing Fluconazole had the lowest amount of adsorbed water: about 2%. It can be inferred that water content has a minor effect on the mechanical properties of films with respect to S addition.

### Tensile tests

The mechanical properties of the films, in terms of maximum stress  $\sigma_{max}$  (MPa), Young's modulus E (MPa) and deformation at break  $\epsilon_b$  (%), were evaluated and reported in Figure 44, together with the sample thickness.

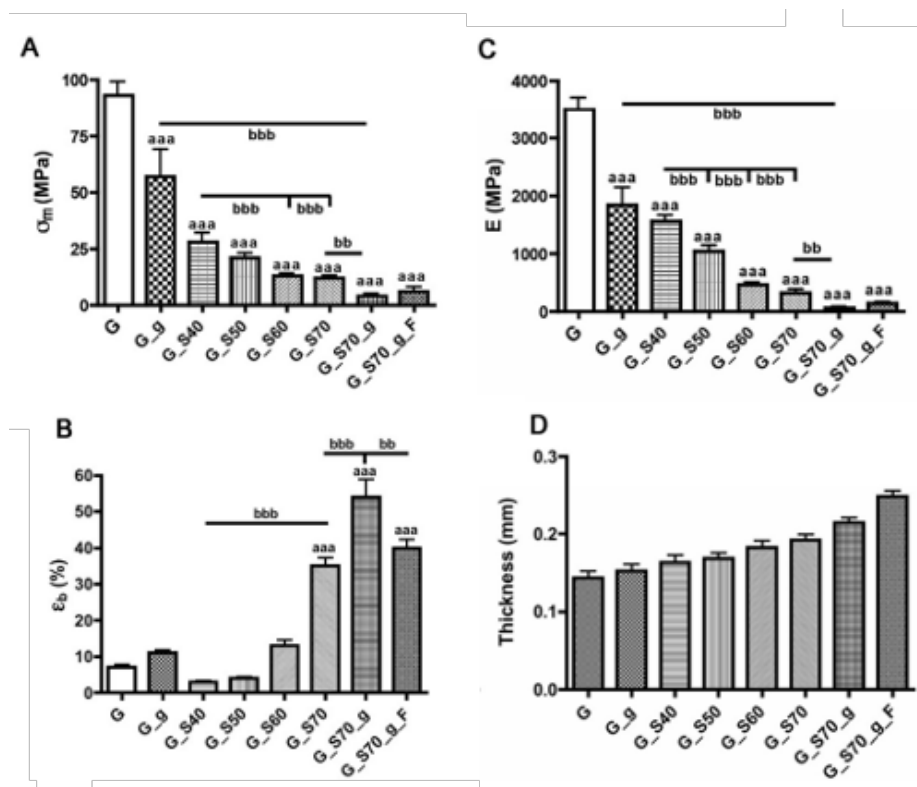


Figure 44. A-C: Mechanical properties of gelatin-based films: A) maximum stress at break (aaa  $p < 0.001$  compared to G; bbb  $p < 0.001$  G\_g vs G\_S70\_g, G\_S40 vs G\_S60 and G\_S40 vs G\_S70); B: Elongation % at break (aaa  $p < 0.001$  compared to G; bbb  $p < 0.001$  G\_S40 vs G\_S70, G\_S70 vs G\_S70\_g and bb  $p < 0.01$  G\_S70\_g vs G\_S70\_g\_F); C: Elastic modulus (aaa  $p < 0.001$  compared to G, bbb  $p < 0.001$  G\_g vs G\_S70\_g, G\_S40 vs G\_S50, G\_S40 vs G\_S60 and G\_S40 vs G\_S70); D: Thickness of gelatin-based films.

Snail slime addition produced a dramatic effect on the tensile properties of the films, as clearly evidenced by graphs reported above. As a matter of fact, an impressive decrease of the maximum stress  $\sigma_{max}$  and of the elastic modulus E was observed after the addition of even the lowest amount of S (G\_S40) (aaa:  $p < 0.001$  compared to G film) and the values of these parameters decrease on increasing S content (aaa:  $p < 0.001$  compared to G film). Ongoing from

G to G\_S70 films, the values of  $\sigma_{\max}$  and E drop by a factor of about ten, while no significant difference was observed between G\_S70, G\_S70\_g and G\_S70\_g\_F ( $p>0.05$ ), thus elucidating that the introduction of Fluconazole and/or glycerol did not affect the maximum stress and the elastic modulus of the films. The deformation at break (Figure 44B) slightly decreases up to G\_S50 and then increases up to G\_S70, reaching a value about 5 times greater than that of G (aaa,  $p<0.001$ ). Therefore, it can be inferred that the “plasticizing effect” of snail slime increases with its content (bbb,  $p<0.001$  for G\_S40 compared with G\_S70), providing the films with increasing elongation at break. The reason why this trend was not maintained at relatively low S content is not very clear but might be due to different interactions that occur between the polymer and the components of the slime when mixed in different proportions. As expected, the presence of glycerol significantly reduced the maximum stress (e.g., the  $\sigma_{\max}$  of G\_S70 is about 3 times higher than that of G\_S70\_g; bb,  $p<0.01$ ) and the elastic modulus, while it enhanced the deformation at break, thus amplifying the effect due to S addition (aaa,  $p<0.001$  for G\_S70 and G\_S70\_g compared to G). Moreover, the presence of glycerol affects the deformation at break (G\_S70 compared to G\_S70\_g; bbb,  $p<0.001$ ) in agreement with its plasticizer effect. In fact, being glycerol a polyhydroxy-alcohol with small molecules, it can easily enter the protein matrix to interact with polar amino acids and form hydrogen bonding involving hydroxyl groups, which could alter the forces holding the protein chains together and add free volume between them<sup>93</sup>. Addition of the drug provoked a small increase of the values of stress at break and elastic modulus together with a slight decrease of the deformation at break, probably due to the lower water content with respect to G\_S70\_g. Finally, film's thickness (Figure 44D) increased on increasing the amount of S, according to the larger amount of solid matter: in fact, snail slime is a mixture of proteins, glycolic acid, allantoin, which represent about a 5% (w/v) of dry matter.

### **Swelling degree**

Considering that this film is intended for skin application, swelling of the drug-loaded polymeric film may play an important role on both bioadhesion and controlled drug release<sup>8</sup>. In fact, hydrophilic polymers with different structures possess a varying degree of swelling, based on the relative resistance of matrix network structure to water molecules movement. This may be due to the formation of hydrogen bonding among the polymeric matrix and the other additives: glycerol, snail slime and the drug. The swelling degree of the films as a function of snail mucus content, glycerol and Fluconazole was measured in PB at a pH value of 4.5 and reported in Figure 45.

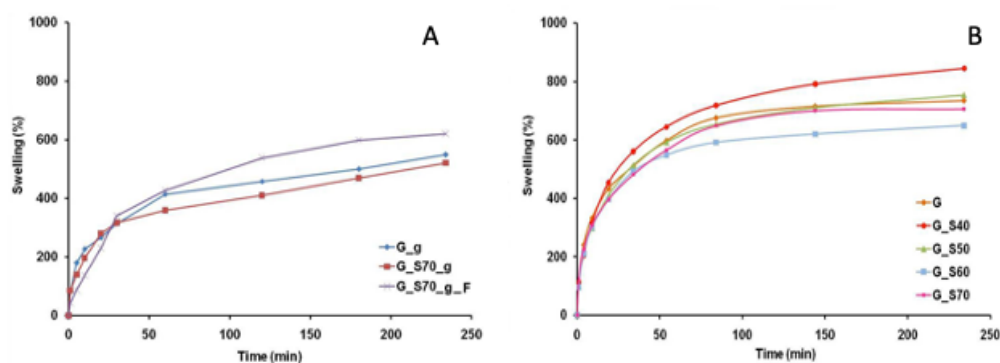


Figure 45. Swelling curves of the gelatin-based films: a) influence of snail slime and b) influence of glycerol and drug addition.

As shown in figure, the swelling of all samples gradually increased up to about 150 min, when it reached an almost constant plateau. The presence of the snail slime did not seem to significantly affect the swelling properties of the films ( $p > 0.05$ ) and a clear trend as a function of the slime content could not be found. All the samples containing glycerol showed a marked reduction of the swelling degree compared to those without glycerol, indicating the formation of strong interactions between glycerol and gelatin. The addition of S at 70% to G\_g (Figure 45A), as well as the addition of Fluconazole, did not significantly modify the swelling ability with respect to the G\_g film.

### Bioadhesive properties

Skin adhesion is one of the most important functional property for a skin drug delivery system. Gelatin and snail lime-based films G\_S70 and G\_S70\_g\_F are slightly adhesive to the touch, but they behave like patch only wetting their surface in contact with the skin. Therefore, such films, once removed from the primary packaging, might be used simply by wetting the skin with water (few droplets) and then applying the film by light finger pressure to allow its adhesion. Moreover, the films ability to remain attached to the skin for several hours was tested up to 8 h: as an example, Figure 46b shows a digital picture of G\_S70\_g film attached to the skin of a hand by means of few drops of water, immediately after adhesion and 8 h later. Film is highly performant and keeps its adhesive force over time.

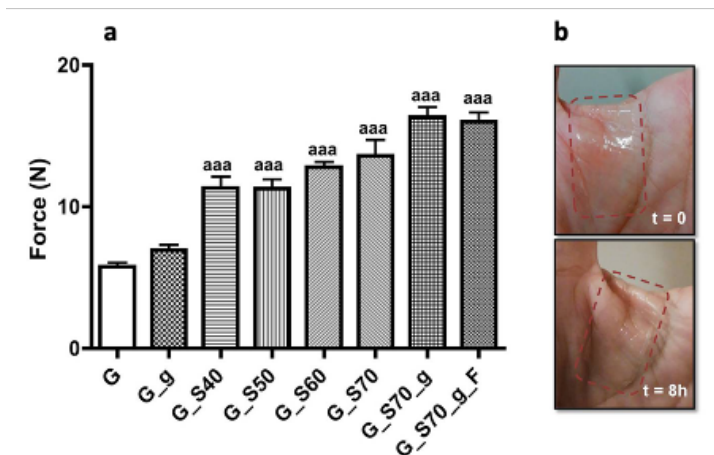


Figure 46. Adhesive strength values of the films expressed as Force (N)  $\pm$  SD (aaa:  $p < 0.001$  all samples compared to G; b:  $p < 0.05$  for G\_S70 vs G\_S70\_g); b) Digital pictures of G\_S70\_g film adhered to the skin of a hand immediately after adhesion ( $t = 0$ ) and after 8 h.

The results of the adhesion strength measurements, expressed as the Force (N) necessary to detach the film adhered to the skin, are shown in Figure 46a. The trend suggests that increasing quantities of slime increase bioadhesion. The film with the best adhesive capacity is that with the higher amount of S, G\_S70, with a value more than 2 times higher than G (aaa:  $p < 0.001$ ). As highlighted by the histogram, also glycerol was able to increase the adhesive capacity of the samples containing S: in fact, 17% more strength was required to detach the films G\_S70\_g from the skin when compared to G\_S70 ( $p < 0.05$ ). Interestingly, even if the adhesion capacity of the G\_g film is higher than that of the G film, it is lower compared to G\_S40, suggesting that snail slime played a major role on promoting adhesion. On the other hand, the presence of the drug did not significantly affect the adhesive ability of the film. In general, all the obtained films showed good detachment forces from the skin, guaranteeing their adhesion to the skin without the addition of glues, like pressure sensitive adhesives generally used in patch development.

### ***In vitro* permeation studies**

To assess the permeation profile of Fluconazole from the film, the effective amount of F loaded into the film was first assessed. The experimental drug content was  $4.53\% \pm 0.07$  w/w (corresponding to  $1.84 \pm 0.05$  mg/cm<sup>2</sup>) very close to the theoretical one (4.76% w/w), suggesting that the preparative method allowed to obtain a homogenous drug distribution within the formulation. Permeation results obtained from film G\_S70\_g\_F were compared with a control solution containing a drug concentration of  $4.14 \pm 0.02$  mg/mL. Ethanol (20% m/V) was added in the control solution to prevent F precipitation, since the drug saturated solubility in pH 5.5 phosphate buffer solution at 25 °C was  $5.05 \pm 0.05$  mg/mL, very close to the reported water solubility (4.37 mg/mL). The drug solubility increased up to  $16.43 \pm 0.85$  mg/mL in the

control solution. The same solution was used in the receiver compartment to ensure sink conditions in the permeation experiments and the drug concentration did not exceed 20% of the saturated solubility ( $20.07 \pm 1.09$  mg/mL).

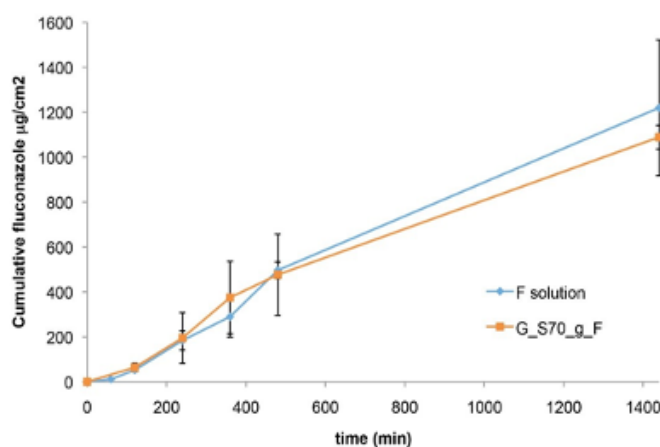


Figure 47. Cumulative Fluconazole concentration permeated through pig ear skin: G\_S70\_g\_F (orange) and F solution (blue) as a control (0.45% w/V solution of F in PB supplemented with 20% w/w EtOH corresponding to the same amount of F loaded into the film).

Analyzing the permeation results, the amount of permeated drug from the solid formulation was superimposable to that of the drug in solution (Figure 47). In particular, in both systems the cumulative amount of F permeated through the skin was about  $60 \mu\text{g}/\text{cm}^2$  (corresponding to 5% of F) after two hours,  $200 \mu\text{g}/\text{cm}^2$  after 4 h and approximately  $500 \mu\text{g}/\text{cm}^2$  in 8 h. After 24 h the drug permeation reached  $1000 \mu\text{g}/\text{cm}^2$ , corresponding to 60% of F loaded into the film. These results evidence that the film formulation enhanced the drug permeation into the skin layer, displaying a similar behavior to the control solution containing 20% of ethanol w/V, which is known for its penetration enhancement property<sup>117</sup>. A possible explanation of the film behavior can be related to the different thermodynamic activity of the examined samples. The drug loaded film formulation (G\_S70\_g\_F) is an example of a supersaturating drug delivery system. As reported in the Section “Structural characterization”, the obtained film is an amorphous solid dispersion, which demonstrated a supersaturation stability for 6 months, unlike the films without snail slime, in which Fluconazole quickly recrystallized. On the other hand, the control solution contains the drug at a lower concentration than its saturated solubility ( $16.43 \pm 0.85$  mg/mL). Thus, for the control solution, the permeation profile of F across the skin is promoted by the enhancer, mainly through a lipid extraction mechanism<sup>118</sup>, rather than by the thermodynamic activity of the subsaturated drug solution. In contrast to chemical penetration enhancers, like ethanol, supersaturation has proved to increase skin penetration without alteration of the *stratum corneum*<sup>119</sup>. The increased thermodynamic activity associated to the supersaturation degree of the film formulation might be a valid explanation of the permeation behavior of the drug. In fact, the film maintained a sufficient level of

supersaturation over the analysis time, ensuring complete dissolution and good permeation. Thus, the hybrid film containing the biopolymer and the snail slime might represent an effective drug delivery system to the skin. Finally, the amount of drug accumulated in viable skin measured at the end of the experiments were  $9.6 \pm 0.6\%$  (corresponding to  $176.0 \pm 11.1 \mu\text{g}/\text{cm}^2$ ) and  $6.8 \pm 1.9\%$  (corresponding to  $140.8 \pm 39.1 \mu\text{g}/\text{cm}^2$ ) for film and solution, respectively, indicating a certain drug accumulation into the skin.

### Antimicrobial tests

The Fluconazole-loaded gelatin films were tested *in vitro* for the evaluation of the antifungal activity against the reference strain *C. albicans* ATCC 10231 and 10 clinical isolates of *Candida spp.* Unloaded gelatin films (based on plain gelatin and on the gelatin and snail slime mixture) as negative controls and Fluconazole paper disks as positive controls were included in each experiment.

Table 11. Measurements of the inhibition zone diameters (mm) detected for unloaded and Fluconazole-loaded gelatin films.

	G g	G S70 g	G S70 g F	F
<i>C. albicans</i> ATCC 10231	N.A.*	N.A.*	$26,5 \pm 0,6$	$25,6 \pm 0,6$
<i>C. albicans</i> (n = 2)	N.A.*	N.A.*	$23,5 \pm 4,7$	$23,6 \pm 2,1$
<i>C. glabrata</i> (n = 2)	N.A.*	N.A.*	$24,5 \pm 1,3$	$25,0 \pm 0,9$
<i>C. parapsilosis</i> (n = 2)	N.A.*	N.A.*	$23,5 \pm 0,7$	$22,7 \pm 1,2$
<i>C. tropicalis</i> (n = 2)	N.A.*	N.A.*	$22,0 \pm 1,8$	$22,6 \pm 1,8$
<i>C. krusei</i> (n = 2)	N.A.*	N.A.*	$21,5 \pm 2,4$	$23,1 \pm 1,6$

Values are mean and SD of two independent experiments performed on the reference strain and on two isolates for each *Candida spp.*

\*N.A.= Not Appearing.

Table 11 reports the diameters of the inhibition growth zones, measured around the tested disks and the Fluconazole control (300  $\mu\text{g}$ ). As expected, the unloaded films did not display any antifungal activity. No statistically significant differences between G\_S70\_g\_F and the positive control were observed on the two sets of measurements. These results agree with the permeation studies and are attributable to the supersaturating status of the novel film formulation. Therefore, Fluconazole-loaded gelatin and snail slime-based films, containing 320–360  $\mu\text{g}$  of drug, proved to be effective towards *Candida spp.* as well as the positive control, indicating that the drug loaded into the film quickly dissolved and diffused through the agar maintaining its high potency and with the same activity of the drug solution.

### Conclusions

A new film-forming patch based on gelatin and snail slime for the local delivery of Fluconazole was successfully developed. Film properties significantly depend on the amount of snail slime:

in particular, formulations with the higher content of S were more flexible and stretchable and the presence of the slime provided the films with the desirable adhesive properties towards the skin. Films were easy to handle and, once applied to the skin, the adhesion was provided for more than 8 h. The film containing the largest volume of extract was selected as potential delivery platform of Fluconazole. The presence of snail slime promoted drug solubilization into the film forming solution and hindered Fluconazole recrystallization inside the film. Furthermore, snail mucus was crucial in stabilizing the amorphous form over the time, until 6 months of storage. Patches containing Fluconazole demonstrated an effective antifungal activity against all the tested *Candida* strains and promoted the drug permeation across the skin. In conclusion, the novel patch-formulation based on natural and biodegradable materials can adhere to wet skin, promoting Fluconazole permeation, and can be easily washed off, avoiding waste, or thrown into compost after use.

## 2.8 MUCOADHESIVE GELATIN-BASED FILMS LOADED WITH ECONAZOLE

### Introduction

In the last decade, vaginal films have received a great deal of attention with respect to traditional vaginal dosage forms such as creams, gels and vaginal suppositories<sup>120</sup>. Good retention ability, bio-adhesiveness, negligible discomfort, low cost, easy storage, decreased product leakage, ease of administration and wide formulation flexibility are the main interesting features of these thin strips<sup>121</sup>. Vaginal films have been formulated using a variety of polymers, both semi/synthetic and natural, such as polyacrylates, cellulose derivatives, polyvinyl alcohol, carrageenan, pectin and chitosan<sup>122–125</sup> and, among them, gelatin is very promising.

Beside to the prolonged residence time at the site of infection, for effective local vaginal delivery of therapeutic agents, the dosage form needs to control the release of the active substance, while assuring its minimum effective concentration. Econazole nitrate (ECN) is an imidazole antifungal agent widely used for the treatment of mucosal candidiasis since its transmucosal absorption is negligible; thus, it could be useful for a topical therapy of vaginal candidiasis. However, the ECN poor water solubility along with the limited volume of the vaginal fluid (it was reported to be in the range of 2–3 g/24 h and it is decreasing with increasing age<sup>121</sup>) can compromise the drug availability<sup>126,127</sup>.

Several strategies and different dosage forms have been explored to assure ECN concentrations significantly higher than its minimum inhibitory concentration (MIC) for a prolonged time. Polymer-lipid based mucoadhesive microparticles were designed as innovative vaginal delivery systems for ECN able to enhance the drug antifungal activity<sup>128</sup>. Another approach used to optimize the dissolution process of a different hydrophobic microbicide and thus its bioavailability, was to develop vaginal films as an amorphous solid dispersion of the drug in a hydroxypropyl methylcellulose and polyethylene glycol 400 mixture<sup>129</sup>. Other strategies to overcome the limitations of conventional therapy include nano-formulations. In particular, nanoparticles-in-film formulation have been considered for the vaginal administration of various microbicide drugs<sup>130</sup>. More recently, a new ECN loaded chitosan-coated nano-capsule carrier, which might be used to load films, has been developed for the treatment of vaginal candidiasis<sup>131</sup>.

The aim of this study was to develop an innovative vaginal mucoadhesive delivery system able on one hand to enhance the solubility of ECN, and thus its effective concentration at the site of action, and on the other to achieve a sustained drug release. Specifically, different ECN solid dispersions (SD) were prepared and characterized using different polymers (Soluplus®, PVPs and Gelucire® 50/13) and loaded into gelatin-based films. As described in the Experimental

part (Paragraph 2.2.6), vaginal films were produced by solvent casting comprising either raw ECN or the corresponding SD. Crosslinked films by means of genipin (2% w/w) were also prepared for comparison purpose. Morphological and structural characterizations of the films were performed by means of scanning electron microscopy (SEM) and X-ray diffraction (XRD). Moreover, their mechanical, swelling and mucoadhesive properties as well as their *in vitro* drug release behavior were assessed. Finally, the antifungal activity of the developed films was evaluated *in vitro* against *Candida albicans* reference strain and clinical isolates recovered from human specimens. Effects of the films on cell viability and cell damage were assessed on a human genital epithelial cell line using two different assays.

## **Results and discussion**

In the development of controlled release bioadhesive systems, both drug release control and swelling capability play an important key role. Films should also ensure appropriate concentration of the active ingredient at the site of application according to the treatment. Therefore, with the aim of improving the drug solubility and, consequently, its potential bioavailability, I first studied the effect of several polymers on the ECN solubility by designing three different solid dispersions, which were then loaded into gelatin films for vaginal application and compared to the neat drug-loaded films. In particular, the influence of different drug solid dispersions and of a cross-linker additive on the properties of the gelatin matrix were investigated.

### **Characterization of the ECN solid dispersions**

Solid dispersions (SD) are widely used to improve the bioavailability of poorly water-soluble drugs<sup>132</sup>. SD increase drug bioavailability owing to different mechanisms, which involve either the conversion of the crystalline drugs into amorphous forms or the formation of nanocrystalline phase using hydrophilic polymers (such as PVP and HPMC), or through the enhancement of drug wettability, dispersibility and supersaturated solubility by means of amphiphilic carriers<sup>133</sup>. In this study, polymers with different physical-chemical characteristics for solid dispersion production, as PVP, Soluplus®, and Gelucire® 53/10 were tested for their ability to solubilize ECN. In particular, a blend of Kollidon® 30 and Kollidon® VA64, also known as copovidone, was selected as amorphous hydrophilic polymer able to form water soluble complexes and as amorphous APIs stabilizer<sup>134,135</sup>, especially using PVPs blends<sup>136</sup>. Soluplus® is an amorphous polymer with an amphiphilic chemical structure able to solubilize poorly soluble drugs in aqueous media<sup>137,138</sup>. Conversely, Gelucire® 50/13 is a semisolid waxy semi-crystalline material with amphiphilic nature used as solubilizer for poorly soluble compounds due to its property of forming micelles/self-emulsifying systems<sup>133,139,140</sup>.

The solubility of pure ECN in PB pH 4.5 was  $331 \pm 6 \mu\text{g/mL}$  due to the acidic pH, which favored the solubilization of the weakly basic drug (Table 5 of Paragraph 2.2.6). All the SD increased the drug solubility: Kollidon® and Soluplus® increased the ECN solubility 3.4 times ( $1114 \pm 182 \mu\text{g/mL}$ ) and 2.5 times ( $813 \pm 46 \mu\text{g/mL}$ ), respectively, while Gelucire® 50/13 increased the drug solubility of 9.2-fold ( $3064 \pm 159 \mu\text{g/mL}$ ). Therefore, this additive demonstrated the higher ability in solubilizing ECN.

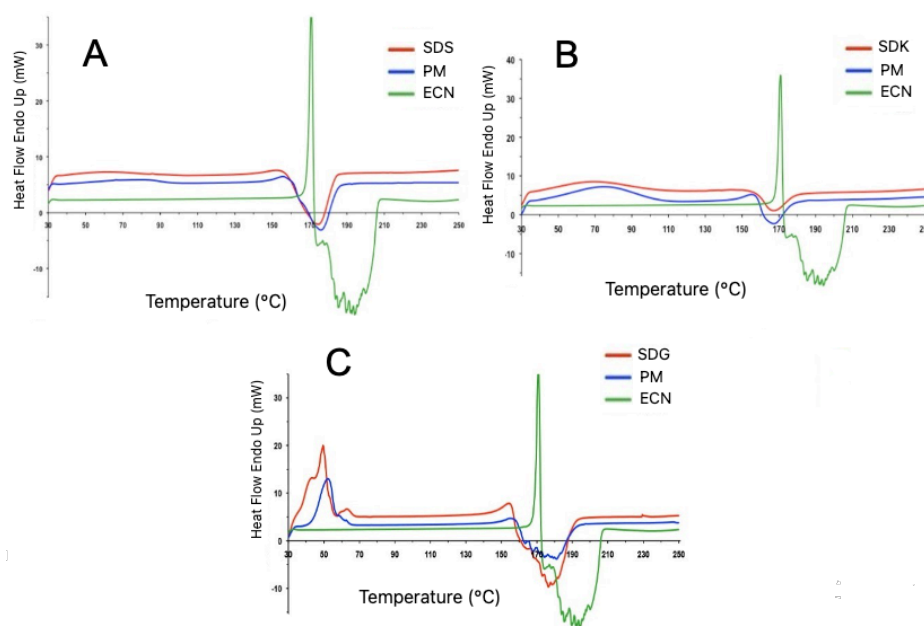


Figure 48. DSC curves of ECN-SD (red line), pure ECN (green line) and of the corresponding physical mixtures (PM, blue line).

In order to detect possible drug solid state modifications during the SD preparation, characterization of the ECN-SD was carried out by means of DSC (Figure 48A-C) and XRD (Figure 49A-C). Raw ECN showed an endothermic peak with a maximum at about 168 °C followed by a large and irregular exothermic peak, which made the endotherm quantification difficult<sup>128</sup>. Both PM and SD showed a lowering and broadening of the drug endothermic peak with respect to ECN. In particular, the melting peak of the drug shifted to about 156 °C for all PM, reached slightly lower values for SDG (about 154 °C, Figure 48C) and was practically undetectable for SDS (Figure 48A) and SDK (Figure 48B). This modification may be due to the partial solubilization of the drug into the polymer during the DSC scan (hence justifying the similar behavior of the PM). In fact, ECN may partially solubilize either in the molten Gelucire at about 60 °C<sup>128</sup>, or in the polymeric carriers, since their T<sub>g</sub> values are lower than the melting point of ECN (T<sub>g</sub> = 70 °C, 149 °C and 101 °C for Soluplus, Kollidon 30 and VA64, respectively)<sup>141</sup>. On the other hand, the lowering and broadening of the ECN endothermic peak could be related to the presence of a drug nano/micro crystalline phase within the SD, as

previously reported in literature <sup>142</sup>. In order to better define the solid state of the ECN within the SD, samples were analyzed by X-rays diffraction.

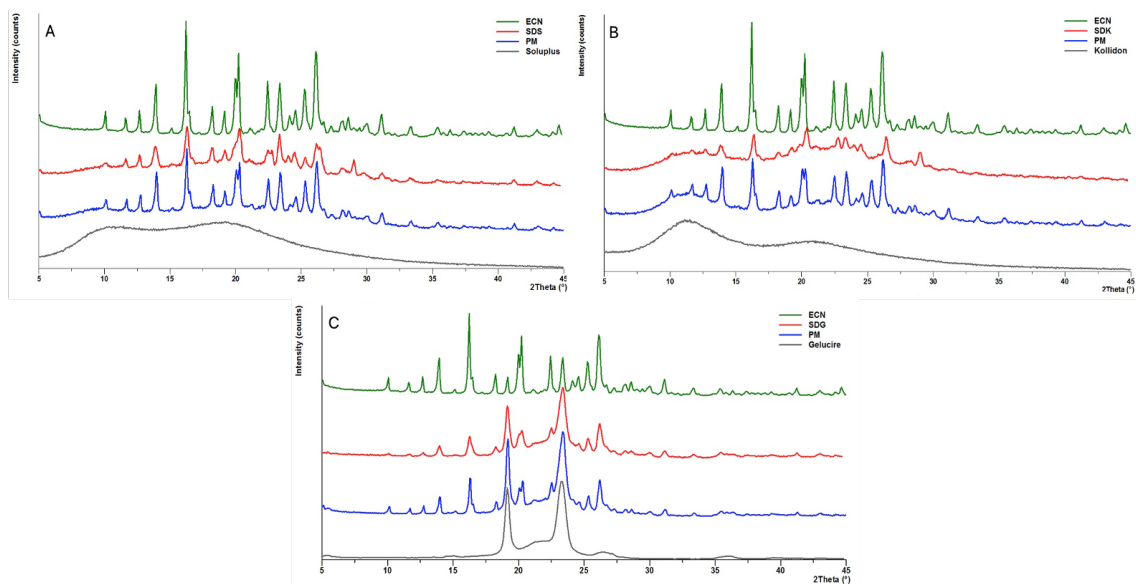


Figure 49. XRD patterns of additives (black line), physical mixtures (PM, blue line) and of ECN-SD (red line) compared to that of pure ECN (green line).

The diffraction patterns of SDS (Figure 49A) and SDG (Figure 49C) samples displayed the permanence of the ECN crystalline structure; the reduced intensity of the reflections may be simply due to drug-additive blend (1:2 w/w ratio). Regarding SDK (Figure 49B), a certain reduction of the drug crystallinity could be appreciated since the majority of the reflections decreased in intensity and those at about  $26^\circ$  and  $32^\circ/2\theta$  completely disappeared. Thus, despite the partial drug amorphization using PVPs, the SD with Gelucire 50/13 showed the highest enhancement in drug solubility, while maintaining the drug crystallinity. These results suggest that the solubility improvement was not related to the drug solid state in the SD, but rather to the ability of the amphiphilic carrier to increase API solubility as a result of the formation of a micellar dispersion <sup>143,144</sup>.

### Characterization of vaginal films containing the SDs

Gelatin-based films containing either the drug or the SD were then prepared at 10% w/w ECN. In a recently published paper, it was found that ECN was able to interact with gelatin by base-acid reaction between the basic  $\epsilon$ -amino groups of gelatin residues and the acidic hydrogen of ECN, resulting in transformation of econazole nitrate into econazole, EC <sup>145</sup>. Since this topotactic transformation occurred during film preparation, films containing the SD were characterized to evaluate the eventual drug modification, even in the presence of polymers.

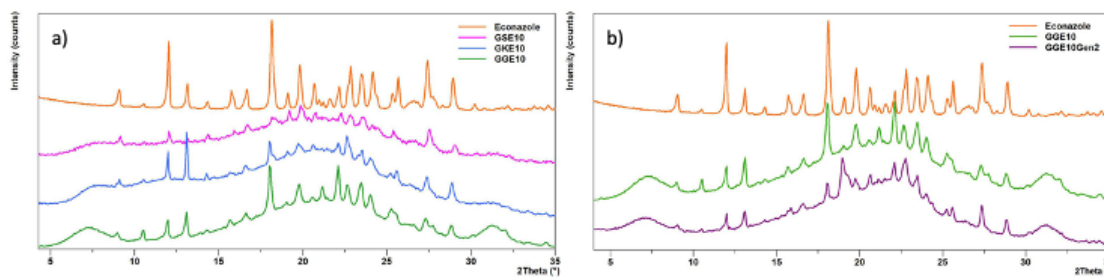


Figure 50. XRD analysis of a) EC powders (orange line) and of gelatin-based films: GGE10 (green line), GKE10 (blue line) and GSE10 (pink line); b) XRD patterns of EC powder (orange line) compared to those of GGE10 (green line) and GGE10gen (purple line).

Figure 50 reports XRD patterns of the films compared to the pattern of EC as reference: all the reflections matched with those of EC powder (orange line), thus confirming that the presence of additives did not prevent the base-acid interaction between ECN and gelatin.

Films should also display a suitable mechanical behavior; thus tensile properties of films were evaluated. The values of stress at break ( $\sigma_b$ ), deformation at break ( $\epsilon_b$ ) and Young's Modulus (E) are reported in Table 12.

Table 12. Thickness, stress at break  $\sigma_b$ , strain at break  $\epsilon_b$  and Young's modulus, E; of gelatin-based films. Each value is the mean of ten determinations and is reported with its standard deviation.

Films	Thickness ( $\mu\text{m}$ )	$\sigma_b$ (Mpa) $\pm$ SD	$\epsilon_b$ (%) $\pm$ SD	E (Mpa) $\pm$ SD
G	91	93 $\pm$ 6	7 $\pm$ 2	3600 $\pm$ 200
GG	115	40 $\pm$ 5	5 $\pm$ 2	1630 $\pm$ 250
GK	105	37 $\pm$ 8	2.0 $\pm$ 0.4	2500 $\pm$ 300
GS	101	30 $\pm$ 7	3.0 $\pm$ 0.3	2090 $\pm$ 160
GE10	110	83 $\pm$ 7*	8 $\pm$ 2*	3640 $\pm$ 250*
GGE10	115	56 $\pm$ 6	11 $\pm$ 2	2070 $\pm$ 140
GKE10	107	67 $\pm$ 5	7 $\pm$ 2	2300 $\pm$ 200
GSE10	102	73 $\pm$ 7	7 $\pm$ 2	2700 $\pm$ 240
GE10gen	98	78 $\pm$ 10*	6 $\pm$ 1*	3400 $\pm$ 200*
GGE10gen	100	62 $\pm$ 10	4 $\pm$ 1	2640 $\pm$ 240

\*Data from literature<sup>145</sup>, here reported for comparison purpose.

G films were brittle and rigid, with high elastic modulus and stress at break. As previously reported<sup>145</sup>, the addition of ECN did not significantly affect the mechanical parameters, while the introduction of the additives induced a significant decrease of the stress at break and of the elastic modulus for all the tested formulations. Films GG, GK and GS showed a noticeable decrease of all the mechanical parameters with respect to G. When SD were added, the most remarkable differences between GKE10 and GSE10 were the stress values, which were almost double with respect to GK and GS, whereas GGE10 displayed the lowest stress and modulus and the highest deformation. These features highlighted that GGE films were the less brittle and rigid materials among all the tested compositions. Gelatin films were highly soluble in aqueous media, with a swelling of about 1000% after few hours in saline solutions<sup>146</sup>. The

incorporation of ECN increased the gelatin solubility, as GE10 films were not recoverable in pH 4.5 PB after 30 min (Figure 51).

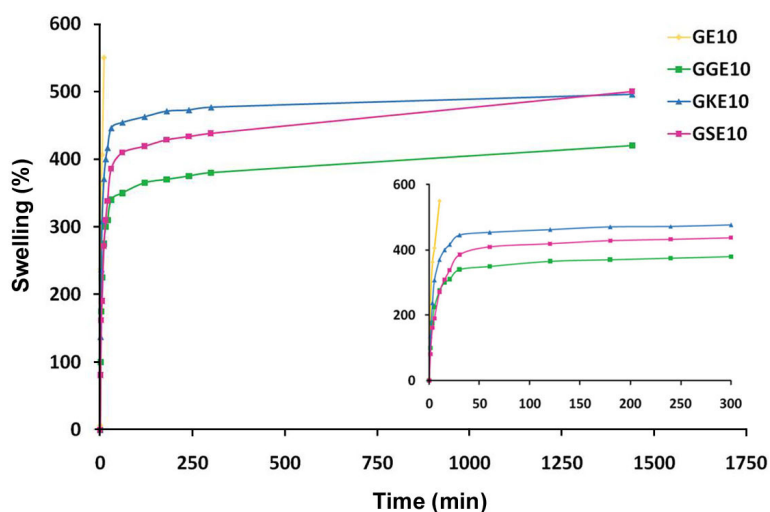


Figure 51. Influence of the additives on the swelling ability of G-films.

When the solid dispersions SD of different compositions were added, all the films swelled considerably lower than G and GE10: in particular, GKE10 and GGE10 showed a swelling degree of about 450 and 350%, respectively, after 5 h. GSE10 displayed an intermediate swelling degree. At longer times all the films gradually dissolved: after 24 h only GGE10 and GSE10 films were still well recognizable. Therefore, comparing the gelatin films, those containing Gelucire® 50/13 demonstrated good flexibility and structural integrity after 24 h of incubation in aqueous media. Based on these results, only gelatin films containing SDG were further investigated and cross-linked with genipin.

### Characterization of gelatin films containing SDG

Gelatin-based films containing ECN at 10% w/w, added either as a powder or as a SD, were then studied. Due to the high solubility of the gelatin films, stabilization with a suitable crosslinking method is mandatory for mucosal application. Genipin, a natural product obtained from gardenia fruits, is a valid alternative to the cytotoxic glutaraldehyde useful to crosslink gelatin<sup>145,147</sup>. Therefore, gelatin films crosslinked with genipin (2% w/w) were investigated and compared with the uncrossed-linked ones regarding mechanical properties, morphology, drug solid state and drug-excipient interactions, swelling behavior and drug release. The elongation at break ( $\epsilon$ ), the stress at break ( $\sigma_b$ ) and the Young's modulus (E) of the films were measured. The results (Table 12) evidenced that genipin crosslinking did not modify the tensile properties of the films (compare GE10/GE10gen), while the addition of SDG provoked a significant decrease of both stress at break and elastic modulus.

XRD patterns of genipin cross-linked films (GE10gen) revealed the permanence of EC crystals<sup>145</sup>. The XRD analysis of the films containing SDG (GGE10) showed that the treatment with genipin did not alter the EC solid state with respect to the uncross-linked samples, as shown in Figure 50b.

These results suggested that neither Gelucire® 50/13 nor genipin interfered in gelatin-ECN acid-base interaction. The IR spectrum of the drug (not reported) evidenced several characteristic peaks at 3174 and 3108  $\text{cm}^{-1}$  (aromatic C–H stretching vibrations); 1585 and 1547  $\text{cm}^{-1}$  (aromatic C–C and C–N stretching vibrations); 1218  $\text{cm}^{-1}$  (aromatic C–Cl stretching vibrations); 1108  $\text{cm}^{-1}$  (C–O–C stretching vibrations); 828 and 803  $\text{cm}^{-1}$  (out of plane C–H deformation vibration) and finally at 761  $\text{cm}^{-1}$  (out of plane C–H deformation vibration of the tri-substituted phenyl group)<sup>128</sup>. FT-IR spectra recorded on GE10 showed several absorption bands corresponding to amide I, II and III typical of gelatin superimposed on those of EC<sup>148</sup> and after genipin crosslinking (GE10gen) no remarkable differences of peaks shapes and intensities were evidenced. The IR spectrum of Gelucire® 50/13 (not reported) displayed a broad band between 3100 and 3600  $\text{cm}^{-1}$  (stretching of free OH groups), at 1738.5  $\text{cm}^{-1}$  (stretching C=O group), at 1469.5  $\text{cm}^{-1}$  (C–H deformation of alkyl group), at 1113.7  $\text{cm}^{-1}$  (–C–O stretching) and at 963.3  $\text{cm}^{-1}$  (double band, characteristic of the polyethylene glycol groups)<sup>133</sup>. Comparing the FT-IR spectrum of GE10 to the GGE10 ones (not reported), the film containing SDG showed all the characteristic adsorption bands of both gelatin and Gelucire, suggesting the absence of interactions between the components of the formulation.

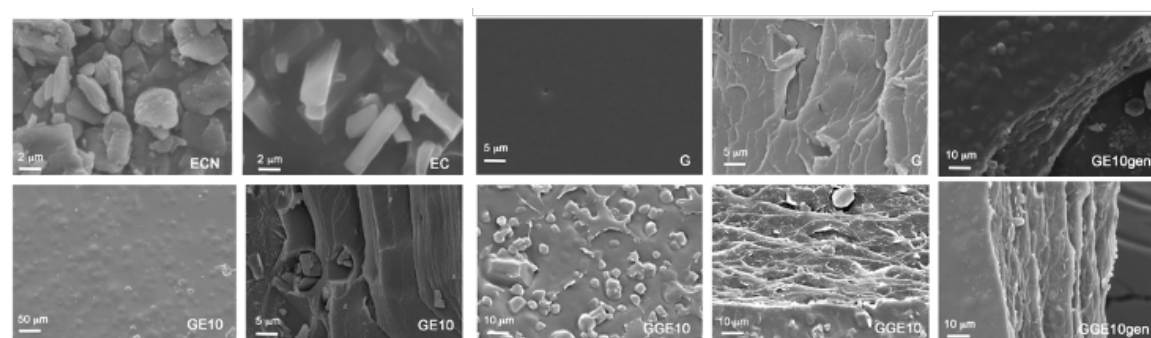


*Figure 52. SEM images of ECN crystals, EC crystals, G film (surface, left and cross-section, right), GE10 film (surface, left and cross-section, right), GGE10 film (surface left and cross-section right) and images of GE10gen (top) and GGE10gen (bottom).*

SEM images, reported in Figure 52, showed the different morphology between the drug crystals of pure drug (ECN) and the modified drug within the film formulation (EC). The unloaded film (G) presented a smooth surface, while films loaded with the drug or with the SDG (GE10 and GGE10) presented small crystals of the drug underneath the film surface, due to the suspended drug within the polymeric matrix, as reported in literature<sup>149</sup>. The images of GE10 and GGE10 revealed a uniform distribution of the drug into the film with the EC crystals distinctly

recognizable. Moreover, SEM analysis evidenced that there are no differences in terms of drug crystal morphology in the presence or absence of the solid dispersion. The morphology of the cross sections showed the typical leaflet structure of gelatin film, even if GGE10 films showed a more compact structure than GE10 ones. Moreover, the morphology did not change after chemical cross-linking (GE10gen and GGE10gen). The HPLC analysis of the solubilized samples evidenced that the drug recovery was in the range 86–93% ( $92.6 \pm 0.5$ ,  $89.6 \pm 1.2$ ,  $87.9 \pm 1.8$  and  $89.8 \pm 1.9$  for GE10, GGE10, GE10gen and GGE10gen, respectively), suggesting that a certain amount of drug remained bounded with gelatin after its topotactic transformation, thus decreasing the free drug extent, regardless the presence of the additives (neither Gelucire® 50/13 nor genipin). To confirm this hypothesis, uncross-linked films (GE10 and GGE10) were also prepared by apart solubilizing ECN or SDG and gelatin in DDW at pH 1.5 while maintaining the same proportion and conditions of stirring and temperature previously reported for film preparation. The pH was adjusted at 1.5 by adding HCl (6 M) before the solvent casting process. The results confirmed a greater availability of free drug, as the drug recovery was about the 100% for all the samples ( $100.2 \pm 2.1$  and  $101.2 \pm 2.1$  for GE10 and GGE10, respectively), confirming our hypothesis.

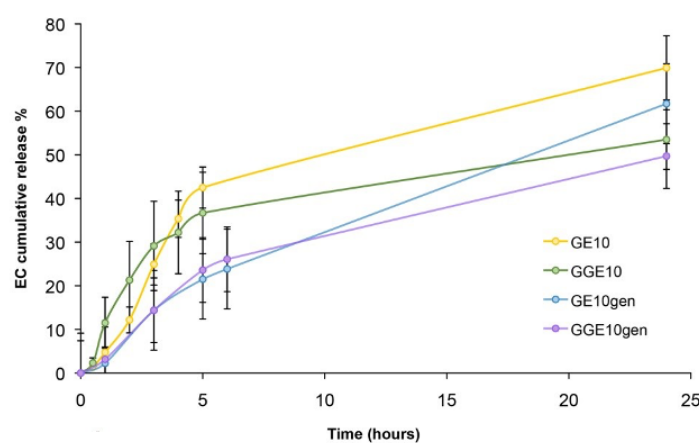


Figure 53. Release studies performed using Franz diffusion cells. EC release profiles from both uncross-linked gelatin-based films and genipin cross-linked gelatin-based films.

The release profiles of both uncross-linked films and genipin crosslinked films are reported in Figure 53. The drug release profile from GE10 and GGE10 was controlled during the first 5 h and reached about 40% of drug dissolved: GGE10 films displayed a greater burst release than neat GE10 films due to the high solubility of the SDG. In particular, the amount of drug released after 2 h was 21,5% and 12% for GGE10 and GE10, respectively. Then, both films exhibited a sustained slow drug release up to 24 h. In particular, the amount of EC released was 70% and 55% for GE10 and GGE10, respectively. Noteworthy, GGE10 film appeared swelled but still intact, while GE10 dissolved forming a gel layer. GE10gen e GGE10gen showed a more

controlled drug release up to 24 h and intact swollen films were still present at the donor sites of Franz cells at the end of the experiment. These results indicated that all film formulations controlled the drug release up to 24 h and only the uncrossed-linked ones (GE10 and GGE10) could achieve a higher drug concentration (about 40%) at the site of application during the first 5 h. Comparing the release profiles of GE10 and GGE10 after the first 5 h, the addition of Gelucire® 50/13 enabled a more controlled drug release, due to its amphiphilic nature with respect to the hydrophilic gelatin. Then, genipin cross-linking exhibited a greater effect on the release profile of films without Gelucire: after 5 h the difference of drug released from GE10 and GE10gen is about 21%, while it was merely 13% from GGE10 and GGE10gen, suggesting that Gelucire might have reduced the extent of cross-linking between the  $\epsilon$ -amino groups of gelatin and genipin. After 24 h, around 55% and 62% of drug were released from GGE10 and GE10gen films, respectively. Therefore, Gelucire® 50/13, due to its peculiar amphiphilic property, ensured an appropriate release of the active ingredient, both enhancing the drug release at the beginning of the treatment and controlling the drug release over time, as genipin. Moreover, genipin is relatively expensive and imbues crosslinked-gelatin films with a dark blue color, which could represent a limit for some applications. Finally, the ability of the film to adhere to the mucosa, measured as the force required to detach the film from the mucosa, was investigated and the results are reported in Figure 54.

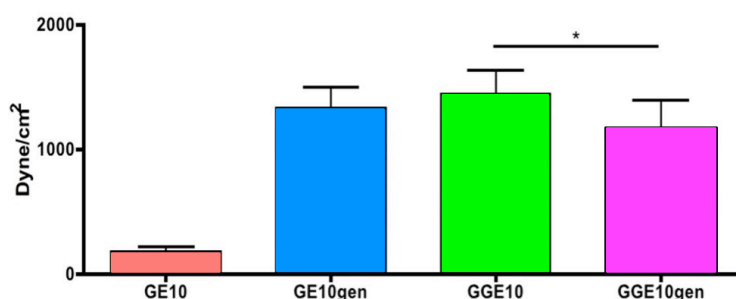


Figure 54. Mucoadhesive strength values of the films: GE10, GE10gen, GGE10 e GGE10gen (\*\* $p < 0.01$ ).

GE10 film did not present a significant mucoadhesive strength, owing to the high water solubility of gelatin in the absence of crosslinking. On the contrary, the addition of genipin to the ECN loaded film (GE10gen) showed a strong increase of mucoadhesive properties. It is interesting to note that the mucoadhesive strength value of GGE10 resulted to be comparable to the cross-linked GE10gen film ( $p > 0.05$ ). Therefore, the addition of Gelucire® increases the structural integrity of the gelatin film allowing the adhesion of the film to the mucosa pivotal for gelatin film application, while avoiding the cross-linking step. Furthermore, a small difference was observed between the samples GGE10 and GGE10gen (\*\* $p < 0.01$ ). Therefore, these results highlight that the presence of Gelucire® solid dispersion within gelatin films had

a significant effect on the strength of adhesion to the mucosa tissue, thus improving the residence time at the site of application.

### Biological activity

The anti-Candida activity of the different gelatin-based films was assessed *in vitro* against both *C. albicans* reference strain ATCC 10231 and six clinical isolates recovered from genitourinary tract infections. The diameters of the inhibition zones are reported in Figure 55.

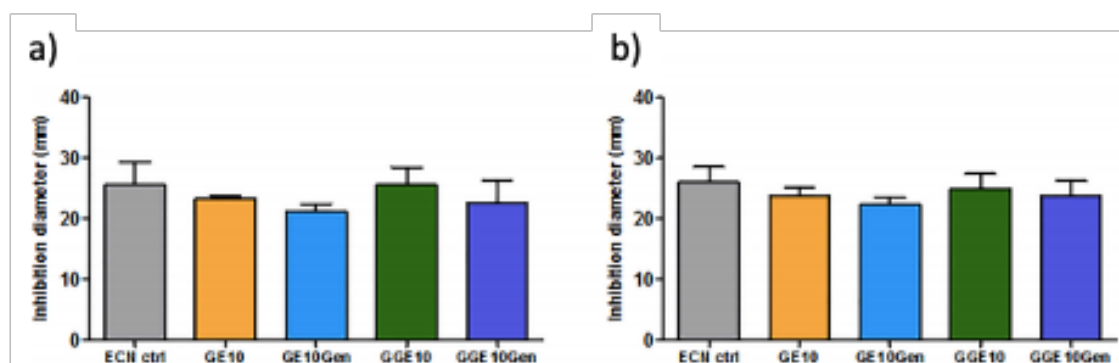


Figure 55. Anti-Candida activity of gelatin-based films loaded with ECN against the *C. albicans* reference strain (a), and six clinical isolates (b), whose results were pooled together. Data are expressed as the diameter (mm) of the clear free zone measured around the disk-shaped samples. Negative films (GG10 and Ggen) were included in the analysis and no inhibition was measured.

Data indicated that the gelatin films inhibited fungal growth with the same effectiveness, and no statistically significant differences were measured in the diameter values between these formulations and the ECN positive control (ECN 300  $\mu$ g). Considering the ECN amount loaded on the film samples, and the weight of gelatin-based films, the drug concentration ranged from 300 to 340  $\mu$ g, depending on the formulation. The four gelatin-based films displayed similar inhibitory activity towards the reference and the clinical strains, which are representative of pathogens circulating in the population, however the best result was achieved for GGE10. The cross-linking step with genipin slightly decreased the effectiveness of the films as diameters of the fungal-clear zones reduced, even if not at significant levels. Overall, these data confirm the suitability of Gelucire® as polymer for ECN delivery system. As an *in vitro* proof-of-concept on the safety of the gelatin-based films, G, GG, and GGE10 disk-shaped samples were dissolved in cell culture medium and solutions were used to treat HeLa cells. To obtain an accurate result in cytotoxicity assay, the samples were evaluated by different methods, such as the determination of NADH in living cells and the release of LDH from dead cells. Results at 48 h of culture are reported in Figure 56.

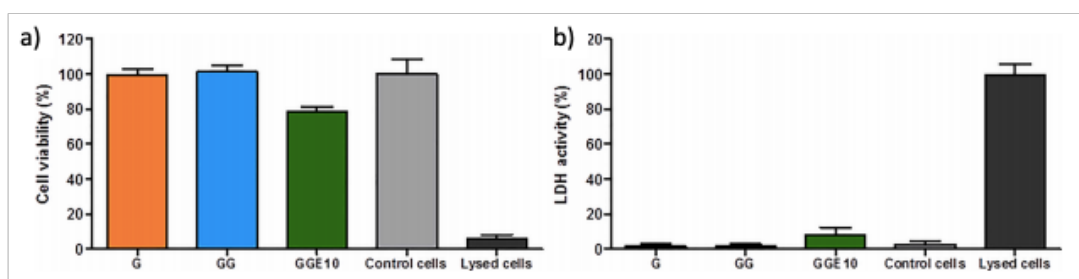


Figure 56. Cell viability assay (a) and LDH release (b) of HeLa cells following 48 h of culture with the experimental samples. Results are percentage values relative to both cells and lysed cells.

As a sample is considered cytotoxic when its viability is <70% in comparison to untreated cells (control cells), none of the tested solutions is cytotoxic, at the used experimental conditions. Only a slight reduction of cell viability (22%) was measured for GGE10, while analysis of cell damage by LDH evaluation confirmed the safety of this sample as LDH activity was measured at negligible level (10%).

## Conclusions

Econazole-loaded vaginal films based on plain gelatin and films containing a drug solid dispersion based on different polymers (Soluplus®, PVPs and Gelucire® 50/13) were successfully prepared and characterized. The solubility of ECN increased for all SD, though the drug remained almost crystalline within the SD. Once the SD was combined with gelatin matrix, XRD patterns demonstrated the occurrence of the base-acid interaction between the drug and the polymer, resulting in transformation of ECN into EC. Among the tested formulations, GGE films demonstrated good flexibility and swelling ability combined with a certain structural integrity after 24 h of incubation in PB pH 4.5. Additionally, GGE films displayed greater adhesiveness and activity against *Candida albicans* than gelatin films alone and those crosslinked with genipin, without a cytotoxic effect. Thus, the use of Gelucire® 50/13 within the polymeric film matrix could represent a valid alternative to the use of chemical crosslinkers to obtain gelatin-based delivery systems for prolonged drug release. In conclusion, the overall *in vitro* results demonstrated that formulated films containing Gelucire improved the drug solubility, while controlling the drug release for an extended period of time, suggesting their potential use for the treatment of vaginal candidiasis with a single application per day. Moreover, being films very flexible in dose according to the final size, they enable a customized dose according to the need.

## 2.9 BIBLIOGRAPHY

- (1) Borges, A.; Silva, C.; Coelho, J.; Simões, S. Oral Films: Current Status and Future Perspectives: I - Galenical Development and Quality Attributes. *J. Control. release* **2015**, *206*, 1–19, DOI:10.1016/J.JCONREL.2015.03.006.
- (2) Shanmugapriya, K.; Kim, H.; Saravana, P.; Chun, B.; Kang, H. Fabrication of Multifunctional Chitosan-Based Nanocomposite Film with Rapid Healing and Antibacterial Effect for Wound Management. *Int. J. Biol. Macromol.* **2018**, *118* (Pt B), 1713–1725, DOI:10.1016/J.IJBIOMAC.2018.07.018.
- (3) Maver, T.; Mohan, T.; Gradišnik, L.; Finšgar, M.; Stana Kleinschek, K.; Maver, U. Polysaccharide Thin Solid Films for Analgesic Drug Delivery and Growth of Human Skin Cells. *Front. Chem.* **2019**, *7* (217) DOI:10.3389/FCHEM.2019.00217.
- (4) Lieb, S.; Szeimies, R. M.; Lee, G. Self-Adhesive Thin Films for Topical Delivery of 5-Aminolevulinic Acid. *Eur. J. Pharm. Biopharm.* **2002**, *53* (1), 99–106, DOI:10.1016/S0939-6411(01)00193-X.
- (5) Padula, C.; Nicoli, S.; Aversa, V.; Colombo, P.; Falson, F.; Pirot, F.; Santi, P. Bioadhesive Film for Dermal and Transdermal Drug Delivery. *Eur. J. Dermatol.* **2007**, *17* (4), 309–312, DOI:10.1684/EJD.2007.0205.
- (6) Fleck, C. A.; Simman, R. Modern Collagen Wound Dressings: Function and Purpose. *J. Am. Col. Certif. Wound Spec.* **2010**, *2* (3), 54, DOI:10.1016/J.JCWS.2010.12.003.
- (7) Dutta, P. K.; Tripathi, S.; Mehrotra, G. K.; Dutta, J. Perspectives for Chitosan Based Antimicrobial Films in Food Applications. *Food Chem.* **2009**, *114* (4), 1173–1182, DOI:10.1016/J.FOODCHEM.2008.11.047.
- (8) Karki, S.; Kim, H.; Na, S. J.; Shin, D.; Jo, K.; Lee, J. Thin Films as an Emerging Platform for Drug Delivery. *Asian J. Pharm. Sci.* **2016**, *11* (5), 559–574, DOI:10.1016/J.AJPS.2016.05.004.
- (9) Vieira, M. G. A.; Da Silva, M. A.; Dos Santos, L. O.; Beppu, M. M. Natural-Based Plasticizers and Biopolymer Films: A Review. *Eur. Polym. J.* **2011**, *47* (3), 254–263, DOI:10.1016/j.eurpolymj.2010.12.011.
- (10) Vieira, J. M.; Flores-López, M. L.; de Rodríguez, D. J.; Sousa, M. C.; Vicente, A. A.; Martins, J. T. Effect of Chitosan-Aloe Vera Coating on Postharvest Quality of Blueberry (*Vaccinium Corymbosum*) Fruit. *Postharvest Biol. Technol.* **2016**, *116*, 88–97, DOI:10.1016/j.postharvbio.2016.01.011.
- (11) Zhao, J.; Wei, F.; Xu, W.; Han, X. Enhanced Antibacterial Performance of Gelatin/Chitosan Film Containing Capsaicin Loaded MOFs for Food Packaging. *Appl. Surf. Sci.* **2020**, *510* (December 2019), 145418, DOI:10.1016/j.apsusc.2020.145418.
- (12) Liu, H.; Adhikari, R.; Guo, Q.; Adhikari, B. Preparation and Characterization of Glycerol Plasticized (High-Amylose) Starch-Chitosan Films. *J. Food Eng.* **2013**, *116* (2), 588–597, DOI:10.1016/j.jfoodeng.2012.12.037.
- (13) Souza, V. G. L.; Fernando, A. L.; Pires, J. R. A.; Rodrigues, P. F.; Lopes, A. A. S.; Fernandes, F. M. B. Physical Properties of Chitosan Films Incorporated with Natural Antioxidants. *Ind. Crops Prod.* **2017**, *107*, 565–572, DOI:10.1016/J.INDCROP.2017.04.056.
- (14) Akyuz, L.; Kaya, M.; Mujtaba, M.; Ilk, S.; Sargin, I.; Salaberria, A.; Labidi, J.; Cakmak, Y.; Islek, C. Supplementing Capsaicin with Chitosan-Based Films Enhanced the Anti-Quorum Sensing, Antimicrobial, Antioxidant, Transparency, Elasticity and Hydrophobicity. *Int. J. Biol. Macromol.* **2018**, *115*, 438–446, DOI:10.1016/J.IJBIOMAC.2018.04.040.
- (15) Kaya, M.; Khadem, S.; Cakmak, Y. S.; Mujtaba, M.; Ilk, S.; Akyuz, L.; Salaberria, A. M.; Labidi, J.; Abdulqadir, A. H.; Deligöz, E. Antioxidative and Antimicrobial Edible Chitosan Films Blended with Stem, Leaf and Seed Extracts of Pistacia Terebinthus for Active Food Packaging. *RSC Adv.* **2018**, *8* (8), 3941–3950, DOI:10.1039/C7RA12070B.
- (16) Siripatrawan, U.; Vitchayakitti, W. Improving Functional Properties of Chitosan Films as Active

- Food Packaging by Incorporating with Propolis. *Food Hydrocoll.* **2016**, *61*, 695–702, DOI:10.1016/j.foodhyd.2016.06.001.
- (17) Albertini, B.; Passerini, N.; Panzavolta, S.; Dolci, L. WO2020201439A1 - Polymer Films Comprising Material Secreted by Gastropods. WO2020/201439 A1, 2020.
  - (18) Di Filippo, M. F.; Panzavolta, S.; Albertini, B.; Bonvicini, F.; Gentilomi, G. A.; Orlacchio, R.; Passerini, N.; Bigi, A.; Dolci, L. S. Functional Properties of Chitosan Films Modified by Snail Mucus Extract. *Int. J. Biol. Macromol.* **2020**, DOI:10.1016/j.ijbiomac.2019.11.230.
  - (19) Di Filippo, M. F.; Dolci, L. S.; Liccardo, L.; Bigi, A.; Bonvicini, F.; Gentilomi, G. A.; Passerini, N.; Panzavolta, S.; Albertini, B. Cellulose Derivatives-Snail Slime Films: New Disposable Eco-Friendly Materials for Food Packaging. *Food Hydrocoll.* **2021**, *111* (July 2020), 106247, DOI:10.1016/j.foodhyd.2020.106247.
  - (20) Di Filippo, M. F.; Albertini, B.; Dolci, L. S.; Bonvicini, F.; Bigi, A.; Gentilomi, G. A.; Passerini, N.; Panzavolta, S. Novel Drug-Loaded Film Forming Patch Based on Gelatin and Snail Slime. *Int. J. Pharm.* **2021**, *598* (February), 120408, DOI:10.1016/j.ijpharm.2021.120408.
  - (21) Dolci, L. S.; Albertini, B.; Di Filippo, M. F.; Bonvicini, F.; Passerini, N.; Panzavolta, S. Development and in Vitro Evaluation of Mucoadhesive Gelatin Films for the Vaginal Delivery of Econazole. *Int. J. Pharm.* **2020**, *591* (July), 119979, DOI:10.1016/j.ijpharm.2020.119979.
  - (22) Sala, M.; Diab, R.; Elaissari, A.; Fessi, H. Lipid Nanocarriers as Skin Drug Delivery Systems: Properties, Mechanisms of Skin Interactions and Medical Applications. *Int. J. Pharm.* **2018**, *535* (1–2), 1–17, DOI:10.1016/j.ijpharm.2017.10.046.
  - (23) Hosseini, S. F.; Rezaei, M.; Zandi, M.; Farahmandghavi, F. Fabrication of Bio-Nanocomposite Films Based on Fish Gelatin Reinforced with Chitosan Nanoparticles. *Food Hydrocoll.* **2015**, *44*, 172–182, DOI:10.1016/j.foodhyd.2014.09.004.
  - (24) Zhao, G.; Lyu, X.; Lee, J.; Cui, X.; Chen, W. N. Biodegradable and Transparent Cellulose Film Prepared Eco-Friendly from Durian Rind for Packaging Application. *Food Packag. Shelf Life* **2019**, *21* (June), DOI:10.1016/j.fpsl.2019.100345.
  - (25) Gennari, C. G. M.; Quaroni, G. M. G.; Creton, C.; Minghetti, P.; Cilurzo, F. SEBS Block Copolymers as Novel Materials to Design Transdermal Patches. *Int. J. Pharm.* **2020**, *575*, 118975, DOI:10.1016/J.IJPHARM.2019.118975.
  - (26) Bachhav, Y. G.; Mondon, K.; Kalia, Y. N.; Gurny, R.; Möller, M. Novel Micelle Formulations to Increase Cutaneous Bioavailability of Azole Antifungals. *J. Control. Release* **2011**, *153* (2), 126–132, DOI:10.1016/j.jconrel.2011.03.003.
  - (27) Özgür Altan, B.; Mehemet, T. Plasticiser Effect on Water Vapour Permeability Properties of Locust Bean Gum-Based Edible Films. *Turk J Chem* **2003**, *27*, 773–782, .
  - (28) Collado-González, M.; Espinosa, Y. G.; Goycoolea, F. M. Interaction Between Chitosan and Mucin: Fundamentals and Applications. *Biomimetics 2019, Vol. 4, Page 32* **2019**, *4* (2), 32, DOI:10.3390/BIOMIMETICS4020032.
  - (29) Singh Dhillon, G.; Kaur, S.; Jyoti Sarma, S.; Kaur Brar, S.; Verma, M.; Yadagiri Surampalli, R. Recent Development in Applications of Important Biopolymer Chitosan in Biomedicine, Pharmaceuticals and Personal Care Products. *Curr. Tissue Eng.* **2013**, *2* (1), 20–40, DOI:10.2174/2211542011302010004.
  - (30) Wang, H.; Qian, J.; Ding, F. Emerging Chitosan-Based Films for Food Packaging Applications. *J. Agric. Food Chem.* **2018**, *66* (2), 395–413, DOI:10.1021/acs.jafc.7b04528.
  - (31) Nataraj, D.; Sakkara, S.; Meghwal, M.; Reddy, N. Crosslinked Chitosan Films with Controllable Properties for Commercial Applications. *Int. J. Biol. Macromol.* **2018**, *120*, 1256–1264, DOI:10.1016/j.ijbiomac.2018.08.187.
  - (32) Mujtaba, M.; Morsi, R. E.; Kerch, G.; Elsabee, M. Z.; Kaya, M.; Labidi, J.; Khawar, K. M. Current Advancements in Chitosan-Based Film Production for Food Technology; A Review. *Int. J. Biol. Macromol.* **2019**, *121*, 889–904, DOI:10.1016/j.ijbiomac.2018.10.109.

- (33) Shariatinia, Z. Pharmaceutical Applications of Chitosan. *Adv. Colloid Interface Sci.* **2019**, *263*, 131–194, DOI:10.1016/j.cis.2018.11.008.
- (34) Wu, Q. X.; Lin, D. Q.; Yao, S. J. Design of Chitosan and Its Water Soluble Derivatives-Based Drug Carriers with Polyelectrolyte Complexes. *Mar. Drugs* **2014**, *12* (12), 6236–6253, DOI:10.3390/md12126236.
- (35) Sah, A. K.; Dewangan, M.; Suresh, P. K. Potential of Chitosan-Based Carrier for Periodontal Drug Delivery. *Colloids Surfaces B Biointerfaces* **2019**, *178* (February), 185–198, DOI:10.1016/j.colsurfb.2019.02.044.
- (36) Jayakumar, R.; Prabakaran, M.; Sudheesh Kumar, P. T.; Nair, S. V.; Tamura, H. Biomaterials Based on Chitin and Chitosan in Wound Dressing Applications. *Biotechnol. Adv.* **2011**, *29* (3), 322–337, DOI:10.1016/j.biotechadv.2011.01.005.
- (37) Argüelles-Monal, W.; Goycoolea, F. M.; Lizardi, J.; Peniche, C.; Higuera-Ciajara, I. Chitin and Chitosan in Gel Network Systems. *ACS Symp. Ser.* **2002**, *833*, 102–121, DOI:10.1021/BK-2002-0833.CH007.
- (38) Kubota, N.; Eguchi, Y. Facile Preparation of Water-Soluble N-Acetylated Chitosan and Molecular Weight Dependence of Its Water-Solubility. *Polym. J.* **1997**, *29* (2), 123–127, DOI:10.1295/polymj.29.123.
- (39) Rinaudo, M.; Domard, A. Solution Properties of Chitosan. Chitin and Chitosan; Skjak-Braek, G., Anthonsen, T., Sandford, P., Eds.; Elsevier: London and NY, 1989; pp 71–86.
- (40) Muxika, A.; Etxabide, A.; Uranga, J.; Guerrero, P.; de la Caba, K. Chitosan as a Bioactive Polymer: Processing, Properties and Applications. *Int. J. Biol. Macromol.* **2017**, *105*, 1358–1368, DOI:10.1016/j.ijbiomac.2017.07.087.
- (41) Kim, K. M.; Son, J. H.; Kim, S.-K.; Weller, C. L.; Hanna, M. A. Properties of Chitosan Films as a Function of PH and Solvent Type. *J. Food Sci.* **2006**, *71* (3), E119–E124, DOI:10.1111/J.1365-2621.2006.TB15624.X.
- (42) Bégin, A.; Van Calsteren, M. R. Antimicrobial Films Produced from Chitosan. *Int. J. Biol. Macromol.* **1999**, *26* (1), 63–67, DOI:10.1016/S0141-8130(99)00064-1.
- (43) Khoshgozaran-Abras, S.; Azizi, M. H.; Hamidy, Z.; Bagheripoor-Fallah, N. Mechanical, Physicochemical and Color Properties of Chitosan Based-Films as a Function of Aloe Vera Gel Incorporation. *Carbohydr. Polym.* **2012**, *87* (3), 2058–2062, DOI:10.1016/j.carbpol.2011.10.020.
- (44) Caner, C.; Vergano, P. J.; Wiles, J. L. Chitosan Film Mechanical and Permeation Properties as Affected by Acid, Plasticizer, and Storage. *J. Food Sci.* **2006**, *63* (6), 1049–1053, DOI:10.1111/j.1365-2621.1998.tb15852.x.
- (45) Lourdin, D.; Bizot, H.; Colonna, P. ““ Antiplasticization ”” in Starch – Glycerol Films ? **1996**, No. February, 1047–1053, .
- (46) Boesel, L. F. Effect of Plasticizers on the Barrier and Mechanical Properties of Biomimetic Composites of Chitosan and Clay. *Carbohydr. Polym.* **2015**, *115*, 356–363, DOI:10.1016/j.carbpol.2014.08.064.
- (47) Samuels, R. J. Solid State Characterization of the Structure of Chitosan Films.
- (48) Saitô, H.; Tabeta, R.; Ogawa, K. High-Resolution Solid-State<sup>13</sup>C NMR Study of Chitosan and Its Salts with Acids: Conformational Characterization of Polymorphs and Helical Structures as Viewed from the Conformation-Dependent<sup>13</sup>C Chemical Shifts. *Macromolecules* **1987**, *20* (10), 2424–2430, DOI:10.1021/ma00176a017.
- (49) Jong-Whan Rhim; Seok-In Hong; Hwan-Man Park; Ng, P. K. W. Preparation and Characterization of Chitosan-Based Nanocomposite Films with Antimicrobial Activity. *J. Agric. Food Chem.* **2006**, *54* (16), 5814–5822, DOI:10.1021/JF060658H.
- (50) Chang, W.; Liu, F.; Sharif, H. R.; Huang, Z.; Goff, H. D.; Zhong, F. Preparation of Chitosan Films by Neutralization for Improving Their Preservation Effects on Chilled Meat. *Food*

- Hydrocoll.* **2019**, *90* (June 2018), 50–61, DOI:10.1016/j.foodhyd.2018.09.026.
- (51) Qiao, C.; Ma, X.; Zhang, J.; Yao, J. Effect of Hydration on Water State, Glass Transition Dynamics and Crystalline Structure in Chitosan Films. *Carbohydr. Polym.* **2019**, *206*, 602–608, DOI:10.1016/J.CARBPOL.2018.11.045.
  - (52) Leceta, I.; Guerrero, P.; De La Caba, K. Functional Properties of Chitosan-Based Films. *Carbohydr. Polym.* **2013**, *93* (1), 339–346, DOI:10.1016/j.carbpol.2012.04.031.
  - (53) Trapella, C.; Rizzo, R.; Gallo, S.; Alogna, A.; Bortolotti, D.; Casciano, F.; Zauli, G.; Secchiero, P.; Voltan, R. HelixComplex Snail Mucus Exhibits Pro-Survival, Proliferative and pro-Migration Effects on Mammalian Fibroblasts. *Sci. Rep.* **2018**, *8* (1), 1–10, DOI:10.1038/s41598-018-35816-3.
  - (54) Bajić, M.; Jalšovec, H.; Travan, A.; Novak, U.; Likozar, B. Chitosan-Based Films with Incorporated Supercritical CO<sub>2</sub> Hop Extract: Structural, Physicochemical, and Antibacterial Properties. *Carbohydr. Polym.* **2019**, *219*, 261–268, DOI:10.1016/J.CARBPOL.2019.05.003.
  - (55) Lavorgna, M.; Piscitelli, F.; Mangiacapra, P.; Buonocore, G. G. Study of the Combined Effect of Both Clay and Glycerol Plasticizer on the Properties of Chitosan Films. *Carbohydr. Polym.* **2010**, *82* (2), 291–298, DOI:10.1016/j.carbpol.2010.04.054.
  - (56) Wang, S. F.; Shen, L.; Tong, Y. J.; Chen, L.; Phang, I. Y.; Lim, P. Q.; Liu, T. X. Biopolymer Chitosan/Montmorillonite Nanocomposites: Preparation and Characterization. *Polym. Degrad. Stab.* **2005**, *90* (1), 123–131, DOI:10.1016/J.POLYMDEGRADSTAB.2005.03.001.
  - (57) ISO/TC 194. UNI EN, ISO 10993-5:2009, Biological Evaluation of Medical Devices — Part 5: Tests for in Vitro Cytotoxicity. 2009, p 34.
  - (58) Verlee, A.; Mincke, S.; Stevens, C. V. Recent Developments in Antibacterial and Antifungal Chitosan and Its Derivatives | Elsevier Enhanced Reader. *Carbohydr. Polym.* **2017**, *164*, 268–283, DOI:http://dx.doi.org/10.1016/j.carbpol.2017.02.001.
  - (59) Foster, L. J. R.; Butt, J. Chitosan Films Are NOT Antimicrobial. *Biotechnol. Lett.* **2011**, *33* (2), 417–421, DOI:10.1007/s10529-010-0435-1.
  - (60) Ferrer, A.; Pal, L.; Hubbe, M. Nanocellulose in Packaging: Advances in Barrier Layer Technologies. *Ind. Crops Prod.* **2017**, *95*, 574–582, DOI:10.1016/J.INDCROP.2016.11.012.
  - (61) Al-Tayyar, N. A.; Youssef, A. M.; Al-hindi, R. Antimicrobial Food Packaging Based on Sustainable Bio-Based Materials for Reducing Foodborne Pathogens: A Review. *Food Chem.* **2020**, *310*, 125915, DOI:10.1016/J.FOODCHEM.2019.125915.
  - (62) Lee, D. S.; Yam, K. L.; Piergiovanni, L. Food Packaging Science and Technology. **2008**, DOI:10.1201/9781439894071.
  - (63) European Commission. Commission Regulation (EU) No 10/2011 on Plastic Materials and Articles Intended to Come into Contact with Food. *Official Journal of the European Union*. January 2011, pp 1–89.
  - (64) Wrona, M.; Cran, M. J.; Nerín, C.; Bigger, S. W. Development and Characterisation of HPMC Films Containing PLA Nanoparticles Loaded with Green Tea Extract for Food Packaging Applications. *Carbohydr. Polym.* **2017**, *156*, 108–117, DOI:10.1016/J.CARBPOL.2016.08.094.
  - (65) Bahrami, A.; Rezaei Mokarram, R.; Sowti Khiabani, M.; Ghanbarzadeh, B.; Salehi, R. Physico-Mechanical and Antimicrobial Properties of Tragacanth/Hydroxypropyl Methylcellulose/Beeswax Edible Films Reinforced with Silver Nanoparticles. *Int. J. Biol. Macromol.* **2019**, *129*, 1103–1112, DOI:10.1016/J.IJBIOMAC.2018.09.045.
  - (66) Arslan, N.; Togrul, H. Modelling of Water Sorption Isotherms of Macaroni Stored in Achamber under Controlled Humidity and Thermodynamic Approach. *J. Food Eng.* **2005**, *69*, 133–145, DOI:doi:10.1016/j.jfoodeng.2004.08.004.
  - (67) Quintavalla, S.; Vicini, L. Antimicrobial Food Packaging in Meat Industry. *Meat Sci.* **2002**, *62* (3), 373–380, DOI:10.1016/S0309-1740(02)00121-3.
  - (68) Appendini, P.; Hotchkiss, J. H. Review of Antimicrobial Food Packaging. *Innov. Food Sci.*

- Emerg. Technol.* **2002**, 3 (2), 113–126, DOI:10.1016/S1466-8564(02)00012-7.
- (69) Gómez-Estaca, J.; López de Lacey, A.; López-Caballero, M. E.; Gómez-Guillén, M. C.; Montero, P. Biodegradable Gelatin–Chitosan Films Incorporated with Essential Oils as Antimicrobial Agents for Fish Preservation. *Food Microbiol.* **2010**, 27 (7), 889–896, DOI:10.1016/J.FM.2010.05.012.
- (70) Muppalla, S. R.; Kanatt, S. R.; Chawla, S. P.; Sharma, A. Carboxymethyl Cellulose-Polyvinyl Alcohol Films with Clove Oil for Active Packaging of Ground Chicken Meat. *Food Packag. Shelf Life* **2014**, 2 (2), 51–58, DOI:10.1016/j.fpsl.2014.07.002.
- (71) Siracusa, V.; Rocculi, P.; Romani, S.; Rosa, M. D. Biodegradable Polymers for Food Packaging: A Review. *Trends Food Sci. Technol.* **2008**, 19 (12), 634–643, DOI:10.1016/J.TIFS.2008.07.003.
- (72) Zeman, S.; Kubík, L. Permeability of Polymeric Packaging Materials. *Tech. Sci.* **2007**, 10, 33–34, DOI:10.2478/V10022-007-0004-6.
- (73) Haghghi, H.; Biard, S.; Bigi, F.; De Leo, R.; Bedin, E.; Pfeifer, F.; Siesler, H. W.; Licciardello, F.; Pulvirenti, A. Comprehensive Characterization of Active Chitosan-Gelatin Blend Films Enriched with Different Essential Oils. *Food Hydrocoll.* **2019**, 95 (February), 33–42, DOI:10.1016/j.foodhyd.2019.04.019.
- (74) Wu, J.; Sun, X.; Guo, X.; Ge, S.; Zhang, Q. Physicochemical Properties, Antimicrobial Activity and Oil Release of Fish Gelatin Films Incorporated with Cinnamon Essential Oil. *Aquac. Fish.* **2017**, 2 (4), 185–192, DOI:10.1016/J.AAF.2017.06.004.
- (75) Guo, J.; Ge, L.; Li, X.; Mu, C.; Li, D. Periodate Oxidation of Xanthan Gum and Its Crosslinking Effects on Gelatin-Based Edible Films. *Food Hydrocoll.* **2014**, Complete (39), 243–250, DOI:10.1016/J.FOODHYD.2014.01.026.
- (76) Haghghi, H.; De Leo, R.; Bedin, E.; Pfeifer, F.; Siesler, H. W.; Pulvirenti, A. Comparative Analysis of Blend and Bilayer Films Based on Chitosan and Gelatin Enriched with LAE (Lauroyl Arginate Ethyl) with Antimicrobial Activity for Food Packaging Applications. *Food Packag. Shelf Life* **2019**, 19 (November 2018), 31–39, DOI:10.1016/j.fpsl.2018.11.015.
- (77) Nur Hazirah, M. A. S. P.; Isa, M. I. N.; Sarbon, N. M. Effect of Xanthan Gum on the Physical and Mechanical Properties of Gelatin-Carboxymethyl Cellulose Film Blends. *Food Packag. Shelf Life* **2016**, 9, 55–63, DOI:10.1016/J.FPSL.2016.05.008.
- (78) Theerawitayaart, W.; Prodpran, T.; Benjakul, S.; Sookchoo, P. Properties of Films from Fish Gelatin Prepared by Molecular Modification and Direct Addition of Oxidized Linoleic Acid. *Food Hydrocoll.* **2019**, 88, 291–300, DOI:10.1016/J.FOODHYD.2018.10.022.
- (79) Hamaguchi, P. Y.; WuYin, W.; Tanaka, M. Effect of PH on the Formation of Edible Films Made from the Muscle Proteins of Blue Marlin (Makaira Mazara). *Food Chem.* **2007**, 100 (3), 914–920, DOI:10.1016/j.foodchem.2005.10.045.
- (80) Bajpai, S. K.; Chand, N.; Chaurasia, V. Investigation of Water Vapor Permeability and Antimicrobial Property of Zinc Oxide Nanoparticles-Loaded Chitosan-Based Edible Film. *J. Appl. Polym. Sci.* **2010**, 115 (2), 674–683, DOI:10.1002/APP.30550.
- (81) Bertuzzi, M. A.; Armada, M.; Gottifredi, J. C. Physicochemical Characterization of Starch Based Films. *J. Food Eng.* **2007**, 82 (1), 17–25, DOI:10.1016/J.JFOODENG.2006.12.016.
- (82) Qiu, L.; Shao, Z.; Liu, M.; Wang, J.; Li, P.; Zhao, M. Synthesis and Electrospinning Carboxymethyl Cellulose Lithium (CMC-Li) Modified 9,10-Anthraquinone (AQ) High-Rate Lithium-Ion Battery. *Carbohydr. Polym.* **2014**, 102 (1), 986–992, DOI:10.1016/J.CARBPOL.2013.09.105.
- (83) Ding, C.; Zhang, M.; Li, G. Preparation and Characterization of Collagen/Hydroxypropyl Methylcellulose (HPMC) Blend Film. *Carbohydr. Polym.* **2015**, 119, 194–201, DOI:10.1016/j.carbpol.2014.11.057.
- (84) Tong, Q.; Xiao, Q.; Lim, L. T. Preparation and Properties of Pullulan-Alginate-Carboxymethylcellulose Blend Films. *Food Res. Int.* **2008**, 41 (10), 1007–1014,

DOI:10.1016/j.foodres.2008.08.005.

- (85) Sunardi; Febriani, N. M.; Junaidi, A. B. Preparation of Carboxymethyl Cellulose Produced from Purun Tikus (*Eleocharis Dulcis*). *AIP Conf. Proc.* **2017**, *1868* (1), 020008, DOI:10.1063/1.4995094.
- (86) Kamide, K.; Okajima, K.; Kowsaka, K.; Matsui, T.; Nomura, S.; Hikichi, K. Effect of the Distribution of Substitution of the Sodium Salt of Carboxymethylcellulose on Its Absorbency toward Aqueous Liquid. *Polym. J.* **1985**, *17* (8), 909–918, DOI:10.1295/polymj.17.909.
- (87) O'SULLIVAN, A. C. Cellulose: The Structure Slowly Unravels. *Cellul. 1997* **43** **1997**, *4* (3), 173–207, DOI:10.1023/A:1018431705579.
- (88) Pérez, S.; Mazeau, K. Conformations, Structures, and Morphologies of Celluloses. In *Polysaccharides: Structural diversity and functional versatility*; Dumitriu, S., Ed.; Marcel Dekker: New York, 2005; pp 41–68, DOI:https://doi.org/10.1021/ja0410486.
- (89) Hosseini, S. F.; Rezaei, M.; Zandi, M.; Farahmandghavi, F. Fabrication of Bio-Nanocomposite Films Based on Fish Gelatin Reinforced with Chitosan Nanoparticles. *Food Hydrocoll.* **2015**, *44*, 172–182, DOI:10.1016/J.FOODHYD.2014.09.004.
- (90) Kim, Y. J. I. N.; Lee, M.; Park, O. K. Processabilities and Mechanical Properties of Surlyn-Treated Starch/ LDPE Blends.
- (91) Shyu, Y. S.; Chen, G. W.; Chiang, S. C.; Sung, W. C. Effect of Chitosan and Fish Gelatin Coatings on Preventing the Deterioration and Preserving the Quality of Fresh-Cut Apples. *Molecules* **2019**, *24* (10) DOI:10.3390/molecules24102008.
- (92) Opstelten, W.; Knuistingh Neven, A.; Eekhof, J. A. H. Treatment and Prevention of Herpes Labialis. *Can. Fam. Physician* **2008**, *54*, 1683–1687, .
- (93) Dou, Y.; Zhang, L.; Zhang, B.; He, M.; Shi, W.; Yang, S.; Cui, Y.; Yin, G. Preparation and Characterization of Edible Dialdehyde Carboxymethyl Cellulose Crosslinked Feather Keratin Films for Food Packaging. *Polym. 2020, Vol. 12, Page 158* **2020**, *12* (1), 158, DOI:10.3390/POLYM12010158.
- (94) Quiñones, J. P.; Brüggemann, O.; Covas, C. P.; Ossipov, D. A. Self-Assembled Hyaluronic Acid Nanoparticles for Controlled Release of Agrochemicals and Diosgenin. *Carbohydr. Polym.* **2017**, *173*, 157–169, DOI:10.1016/J.CARPOL.2017.05.048.
- (95) Pechter, P. M.; Gil, J.; Valdes, J.; Tomic-Canic, M.; Pastar, I.; Stojadinovic, O.; Kirsner, R. S.; Davis, S. C. Keratin Dressings Speed Epithelialization of Deep Partial-Thickness Wounds. *Wound Repair Regen.* **2011**, *20*, 236–242, DOI:10.1111/j.1524-475X.2012.00768.x.
- (96) Jangchud, A.; Chinnan, M. S. Properties of Peanut Protein Film: Sorption Isotherm and Plasticizer Effect. *LWT - Food Sci. Technol.* **1999**, *32* (2), 89–94, DOI:10.1006/FSTL.1998.0498.
- (97) Vanin, F. M.; Sobral, P. J. A.; Menegalli, F. C.; Carvalho, R. A.; Habitante, A. M. Q. B. Effects of Plasticizers and Their Concentrations on Thermal and Functional Properties of Gelatin-Based Films. *Food Hydrocoll.* **2005**, *19* (5), 899–907, DOI:10.1016/J.FOODHYD.2004.12.003.
- (98) Guerrero, P.; De La Caba, K. Thermal and Mechanical Properties of Soy Protein Films Processed at Different PH by Compression. *J. Food Eng.* **2010**, *100* (2), 261–269, DOI:10.1016/J.JFOODENG.2010.04.008.
- (99) Gómez-Siurana, A.; Marcilla, A.; Beltrán, M.; Berenguer, D.; Martínez-Castellanos, I.; Menargues, S. TGA/FTIR Study of Tobacco and Glycerol–Tobacco Mixtures. *Thermochim. Acta* **2013**, *573*, 146–157, DOI:10.1016/J.TCA.2013.09.007.
- (100) Rocha Plácido Moore, G.; Martelli, S. M.; Gandolfo, C.; do Amaral Sobral, P. J.; Laurindo, J. B. Influence of the Glycerol Concentration on Some Physical Properties of Feather Keratin Films. *Food Hydrocoll.* **2006**, *20* (7), 975–982, DOI:10.1016/J.FOODHYD.2005.11.001.
- (101) Tanabe, T.; Okitsu, N.; Yamauchi, K. Fabrication and Characterization of Chemically Crosslinked Keratin Films. *Mater. Sci. Eng. C* **2004**, *24* (3), 441–446,

DOI:10.1016/J.MSEC.2003.11.004.

- (102) Dixit, R. P.; Puthli, S. P. Oral Strip Technology: Overview and Future Potential. *J. Control. Release* **2009**, *139* (2), 94–107, DOI:10.1016/J.JCONREL.2009.06.014.
- (103) Paolicelli, P.; Varani, G.; Pacelli, S.; Oglioni, E.; Nardoni, M.; Petralito, S.; Adrover, A.; Casadei, M. A. Design and Characterization of a Biocompatible Physical Hydrogel Based on Scleroglucan for Topical Drug Delivery. *Carbohydr. Polym.* **2017**, *174*, 960–969, DOI:10.1016/j.carbpol.2017.07.008.
- (104) Ayub, A. C.; Gomes, A. D. M.; Lima, M. V. C.; Vianna-Soares, C. D.; Ferreira, L. A. M. Topical Delivery of Fluconazole: In Vitro Skin Penetration and Permeation Using Emulsions as Dosage Forms. <http://dx.doi.org/10.1080/03639040600829989> **2008**, *33* (3), 273–280, DOI:10.1080/03639040600829989.
- (105) El-Housiny, S.; Eldeen, M. A. S.; El-Attar, Y. A.; Salem, H. A.; Attia, D.; Bendas, E. R.; El-Nabarawi, M. A. Fluconazole-Loaded Solid Lipid Nanoparticles Topical Gel for Treatment of Pityriasis Versicolor: Formulation and Clinical Study. <https://doi.org/10.1080/10717544.2017.1413444> **2017**, *25* (1), 78–90, DOI:10.1080/10717544.2017.1413444.
- (106) Salerno, C.; Carlucci, A. M.; Bregni, C. Study of In Vitro Drug Release and Percutaneous Absorption of Fluconazole from Topical Dosage Forms. *AAPS PharmSciTech* **2010**, *11* (2), 986–993, DOI:10.1208/S12249-010-9457-1.
- (107) Gupta, M.; Vyas, S. P. Development, Characterization and in Vivo Assessment of Effective Lipidic Nanoparticles for Dermal Delivery of Fluconazole against Cutaneous Candidiasis. *Chem. Phys. Lipids* **2012**, *165* (4), 454–461, DOI:10.1016/J.CHEMPHYSLIP.2012.01.006.
- (108) Dash, A. K.; Elmquist, W. F. Fluconazole. In *Analytical Profiles of Drug Substances and Excipients*; Elsevier Inc., 2001; Vol. 27, pp 67–113 DOI:10.1016/S1075-6280(01)27005-0.
- (109) Uranga, J.; Leceta, I.; Etxabide, A.; Guerrero, P.; De La Caba, K. Cross-Linking of Fish Gelatins to Develop Sustainable Films with Enhanced Properties. *Eur. Polym. J.* **2016**, *78*, 82–90, DOI:10.1016/j.eurpolymj.2016.03.017.
- (110) Cai, L.; Shi, H.; Cao, A.; Jia, J. Characterization of Gelatin/Chitosan Polymer Films Integrated with Docosahexaenoic Acids Fabricated by Different Methods. *Sci. Reports* **2019**, *9* (1), 1–11, DOI:10.1038/s41598-019-44807-x.
- (111) Okuyama, K. Revisiting the Molecular Structure of Collagen Connective Tissue. *Connect. Tissue Res.* **2008**, *49* (5), 299–310, DOI:10.1080/03008200802325110.
- (112) K, W.; W, W.; R, Y.; J, X.; Y, L.; J, D.; S, Z.; A, L. Mechanical and Barrier Properties of Maize Starch-Gelatin Composite Films: Effects of Amylose Content. *J. Sci. Food Agric.* **2017**, *97* (11), 3613–3622, DOI:10.1002/JSFA.8220.
- (113) Nowak, M.; Gajda, M.; Baranowski, P.; Szymczyk, P.; Karolewicz, B.; Nartowski, K. P. Stabilisation and Growth of Metastable Form II of Fluconazole in Amorphous Solid Dispersions. *Pharm.* **2020**, *Vol. 12, Page 12* **2019**, *12* (1), 12, DOI:10.3390/PHARMACEUTICS12010012.
- (114) Papageorgiou, G. Z.; Bikiaris, D.; Kanaze, F. I.; Karavas, E.; Stergiou, A.; Georgarakis, E. Tailoring the Release Rates of Fluconazole Using Solid Dispersions in Polymer Blends. <https://doi.org/10.1080/03639040701662669> **2008**, *34* (3), 336–346, DOI:10.1080/03639040701662669.
- (115) Karanam, M.; Dev, S.; Choudhury, A. R. New Polymorphs of Fluconazole: Results from Cocrystallization Experiments. *Cryst. Growth Des.* **2011**, *12* (1), 240–252, DOI:10.1021/CG201005Y.
- (116) Newman, A.; Knipp, G.; Zograf, G. Assessing the Performance of Amorphous Solid Dispersions. *J Pharm Sci* **2012**, *101*, 1355–1377, DOI:10.1002/jps.23031.
- (117) I, A.; YN, K.; A, N.; J, B.; RH, G. Effect of Ethanol and Isopropyl Myristate on the Availability of Topical Terbinafine in Human Stratum Corneum, in Vivo. *Int. J. Pharm.* **2001**, *219* (1–2), 11–19, DOI:10.1016/S0378-5173(01)00616-0.

- (118) Gupta, R.; Badhe, Y.; Rai, B.; Mitragotri, S. Molecular Mechanism of the Skin Permeation Enhancing Effect of Ethanol: A Molecular Dynamics Study. *RSC Adv.* **2020**, *10* (21), 12234–12248, DOI:10.1039/D0RA01692F.
- (119) Moser, K.; Kriwet, K.; Froehlich, C.; Kalia, Y. N.; Guy, R. H. Supersaturation: Enhancement of Skin Penetration and Permeation of a Lipophilic Drug. *Pharm. Res.* **2001**, *18* (7), 1006–1011, DOI:10.1023/A:1010948630296.
- (120) Machado, R. M.; Palmeira-De-Oliveira, A.; Jos', J.; Martinez-De-Oliveira, J.; Palmeira-De-Oliveira, R. *Vaginal Films for Drug Delivery*; 2013; Vol. 102 DOI:10.1002/jps.23577.
- (121) Valenta, C. The Use of Mucoadhesive Polymers in Vaginal Delivery. *Adv. Drug Deliv. Rev.* **2005**, *57* (11), 1692–1712, DOI:10.1016/J.ADDR.2005.07.004.
- (122) Garg, S.; Vermani, K.; Garg, A.; Anderson, R. A.; Rencher, W. B.; Zaneveld, L. J. D. Development and Characterization of Bioadhesive Vaginal Films of Sodium Polystyrene Sulfonate (PSS), a Novel Contraceptive Antimicrobial Agent. *Pharm. Res.* **2005**, *22* (4), 584–595, DOI:10.1007/S11095-005-2490-1.
- (123) Dobaria, N. B.; Badhan, A. C.; Mashru, R. C. A Novel Itraconazole Bioadhesive Film for Vaginal Delivery: Design, Optimization, and Physicodynamic Characterization. *AAPS PharmSciTech* **2009**, *10* (3), 951–959, DOI:10.1208/S12249-009-9288-0.
- (124) Calvo, N. L.; Svetaz, L. A.; Alvarez, V. A.; Quiroga, A. D.; Lamas, M. C.; Leonardi, D. Chitosan-Hydroxypropyl Methylcellulose Tioconazole Films: A Promising Alternative Dosage Form for the Treatment of Vaginal Candidiasis. *Int. J. Pharm.* **2019**, *556* (September 2018), 181–191, DOI:10.1016/j.ijpharm.2018.12.011.
- (125) Cautela, M. P.; Moshe, H.; Sosnik, A.; Sarmiento, B.; das Neves, J. Composite Films for Vaginal Delivery of Tenofovir Disoproxil Fumarate and Emtricitabine. *Eur. J. Pharm. Biopharm.* **2019**, *138*, 3–10, DOI:10.1016/J.EJPB.2018.02.001.
- (126) Elkasabgy, N. A. Ocular Supersaturated Self-Nanoemulsifying Drug Delivery Systems (S-SNEDDS) to Enhance Econazole Nitrate Bioavailability. *Int. J. Pharm.* **2014**, *460* (1–2), 33–44, DOI:10.1016/J.IJPHARM.2013.10.044.
- (127) Firooz, A.; Nafisi, S.; Maibach, H. I. Novel Drug Delivery Strategies for Improving Econazole Antifungal Action. *Int. J. Pharm.* **2015**, *495* (1), 599–607, DOI:10.1016/J.IJPHARM.2015.09.015.
- (128) Albertini, B.; Passerini, N.; Di Sabatino, M.; Vitali, B.; Brigidi, P.; Rodriguez, L. Polymer–Lipid Based Mucoadhesive Microspheres Prepared by Spray-Congeeing for the Vaginal Delivery of Econazole Nitrate. *Eur. J. Pharm. Sci.* **2009**, *36* (4–5), 591–601, DOI:10.1016/J.EJPS.2008.12.009.
- (129) Grammen, C.; Van Den Mooter, G.; Appeltans, B.; Michiels, J.; Crucitti, T.; Ariën, K. K.; Augustyns, K.; Augustijns, P.; Brouwers, J. Development and Characterization of a Solid Dispersion Film for the Vaginal Application of the Anti-HIV Microbicide UAMC01398. *Int. J. Pharm.* **2014**, *475* (1–2), 238–244, DOI:10.1016/J.IJPHARM.2014.08.054.
- (130) Neves, J. das; Sarmiento, B. Antiretroviral Drug-Loaded Nanoparticles-in-Films: A New Option for Developing Vaginal Microbicides? <https://doi.org/10.1080/17425247.2017.1270938> **2016**, *14* (4), 449–452, DOI:10.1080/17425247.2017.1270938.
- (131) Calvo, N. L.; Sreekumar, S.; Svetaz, L. A.; Lamas, M. C.; Moerschbacher, B. M.; Leonardi, D. Design and Characterization of Chitosan Nanoformulations for the Delivery of Antifungal Agents. *Int. J. Mol. Sci.* **2019**, *20*, Page 3686 **2019**, *20* (15), 3686, DOI:10.3390/IJMS20153686.
- (132) Tran, P.; Pyo, Y.-C.; Kim, D.-H.; Lee, S.-E.; Kim, J.-K.; Park, J.-S. Overview of the Manufacturing Methods of Solid Dispersion Technology for Improving the Solubility of Poorly Water-Soluble Drugs and Application to Anticancer Drugs. *Pharm.* **2019**, *11*, Page 132 **2019**, *11* (3), 132, DOI:10.3390/PHARMACEUTICS11030132.
- (133) Bertoni, S.; Albertini, B.; Ferraro, L.; Beggiano, S.; Dalpiaz, A.; Passerini, N. Exploring the Use

- of Spray Congealing to Produce Solid Dispersions with Enhanced Indomethacin Bioavailability: In Vitro Characterization and in Vivo Study. *Eur. J. Pharm. Biopharm.* **2019**, *139*, 132–141, DOI:10.1016/J.EJPB.2019.03.020.
- (134) Lehmkemper, K.; Kyeremateng, S. O.; Heinzerling, O.; Degenhardt, M.; Sadowski, G. Impact of Polymer Type and Relative Humidity on the Long-Term Physical Stability of Amorphous Solid Dispersions. *Mol. Pharm.* **2017**, *14* (12), 4374–4386, DOI:10.1021/ACS.MOLPHARMACEUT.7B00492.
- (135) Lehmkemper, K.; Kyeremateng, S. O.; Bartels, M.; Degenhardt, M.; Sadowski, G. Physical Stability of API/Polymer-Blend Amorphous Solid Dispersions. *Eur. J. Pharm. Biopharm.* **2018**, *124*, 147–157, DOI:10.1016/J.EJPB.2017.12.002.
- (136) Forster, A.; Hemenstall, J.; Rades, T. Characterization of Glass Solutions of Poorly Water-Soluble Drugs Produced by Melt Extrusion with Hydrophilic Amorphous Polymers. *J. Pharm. Pharmacol.* **2001**, *53* (3), 303–315, DOI:10.1211/0022357011775532.
- (137) Caron, V.; Hu, Y.; Tajber, L.; Erxleben, A.; Corrigan, O. I.; McArdle, P.; Healy, A. M. Amorphous Solid Dispersions of Sulfonamide/Soluplus® and Sulfonamide/PVP Prepared by Ball Milling. *AAPS PharmSciTech* **2013**, *14* (1), 464–474, DOI:10.1208/S12249-013-9931-7.
- (138) Zi, P.; Zhang, C.; Ju, C.; Su, Z.; Bao, Y.; Gao, J.; Sun, J.; Lu, J.; Zhang, C. Solubility and Bioavailability Enhancement Study of Lopinavir Solid Dispersion Matrixed with a Polymeric Surfactant - Soluplus. *Eur. J. Pharm. Sci.* **2019**, *134*, 233–245, DOI:10.1016/J.EJPS.2019.04.022.
- (139) Albertini, B.; Sabatino, M. Di; Melegari, C.; Passerini, N. Formulation of Spray Congealed Microparticles with Self-Emulsifying Ability for Enhanced Glibenclamide Dissolution Performance. <http://dx.doi.org/10.3109/02652048.2014.985341> **2015**, *32* (2), 181–192, DOI:10.3109/02652048.2014.985341.
- (140) Bertoni, S.; Albertini, B.; Passerini, N. Spray Congealing: An Emerging Technology to Prepare Solid Dispersions with Enhanced Oral Bioavailability of Poorly Water Soluble Drugs. *Mol. 2019, Vol. 24, Page 3471* **2019**, *24* (19), 3471, DOI:10.3390/MOLECULES24193471.
- (141) Haaf, F.; Sanner, A.; Straub, F. Polymers of N-Vinylpyrrolidone: Synthesis, Characterization and Uses. *Polym. J.* **1985**, *17* (1), 143–152, DOI:10.1295/polymj.17.143.
- (142) Hasa, D.; Voinovich, D.; Perissutti, B.; Grassi, G.; Fiorentino, S.; Farra, R.; Abrami, M.; Colombo, I.; Grassi, M. Reduction of Melting Temperature and Enthalpy of Drug Crystals: Theoretical Aspects. *Eur. J. Pharm. Sci.* **2013**, *50* (1), 17–28, DOI:10.1016/J.EJPS.2013.03.018.
- (143) Shaker, M. A. Dissolution and Bioavailability Enhancement of Atorvastatin: Gelucire Semi-Solid Binary System. *J. Drug Deliv. Sci. Technol.* **2018**, *43*, 178–184, DOI:10.1016/J.JDDST.2017.10.003.
- (144) Bertoni, S.; Albertini, B.; Passerini, N. Different BCS Class II Drug-Gelucire Solid Dispersions Prepared by Spray Congealing: Evaluation of Solid State Properties and In Vitro Performances. *Pharm. 2020, Vol. 12, Page 548* **2020**, *12* (6), 548, DOI:10.3390/PHARMACEUTICS12060548.
- (145) Dolci, L. S.; Liguori, A.; Panzavolta, S.; Misericocchi, A.; Passerini, N.; Gherardi, M.; Colombo, V.; Bigi, A.; Albertini, B. Non-Equilibrium Atmospheric Pressure Plasma as Innovative Method to Crosslink and Enhance Mucoadhesion of Econazole-Loaded Gelatin Films for Buccal Drug Delivery. *Colloids Surfaces B Biointerfaces* **2018**, *163*, 73–82, DOI:10.1016/j.colsurfb.2017.12.030.
- (146) Amadori, S.; Torricelli, P.; Rubini, K.; Fini, M.; Panzavolta, S.; Bigi, A. Effect of Sterilization and Crosslinking on Gelatin Films. *J. Mater. Sci. Mater. Med.* **2015**, *26* (2), 1–9, DOI:10.1007/S10856-015-5396-4.
- (147) Bigi, A.; Cojazzi, G.; Panzavolta, S.; Roveri, N.; Rubini, K. Stabilization of Gelatin Films by Crosslinking with Genipin. *Biomaterials* **2002**, *23* (24), 4827–4832, DOI:10.1016/S0142-9612(02)00235-1.

- (148) Kujawski, J.; Czaja, K.; Jodłowska, E.; Dettlaff, K.; Politańska, M.; Zwawiak, J.; Kujawski, R.; Ratajczak, T.; Chmielewski, M. K.; Bernard, M. K. Structural and Spectroscopic Properties of Econazole and Sulconazole – Experimental and Theoretical Studies. *J. Mol. Struct.* **2016**, *1119*, 250–258, DOI:10.1016/J.MOLSTRUC.2016.04.065.
- (149) Tejada, G.; Lamas, M. C.; Svetaz, L.; Salomón, C. J.; Alvarez, V. A.; Leonardi, D. Effect of Drug Incorporation Technique and Polymer Combination on the Performance of Biopolymeric Antifungal Buccal Films. *Int. J. Pharm.* **2018**, *548* (1), 431–442, DOI:10.1016/J.IJP.2018.07.023.

## **Chapter 3.** **SCAFFOLDS**

### **3.1 INTRODUCTION**

Chondral and osteochondral defects are challenging problems, since the native structure of cartilage and subchondral bone cannot be regenerated with any of the available treatments <sup>1</sup>.

The staggering growth of procedures points toward a need for regenerative solutions for bone and cartilage, that are scalable and can remain successful throughout the life of the patient.

Tissue engineering approaches are well underway to regenerate the most complex of tissues through the use of external templates (scaffolds) which simulate the cell growth microenvironment and combine the body's self-healing ability to guide the regeneration in damaged or defective tissue sites.

As introduced in the 'Tissue engineering' section of Paragraph 1.3, the 3D biomaterial scaffolds act as templates for cell attachment and tissue repair <sup>2</sup>: cells are allowed to proliferate and organize their extracellular matrix in a three-dimensional (3D) lattice to form *ex vivo* a clinically functional tissue, exhibiting histochemical, biochemical and biomechanical properties identical to native, healthy tissue <sup>3</sup>. Hence, far from being passive components, tissue engineering scaffolds provide a promising way to repair and regenerate damaged tissues by mimicking the structural and functional profile of the natural extra-cellular matrix (ECM) <sup>4</sup>, providing a friendly interaction with biological tissues and promoting tissue repair. Furthermore, an ideal scaffold should fill the missing segment of the defective tissue and provide a sufficient mechanical support for host tissue immediately after implantation <sup>5</sup>. In fact, at the most basic level, the tissue engineering scaffolds serve as a mechanical support for the regeneration of tissues, especially in load-bearing areas.

However, the scaffold design is very complex: an adequate macro- and micro-porosity must be achieved together with pore interconnection to allow cell spread and proliferation, tissue infiltration, nutrient and waste exchange, as well as blood vessel and nerve growth. Hence, a successful scaffold should combine a mechanical function (similar to that of the native tissue) with the delivery of biologically relevant molecules, providing a sequential transition in which the regenerated tissue assumes function as the scaffold degrades <sup>6</sup>. For example, for bone tissue regeneration, it has been reported that the minimum requirement for pore diameters is considered 100  $\mu\text{m}$ , necessary for cell attachment, migration and transport; while pore diameters over 300  $\mu\text{m}$  are recommended for tissue ingrowth <sup>7</sup>. Additional studies have also shown the importance of pore size on the progression of osteogenesis, due to vascularization, and the role of scaffold morphology <sup>8</sup>: since there is no consensus on the ideal pore size, maybe

the best way is to create scaffolds with gradients of porosity to serve specific functions during the healing process <sup>7</sup>.

Approaches in scaffold design must meet all the mentioned requirements and, to this aim, several fabrication techniques have been employed, from conventional to rapid prototyping methods. Conventional techniques include porogen leaching, gas foaming, phase separation, fiber meshing, supercritical fluid processing, microsphere sintering, electrospinning and freeze-drying <sup>9,10</sup>, while 3D printing and additive manufacturing are examples of non-conventional methods. The different preparation methods allow to have a different control on the morphology, porosity and final properties of the scaffolds, and the most suitable method for the synthesis must be chosen according to the use.

Bone and cartilage are included under the same orthopedic field, but they are very different tissues and hence require different approaches to regenerate. In fact, unlike bone, which has a high regenerative potential, cartilage does not have a vascular network and has limited self-repair and regeneration ability: once damaged, it cannot effectively repair, eventually leading to the occurrence of osteoarthritis <sup>11</sup>. Even the repair of small cartilage defects is hampered by its avascular nature, low cell density and slow diffusion of nutrients <sup>2</sup>.

Nowadays, the materials employed for scaffolds fabrication are natural or synthetic polymers such as polysaccharides, poly( $\alpha$ -hydroxy ester), hydrogels or thermoplastic elastomers <sup>12</sup>. However, freestanding polymeric scaffolds lack mechanical strength and other desired functions to serve as graft material <sup>12</sup>. In order to customize the mechanical, structural and surface properties, it is possible to vary the ratios and combination of different polymers; even the degradability can be tuned by modifying the chain length or using polymeric mixtures. With this aim, composites of polymers and ceramics have been developed <sup>13</sup> and also scaffolds loaded with bioactive molecules were produced in order to confer them drug delivery capacity.

During my doctorate I developed both scaffold for bone and cartilage tissue repair and the main results are reported in Chapters 3.3 and 3.4, respectively.

For the production of scaffolds for bone repair, I selected gelatin as biopolymer since it is not antigenic, it is biocompatible and biodegradable under physiological conditions. As explained in the 'Gelatin' section of Paragraph 1.2, it is obtained by thermal denaturation or physical and chemical degradation of collagen through the breaking of the triple-helix structure into random coils; hence, it is completely resorbable *in vivo* <sup>14</sup>. However, due to its high solubility in aqueous environment, a crosslinking reaction is mandatory <sup>15</sup>. Crosslinking, defined as induction of chemical or physical links among polymer chains, is a simple method that usually involves the  $\epsilon$ -amino groups of the lysine residues and is generally used to modify mechanical, biological

and degradation properties of hydrogels <sup>16</sup>. Different crosslinking methods may be used, including chemical, plasma and enzymatic methods, together with the use of small crosslinkers, such as glutaraldehyde and genipin <sup>16</sup>.

To produce materials for bone regeneration able to reduce osteoclast activity in osteoporotic bones, I designed layered scaffolds with different crosslinking degree to modulate their stability in physiological conditions, and hence the lifetime of the structure. The mechanical properties of these gelatin lattices, already enhanced by the anisotropic curled structure, were improved by the addition of an inorganic phase. The Sr-substituted hydroxyapatite loaded into the scaffolds conferred drug delivery ability to the scaffold, which showed a sustained release of Sr ions in the surrounding media. Overall, the results of this work proposed an alternative method for reinforcing and modulating the final properties of bone scaffolds, and have been published in a scientific international journal <sup>17</sup>.

Scaffolds for cartilage repair were obtained by combining different types of gelatin (derived from mammalian or from fish) with chitosan, a natural aminopolysaccharide obtained by alkaline deacetylation of chitin, the main component of crabs and shrimps shells <sup>18</sup>. Chitosan is particularly suitable for cartilage repair, since its structure is similar to the glycosaminoglycans (GAG) that are naturally present in the cartilage extracellular matrix, and probably this is the reason of its superior biocompatibility. As for bone tissue, cartilage scaffolds must initially have a certain mechanical stability and must allow a regular distribution of cells: balancing the ratio between the amount of chitosan and gelatin allowed us to tune both the porosity and solubility of the material.

Given the experience of the research team and the previous studies on film formulations, the composition of these biomaterials was enriched with snail slime. The preparation of these materials posed several challenges: at first, the amount and the type of gelatin used in the scaffold fabrication significantly influenced the morphology and the stability of the final material. Moreover, the high solubility of the scaffold made it necessary to find a non-toxic crosslinker acting on both gelatin and chitosan, and able to maintain the sustainability of the whole process.

Even if the method employed was effective for scaffolds prepared with porcine gelatin, it revealed to be inadequate in the case of fish gelatin. Additionally, the presence of snail slime limited the cross-linking degree of the biomaterials: its role in the scaffold's composition and its contribution to scaffolds properties must be studied deeper.

While the biomaterials used without cells have been successful in bone repair (as guide for tissue regeneration mechanisms, or for the migration of cell populations to lesion from adjacent tissue), these have proven to be inadequate for cartilage treatment, probably due to the limited

proliferative and migratory capacity of chondrocytes <sup>19</sup>. However, the preliminary results of this work are promising, even if other analyses are needed to evaluate their biological activity and ability to express the genetic markers necessary for cartilage repair.

## 3.2 EXPERIMENTAL PART

### 3.2.1 Gelatin-based scaffolds for bone tissue engineering

#### Materials

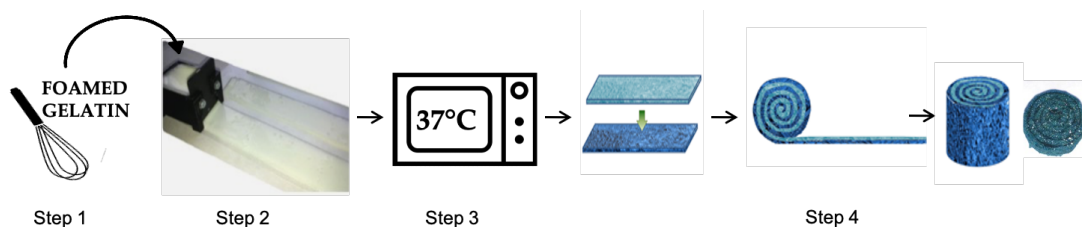
Porcine gelatin (type A, 300 Bloom) and Glycine were purchased from Sigma Aldrich (St. Louis, MO, USA). Genipin was purchased from Wako Chemicals (Osaka, Japan).

#### Synthesis of Sr-substituted hydroxyapatite

Strontium-substituted hydroxyapatite (Sr-HA) synthesis was performed through direct synthesis in aqueous solution. Briefly, 50 mL of 0.65 M  $(\text{NH}_4)_2\text{HPO}_4$  solution (pH 10 adjusted with  $\text{NH}_3$ ) was added dropwise under stirring to the 1.08 M cationic solution  $\text{Ca}(\text{NO}_3)_2 \cdot 4\text{H}_2\text{O}$  +  $\text{Sr}(\text{NO}_3)_2$ , with a Sr/(Ca + Sr) ratio of 0.10 and heated at 90 °C for 4 h. The precipitate was centrifuged, dried at 37 °C, finely ground in a mortar and sieved.

#### Preparation of gelatin-based scaffolds

To produce gelatin-based scaffolds, gelatin was dissolved in distilled water at 55 °C under magnetic stirring and foamed for 90 seconds. Based on the desired lifetime of the scaffold, 2.5 mL of genipin solution at different concentrations in distilled water were used (Step 1): solution 0.05, 0.1, 0.15 and 0.2% (w/w of genipin with respect to the amount of gelatin). 2.5 mL of PBS (1 M at pH 7.4) were added to accelerate the cross-linking reaction. The foam was then shaped in strips with a uniform thickness of 1 mm and length of 18 cm using a 3D-printed doctor-blade (Step 2)<sup>20</sup>. The strips were kept at 37 °C for 1 h in order to start the cross-linking reaction which led to a change of the scaffold's color from white to blue (Step 3). Cylindrical single- and double-layer scaffolds with a spiral cross-section were obtained by hand rolling a single damp gelatin stripe and two overlapped gelatin stripes of different composition, respectively. The obtained scaffolds were immersed in glycine 0.1 M for 30 min, washed with distilled water, immersed in ethanol for 24 h and then freeze-dried overnight. The obtained scaffolds were labeled according to their genipin content: G\_0.05, G\_0.1, G\_0.15, G\_0.2 (Step 4). In the case of double-layer scaffolds, the outer layer was always the stripe cross-linked with the major genipin concentration (G\_0.2). Samples obtained by overlapping stripes with different genipin content were labelled G\_0.05/G\_0.2, G\_0.1/G\_0.2 and G\_0.15/G\_0.2. The preparation method is summarized in Scheme 1.



*Scheme 1. Scheme of preparation of the spiral cross-section scaffolds.*

In order to evaluate the scaffolds' ability to be loaded with drugs, active molecules or inorganic phases and then to release them, the composition of G\_0.1 stripe was enriched with 30% of Sr-HA (w/w of Sr-HA with respect to the total weight of Sr-HA and gelatin) by adding it to the gelatin suspension before foaming. Cylindrical single- and double-layer scaffolds were obtained by curling one strip as previously described (obtaining samples labeled as G\_0.1\_HA), or two superimposed stripes rolled with the G\_0.2 strip (double-layer samples labeled as G\_0.1\_HA/G\_0.2). Non-curved strips of the same composition as G\_0.1\_HA were used as control and labeled S\_0.1\_HA. Samples were labeled according to their genipin content, expressed as ratio (%) between the weight of genipin and gelatin. S\_0.1\_HA is the single flat layer (non-rolled) scaffold used as reference. The compositions of the obtained scaffolds are summarized in Table 13.

*Table 13. Composition of the obtained single-layer and double-layer scaffolds.*

Single-layer scaffolds	Genipin % (w genipin/w gelatin)	Double-layer scaffolds	Genipin % (w genipin/w gelatin)	
			Inner layer	Outer layer
S_0.1 Sr-HA	0.1			
G_0.05	0.05			
G_0.1	0.1	G_0.05/G_0.2	0.05	0.2
G_0.15	0.15	G_0.1/G_0.2	0.1	0.2
G_0.2	0.2	G_0.15/G_0.2	0.15	0.2
G_0.1 Sr-HA	0.1	G_0.1 Sr-HA/G_0.2	0.1	0.2

Samples were labeled according to their genipin content, expressed as ratio (%) between the weight of genipin and gelatin. G refers to rolled scaffolds, while S\_0.1\_Sr-HA is the single flat layer (non-rolled) scaffold used as reference.

### **Scaffold Characterization**

Scaffolds were characterized as described in 'Compressive Tests' and 'Scanning Electron Microscopy' sections of Paragraph 3.2.3.

### **X-ray Diffraction**

X-ray diffraction analyses were carried out by means of an X'Pert powder diffractometer (Philips, Eindhoven, Netherlands) equipped with a graphite monochromator in the diffracted beam. CuK $\alpha$  radiation ( $\lambda = 15,418 \text{ \AA}$ ; 40 mA; 40 kV) was used. XRD patterns were obtained in the 3–50°/2 $\theta$  range using a 0.03 step and a 3°/min speed.

### **Extent of crosslinking**

The measurement of the extent of cross-linking is based on the determination of the unreacted  $\epsilon$ -amino groups belonging to lysine residues. Briefly, selected samples were allowed to react with TNBS (trinitro-benzen sulfonic acid) and, after hydrolysis in HCl 6 N, the absorbance of the solution was measured at 346 nm against a blank. The moles of  $\epsilon$ -amino groups per gram of gelatin are obtained by the following formula:

$$\text{Moles of } \epsilon\text{-amino groups/g of gelatin} = \frac{2 \cdot A \cdot V}{\epsilon \cdot b \cdot x} \quad 7)$$

where A is the absorbance value, V is the final volume of the sample,  $\epsilon$  is the molar absorptivity, x is the optical path and b is the weight of the tested sample, expressed in grams. The degree of cross-linking (%) was determined from the ratio between the moles of free  $\epsilon$ -amino groups in genipin treated gelatin and those in non-crosslinked gelatin.

### **Water Uptake Ability (WUA)**

The equilibrium water uptake ability was determined after immersion of the pre-weighted dry samples in phosphate buffered saline (PBS 0.1 M, pH= 7.4) at 37 °C for 20 s. The weight of the wet samples was measured after PBS excess removal. Then, the WUA was calculated according to the following equation:

$$WUA = \frac{W_w - W_d}{W_d} \quad 8)$$

where  $W_w$  and  $W_d$  represent the weight of the wet and dry sample, respectively. The process was repeated in triplicate and data were reported as mean and standard deviation.

### **Gelatin release**

Gelatin release in NaCl 0.9% solution at 37 °C was determined at increasing times, from 2 to 70 days by colorimetric method using a bicinchoninic acid protein assay (Sigma Chemicals, St. Louis, MO, USA).

### **Strontium release**

For the evaluation of strontium release kinetics, samples G\_0.1\_HA/G\_0.2, G\_0.1\_HA and S\_0.1\_HA were weighted, immersed in 5 mL of saline solution (NaCl 0.9% in ultrapure water, added with sodium azide to prevent microbial contamination) and stored at 37 °C for different periods of time up to 7 days. At every selected time, the medium was removed and replaced with 5 mL of saline solution. Three different samples for each time were analyzed. Aliquots of the collected medium were suitably diluted with HNO<sub>3</sub> 0.5 M, containing 10% (w/V) of LaCl<sub>3</sub>·H<sub>2</sub>O (99% trace metal basis, Sigma Aldrich). Quantitative determination of strontium content was made by means of atomic absorption spectrophotometer (AAS, Analyst 400, Perkin

Elmer Italia, Milano, Italy) equipped with an air-acetylene burner and a strontium lamp working at a wavelength of 460.73 nm. The standard additions method was used.

### **Statistical analysis**

Statistical evaluation of data was performed using the software package SPSS/PC+ Statistics 23.0 (SPSS Inc., Chicago, IL, USA). The results presented are the mean of six independent values. Data are reported as mean  $\pm$  standard deviations (SD) at a significance level of  $p < 0.05$ . After having verified normal distribution and homogeneity of variance, a one-way ANOVA was done for comparison

## **3.2.2 Chitosan and gelatin-based scaffolds for cartilage repair**

### **Materials**

Chitosan (C, degree of deacetylation = 93%, M.W.=100 KDa) was purchased from Faravelli (Milan, Italy). Gelatin (G) from cold water fish (MW=60 KDa) and porcine skin (type A, 300 Bloom, MW=50-100 KDa) were purchased by Sigma-Aldrich. Acetic acid was purchased from Sigma Aldrich (Milan, Italy). Snail slime from *Helix Aspersa* Muller snails extracted by MullerOne method was provided by “I Poderi” farm (Montemerano, Italy), and details are reported in Appendix I.

### **Preparation of chitosan and gelatin-based scaffolds with snail slime**

Chitosan and gelatin-based scaffolds were prepared by suspending the proper amount of gelatin (10 % w/v) in acetic acid (2% w/v) under stirring at 35 °C. After complete gelatin dissolution, chitosan (2% w/v) was added at RT and the mixture was left under stirring for 2 h. Then, the solution was foamed for 5 minutes at room temperature, put in Petri dishes and kept at -20°C for 2 hours. The scaffolds were obtained by freeze-drying and labelled GpC and GfC for porcine and fish gelatin-based scaffolds, respectively.

To obtain chitosan and gelatin-based scaffolds containing different amount of snail slime (S), the relative volume of S (10 and 30 % v/v) was added to the solution of gelatin and chitosan previously dissolved in the remaining volume of acetic acid (2% w/v). The solution was foamed for 5 minutes at RT, put in Petri dishes, and kept at -20°C for 2 hours. The obtained scaffolds were labelled GpC\_S10, GpC\_S30 and GfC\_S10, GfC\_S30, according to the gelatin used and the amount of slime employed. The compositions and labels of the obtained samples are summarized in Table 14.

The dry scaffolds were crosslinked by immersion in a tripolyphosphate (TPP) aqueous solution (10% w/V, pH<6) at 4°C for 2 h. Then, the scaffolds were repeatedly washed with abundant distilled water, kept for 2 hours at -20°C and then lyophilized.

Table 14. Compositions and labels of the obtained chitosan/gelatin-based scaffolds.

Sample	Chitosan % (w/v)	Gelatin % (w/v)		Acetic acid % (v/v)	Snail slime % (v/v)
		Fish	Porcine		
GpC	2	-	10	100	0
GfC	2	10	-	100	0
GpC_S10	2	-	10	90	10
GfC_S10	2	10	-	90	10
GpC_S30	2	-	10	70	30
GfC_S30	2	10	-	70	30

### **Scaffold Characterization**

The mechanical properties were tested as described in section ‘Compressive Tests’ while morphological evaluation by means of scanning electron microscopy (SEM) of the obtained scaffolds was performed as described in section ‘Electron Microscopy’ of Paragraph 3.2.3.

### **Swelling degree**

Cubic-shaped (1 cm<sup>3</sup>) scaffolds were weighted and immersed in 5 mL of PB at 37°C. After fixed time intervals (1, 3, 5, 10, 20, 30, 60, 120, 180, 240 and 300 minutes) the samples were removed from the solution, wiped with filter paper to remove the excess of liquid and then reweighted. The swelling degree was obtained using the following equation:

$$Swelling (\%) = \frac{Ww - Wd}{Wd} \cdot 100 \quad 9)$$

where Ww and Wd are the weights of the wet and the air-dried sample, respectively.

### **Scaffold solubility**

After 24 h from the swelling studies, the scaffolds not completely dissolved were removed from the solution and dried at 37°C until a constant weight is obtained. The solubility was calculated as following:

$$Solubilization (\%) = \frac{Wi - Wf}{Wi} \cdot 100 \quad 10)$$

where Wi and Wf are the weights of the sample before and after immersion in water, respectively.

### **3.2.3 Methods of Characterization**

#### **Compressive Tests**

Mechanical characterization of the scaffolds was performed on samples in dry conditions. Compression tests were carried out using a 4465 Instron testing machine, equipped with a 1 kN load cell. Six samples were tested for each composition, at a loading rate of 1.0 mm/min.

#### **Scanning Electron Microscopy**

Morphological and micro-structural analyses were performed with a Philips XL-20 scanning electron microscope (SEM) operating at 15 kV. Scaffolds were sputter-coated with gold before the analysis.

Energy dispersive X-ray spectrometry (EDS) maps were performed on composite scaffolds using a Philips XL-20 Scanning Electron Microscope operating at 15 kV.

Transmission electron microscopy (TEM) investigation of the synthesized powders was carried out using a Philips CM 100 transmission electron microscope operating at 80 kV. A small amount of powder was dispersed in ethanol and submitted to ultrasonication; then, a drop of the suspension was transferred onto holey carbon foils supported on conventional copper micro grids.

### 3.3 GELATIN-BASED SCAFFOLDS FOR BONE TISSUE ENGINEERING

#### Introduction

The structure of the scaffold plays a critical role in the reconstruction of bone tissues, but conventional porous scaffolds exhibit isotropic transmission of stress <sup>21</sup>, which hampers their integration with the anisotropic host bone. Accordingly, finely designed 3D scaffolds with similar structures of natural bone are required for better bone integration and even for successful osteointegration and functional reconstruction of bone defects. In fact, it has been demonstrated that that spiral- cylindrical arrangement of hybrid chitosan/cellulose/nano-hydroxyapatite membranes can promote complete infiltration of bone tissues *in vivo* <sup>22</sup>. Hence, the rolling-up strategy has been applied by several groups in scaffold fabrication, also made by nanofibers <sup>23–26</sup>, with the purpose to increase the surface to volume ratio for cell attachment and form a 3D non-planar cell matrix <sup>27</sup>.

In this study, I developed new anisotropic gelatin scaffolds for bone tissue engineering by assembling gelatin foamed strips, which were curled concentrically to generate a cylindrical scaffold with a spiral cross-section, which composition and structure mimic the osteon concentric arrangement. The 3D rolled scaffolds were stabilized by crosslinking with genipin, a natural crosslinking molecule extracted from the fruits of *Gardenia jasminoides Ellis*, which exhibits low cytotoxicity when compared to other chemical crosslinking agents. Genipin can efficiently crosslink cellular tissues and biomaterials containing primary amino-groups to form blue pigments <sup>28–31</sup>. Different genipin concentrations were tested in order to obtain strips with different crosslinking degrees and hence a tunable stability in biological environment.

Furthermore, the possibility to enrich the material with an inorganic phase was investigated: enrichment with strontium substituted hydroxyapatite (Sr-HA) was performed to obtain systems with improved mechanical performances and with an anti-osteoporotic activity, thanks to a sustained release of strontium over time. Indeed, strontium is known to display a beneficial role on bone remodeling, and it has been proposed for the treatment of pathologies associated to excessive bone resorption (e.g., osteoporosis) <sup>32,33</sup>: its action on bone turnover has been ascribed to the combined effect of decrease of bone resorption and enhancement of bone formation <sup>34,35</sup>, and clinical studies showed a beneficial effect of strontium treatment in osteoporotic patients <sup>36,37</sup>.

The approach used (see Scheme 1) provided highly porous multi-layered scaffolds with anisotropic mechanical properties and a sustained strontium release, suggesting possible applications for the local treatment of abnormally high bone resorption. Moreover, this study demonstrates that assembly of layers of different composition can be used as a tool to obtain

scaffolds with modulated properties, which can be loaded with drugs or biologically active molecules to provide properties tailored upon the needs.

## Results and discussion

Porous gelatin scaffolds can be obtained through foaming and freeze-drying of gelatin aqueous solutions<sup>38–40</sup>. Herein, we employed an extremely versatile method to prepare composite multi-layered scaffolds in a very simple way: cylindrical scaffolds were prepared by rolling up one or two overlapped layers at different degree of crosslinking, as depicted in Scheme 1. The use of doctor-blade, a technique in which a blade with a certain gap height is used to produce porous large strips<sup>41</sup>, allowed us to obtain regular strips of foamed gelatin (step 2) with a set width and thickness and provided highly porous multi-layered scaffolds with anisotropic mechanical properties. The compositions and labels of each scaffold are reported in Table 1 (Paragraph 3.2.1).

### Sr-HA Characterization

It is well known that strontium is present in the mineral phase of bone, especially in the regions of high metabolic turn-over<sup>42</sup>, and that its administration to post-menopausal women has beneficial effect in the treatment of osteoporosis, reducing bone resorption and enhancing bone formation. Strontium can easily replace calcium in the hydroxyapatite structure, because of the chemical similarity between the two cations. For this reason, Sr-substituted hydroxyapatite, with a Sr content of 10% (in atoms), was synthesized and employed for scaffold manufacturing. The X-ray powder diffraction pattern of the obtained Sr-HA is reported in Figure 57a, together with the pattern of hydroxyapatite (HA) as comparison.

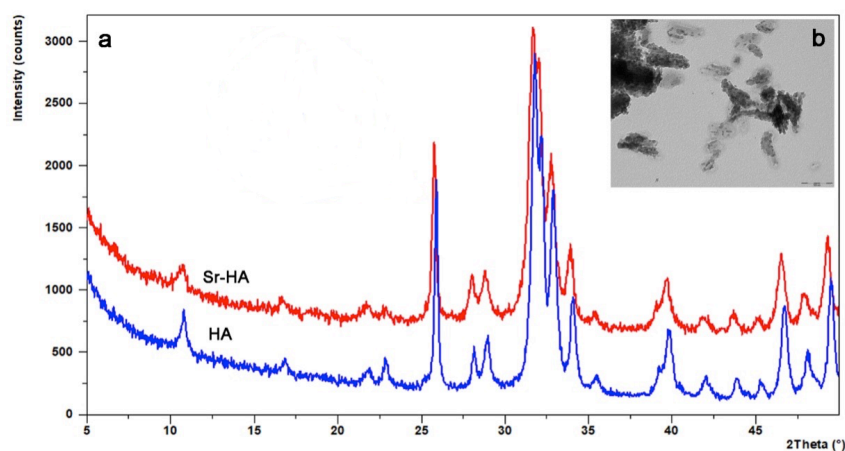


Figure 57. a) X-Ray diffraction pattern of strontium-substituted hydroxyapatite (Sr-HA) and of hydroxyapatite (HA); b) TEM image of Sr-HA nanocrystals (bar = 100nm).

All the peaks in Sr-HA pattern are characteristic of hydroxyapatite, which is the only crystalline phase obtained from the synthesis. The incorporation of Sr into the crystal lattice of

hydroxyapatite is confirmed by the shift of the main diffraction peaks of Sr-HA (25-26.5°/2theta range), at lower angles when compared to those present in the X-ray diffraction pattern of the samples synthesized in the absence of strontium (HA), as reported in literature <sup>43</sup>. This shift is in agreement with the substitution of calcium with the bigger strontium ion into the hydroxyapatite structure. Sr-HA appears constituted of nanocrystals with small dimensions (about 20 nm long) and an irregular shape, as shown in the TEM image (Figure 57b).

### Structural characterization

The preparation of the scaffolds implied gelatin foaming, crosslinking, and air drying. The structural modifications induced by this procedure on gelatin was analyzed using X-ray diffraction analysis: the wide-angle X-ray diffraction peak of collagen at about 1.1 nm, which is related to the diameter of the triple helix, can be used as an index of the degree of renaturation of gelatin <sup>44</sup>.

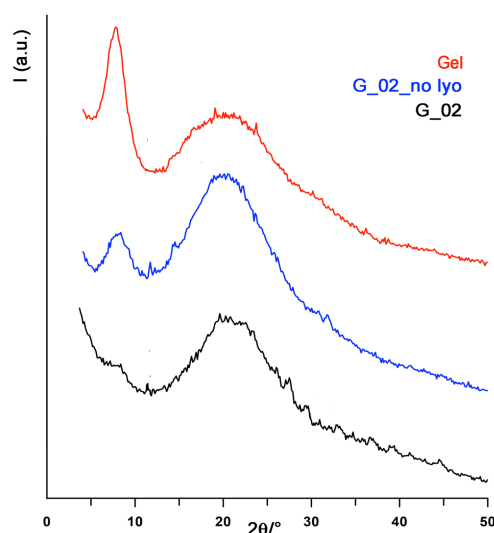


Figure 58. X-rays powder diffraction patterns recorded on gelatin foam (Gel, red), gelatin foam containing genipin before lyophilization (G\_02\_no lyo, blue) and the same sample after lyophilization (G\_02, black).

Figure 58 reports the wide-angle X-ray diffraction patterns of samples during the different steps of the scaffold's preparation. All the patterns displayed a diffraction peak at about 8°/2θ, corresponding to the periodicity of 1.1 nm, and a broad halo centered around 20°/2θ corresponding to a periodicity of about 0.45 nm, due to the distance between adjacent polypeptide strands <sup>45</sup>. The presence of genipin during the cooling of the foam involved the formation of crosslinks which inhibited the conformational disorder-order transition: in fact, the 1.1 nm peak displayed a high relative intensity in the pattern recorded from gelatin foam (Gel), while it seemed reduced in the XRD pattern of the sample obtained after foaming in presence of genipin before lyophilization (G\_02\_no lyo), suggesting a decrease of the triple helix content. The further reduction of the relative intensity of the diffraction peak observed on

the scaffold after freeze-drying (G\_02) is consistent with a further decrease of the triple helix content, in agreement with what previously reported for wet and freeze-dried collagen <sup>46</sup>.

### Morphological evaluation

The morphology of the obtained scaffolds was investigated by means of scanning electron microscopy. The images in Figure 59a-d, related to single layer rolled scaffolds, confirm the high porosity and the interconnection of pores; furthermore, the layers appeared strictly joined, forming a continuous network without uneven areas at the joint points.

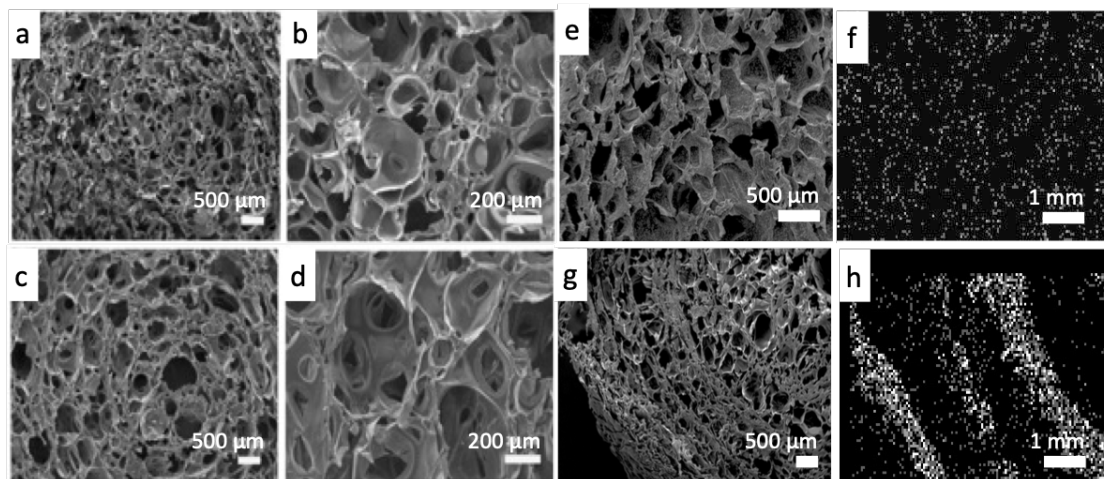


Figure 59. SEM images of single-layer curled scaffolds (a-d): G\_0.1 (a,b) and G\_0.15 (c,d); flat layer scaffold S\_0.1\_Sr-HA (e) and double-layer rolled scaffold G\_0.1\_Sr-HA/G\_0.2 (g) with their EDS map showing the presence of Sr (f and h, respectively).

Figure 59e shows the structure of a single flat layer (S\_0.1\_Sr-HA) containing Sr-HA: the homogeneous distribution of Sr-HA nanocrystals inside the gelatin network is confirmed by the EDS maps reported in Figure 59f, where the small bright zones indicate the presence of strontium.

The morphology of the double layered scaffold G\_0.1\_Sr-HA/G\_0.2 is showed in Figure 59g, together with its EDS map (Figure 59h): the layered structure is well evident, since the layers containing the inorganic phase appear more compact. These images suggest that rolling up layers containing Sr-HA provokes a reduction of the pore's dimensions in comparison with those of the flat layer. Moreover, a clear separation between the layers was found: these gaps are very important for an improved nutrient transport within the matrix because they could meet the nutrient requirement of the inner regenerated tissue which is subject to the restrained diffusion rate of oxygen and other nutrient <sup>27</sup>. Furthermore, the Sr-HA containing layers can be easily identified by the EDS map, which localizes the presence of strontium inside the cylindrical structure.

## Mechanical properties

Mechanical properties were measured under compression both in longitudinal and transverse direction and the results are reported in Figure 60.

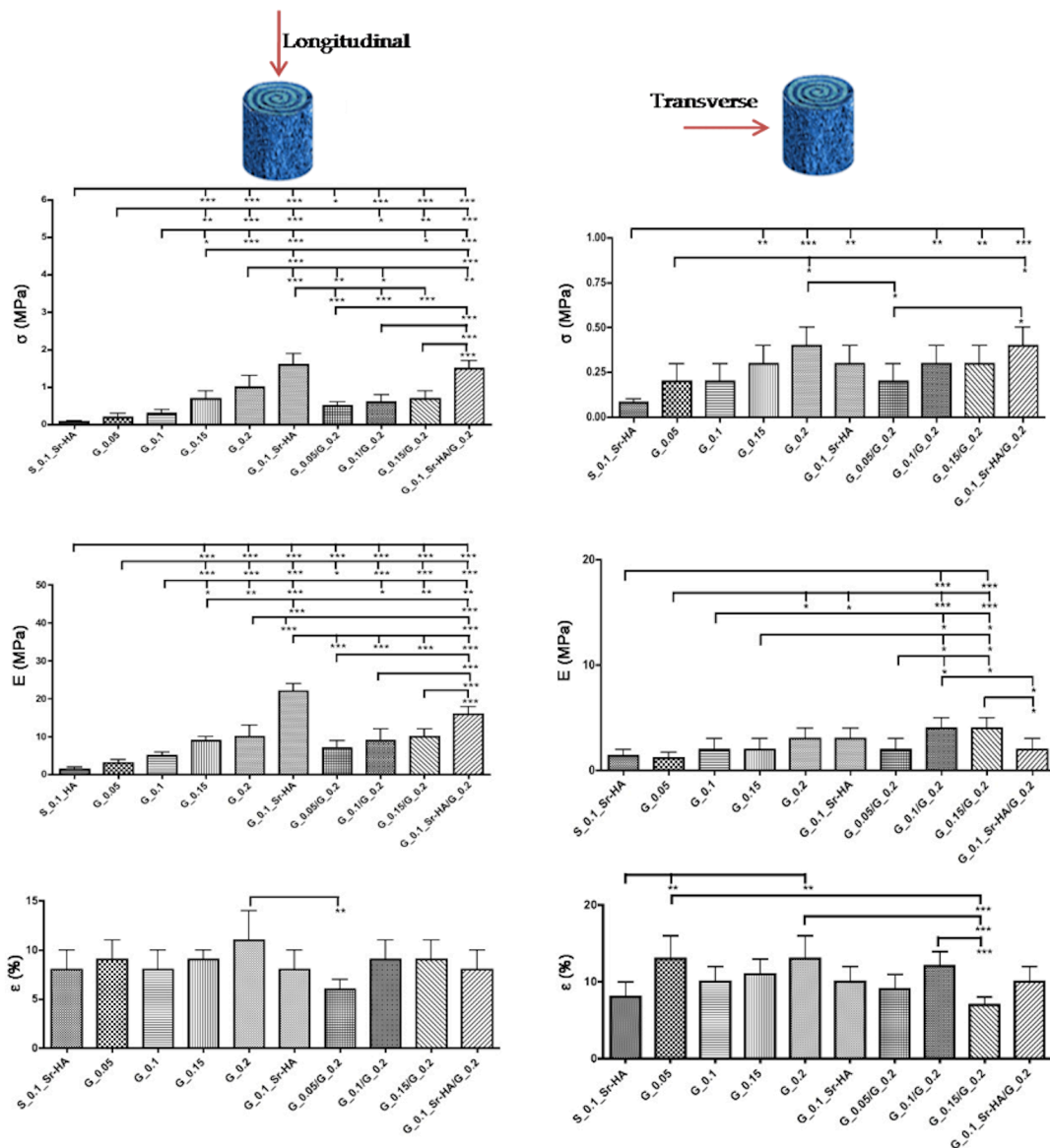


Figure 60. Mechanical properties in compression, measured in longitudinal and transverse direction. Each value is the average of six determinations and is reported with its standard deviation and statistical analysis. Asterisks indicate the results of Turkey post-hoc test (\* $p < 0.05$ , \*\* $p < 0.01$  and \*\*\* $p < 0.001$ ).

At variance with the great majority of the porous scaffolds proposed for bone repair<sup>47</sup>, the peculiar three-dimensional structure of the scaffold resulted in anisotropic mechanical properties: both the values of maximum stress at break and of elastic modulus in compression were significantly higher when measured along the longitudinal (parallel to the long axis of the cylindrical scaffold) than the transverse direction of the scaffolds. Also the values measured in the transverse direction were higher than those measured for the flat-layer scaffold S\_0.1\_Sr-HA, which showed isotropic mechanical properties when tested both longitudinally and

transversely. An improvement of the mechanical properties, especially along the longitudinal direction, was obtained through the variation of the crosslinker's concentration: increasing of genipin concentration up to 0.2% (w/w of genipin with respect to the amount of gelatin) provoked an increase in the degree of crosslinking up to about 30% and, as a consequence, an improvement of both the values of maximum stress at break and of Young's modulus, as found in literature <sup>48</sup>. The scaffolds prepared with two different layers exhibited intermediate mechanical properties between those of the single-layered scaffolds, while the compaction caused by rolling the scaffolds enhanced the mechanical properties (compare the values of S\_0.1\_Sr-HA with those of G\_0.1\_Sr-HA). The introduction of Sr-HA in the composition of the scaffolds provoked a further enhancement of the mechanical properties, in agreement with what previously reported for isotropic scaffolds, which showed increasing mechanical performances on increasing the inorganic phase content <sup>49</sup>: the stress at break of G\_0.1\_Sr-HA measured in longitudinal direction was five times higher than that of G\_0.1 ( $1.6 \pm 0.3$  for G\_0.1\_Sr-HA and  $0.3 \pm 0.1$  for G\_0.1), whereas the values of the mechanical parameters along the transverse direction did not show significant variation as a function of composition.

### Extent of crosslinking

The extent of crosslinking calculated for single-layer rolled scaffolds is reported in Table 15. The crosslinking degree significantly increased from G\_0.05 to G\_0.2, in agreement with the increase of genipin concentration used for the preparation of the scaffolds.

*Table 15. Extent of crosslinking (%).*

Sample	Crosslinking
G_0.05	$8 \pm 1$
G_0.1	$14 \pm 3$
G_0.15	$26 \pm 2$
G_0.2	$30 \pm 1$
G_0.1_Sr-HA	$15 \pm 3$

Each value corresponds to the average of three determinations and it is reported with its own standard deviation.

### Water Uptake Ability

The water uptake ability (WUA) of the samples was calculated by means of Equation 2: when the composition was enriched with Sr-HA, the values were normalized to the weight of gelatin alone. Values reported in Table 16 highlight that the amount of adsorbed PBS depends on the number of layers used to prepare the scaffolds. Indeed, the double-layered samples displayed WUA values higher than those of single-layer scaffolds (e.g., G\_0.1/G\_0.2 vs G\_0.1 or G\_0.15/G\_0.2 vs G\_0.15), most likely because of the presence of uneven areas between

different layers, which could provide more space for the solution uptake. The presence of Sr-HA inside the scaffolds did not influence significantly the WUA.

*Table 16. Water Uptake Abilities.*

<b>Sample</b>	<b>WUA (gPBS / ggelatin)</b>
S_0.1-Sr-HA	1.7 ± 0.3
G_0.05	3.1 ± 0.9
G_0.1	2.2 ± 0.8
G_0.15	2.2 ± 0.3
G_0.2	2.1 ± 0.4
G_0.1_Sr-HA	1.8 ± 0.3
G_0.1/G_0.2	5.0 ± 0.6
G_0.15/G_0.2	6.9 ± 0.7
G_0.1 Sr-HA/G_0.2	5.0 ± 0.4

Each value in the table corresponds to the average of three determinations and it is reported with its own standard deviation.

### Gelatin release

Average values of the amount of gelatin released from the samples after immersion in NaCl 0.9% at 37°C are reported in

Table 17. The higher the concentration of genipin used to crosslink the scaffold, the longer the lifetime of the material: the scaffold with the highest percentage of genipin achieved a strong stability and it did not dissolve even after 70 days, while the dissolution of samples cross-linked with lower genipin concentrations started already at 14 days.

*Table 17. Gelatin release (% w).*

<b>Sample</b>	<b>Time (days)</b>						
	<b>2</b>	<b>7</b>	<b>14</b>	<b>21</b>	<b>28</b>	<b>49</b>	<b>70</b>
S_0.1_Sr-HA	14.8± 0.1	22.7± 0.1	33.7± 2	39.3± 1.3	49± 2	dissolved	dissolved
G_0.05	26± 2	47± 2	dissolved	dissolved	dissolved	dissolved	dissolved
G_0.1	16± 1	26.9± 0.9	36.8± 0.4	44.3± 0.8	52.1± 0.6	dissolved	dissolved
G_0.15	12± 1	20.7± 1	28.1± 0.4	34.6± 0.2	40.9± 0.2	66± 1	dissolved
G_0.2	11± 1	17.6± 0.8	23.7± 0.9	28.7± 0.5	32.7± 0.6	38.6± 0.6	56± 2
G_0.1_Sr-HA	16.5± 1	27± 0.6	36.5± 0.8	44± 1	52.8± 0.5	dissolved	dissolved
G_0.05/G_0.2	22± 1	39± 1	44± 1	50± 2	54± 2	60± 2	dissolved
G_0.1/G_0.2	14.7± 0.8	24± 1	34± 2	42± 1	49± 1	61± 1	dissolved
G_0.15/G_0.2	11± 0.6	20± 0.8	25± 0.8	34± 1	42± 2	50± 2	65± 2
G_0.1_Sr-HA/G_0.2	15± 1	24.3± 0.6	33± 1.4	40.8± 2	48.3± 1	61.3± 1	dissolved

Each value is the average of tree determinations and is reported with its standard deviation.

### Strontium release

The amount of strontium released as a function of soaking time in NaCl 0.9% at 37°C was evaluated by means of atomic absorption spectrophotometric analysis. The results reported in Figure 5 show that the strontium cumulative release after seven days reached values of about 23% for the double-layer rolled scaffolds, 16% for the single-layer rolled scaffolds and 14% for the flat layer, following the same trend of the water uptake ability results.

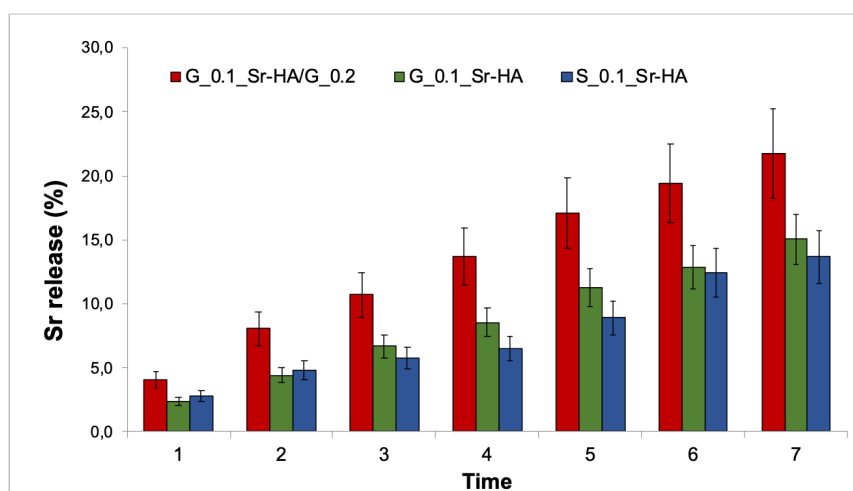


Figure 61. Strontium cumulative release from samples G\_0.1\_Sr-HA/G\_0.2 (red), G\_0.1\_Sr-HA (green) and S\_0.1\_Sr-HA (blue) as a function of soaking time (days) in NaCl 0,9% at 37°C.

These results suggest that the greater amount of solution that the double-layer rolled scaffolds were able to absorb could be responsible for the greater strontium release in solution.

## Conclusions

Cylindrical layered scaffolds were obtained through curling of one or two gelatin strips on themselves, combining stripes with different crosslinking degree. The rolled scaffolds displayed high porosity, although slightly lesser than that of the flat scaffold, because the rolling up provoked shrinkage of the pores. Morphological investigation showed the clear separation between the layers of the double-layered curled scaffolds, responsible for the greater water uptake ability of these materials in comparison with those measured for the single-layer rolled scaffolds. On the other hand, the separation between the layers did not seem to influence the mechanical properties. In fact, the mean values of the elastic moduli were in the range reported for normal cancellous bones<sup>50</sup>, which also display anisotropic behavior<sup>51,52</sup>. It follows that the rolled scaffolds developed in this work could find useful applications in defects of trabecular bone tissue. Moreover, the mechanical compressive tests revealed the anisotropic behavior of the samples, which exhibited better mechanical properties when compressed along the longitudinal direction; only the flat scaffold showed isotropic performances. An improvement of the mechanical properties was achieved by increasing the crosslinking degree, which also modulated the scaffold stability. All scaffolds displayed a sustained strontium release over time, especially for the double-layered rolled scaffolds. The release can be tuned by varying the layer where the drug is loaded or loading the drug in both layers, as well as increasing the gap between layers, indicating that these scaffolds can be used as systems for the local treatment of pathologies characterized by abnormally high bone resorption.

### 3.4 CHITOSAN AND GELATIN-BASED SCAFFOLDS FOR CARTILAGE REPAIR

#### Introduction

There are different types of cartilage (hyaline, elastic, and fibrous cartilage), that differ by their position within the body and their composition. Hyaline cartilage is a tough and flexible tissue that allows the nearby bones to slide over one another, it is subjected to a high stress and acts as shock absorber. For these reasons, damages to cartilage are quite common both as sport injury and due to osteoarthritis. However, self-repair ability of cartilage is limited by its avascular nature and by the limited proliferation capacity, low density, and tendency to de-differentiate of cartilage cells (chondrocytes) <sup>53,54</sup>. Common treatments are mosaicplasty and autologous chondrocytes injection, but the structure of the native cartilage is not reproduced. Tissue engineering is a promising strategy to overcome these problems, using scaffolds to deliver cells and signalling molecules, thus allowing the repair of the damaged tissue <sup>55</sup>.

Natural biopolymers are inherently biomimetic and may be biodegraded through enzymatic and hydrolytic degradation. On the other hand, these materials have inadequate mechanical properties and hence they are normally used in blend. Among the most used biopolymers in tissue engineering, chitosan and gelatin were selected in this project for scaffold preparation.

Indeed, chitosan has repetitive units in common with the main cartilage glycosaminoglycans, allowing the formation of a structure similar to the cartilage extracellular matrix through electrostatic interactions, and thus creating a favorable environment for normal cellular processes of chondrocytes. Chitosan is also able to promote the chondrogenic activity and the cartilage-specific protein expression <sup>56</sup> and so, chitosan-based composite scaffolds have become very appealing for the restoration of articular cartilage <sup>57</sup>.

The combination of chitosan and a biopolymer like gelatin or collagen has gained attraction in cartilage tissue engineering, due to the non-toxicity and biocompatibility of the biopolymers <sup>58</sup>. Gelatin was introduced to improve the mechanical properties of the scaffolds and to obtain a controlled and regular porosity, a fundamental requirement to promote cell proliferation. Two types of gelatins were used: one extracted from cold water fish, and one extracted from porcine skin. In fact, nowadays the use of fish gelatin overcomes some concerns related to gelatin extracted from mammals (such as the increasing number of vegetarians, religious issues and the possibility of pathogen transmission) and, in addition, could provide a valuable alternative source of gelatin, being the major by-product of the fish-processing industry. Furthermore, blending chitosan with fish gelatin improved the mechanical properties and decreased the permeability of films, as reported in literature <sup>59</sup>.

Since we have previously demonstrated that snail slime is able to induce modifications to the properties of film based on chitosan and gelatin, we wanted to investigate its influence on the

properties of scaffold designed for cartilage regeneration. Herein, scaffolds with different percentage by volume of snail slime (0, 10, 30 % v/v) and with different types of gelatins were produced. At present, the mechanical and solubility properties were evaluated, together with the swelling degree and the morphology of all formulations. Further analyses will be performed to assess the biological compatibility of these scaffolds and their effectiveness as potential platforms for cartilage tissue engineering.

## **Results and discussion**

Preliminary attempts have been made to set up the experimental conditions for the preparation of chitosan and gelatin-based scaffolds with snail slime. The scaffolds were prepared with two different types of gelatins, from porcine skin and from cold water fish skin, following the same procedure. As for film preparation (see Paragraph 2.2.1), chitosan concentration was set to 2% w/v, while gelatin concentration was set to 10% w/v: a lower amount of gelatin provided an insufficient porosity while higher percentages did not improve the porosity but only the scaffold solubility.

### **Crosslinking**

Scaffolds were crosslinked through immersion for 2 hours at 4 °C in an aqueous tripolyphosphate solution: tripolyphosphate (TPP) has indeed received increasing attention as an alternative crosslinking agent with respect to glutaraldehyde and genipin, due to its excellent biocompatibility<sup>60</sup>. Moreover, the multiple phosphate groups interact with the protonated amino groups present in chitosan and in some amino acid residues, so it could be an effective crosslinker for both chitosan and gelatin. However, while scaffolds prepared with porcine gelatine were crosslinked, the same process was ineffective for scaffolds containing fish gelatin: this method was not able to crosslink the fish gelatin, while provided a strong ionic interaction with the porcine one. This result can be explained by a different amount of -NH<sub>2</sub> moieties occurring in fish and porcine gelatin. The number of moles of ε-amino groups per gram of gelatin was evaluated through Equation 1, resulting in  $7,14 \cdot 10^{-5}$  and  $2,16 \cdot 10^{-4}$  for fish and porcine gelatine, respectively, thus confirming our hypothesis.

In accordance with the obtained results, further characterizations were performed on non-crosslinked fish gelatin scaffolds, and on crosslinked porcine gelatin scaffolds.

### **Swelling degree**

In contact with body fluids, the scaffolds absorb physiological fluids, thus increasing volume and weight. In order to get information about scaffolds' behaviour in physiological conditions,

swelling and solubility tests were performed in PB at pH 7.4. The swelling profiles of all the obtained scaffolds are reported in Figure 62.

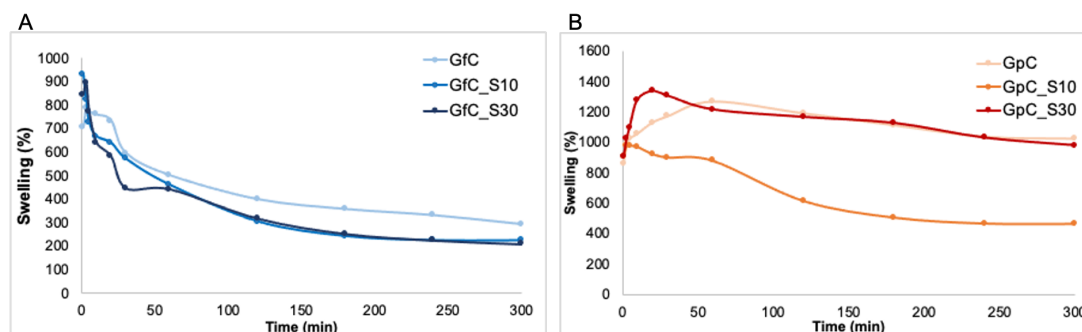


Figure 62. Swelling curves obtained for scaffolds prepared using fish (A) and porcine 138elatin (B) in combination with chitosan and snail slime.

The swelling curves of the fish gelatin-based scaffolds prepared with different amount of snail slime were very similar: scaffolds reached immediately the maximum water content and then decreased in weight (see Figure 62A). This trend is associated to the faster solubilization of fish gelatin-containing scaffolds compared to porcine gelatin-based scaffolds (Figure 62B). The addition of snail slime did not seem to affect the water absorption of the biomaterials.

Porcine gelatin-based scaffolds without snail slime (GpC) and with 30% v/v of slime (GpC\_S30) showed a similar swelling trend, while the samples containing 10% v/v of snail slime (GpC\_S10) showed lower swelling values. A probable explanation could be the ability of some macromolecules present into snail slime to act as crosslinker for gelatin.

### Scaffold solubility

In order to modulate the lifetime of the scaffold in physiological conditions a crosslinking step by immersing the scaffolds in TTP for 2 hours was performed. The scaffolds' solubility values (%) after 24 h of immersion in PB at 37 °C and after the crosslinking step are listed in Table 18.

Table 18. Solubility values at 24 hours and after the crosslinking step.

Sample	Solubility %	Solubility % after cosslinking
GfC	74.1 ± 0.5	
GpC	71.1 ± 3.0	38.1 ± 8.5
GfC_S10	85.9 ± 0.5	
GpC_S10	79.2 ± 0.1	71.7 ± 1.2
GfC_S30	83.4 ± 0.5	
GpC_S30	74.6 ± 0.4	67.0 ± 2.8

All the scaffolds were characterized by a very high solubility after 24 h, limiting their possible applications in the biological field. The comparison between the solubility before and after immersion in TPP solution (Table 18) is a further evidence of the crosslinking occurrence, even

if the extent of crosslinking is probably low. While the crosslinking of fish gelatin-based scaffolds was not efficient, that of porcine gelatin-based scaffolds is evident from the table: the solubility of GpC was 71.1% before the crosslinking step and reached 38% following immersion in TPP. Interestingly, the presence of snail slime in the formulations of the scaffolds led to a decrease of the effectiveness of the cross-linking step: indeed, the solubility values for samples containing 10% and 30% (GpC\_S10 and GpC\_S30, respectively) of slime differed only slightly from the original values.

### Compressive Tests

Mechanical tests in compression were carried out on dry specimens and the stress-strain curves are reported in Figure 63.

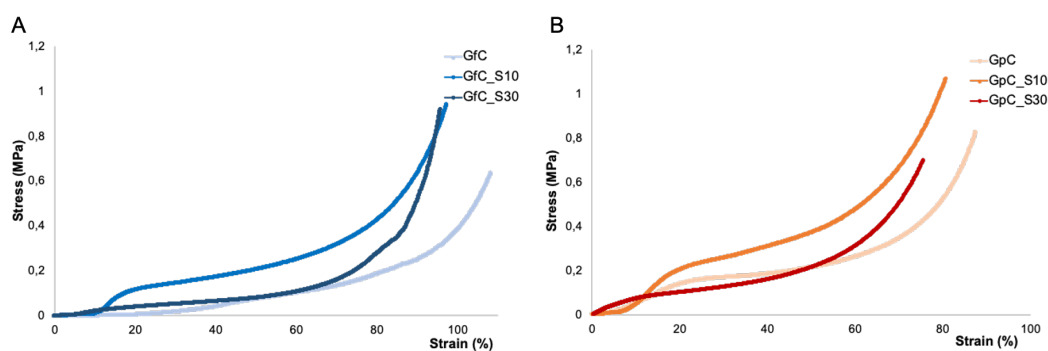


Figure 63. Stress-strain curves of the chitosan scaffolds in combination with A) fish gelatin and B) porcine gelatin.

As usual, the compressive stress–strain curves of the porous scaffolds showed three distinct zones: a first linear elastic part, a collapse plateau since the area increases during compression, and a quick increase in slope due to a densification.

The ideal Young’s modulus of a scaffold for cartilage replacement is in the range of 0,4 and 0,8 Mpa <sup>61,62</sup>. The moduli of dry scaffolds are graphed in Figure 64: reference scaffolds containing porcine gelatin exhibited a higher elastic modulus than those containing fish gelatin, and both these values are not far from the suggested working range. Addition of 10% v/v of snail slime greatly enhanced the elastic modulus of fish gelatin-based scaffolds: the value of GfC\_S10 was about six times higher than that of GfC, while 30% v/v of slime produced only a minimum increase. The elastic modulus of GpC\_S10 was not significantly different from that of GpC, while a higher amount of slime (GpC\_S30) led to a decrease of about 40%, even if the modulus value fits to the required ones (Figure 64). Overall, the values for dry samples are adequate for cartilage replacement.

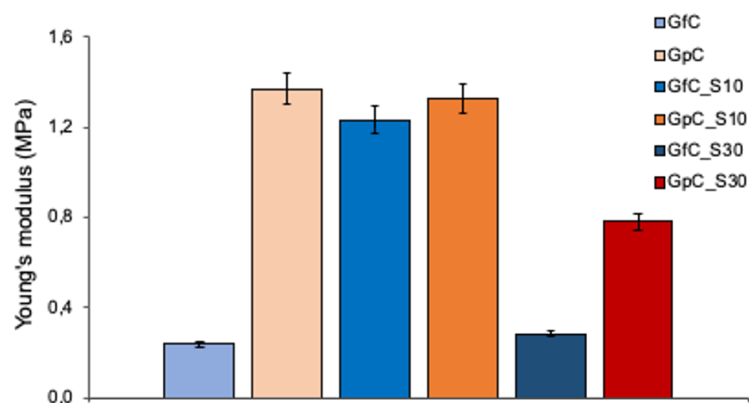


Figure 64. Elastic Young's moduli of the obtained scaffolds.

### Scanning Electron Microscopy

Scanning electron microscopy images, reported in *Figure 65*, were collected on dry samples to evaluate any morphological change on scaffolds before and after solubility tests.

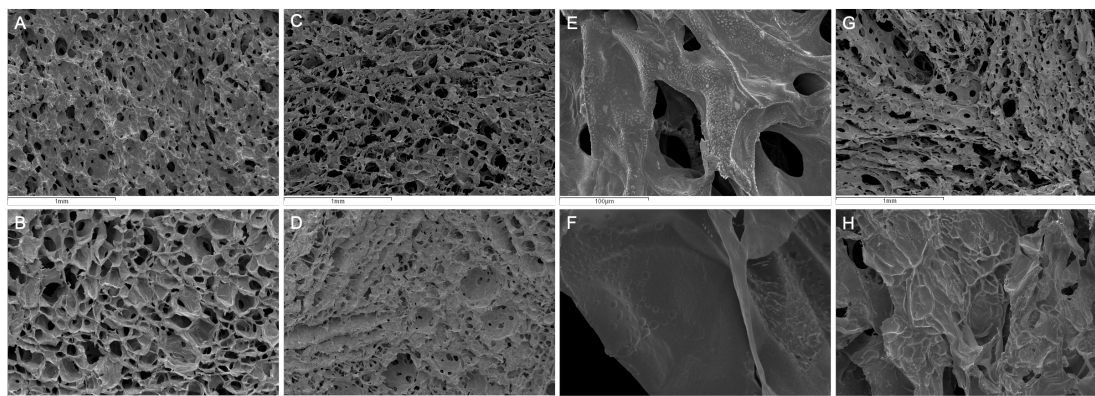


Figure 65. SEM images of the obtained scaffolds: A) GpC; B) GpC after 24 h of immersion in PB; C) GpC\_S10 after 24 h of immersion in PB; D) GpC\_S30; E) Surface of GpC; F) Surface of GpC after 24 h of immersion in PB; G) GfP and H) GfP\_S30 after 24 h of immersion in PB.

All the scaffolds showed a porous structure with interconnected pores. Scaffold GpC was characterized by a compact structure with well-defined and separated pores (Figure 65A). After 24 h in PB at 37°C the pore size increased (Figure 65B), probably as a consequence of the scaffold's partial solubilization. The addition of snail slime increased the porosity and provided jagged pore edges: a more open structure was indeed observed in GpC\_S10 samples, which showed an ordered structure with more defined pore borders after the solubility tests (Figure 65C). Increasing amount of snail slime (GpC\_S30) led to a layered structure with small pores (Figure 65D). Higher magnifications of porcine gelatin-based scaffolds revealed surfaces characterized by well-defined bubbles (Figure 65E), probably due to the precipitated TTP salt after the crosslinking step. It is very likely that, thanks to its affinity to the scaffold, the phosphorus salt re-precipitates on its surface and is not eliminated after the solubility tests (Figure 65F). This could be the reason why an increase in weight of above 20% after crosslinking was found.

The scaffold GfC seemed more layered than the corresponding formulation with pig gelatin (Figure 65G) and no differences were observed before and after solubility. Scaffolds with 30 % v/v of snail slime, made both with fish and porcine gelatin, were characterized by a different microstructure, as showed in Figure 9H, probably due to the high volume of slime added that contains macromolecular aggregates.

## **Conclusions**

Herein, chitosan and gelatin-based scaffolds in combination with different percentages in volume of snail slime were produced. The biomaterials were fabricated employing both gelatin from cold water fish and that from porcine skin, to overcome some of the concerns related to the use of porcine derivatives. However, the fish gelatin-based scaffolds revealed lower performances when compared to those of porcine gelatin-based ones. All scaffolds were subjected to a crosslinking step in order to modulate their solubility and thus their stability in physiological conditions. The crosslinking step performed by dipping the scaffold into TPP for 2 hours was not very effective for scaffolds containing snail slime and was only suitable for scaffolds based on porcine gelatin. It is therefore necessary to find an alternative method of crosslinking chitosan and gelatin in a natural way and avoiding toxic products. The morphologic analysis revealed highly porous structures, with an increased general porosity after 24 hours of immersion in PB, probably due to the relative solubility of the scaffolds. The mechanical properties performed on dry scaffolds were suitable and the Young's elastic moduli were in the range of those of native cartilage. Further analyses are necessary to verify the effective biocompatibility of these materials and their ability to produce type II collagen.

### 3.5 BIBLIOGRAPHY

- (1) Gomoll, A. H.; Filardo, G.; Almqvist, F. K.; Bugbee, W. D.; Jelic, M.; Monllau, J. C.; Puddu, G.; Rodkey, W. G.; Verdonk, P.; Verdonk, R.; Zaffagnini, S.; Marcacci, M. Surgical Treatment for Early Osteoarthritis. Part II: Allografts and Concurrent Procedures. *Knee Surgery, Sport. Traumatol. Arthrosc.* **2011**, *20* (3), 468–486, DOI:10.1007/S00167-011-1714-7.
- (2) Curtin, C. M.; Castaño, I. M.; O'Brien, F. J. Scaffold-Based MicroRNA Therapies in Regenerative Medicine and Cancer. *Adv. Healthc. Mater.* **2018**, *7* (1), 1700695, DOI:10.1002/ADHM.201700695.
- (3) Griffon, D. J.; Sedighi, M. R.; Schaeffer, D. V.; Eurell, J. A.; Johnson, A. L. Chitosan Scaffolds: Interconnective Pore Size and Cartilage Engineering. *Acta Biomater.* **2006**, *2* (3), 313–320, DOI:10.1016/J.ACTBIO.2005.12.007.
- (4) Cheng, A.; Schwartz, Z.; Kahn, A.; Li, X.; Shao, Z.; Sun, M.; Ao, Y.; Boyan, B. D.; Chen, H. Advances in Porous Scaffold Design for Bone and Cartilage Tissue Engineering and Regeneration. *Tissue Eng. - Part B Rev.* **2019**, *25* (1), 14–29, DOI:10.1089/TEN.TEB.2018.0119.
- (5) Petite, H.; Viateau, V.; Bensaid, W.; Meunier, A.; Bourguignon, M.; Oudina, K.; Sedel, L.; Guillemain, G. Tissue-Engineered Bone Regeneration. *Nat. Biotechnol.* **2000**, *18* (9), 959–963, .
- (6) Hollister, S. J. Porous Scaffold Design for Tissue Engineering. **2005**.
- (7) Karageorgiou, V.; Kaplan, D. Porosity of 3D Biomaterial Scaffolds and Osteogenesis. *Biomaterials* **2005**, *26* (27), 5474–5491, DOI:10.1016/j.biomaterials.2005.02.002.
- (8) Perez, R. A.; Mestres, G. Role of Pore Size and Morphology in Musculo-Skeletal Tissue Regeneration. *Mater. Sci. Eng. C* **2016**, *61*, 922–939, DOI:10.1016/j.msec.2015.12.087.
- (9) Darder, M.; Aranda, P.; Ferrer, M. L.; Gutiérrez, M. C.; Del Monte, F.; Ruiz-Hitzky, E.; Darder, M.; Aranda, P.; Ferrer, M. L.; Gutiérrez, M. C.; Del Monte, F.; Ruiz-Hitzky, E. Progress in Bionanocomposite and Bioinspired Foams. *Adv. Mater.* **2011**, *23* (44), 5262–5267, DOI:10.1002/adma.201101617.
- (10) Babaie, E.; Bhaduri, S. B. Fabrication Aspects of Porous Biomaterials in Orthopedic Applications: A Review. *ACS Biomater. Sci. Eng.* **2018**, *4* (1), 1–39, DOI:10.1021/acsbiomaterials.7b00615.
- (11) Yan, X.; Chen, Y. R.; Song, Y. F.; Yang, M.; Ye, J.; Zhou, G.; Yu, J. K. Scaffold-Based Gene Therapeutics for Osteochondral Tissue Engineering. *Front. Pharmacol.* **2020**, *10*, DOI:10.3389/FPHAR.2019.01534.
- (12) Rezwan, K.; Chen, Q. Z.; Blaker, J. J.; Boccaccini, A. R. Biodegradable and Bioactive Porous Polymer/Inorganic Composite Scaffolds for Bone Tissue Engineering. *Biomaterials* **2006**, *27* (18), 3413–3431, DOI:10.1016/J.BIOMATERIALS.2006.01.039.
- (13) Hedberg, E. L.; Shih, C. K.; Lemoine, J. J.; Timmer, M. D.; Michael, M. A.; Jansen, J. A.; Mikos, A. G. In Vitro Degradation of Porous Poly(Propylene Fumarate)/Poly(DI-Lactic-Co-Glycolic Acid) Composite Scaffolds. *Biomaterials* **2005**, *26* (16), 3215–3225, DOI:10.1016/J.BIOMATERIALS.2004.09.012.
- (14) Habraken, W. J. E. M.; De Jonge, L. T.; Wolke, J. G. C.; Yubao, L.; Mikos, A. G.; Jansen, J. A. Introduction of Gelatin Microspheres into an Injectable Calcium Phosphate Cement. *J. Biomed. Mater. Res. - Part A* **2008**, *87* (3), 643–655, DOI:10.1002/jbm.a.31703.
- (15) Rault, I.; Frei, V.; Herbage, D.; Abdul-Malak, N.; Huc, A. Evaluation of Different Chemical Methods for Cross-Linking Collagen Gel, Films and Sponges. *J. Mater. Sci. Mater. Med.* **1996**, *7* (4), 215–221, DOI:10.1007/BF00119733.
- (16) Oryan, A.; Kamali, A.; Moshiri, A.; Baharvand, H.; Daemi, H. Chemical Crosslinking of Biopolymeric Scaffolds: Current Knowledge and Future Directions of Crosslinked Engineered Bone Scaffolds. *Int. J. Biol. Macromol.* **2018**, *107* (PartA), 678–688, DOI:10.1016/J.IJBIOMAC.2017.08.184.

- (17) Di Filippo, M. F.; Amadori, S.; Casolari, S.; Bigi, A.; Dolci, L. S.; Panzavolta, S. Cylindrical Layered Bone Scaffolds with Anisotropic Mechanical Properties as Potential Drug Delivery Systems. *Molecules* **2019**, *24* (10), DOI:10.3390/molecules24101931.
- (18) Kaş, H. Chitosan: Properties, Preparations and Application to Microparticulate Systems. *J. Microencapsul.* **1997**, *14* (6), 689–711, DOI:10.3109/02652049709006820.
- (19) Falcone, L.; Marinoni, E.; Rapisarda, V.; Capitani, D.; Veronese, S.; Marazzi, M. Cartilagine Articolare Ingegnerizzata: L'importanza Di Uno Scaffold. Nuove Frontiere. *Artroscopia* **2007**, *VIII* (1), 1–13, .
- (20) Tanimoto, Y.; Hayakawa, T.; Sakae, T.; Nemoto, K. Characterization and Bioactivity of Tape-Cast and Sintered TCP Sheets. *J. Biomed. Mater. Res. Part A* **2006**, *76A* (3), 571–579, DOI:10.1002/JBM.A.30558.
- (21) Weiner, S.; Wagner, H. D. THE MATERIAL BONE: Structure-Mechanical Function Relations. *Annu. Rev. Mater. Sci* **1998**, *28*, 271–298, .
- (22) Jiang, H.; Zuo, Y.; Zou, Q.; Wang, H.; Du, J.; Li, Y.; Yang, X. Biomimetic Spiral-Cylindrical Scaffold Based on Hybrid Chitosan/Cellulose/ Nano-Hydroxyapatite Membrane for Bone Regeneration. *ACS Appl. Mater. Interfaces* **2013**, *5* (22), 12036–12044, DOI:10.1021/am4038432.
- (23) Wan, Y.; Feng, G.; Shen, F. H.; Laurencis, C. T.; Li, X. Biphasic Scaffold for Annulus Fibrosus Tissue Regeneration. *Biomaterials* **2008**, *29*, 643–652, .
- (24) Light, N. D.; MacGregor, J.; Harvey, W.; Watt, P. W. Absorbable Structures for Ligament and Tendon Repair. US5514181A, September 29, 1994.
- (25) Berman, A. B. Resorbable Interposition Arthroplasty Implant. US6017366A, April 18, 1997.
- (26) Sussman, M. B.; Kadouri, Z. Fibrous Matrix for in Vitro Cell Cultivation. U.S. Patent 5, 266, 476, 1993. - Google Patents. 266, 1993.
- (27) Wang, J.; Shah, A.; Yu, X. The Influence of Fiber Thickness, Wall Thickness and Gap Distance on the Spiral Nanofibrous Scaffolds for Bone Tissue Engineering. *Mater. Sci. Eng. C* **2011**, *31*, 50–56, .
- (28) Sung, H.-W.; Liang, I.-L.; Chen, C.-N.; Huang, R.-N.; Liang, H.-F. Stability of a Biological Tissue Fixed with a Naturally Occurring Crosslinking Agent (Genipin). *J. Biomed. Mater. Res.* **2001**, *55* (4), 538–546, .
- (29) Bigi, A.; Cojazzi, G.; Panzavolta, S.; Roveri, N.; Rubini, K. Stabilization of Gelatin Films by Crosslinking with Genipin. *Biomaterials* **2002**, *23* (24), 4827–4832, DOI:10.1016/S0142-9612(02)00235-1.
- (30) Yao, C. H.; Liu, B. S.; Chang, C. J.; Hsu, S. H.; Chen, Y. S. Preparation of Networks of Gelatin and Genipin as Degradable Biomaterials. *Mater. Chem. Phys.* **2004**, *83* (2–3), 204–208, DOI:10.1016/J.MATCHEMPHYS.2003.08.027.
- (31) Huang, K. S.; Lu, K.; Yeh, C. S.; Chung, S. R.; Lin, C. H.; Yang, C. H.; Dong, Y. S. Microfluidic Controlling Monodisperse Microdroplet for 5-Fluorouracil Loaded Genipin-Gelatin Microcapsules. *J. Control. Release* **2009**, *137* (1), 15–19, DOI:10.1016/J.JCONREL.2009.02.019.
- (32) Deeks, E. D.; Dhillon, S. Strontium Ranelate: A Review on Its Use in the Treatment of Postmenopausal Osteoporosis. *Drugs* **2010**, *70* (6), 733–759, DOI:10.2165/10481900-000000000-00000.
- (33) Gallacher, S. J.; Dixon, T. Impact of Treatments for Postmenopausal Osteoporosis (Bisphosphonates, Parathyroid Hormone, Strontium Ranelate, and Denosumab) on Bone Quality: A Systematic Review. *Calcif. Tissue Int.* **2010**, *87* (6), 469–484, DOI:10.1007/S00223-010-9420-X.
- (34) Marie, P. J. Strontium Ranelate: A Novel Mode of Action Optimizing Bone Formation and Resorption. *Osteoporos. Int.* **2004**, *16* (1), S7–S10, DOI:10.1007/S00198-004-1753-8.

- (35) Ammann, P. Strontium Ranelate: A Novel Mode of Action Leading to Renewed Bone Quality. *Osteoporos. Int.* **2004**, *16* (1), S11–S15, DOI:10.1007/S00198-004-1809-9.
- (36) Reginster, J. Y.; Bruyère, O.; Sawicki, A.; Roces-Varela, A.; Fardellone, P.; Roberts, A.; Devogelaer, J. P. Long-Term Treatment of Postmenopausal Osteoporosis with Strontium Ranelate: Results at 8 Years. *Bone* **2009**, *45* (6), 1059–1064, DOI:10.1016/J.BONE.2009.08.004.
- (37) Saidak, Z.; Marie, P. J. Strontium Signaling: Molecular Mechanisms and Therapeutic Implications in Osteoporosis. *Pharmacol. Ther.* **2012**, *136* (2), 216–226, DOI:10.1016/J.PHARMTHERA.2012.07.009.
- (38) Davidenko, N.; Gibb, T.; Schuster, C.; Best, S. M.; Campbell, J. J.; Watson, C. J.; Cameron, R. E. Biomimetic Collagen Scaffolds with Anisotropic Pore Architecture. *Acta Biomater.* **2012**, *8* (2), 667–676, DOI:10.1016/J.ACTBIO.2011.09.033.
- (39) Panzavolta, S.; Torricelli, P.; Amadori, S.; Parrilli, A.; Rubini, K.; della Bella, E.; Fini, M.; Bigi, A.; Bella, della E. 3D Interconnected Porous Biomimetic Scaffolds: In Vitro Cell Response. *J. Biomed. Mater. Res. Part A* **2013**, *101* (12), 3560–3570, DOI:10.1002/jbm.a.34662.
- (40) Panzavolta, S.; Fini, M.; Nicoletti, A.; Bracci, B.; Rubini, K.; Giardino, R.; Bigi, A. Porous Composite Scaffolds Based on Gelatin and Partially Hydrolyzed  $\alpha$ -Tricalcium Phosphate. *Acta Biomater.* **2009**, *5* (2), 636–643, DOI:10.1016/J.ACTBIO.2008.08.017.
- (41) Walther, A.; Bjurhager, I.; Malho, J.-M.; Pere, J.; Ruokolainen, J.; Berglund, L. A.; Ikkala, O. Large-Area, Lightweight and Thick Biomimetic Composites with Superior Material Properties via Fast, Economic, and Green Pathways. *Nano Lett.* **2010**, *10* (8), 2742–2748, DOI:10.1021/nl1003224.
- (42) Dahl, S. G.; Allain, P.; Marie, P. J.; Mauras, Y.; Boivin, G.; Ammann, P.; Tsouderos, Y.; Delmas, P. D.; Christiansen, C. Incorporation and Distribution of Strontium in Bone. *Bone* **2001**, *28* (4), 446–453, DOI:10.1016/S8756-3282(01)00419-7.
- (43) Panzavolta, S.; Torricelli, P.; Casolari, S.; Parrilli, A.; Fini, M.; Bigi, A. Strontium-Substituted Hydroxyapatite-Gelatin Biomimetic Scaffolds Modulate Bone Cell Response. *Macromol. Biosci.* **2018**, *18* (7), 1–10, DOI:10.1002/mabi.201800096.
- (44) Gioffrè, M.; Torricelli, P.; Panzavolta, S.; Rubini, K.; Bigi, A. Role of PH on Stability and Mechanical Properties of Gelatin Films. *J. Bioact. Compat. Polym.* **2012**, *27* (1), 67–77, DOI:10.1177/08839115111431484.
- (45) Okuyama, K. Revisiting the Molecular Structure of Collagen Connective Tissue. *Connect. Tissue Res.* **2008**, *49* (5), 299–310, DOI:10.1080/03008200802325110.
- (46) Miles, C. A.; Ghelashvili, M. Polymer-in-a-Box Mechanism for the Thermal Stabilization of Collagen Molecules in Fibers. *Biophys. J.* **1999**, *76* (6), 3243–3252, DOI:10.1016/S0006-3495(99)77476-X.
- (47) Wubneh, A.; Tsekoura, E. K.; Ayranci, C.; Uludağ, H. Current State of Fabrication Technologies and Materials for Bone Tissue Engineering. *Acta Biomater.* **2018**, *80*, 1–30, DOI:10.1016/j.actbio.2018.09.031.
- (48) Amadori, S.; Torricelli, P.; Panzavolta, S.; Parrilli, A.; Fini, M.; Bigi, A. Highly Porous Gelatin Reinforced 3D Scaffolds for Articular Cartilage Regeneration. *Macromol. Biosci.* **2015**, *15* (7), 941–952, DOI:10.1002/mabi.201500014.
- (49) Amadori, S.; Torricelli, P.; Panzavolta, S.; Parrilli, A.; Fini, M.; Bigi, A. Multi-Layered Scaffolds for Osteochondral Tissue Engineering: In Vitro Response of Co-Cultured Human Mesenchymal Stem Cells. *Macromol. Biosci.* **2015**, *15* (11), 1535–1545, DOI:10.1002/mabi.201500165.
- (50) Goldstein, S. A. The Mechanical Properties of Trabecular Bone: Dependence on Anatomic Location and Function. *J. Biomech.* **1987**, *20* (11–12), 1055–1061, .
- (51) Homminga, J.; McCreadie, B. R.; Ciarelli, T. E.; Weinans, H.; Goldstein, S. A.; Huiskes, R. Cancellous Bone Mechanical Properties from Normals and Patients with Hip Fractures Differ on the Structure Level, Not on the Bone Hard Tissue Level. *Bone* **2002**, *30* (5), 759–764,

DOI:10.1016/S8756-3282(02)00693-2.

- (52) Giesen, E. B. W.; Ding, M.; Dalstra, M.; Van Eijden, T. M. G. J. Mechanical Properties of Cancellous Bone in the Human Mandibular Condyle Are Anisotropic. *J. Biomech.* **2001**, *34* (6), 799–803, DOI:10.1016/S0021-9290(01)00030-6.
- (53) Reed, S.; Wu, B. Biological and Mechanical Characterization of Chitosan-Alginate Scaffolds for Growth Factor Delivery and Chondrogenesis. *J. Biomed. Mater. Res. B. Appl. Biomater.* **2017**, *105* (2), 272–282, DOI:10.1002/JBM.B.33544.
- (54) Mohammad Amin, S.; Ahmad, R.; Hamid, M.; Hamid, M.; Mohebbi-Kalhari, D.; Mohamadreza Baghaban, E. Fabrication and Characterization of Hydrothermal Cross-Linked Chitosan Porous Scaffolds for Cartilage Tissue Engineering Applications. *Mater. Sci. Eng. C* **2017**, *80*, 532–542, DOI:10.1016/j.msec.2017.03.194.
- (55) Chung, C.; Burdick, J. Engineering Cartilage Tissue. *Adv. Drug Deliv. Rev.* **2008**, *60* (2), 243–262, DOI:10.1016/J.ADDR.2007.08.027.
- (56) Neves, S. C.; Moreira Teixeira, L. S.; Moroni, L.; Reis, R. L.; Van Blitterswijk, C. A.; Alves, N. M.; Karperien, M.; Mano, J. F. Chitosan/Poly( $\epsilon$ -Caprolactone) Blend Scaffolds for Cartilage Repair. *Biomaterials* **2011**, *32* (4), 1068–1079, DOI:10.1016/j.biomaterials.2010.09.073.
- (57) Kashi, M.; Baghbani, F.; Moztarzadeh, F.; Mobasheri, H.; Kowsari, E. Green Synthesis of Degradable Conductive Thermosensitive Oligopyrrole/Chitosan Hydrogel Intended for Cartilage Tissue Engineering. *Int. J. Biol. Macromol.* **2018**, *107* (Pt B), 1567–1575, DOI:10.1016/J.IJBIOMAC.2017.10.015.
- (58) Xia, W.; Liu, W.; Cui, L.; Liu, Y.; Zhong, W.; Liu, D.; Wu, J.; Chua, K.; Cao, Y. Tissue Engineering of Cartilage with the Use of Chitosan-Gelatin Complex Scaffolds. *J. Biomed. Mater. Res. B. Appl. Biomater.* **2004**, *71* (2), 373–380, DOI:10.1002/JBM.B.30087.
- (59) Fakhreddin Hosseini, S.; Rezaei, M.; Zandi, M.; Ghavi, F. F. Preparation and Functional Properties of Fish Gelatin-Chitosan Blend Edible Films. *Food Chem.* **2013**, *136* (3–4), 1490–1495, DOI:10.1016/j.foodchem.2012.09.081.
- (60) Fang, Y.; Zhang, T.; Song, Y.; Sun, W. Assessment of Various Crosslinking Agents on Collagen/Chitosan Scaffolds for Myocardial Tissue Engineering. *Biomed. Mater.* **2020**, *15* (4) DOI:10.1088/1748-605X/AB452D.
- (61) Bhumkar, D. R.; Pokharkar, V. B. Studies on Effect of PH on Cross-Linking of Chitosan With Sodium Tripolyphosphate: A Technical Note. *AAPS PharmSciTech- J. Am. Assoc. Pharm. Sci.* **2006**, *7* (2), E1–E6, .
- (62) Thambyah, A.; Nather, A.; Goh, J. Mechanical Properties of Articular Cartilage Covered by the Meniscus. *Osteoarthr. Cartil.* **2006**, *14*, 580–588, DOI:10.1016/j.joca.2006.01.015.

## **Chapter 4.** **BONE CEMENTS**

### **4.1 INTRODUCTION**

Bone is a dynamic tissue that undergoes continual adaptation during vertebrate life by bone remodeling, the process underlying the maintenance of the skeletal system. This is a lifelong process which responds to functional demands and controls the continuous reshaping of bone. Most of the bone-related pathologies lead to an imbalance in the rate of apposition of new bone tissue with respect to bone resorption (e.g. osteoporosis) <sup>1</sup>, and hence to the formation of bone defects. Also, trauma, tumor resection and age-related loss of bone mass can cause bone defects, inducing a high demand for bone filling materials.

Autologous bone grafts are still the ‘golden standard’ filling materials in bone surgery, but in certain settings, especially in extensive bone defects, this method of treatment could be insufficient and could only pose an additional trauma for the patient <sup>2</sup>.

Since natural bone is a complex material with well-designed architecture, to achieve successful bone integration and regeneration, the constituents and structure of bone-repairing materials need to be functionalized synergistically based on biomimetics: in the context of tissue engineering, many attempts to obtain biomimetic-inspired bone-repairing scaffolds or cement have been made, using both organic and inorganic compounds <sup>3</sup>.

Since 1920, compounds of calcium phosphate (CaP) have been investigated as bone repair materials, but they had only limited use in clinical applications until the 1970s. Only in the early 1980s the clinical potential of CaP materials further increased with the development of self-setting calcium phosphate cement (CPC) by Brown and Chow <sup>4,5</sup>. They found that a slurry containing appropriate amounts of tetracalciumphosphate (TTCP:  $\text{Ca}_4(\text{PO}_4)_2\text{O}$ ) and dicalcium phosphate (DCPD:  $\text{CaHPO}_4 \cdot 2\text{H}_2\text{O}$  or DCPA:  $\text{CaHPO}_4$ ) led to the precipitation of hydroxyapatite (HA) and was capable to be moulded into bone defects and implant sites, self-set and harden *in situ* to form a scaffold, providing stability <sup>5</sup>. Being the inorganic phase of bone tissue a poorly crystalline hydroxyapatite, CPCs have the potential to mimic the mineral phase of native bone: hence, bone tissue is formed in direct contact with calcium phosphate cement and without the generation of undesirable fibrous capsules. In fact, the biomimetic CPC provides a preferred substrate for cell attachment and support the proliferation and expression of osteoblast phenotype <sup>6</sup>. CPCs are supposed to be subject to biological degradation and concomitant replacement by bone tissue, but their degradation *in vivo* is very slow <sup>7</sup> due to the low solubility of hydroxyapatite and to the limited extent of porosity of these materials <sup>8</sup>.

In addition to their excellent biological behavior, the main advantage of CPCs is that they can be injected into a defect area, providing intimate adaptation to the surrounding bone even for irregular shaped cavities <sup>9</sup>. CPCs offer great opportunities to decrease the invasiveness and painfulness of surgical procedures, reducing recovery time and increasing the overall benefits for the patient <sup>10</sup>: hence, they gained clinical acceptance for bone substitution and augmentation, especially in percutaneous surgery <sup>6</sup>. Currently, there is no common understanding about the meaning of injectability: for many authors, it is related to the injection force that must be applied to a syringe in order to deliver the cement paste. This definition, however, seems to measure the ease of injection, which depends on the injection system, rather than the injectability of a paste and, in addition, it does not consider the quality of the extruded paste <sup>9</sup>. Bohner and Baroud defined the injectability of a paste as the ability to stay homogeneous during injection, independently from the injection force <sup>9</sup>.

Poor injectability of CPCs primarily arises from the separation of the solid and liquid phases (also called filter-pressing) during cement delivery from a syringe/cannulated needle arrangement <sup>5</sup>. Phase separation probably causes a deviation of the actual composition of the extruded paste from the initial one <sup>9</sup> and extravasation from the surgical site, being detrimental to the final properties of the set CPC <sup>5</sup>. In the last few decades, many of the studies attempting to optimize CPCs for clinical applications have focused on improving their delivery to the surgical site through injection, with vary degrees of success. For this reason, in both studies reported in Paragraph 4.3 and 4.4, the compositions of cements were adjusted in order to obtain injectable formulations.

The properties of bone vary more than in any other organs as one move from its edge to the center: shifting from the dense cortical surface to the lighter trabecular interior and then to the soft bone marrow, porosity, vascularization, and remodeling rate increase and, hence, there is the need for a material with tailored and tunable properties <sup>11</sup>. Depending on age, gender, location within the body and stress imposed on it, the compressive strength of bone varies widely. As a consequence, the required compressive strength depends on the clinical application <sup>5</sup>.

To improve mechanical properties of CPCs, the incorporation of high-strength biomaterials such as chitosan lactate, collagen and other polymers <sup>12</sup> into cements composition has been widely explored. Among them, gelatin would be the preferred material because of its excellent biocompatibility and because it does not express antigenity in physiological conditions <sup>13</sup>: moreover, it is completely resorbable *in vivo* <sup>14</sup>. Due to these properties, gelatin has been chosen to be incorporated in the composition of the cements I prepared.  $\alpha$ -TCP was indeed mixed with

gelatin to form a suspension, that was dried, crushed and sieved (<40 µm). Then, it was combined with the weighed amount of DCPD, constituting the starting powder phase of the cements.

After an orthopedic surgery, one of the most adverse complications is the development of infections (e.g., osteomyelitis), which can lead to pain, prolonged recovery, and re-operation<sup>15</sup>. For this reason, in the research project reported in Paragraph 4.3 and published in a scientific international journal<sup>16</sup>, I investigated the possibility to employ solid lipid microparticles (MPs) loaded with an antibiotic to confer the cement with antibacterial properties. The use of MPs is a strategy for overcoming the adverse effects on the mechanical and hardening properties of cements produced by the addition of a drug (or of any other substance) directly to the starting powders. Moreover, in addition to their ability to represent drug delivery platforms inside the cement, microparticles, as a result of their *in vivo* degradation, are also exploited to enhance cements' macroporosity, which is one of the main critical issues of CPCs. The ability of drug-loaded cements to inhibit bacterial growth has been evaluated *in vitro* by means of Kirby-Bauer tests against a panel of clinical isolates thanks to the collaboration with the research team of Prof. Bonvicini at Microbiology Unit of the St. Orsola-Malpighi University Hospital, with satisfying results. Moreover, the cytotoxicity assessment performed by the IRCCS Rizzoli Orthopedic Institute revealed a good colonization of the cement's surface, confirming the suitability of these platforms.

In Paragraph 4.4 the main limitation of the CPCs is further targeted: their poor mechanical properties are still the major issue limiting their applications. A very effective reinforcement strategy, also used in cements for buildings, is the insertion of fibres in the cement's composition.

In this study I demonstrated the feasibility of obtaining a self-assembly of fibers within the cement paste: a gelator capable of forming supramolecular structures has been used, and the formation of fibres has taken place even in the presence of such a large quantity of powders. Self-assembly occurred thanks to the presence of Ca<sup>2+</sup> ions (introduced as CaCl<sub>2</sub>) as gelator trigger for the self-assembling mechanism. This method has allowed to obtain cements with larger pore diameters and fibres with a good adhesion with the surrounding apatite matrix, ensuring a mechanical reinforcement of the material. Further studies could be addressed to the structural modification and functionalization of the peptidic gelator by means of bioactive molecules or drugs, which would enrich the therapeutic capacity of the CPC platform.

## 4.2 EXPERIMENTAL PART

### 4.2.1 Development of antibacterial calcium phosphate bone cements

#### Materials

Cutin® HR (hydrogenated castor oil) was purchased from Farmalabor S.R.L., Italy. Porcine gelatin (type A, 300 Bloom) was purchased from Sigma Aldrich (St. Louis, MO, USA). Gentamicin sulphate (GS) was purchased by Carlo Erba, Italy.  $\alpha$ -TCP was obtained by solid state reaction of a mixture of  $\text{CaCO}_3$  and  $\text{CaHPO}_4 \cdot 2\text{H}_2\text{O}$  in the molar ratio of 1:2 at 1300 °C for 5 h, crushed in a ball mill and sieved ( $<80\mu\text{m}$ ).

#### Production of microparticles

Microparticles made of Cutin® HR (MPs) were produced by the spray-congealing process. In order to prepare microparticles containing 20% w/w of Gentamicin sulphate (MPsGS), the proper amount of GS was slowly added under stirring to the melted Cutin to obtain a homogeneous suspension, which was then subjected to atomization. Obtained MPs were collected, sieved (range 75-250  $\mu\text{m}$ ) and stored in polyethylene closed bottles at  $4 \pm 2$  °C.

#### Cement preparation

Starting cement powders were made of 475 mg of the gelatin/ $\alpha$ -TCP (15% wt of gelatin with respect to the total amount) and 25 mg of DCPD ( $\text{CaHPO}_4 \cdot 2\text{H}_2\text{O}$ ). Powders were packed in a Teflon mold ( $6 \times 12$  mm) and mixed in an electric mortar (3 M ESPE RotoMix) two times for 20 s. A liquid to powder ratio of 0.24 mL/g was used with distilled water as liquid phase. After addition of the liquid phase, cement powders were mixed in the electric mortar two times for 20 s to obtain a paste of workable consistency and compacted for 1 min inside the Teflon mold by using a 4465 Instron dynamometer set at 70 N. After 10 min from the compaction, cement samples were demolded and immersed in PB at 37 °C and pH 7.4 up to 21 days. These cements were used as control and labeled C. For the preparation of cements enriched with different additives (GS and/or  $\text{BaSO}_4$  and/or MPs and/or MPsGS) the same procedure was followed, maintaining the same amounts of starting cement powders. The amount of each additive was calculated with respect to the weight of the starting powders and was added before mixing with the liquid phase. The cement compositions and the corresponding labels are reported in Table 19.

To obtain cement pastes of flowable consistency, the injectable cements were prepared as described above, adjusting the liquid to powder ratio for each composition and labelling the samples by adding 'in \_', as reported in Table 19.

Table 19. Compositions, labels, and liquid/powder ratio of the obtained cements. Each additive is expressed as % w/w with respect to the starting powders ( $\alpha$ -TCP/gelatin mix +DCPC).

Label	BaSO <sub>4</sub>	GS			MPs	MPsGS	L/P (mL/g)
	%	%			%	%	
	10	2	4	8	10	10	
C							0.24
C GS2		x					0.24
C GS4			x				0.24
C GS8				x			0.24
C Ba	x						0.24
C Ba GS2	x	x					0.24
C Ba GS4	x		x				0.24
C Ba GS8	x			x			0.24
C MPs					x		0.24
C MPsGS						x	0.24
C Ba MPs	x				x		0.24
C Ba MPsGS	x					x	0.24
C Ba GS2 MPsGS	x	x				x	0.24
in C Ba	x						0.55
in C Ba GS2	x	x					0.60
in C Ba MPs	x				x		0.65
in C Ba MPsGS	x					x	0.65
in C Ba GS2 MPsGS	x	x				x	0.75

### Cement preparation for biological assays

For biological assays, the cylindrical cements samples obtained after compaction inside teflon molds were demolded, cut into slices (d= 6mm, h= 1,5 mm) and stored at 37°C for 7 days to allow cement's hardening. After this time, samples were sterilized by gamma irradiation (cobalt-60 at 25 kGy).

### Microparticles Characterization

Morphological evaluation by means of scanning electron microscopy (SEM) of the obtained MPs was performed as described in the 'Scanning Electron Microscopy' section of Paragraph 4.2.3.

### Evaluation of drug content

The drug content was measured by a spectrophotometric method that requires the use of Ninhydrin as derivatizing agent. Ninhydrin, freshly prepared before each determination, was prepared by dissolving 125 mg of powder in 25 mL of phosphate buffer (PB) pH 7.4 at RT. For the calibration curve, proper aliquots of GS standard solution (1 mg/mL in PB) were mixed with 2 mL of Ninhydrin solution and the volume was filled up to 10 mL with PB to obtain a Gentamicin concentration ranging from 70 to 150 µg/mL. The solutions were heated at 95°C for 15 min and then cooled in ice for 10 min. Spectra were registered from 200 to 800 nm and the absorbance was read at 400 nm ( $R^2=0,997$ ). For the determination of drug content, 30 mg of MPsGS were accurately weighted and added to 10 mL of PB pH 7,4. The suspension was

heated at 95°C (~10°C above Cutin melting point), gently shaken for 1 hour and filtered. 2 mL of the filtered solution were poured into a flask with 2 mL of derivatizing agent and properly diluted with PB. The samples were analyzed in duplicate, and the encapsulation efficiency (EE) calculated as follows:

$$EE (\%) = \frac{W_a}{W_t} \cdot 100 \quad 11)$$

where  $W_a$  was the actual drug content and  $W_t$  the theoretic one.

### **Drug release from MPsGS**

For the GS release kinetic from MPsGS measurement, 15 mg of MPsGS were accurately weighted and added to test tubes with 5 mL of 0.1 M phosphate buffer (PB) pH 7,4. Tubes were kept at 37 °C and the solution was completely filtered after set time intervals (15, 30, 60, 120, 180, 240 and 300 min) using a syringe with a straw equipped with 8 µm filter. The same amount of fresh buffer solution was replaced every time in each tube. The analysis was carried out in duplicate. GS content in filtered solution was evaluated by means of Ninhydrin derivatization, as reported above. GS powder (5 mg/5 mL of PB pH 7,4) was used as reference.

### **Hot Stage Microscopy (HSM)**

The measure was carried out on hot stage apparatus (Mettler-Toledo S.p.A) mounted on Nikon Digital Net Camera DN100 for the images acquisition. MPs and MPsGS were heated from 35°C to 110°C (~20°C above the excipient melting point) with a scanning rate of 10°C/min.

### **X-ray diffraction analysis**

X-ray diffraction analyses were carried out by means of a Philips X'Celerator powder diffractometer, using  $\text{CuK}\alpha$  radiation ( $\lambda = 1,5418 \text{ \AA}$ ; 40 mA, 40 kV). MPs were packed into recessed slide and the diffraction patterns were obtained in the 3- 50°/ 2θ range using a 0,03° step and a 3°/min speed.

### **Cement Characterization**

The mechanical properties were tested as described in the 'Compressive Tests' section of Paragraph 4.2.3; then, a two ways analysis of variance (ANOVA) followed by Bonferroni's Multiple comparison test was employed to assess statistical significance of the experimental conditions ( $p < 0.05$ ). Cements were characterized as reported in 'X-ray diffraction', 'Scanning Electron Microscopy', 'Evaluation of injectability' and 'Evaluation of cohesion' sections of Paragraph 4.2.3.

### **Setting times determination**

Initial and final setting times were determined by the Gillmore method (ASTM, American Society for Testing and Materials: C 266- 89). Measurements were performed at 37 °C for the injectable composition and at room temperature for the pastes.

### **Micro-CT characterization**

To obtain a quantitative and tridimensional analysis of cement's porosity, selected samples (C\_Ba, C\_GS2, C\_MPsGS and C\_Ba\_GS2\_MPsGS after 21 days of soaking in PB solution) were scanned using a high-resolution micro-CT SkyScan 1172 (Bruker Micro-CT, Kontich, Belgium) using CTAn software (version 1.17.7.2, Bruker). The voltage source and the current were set at 100 kV and 100  $\mu$ A respectively, using a Cu/Al filter and with a nominal resolution of 6,5  $\mu$ m (pixel dimension). A cylindrical volume of interest (VOI) of 5 mm in diameter and 7 mm in height was defined in each sample. Then, the following 3D parameters related to the material porosity were calculated:

- the closed porosity P.cl (%), defined as the ratio between the volume of the closed and not 3D interconnected pores detected in the scaffolds and the total volume (VOI);
- the open porosity P.op (%), defined as the ratio between the volume of the open and 3D interconnected pores with the scaffold surface detected in the scaffolds and the total volume (VOI);
- the total porosity P.tot (%), defined as the ratio between the volume of the pores detected in the scaffolds and the total volume (VOI).

Moreover, in the same VOI, a 2D analysis of porosity size distribution was carried out calculating the diameter (in mm) of the circle having the same area as the single measured pore detected in each tomographic section and given as percentage in relation to the occupied area.

### **Antibacterial activity**

The antibacterial activity of disk-shaped samples C\_Ba, C\_Ba\_GS2, C\_Ba\_MPs, C\_Ba\_MPsGS and C\_Ba\_GS2\_MPsGS was evaluated *in vitro* against a panel of defined control strains from the American Type Culture Collection (ATCC), including three Gram-positive (*Staphylococcus aureus* ATCC 25923, *Staphylococcus epidermidis* ATCC 12228, *Enterococcus faecalis* ATCC 29212) and three Gram-negative bacterial strains (*Escherichia coli* ATCC 25922, *Pseudomonas aeruginosa* ATCC 27853, *Klebsiella pneumoniae* ATCC 9591). In addition, 20 clinical isolates recovered from patients with chronic bone or prosthetic joint infections at the Microbiology Unit, St Orsola Malpighi University Hospital (Bologna, Italy) were used. Clinical strains were isolated on BD Columbia Agar with 5% sheep blood (Becton Dickinson, GmbH, Germany) and confirmed by MALDI-TOF MS (BrukerDaltonik,

GmbH, Germany) (Croxatto, A 2012). Their antibiotic susceptibility was determined by using the Vitek2 semi-automated system (bioMerieux, France) and interpreted following EUCAST guidelines (EUCAST). For the Kirby-Bauer (KB) disk diffusion assay, the surface of Mueller-Hinton (MH) agar plate (Sigma-Aldrich) was inoculated with the bacterial suspension at 0.5 McFarland, and sterilized disks ( $\varnothing = 6.0$  mm) were placed on the agar plates. As control, gentamicin disk (GMN 10  $\mu$ g) was included in each assay. After 24 h of incubation at 37 °C the agar plate was observed and the inhibition zone diameters (corresponding to the bacterial-free zone around the disk-shaped sample) was measured to the nearest whole millimeter with a ruler. All experiments were performed on duplicate in different days. One-way analysis of variance (ANOVA) followed by Turkey's multiple comparison test was used to compare the antibacterial properties among samples. Differences were considered statistically significant with  $p < 0.05$ .

#### **Antibacterial activity over the time on *S. aureus***

Selected disk-shaped samples, C\_Ba\_GS2, C\_Ba\_MPsGS and C\_Ba\_GS2\_MPsGS, were assayed for their antibacterial activity towards *S. aureus* ATCC 25923 over a long period of incubation in PB solution, at pH 7.3 and at 37 °C to mimic physiological environment. Each biomaterial was prepared in a vial and incubated with 1 mL of PB solution. At set time intervals (1h, 4h, 24h, 3 days, 7 days, 14 and 21 days) the solution was withdrawn and replaced with fresh PB (1 mL). The antibacterial activity of the liquid samples, containing released GS from the different biomaterials, was evaluated *in vitro* against *S. aureus* control strain. In particular, each sample, previously diluted 1:500, was incubated for 24 h at 37°C with the inoculum suspension, prepared at 0.5 McFarland and diluted 1:200 in MH broth, in a final volume of 200  $\mu$ L. Bacterial growth was determined by measuring the optical density at 630 nm (OD) and the effectiveness of the GS released from the different biomaterials in inhibiting *S. aureus* growth was expressed as percentage value relative to the positive growth control (bacterial suspension in regular medium). Experiments were performed in duplicate, and samples were analyzed upon completion of the study. One-way analysis of variance (ANOVA) followed by Bonferroni's Multiple comparison test was used to compare data among the different experimental conditions; statistically significant differences were determined at  $p < 0.05$ . In addition, cements C\_Ba\_GS, C\_Ba\_MPsGS and C\_Ba\_GS2\_MPsGS recovered at the end of the above-described experiments, thus soaked in PB solution for 21 days, were assayed for their residual antibacterial activity towards *S. aureus* strain following the KB procedure.

## **Cytotoxicity tests**

Human osteoblast-like cells MG63 (OB, Istituto Zooprofilattico Sperimentale IZSBS, Brescia, Italy) were cultured in DMEM medium (Dulbecco's Modified Eagle's Medium, Sigma, UK) supplemented with 10% FCS and antibiotics (100 U/ml penicillin, 100 µg/ml streptomycin). Cells were detached from culture flasks by trypsinization, and cell number and viability were checked by erythrosine B dye. OB cells were plated at a density of  $3 \times 10^4$  cells/mL in 24-well plates containing six sterile samples of the biomaterials C\_Ba, C\_Ba\_MPsGS, C\_Ba\_GS2, C\_Ba\_GS2\_MPsGS. Cells were also plated in wells for negative (CTR<sup>-</sup>, DMEM only) and positive (CTR<sup>+</sup>, DMEM + 0.05% phenol solution) controls. Plates were cultured in standard conditions, at  $37 \pm 0.5$  °C with 95% humidity and  $5\% \pm 0.2$  CO<sub>2</sub> up to 72 h. The quantitative evaluation of cytotoxicity was performed by measuring cell viability and lactate dehydrogenase enzyme (LDH) release, whereas cell morphology was performed by Live/Dead® assay (Molecular Probes, Eugene, OR, USA). Cell viability at 72 hours was assessed by WST1 (WST1, Roche Diagnostics GmbH, Mannheim, Germany) colorimetric reagent test. The assay is based on the reduction of tetrazolium salt into a soluble formazan salt by a reductase of the mitochondrial respiratory chain, active only in viable cells. 100 µL of WST1 solution and 900 µL of medium (final dilution: 1:10) were added to the cell monolayer, and the multi-well plates were incubated at 37°C for further 4 h. Supernatants were quantified spectrophotometrically at 450 nm with a reference wavelength of 625 nm. Results of WST1 are reported as optical density (OD) and directly correlate with the cell number. Proliferation percent relative to CTR<sup>-</sup> at 24h are also reported. At the end of experimental times the supernatant was collected from all wells and centrifuged to remove particulates, if any, for LDH measure (LDH enzyme-kinetic test, Roche, D) according to manufacture instruction. A qualitative analysis for cell morphology was performed by Live/Dead® assay (Molecular Probes, Eugene, OR, USA), according to the manufacturer's instructions. Samples were visualized using an inverted microscope equipped with an epifluorescence setup (Eclipse TiU, NIKON Europe BV, NITAL SpA, Milan, Italy): excitation/emission setting of 488/530 nm to detect green fluorescence (live cells) and 530/580 nm to detect red fluorescence (dead cells).

### **4.2.2 Calcium phosphate bone cement enriched with self-assembling fibres**

#### **Synthesis of Boc-L-Dopa(OBn)<sub>2</sub>-OH**

The gelator was synthesized from unprotected and commercially available L-Dopa, which was transformed into Boc-L-Dopa(Bn)<sub>2</sub>-OH following a multistep procedure in solution, as reported in literature<sup>17,18</sup>.

### Preparation of the gelator solutions

The gelator solutions were prepared by dissolving the proper amount (20 and 50 mg, respectively) of Boc-L-Dopa(Bn)<sub>2</sub>-OH in 1 mL of an aqueous NaOH solution (1.3 equivalents), under stirring and sonicating for about 15 min<sup>19</sup>.

### Optimization of preparation steps – preliminary samples

During the development of the cement preparation method, a first attempt was made by mixing the CaCl<sub>2</sub> trigger with the cement powders and subsequently incorporating the liquid phase. The obtained cements were characterized to evaluate the actual presence of the fibres.

In addition, different amounts of CaCl<sub>2</sub> as triggers were used to assess whether this affected the formation and quantity of the fibres. The minimum quantity of trigger required for fibre formation is 1 equivalent compared to the quantity of gelator used. Larger quantities of trigger have been tested to assess the correlation between fibre formation and the amount of trigger used. The weighted amounts of CaCl<sub>2</sub>, corresponding to 1, 1.3 and 1.6 equivalent with respect to the gelator, were added to the vial containing the gelator solution, shaken in an electric mortar (Rotomix, 20 s) and then mixed with cement powders. The cements thus obtained have been labelled as summarized in Table 20.

Table 20. Compositions and labels of preliminary cements.

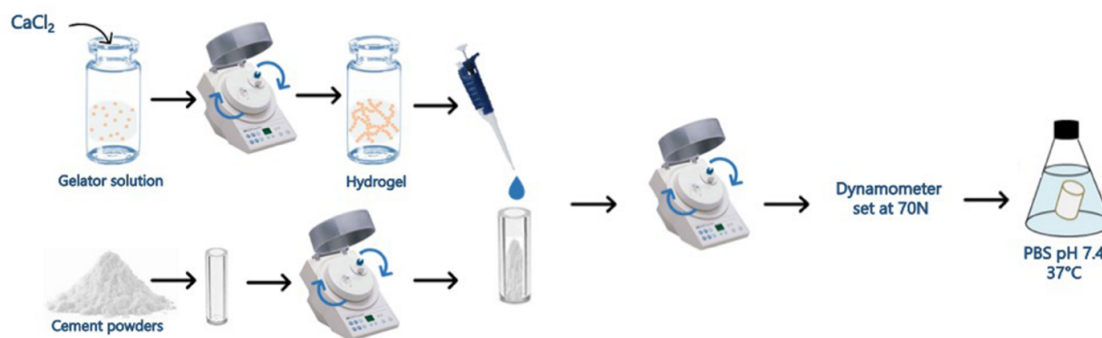
Label	Gelator (% w/w)		BaSO <sub>4</sub> (10% w/w)	CaCl <sub>2</sub> equivalents
	1%	2.6%		
G1_1eq	x			1
G1_1eq_Ba	x		x	1
G1_1.3	x			1.3
G1_1.3_Ba	x		x	1.3
G1_1.6	x			1.6
G1_1.6_Ba	x		x	1.6
G2.6_1eq		x		1
G2.6_1eq_Ba		x	x	1
G2.6_1.3		x		1.3
G2.6_1.3_Ba		x	x	1.3
G2.6_1.6		x		1.6
G2.6_1.6_Ba		x	x	1.6

### Cement preparation

The cement powders are composed of a gelatin/ $\alpha$ -TCP mix (15% w of gelatin with respect to the total amount) and CaHPO<sub>4</sub>·2H<sub>2</sub>O (DCPD). To obtain the reference cement (C), gelatin/ $\alpha$ -TCP powders and DCPD (5% w/w) were mixed in an electric mortar (3M ESPE RotoMix) two times for 20 s. After addition of an aqueous NaOH solution (1.3 equivalents), the powders were mixed again for 20 s with a liquid to powder (L/P) ratio of 0.52 mL/g. The

obtained pastes were compacted in a Teflon mold for 1 min with a 4465 Instron dynamometer set at 70 N. Then, cements were demolded and put in phosphate buffer (PB) at 37°C and pH 7.4 for 7 days.

For the preparation of fibres-containing cements, to ensure a homogeneous dispersion of the fibres inside the paste, the preparation method shown in Scheme 2 was used.



*Scheme 2. Preparation method of the FRCPCs.*

In particular, 1.3 equivalents (with respect to the weighted amount of the gelator) of  $\text{CaCl}_2$  as trigger were added to the gelator solution and mixed for 20 s in the electric mortar. Then, the mixed cement powders were added to the obtained hydrogel (liquid to powder ratio of 0.52 mL/g) and treated as described above. Two different amounts of gelator, 1% and 2.6% (w/w) with respect to the cement powders, were tested. The obtained cements were labeled G1 and G2.6, respectively. For the Ba-containing formulations, 10% (w/total weight of the cement powders) of  $\text{BaSO}_4$  was added to the cement powders before mixing with the liquid phase. The Ba-containing samples were labeled adding “\_Ba” to the above stated tags. The compositions and labels of the obtained cements are summarized in Table 21.

*Table 21. Compositions and labels of the obtained CPC samples.*

Label	$\text{CaCl}_2$ (1.3eq)	$\text{BaSO}_4$ 10%*	Gelator %*
C_Ba	x	x	/
G1	x		1%
G1_Ba	x	x	1%
G2.6	x		2.6%
G2.6_Ba	x	x	2.6%

\* w/w with respect to the weight of the powders mix.

### **Cement Characterization**

Cements were characterized as reported in ‘X-Ray diffraction’, ‘Scanning Electron Microscopy’, ‘Evaluation of injectability’ and ‘Evaluation of cohesion’ sections of Paragraph 4.2.3.

### Measurement of fibres diameters

The mean values of the fibre's diameters were calculated from the SEM images using the Digimizer Image Analysis Software. At least 50 fibres were measured for each composition.

### FT-IR spectroscopy

Fourier-transform infrared spectroscopy (FTIR, Nicolet IS10 spectrophotometer) was performed with a spectral resolution of 4 cm<sup>-1</sup> and 70 scans from 4000 to 500 cm<sup>-1</sup> on samples prepared as KBr disks. Omnic software (Thermo Electron Corp., Woburn, MA) was used for data processing and baseline correction.

### Mechanical characterization

Mechanical characterization of the cements was performed both in compression and in bending mode on samples right after the extraction from PB. The compressive strength tests were performed as reported in the 'Compressive Tests' section of Paragraph 4.2.3.

The specimens employed in the flexural tests were flat rectangular bars (20 x 10 x 3.5 mm) tested in three-point bending using a 4465 Instron testing machine, equipped with a 1 kN load cell at a crosshead speed of 1 mm/min. The flexural strength, Young's flexural modulus and work-of-fracture (WOF) were measured from the load-displacement curves using the following equations:

$$\text{Flexural Strength (MPa)} = \frac{3 \cdot F \cdot L}{2 \cdot b \cdot h^2} \quad (12)$$

where F is the failure load, L is the distance between outer loading points (20 mm), b and d are the width and the thickness of the specimen, respectively <sup>20</sup>.

$$\text{Flexural Modulus (MPa)} = \frac{F \cdot L^3}{4 \cdot d \cdot b \cdot h^3} \quad (13)$$

where d is the deflection at mid-span <sup>21</sup>.

$$\text{Work of Fracture (WOF)} = \frac{A}{b \cdot h} \quad (14)$$

where A indicates the total area under the load-displacement curve.

### Rheological tests

The rheological analyses were carried out to evaluate the viscoelastic behavior of the hydrogels in terms of G' (storage modulus, elastic contribution) and G'' (loss modulus, viscous contribution) moduli. The Anton Paar modular compact rheometer MCR102 was used for these tests. Time sweep tests were carried out on the gel keeping the shear strain (shear strain,  $\gamma =$

0.5%) and the oscillation frequency (10 rad/s) constant, recording a point every 60 seconds for several hours.

### Micro-CT characterization

C, C\_Ba, G1, G1\_Ba, G2.6 and G2.6\_Ba cements were scanned in the SkyScan 1172 micro-CT system (Bruker- MicroCT, Belgium) at a nominal resolution of 5 microns (2096x4000 pixels) employing a 0.5 mm thick aluminum filter and an applied x-ray tube voltage of 70 kV. Camera pixel binning was not applied. The scan orbit was 180 degrees with a rotation step of 0.4 degrees. Reconstruction was carried out using the SkyScanTMNRecon software (version 1.7.4.6, Bruker). Gaussian smoothing, ring artifact reduction and beam hardening correction were applied during the reconstruction process, and specific alignment relative to each single scan when needed. Volume of interest (VOI) selection, segmentation to binary and morphometric analysis were performed using SkyScan CT-Analyser (“CTAn” 1.20.3.0 version, Bruker) software. VOIs were defined considering the most structurally homogeneous region of the samples, starting from the center and measuring a volume of at least  $75\% \pm 5$  of the total volume of each sample (Figure 1).

Then, the following 3D parameters related to the material porosity were calculated:

- the total porosity (%), defined as the ratio between the volume of the pores detected in the scaffolds and the total volume (VOI);
- the normalized frequency of the pore’s distribution in the VOI.

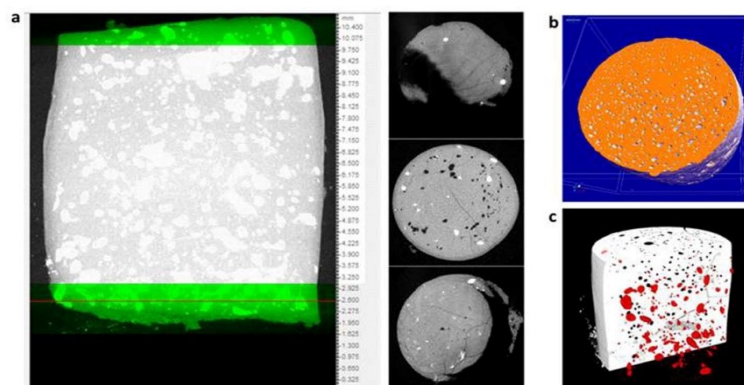


Figure 66. a) Definition of the VOI for the analyses. On the sagittal view, VOI top and bottom excluding incomplete sections (green regions); b) 3D visualization of samples G1 (left) and G1\_Ba (right).

### *In vitro* biocompatibility

Osteoblast-like cells MG63 (Istituto Zooprofilattico Sperimentale IZSLER, Brescia, Italy) were chosen to assess *in vitro* biocompatibility of G1 and G2.6 cements, added or not with barium (G1\_Ba, G2.6\_Ba), and using the sample without the gelator as reference (C\_Ba). MG63 were expanded in DMEM medium (Dulbecco’s Modified Eagle’s Medium, Sigma, UK)

supplemented with 10% FCS and antibiotics (100 U/mL penicillin, 100 µg/mL streptomycin), then plated at a concentration of  $2 \times 10^4$  cells/well in 24-well plates containing sterile samples of experimental biomaterial and reference, and DMEM only without materials as internal control (CTR). Plates were cultured in standard conditions, at  $37 \pm 0.5^\circ\text{C}$  with 95% humidity and  $5\% \pm 0.2 \text{ CO}_2$  up to 7 days. Cell viability was measured after 3 and 7 days of culture by Alamar blue dye (Cell Viability Reagent, Life Technologies Corp., Oregon, USA): the reagent was added (1:10 v/v) to each well and incubated for 4 h at  $37^\circ\text{C}$ . A redox indicator, incorporated in the reagent, changes its color in response to the chemical reduction of the medium resulting from living cells. The result is expressed as relative fluorescence units (RFU). The osteoblast viability was also calculated as percentage according to the following formula:

$$\text{Cell viability \%} = \frac{OD(\text{sample})}{OD(\text{C\_Ba})} \cdot 100 \quad 15)$$

so, referring the value of each sample to the reference material.

Furthermore, both 3- and 7-days supernatants from each well were collected and centrifuged to remove particulates and to measure Lactate Dehydrogenase (LDH detection kit, Roche diagnostics, IN, USA): enzyme released in medium when cell membrane is damaged. The test was performed following manufacturer's instruction and LDH concentration was spectrophotometrically read and reported in function of cell viability.

### Gene expression analysis

Gene expression of the most common markers of osteoblastic differentiation and activity was evaluated on all materials, as well as proinflammatory cytokines. Total RNA was extracted from all samples at each experimental time using PureLink™ RNeasy Mini Kit (AMBION, Life Technologies, Carlsbad, CA, USA), quantified by NANODROP spectrophotometer (NANODROP 2720, Thermal Cycler, Applied Biosystem) and reverse transcribed with SuperScriptVILO cDNA Synthesis Kit (Life Technologies), following the manufacturer's instructions. The obtained cDNA of each sample was diluted to the final concentration of 5 ng/µL and semi-quantitative polymerase chain reaction (PCR) analysis was performed for each sample in duplicate in a LightCycler 2.0 Instrument (Roche Diagnostics GmbH, Mannheim, Germany) using QuantiTect SYBR Green PCR Kit (Qiagen, Hilden, Germany) and gene-specific primers (Table 22). The protocol included a denaturation cycle at  $95^\circ\text{C}$  for 15'', 25 to 40 cycles of amplification ( $95^\circ\text{C}$  for 15'', appropriate annealing temperature for each target for 20'', and  $72^\circ\text{C}$  for 20''). After melting curve analysis to check for amplicon specificity the threshold cycle was determined for each sample and relative gene expression was calculated using the  $2^{-\Delta\Delta\text{Ct}}$  method (Schmittgen and Livak, 2008). For each gene, expression levels were normalized to GAPDH (glyceraldehyde 3-phosphate dehydrogenase) using C\_Ba as calibrator.

Table 22. Specifications of primer used for qPCR analysis.

GENE	Primer forward	Primer reverse	Amplicon Length	Annealing Temperature
GAPDH	5'- TGGTATCGTGGAAGGACTC A-3'	5'- GCAGGGATGATGTTCTG GA -3'	123 bp	56°C
ALPL	QuantiTect Primer Assay (Qiagen) Hs ALPL 1 SG		110 bp	55°C
COL1A1	QuantiTect Primer Assay (Qiagen) Hs COL1A1 1 SG		118 bp	55°C
BGLAP	QuantiTect Primer Assay (Qiagen) Hs BGLAP 1 SG		90 bp	55°C
SPARC	QuantiTect Primer Assay (Qiagen) Hs SPARC 1 SG		60 bp	55°C
IL1b	QuantiTect Primer Assay (Qiagen) Hs IL1B 1 SG		117 bp	55°C
IL6	QuantiTect Primer Assay (Qiagen) Hs IL6 1 SG		107 bp	55°C

### Immunoenzymatic analysis

Supernatants collected at 3 and 7 days were used for immunoenzymatic detection of Alkaline Phosphatase (ALP), Osteocalcin (OSTC), Interleukin 1 $\beta$  (IL1 $\beta$ ), Interleukin 6 (IL6) (ELISA kit, Finetest, Wuhan, China) and Type I Collagen (COL1, ELISA kit Biomatik Corp, Wilmington, USA). Dosages were performed in duplicates for each sample, following customer instructions.

### Statistical analysis

Statistical evaluation of data was performed using the software package SPSS/PC<sup>+</sup> Statistics<sup>TM</sup> 25.0 (SPSS Inc., Chicago, IL USA). The results presented are the mean of six independent values. Data are reported as mean  $\pm$  standard deviations (SD) at a significance level of  $p < 0.05$ . After having verified not normal distribution and homogeneity of variance, not parametric analysis was performed to assess differences among groups.

## 4.2.3 Methods of Characterization

### X-Ray diffraction

Cements were extracted from PB and immediately immersed in liquid nitrogen for few minutes in order to stop the hardening reaction. Samples were ground in a mortar, packed into recessed silicon slides and subjected to X-ray diffraction analysis by means of a Philips X'Celerator powder diffractometer equipped with a graphite monochromator in the diffracted beam. CuK $\alpha$  radiation ( $\lambda = 1,54 \text{ \AA}$ ; 40 mA, 40 kV) was used. The diffraction patterns were obtained in the 3- 50 $^{\circ}$ /2 $\theta$  range using a 0,03 step and a 3 $^{\circ}$ /min speed. For some Ba-containing samples, a Rietveld refinement was applied in order to evaluate the relative content of  $\alpha$ -TCP and HA, because of the superimposition of BaSO<sub>4</sub> reflections to those of phosphates.

## Compressive Tests

Mechanical properties in compression were evaluated on cylindrical specimens (6 mm in diameter, 12 mm in length) using a 4465 Instron dynamometer equipped with a 1 kN load cell. Stress-strain curves were recorded at a crosshead speed of 1 mm/min by the software SERIE IX for Windows. At least 6 specimens for each incubation time were tested.

## Scanning Electron Microscopy

Morphological investigations of MPs were performed by using a Philips XL-20 Scanning Electron Microscope. The samples were placed on metal stubs and sputter-coated with gold prior to examination (30 mA for 2,5 min).

Morphological investigation of the fractured surfaces of the cement samples was performed after stopping the hardening reaction with liquid nitrogen, using a Cambridge Stereoscan 360 Scanning Electron Microscope (SEM) with an electron acceleration voltage of 15kV. Samples were sputter-coated with gold prior to examination.

## Evaluation of injectability

The injectability of the CPC pastes was assessed using a 10 mL syringe fitted with an orifice of 1,2 mm inner diameter and a 14-gauge needle. CPC powders and the liquid phase were manually mixed and packed into the syringe. After that, the syringe plunger was manually shifted to eliminate the trapped air, applying a pre-load onto the paste. Four minutes after the initial mixing of the CPC powders and liquid, the syringe was placed between the compression plates and the CPC paste was extruded from the syringe by a 4465 Instron dynamometer (1kN load cell) at a speed of 15 mm/min until a maximum force was reached. Tests were performed at RT and each measurement was carried out in triplicate. Injectability curves (load applied vs displacement) were recorded. The mass (m) of the paste extruded from the syringe was weighted and divided by the original mass of the paste in order to calculate the percentage of extruded cement:

$$\% \text{ Extruded cement} = \frac{W_f - W_{ef}}{W_f - W_{ei}} \cdot 100 \quad (16)$$

where  $W_f$  is the weight of full syringe,  $W_{ef}$  is the weight of empty syringe after the extrusion and  $W_{ei}$  is the weight of empty syringe before the extrusion.

## Evaluation of cohesion

To assess the cement cohesion, the newly prepared CPC pastes were immediately injected into a saline solution at 37°C, and their behavior (whether disintegration happened or not) was observed during hardening. Pictures were taken immediately and after 24 hours.

### 4.3 DEVELOPMENT OF ANTIBACTERIAL CALCIUM PHOSPHATE BONE CEMENTS

#### Introduction

Calcium Phosphate Cements (CPCs) applications in bone replacement imply risks of infections due to bacterial colonization<sup>22</sup>. It follows that the addition of antibiotics to CPCs composition is of outmost interest, as testified by the high number of studies reported in the literature<sup>11,23,24</sup>. The loading of the antibiotic drug is generally performed by adding it directly to the solid or to the liquid phase of the cement, even if this method has adverse effects on its mechanical and setting properties, thus limiting the amount of drug that could be added<sup>23,25</sup>. The addition to the cement powders of poly(lactic co-glycolic-acid) microspheres as antibiotics carriers has been proposed as a strategy to better control drug release and increase its bioavailability without affecting the cement properties<sup>26,27</sup>. Spray-congealed solid lipid microparticles have previously been demonstrated to be an effective platform for the controlled delivery of sodium alendronate, an osteoporosis contrasting drug able to stimulate bone formation and suppress bone resorption<sup>28</sup>. Moreover, the introduction of loaded microparticles can also prevent the lengthening of setting times and the worsening of mechanical properties caused by the direct loading of the drug into cement composition, thus allowing a higher amount of drug to be incorporated<sup>29,30</sup>. Lipids display a favorable biocompatibility and lower toxicity compared with many polymers: the higher degradability of Cutin with respect to PLGA could favor the development of a microporosity inside the set cements<sup>28</sup>.

In this project, I explored the possibility to employ solid lipid microparticles obtained from Cutin to load an antibiotic into a biomimetic calcium phosphate cement, in order to obtain a material able to sustain a potent antibacterial activity over a long period and avoid the adverse effects of drug direct addition to the starting powders<sup>25</sup>. Gentamicin sulphate (GS) was chosen as model drug, since it is the utmost used agent for the treatment of severe infections caused by Gram positive and Gram-negative bacteria. The effect of the drug on the cement properties was investigated in cements where gentamicin sulphate was (i) loaded directly into the cement powder, (ii) loaded into the solid lipid microparticles, which were added to the cement, and (iii) loaded both directly into the cement powder and into the solid lipid microparticles. Moreover, barium sulphate was added as radiopacifying agent to the composition of cements, in order to allow the material to be monitored during the surgery. The mechanical and structural properties of the cements were investigated, and the formulations were optimized to obtain injectable pastes. The antibacterial activity was tested *in vitro* against a panel of Gram-positive and Gram-negative reference bacterial strains and against a panel of clinical isolates recovered from

patients with chronic bone or prosthetic joint infections at the S. Orsola-Malpighi University Hospital of Bologna.

## Results and discussion

The results of this work demonstrate that Cutin solid lipid microparticles produced by a solvent-free technique can be used as carriers of the antibiotic Gentamicin sulphate, in order to provide cement formulations with antibacterial properties, without worsening their mechanical behavior. MPs, loaded with 20% w/w of GS, were successfully obtained by spray congealing technology. To evaluate the influence of different additives on cement properties, BaSO<sub>4</sub>, GS as powder, MPs and MPsGS were added separately, as well as in mixed compositions, to a weighted amount of cement powder as summarized in Table 1.

### Production and characterization of MPs and MPsGS

Cutin microparticles obtained by spray congealing technique, containing or not 20% w/w of GS (MPs and MPsGS), presented a Gaussian dimensional distribution with a maximum centered at the size fraction 100-150  $\mu\text{m}$ , which was therefore been chosen for cements formulations. Evaluation of encapsulation efficiency of GS confirmed the theoretical value of 20% and did not reveal any significant difference as a function of particles size. MPsGS appeared round shaped and exhibited almost smooth surfaces, although small pores were appreciable on the particles surface (Figure 67b).

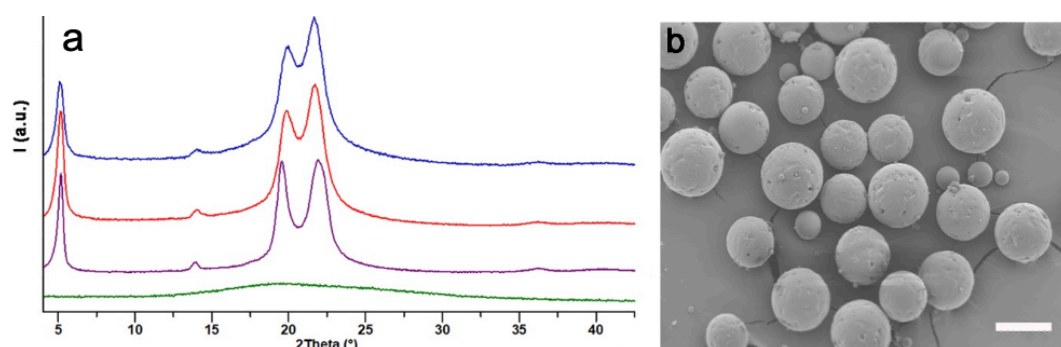


Figure 67. a) X-ray diffraction patterns of: Cutina powder (purple), MPs (red), MPsGS (blue) and GS as received (green); b) SEM image of MPsGS, bar=100  $\mu\text{m}$ .

X-ray diffraction pattern of GS powder showed a very broad halo centered at about 20°/2 $\theta$ , whereas the patterns of MPsGS displayed several diffraction reflections, the most intense centered at 5.2, 19.5 and 21.95°/2 $\theta$ , characteristic of Cutin (Figure 67a). The position and relative intensity of these reflections are not affected by the presence of GS.

Hot Stage microscopy (HSM) showed clear evidence of the presence of GS after fusion of the low-melting excipient (see Figure 68).

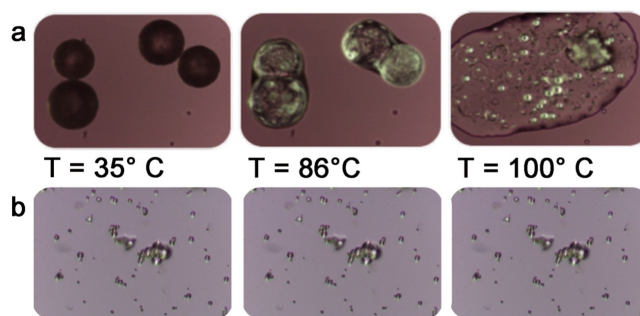


Figure 68. HSM of (a) spray congealed Cutin microparticles loaded with GS and (b) GS powder.

As expected, encapsulation of GS into lipid microparticles led to a prolonged release over time. In fact, due to the high solubility of GS, when the powder is put in aqueous medium, its dissolution is nearly instantaneous and after 15 min the GS was completely recovered, while the release from MPs was completed only after 5 h (data not shown).

#### Cement pastes loaded with GS and/or BaSO<sub>4</sub>

The effect of GS and/or barium sulphate on the mechanical, setting and hardening behavior of the cement pastes was evaluated. Mechanical properties in compression were tested after 7 and 21 days of soaking in PB and the values of maximum stress, obtained from the stress-strain curves, as well as the initial and final setting times, are reported in Table 23, while the effect of both the additives on the hardening reaction was evaluated through X-ray diffraction analysis and subsequent Rietveld refinement.

Table 23. Maximum stress values, initial and final setting times, and relative content (%) of Hydroxyapatite in cements with GS and/or BaSO<sub>4</sub> after different soaking times.

Sample	S <sub>max</sub> (MPa)		t <sub>i</sub> (min)	t <sub>f</sub> (min)	HA content (%)	
	7 days	21 days			7 days	21 days
C	10.1 ± 0.6	15 ± 1	6 ± 1	13 ± 3	100	100
C_GS 2	6.8 ± 0.8***	7.0 ± 2.0***	10 ± 1	22 ± 2	90	95
C_GS 4	5.8 ± 0.8***	5.4 ± 0.9***	10 ± 1	20 ± 3	82	90
C_GS 8	3.4 ± 0.6***	3.3 ± 0.9***	9 ± 2	19 ± 3	70	90
C_Ba	15 ± 2***	13 ± 1***	5 ± 2	8 ± 3	81	98
C_Ba_GS2	10 ± 3	9 ± 2***	11 ± 2	21 ± 2	60	94
C_Ba_GS4	9 ± 2	6 ± 1***	8 ± 3	20 ± 2	50	90
C_Ba_GS8	4.3 ± 0.9***	4 ± 1***	8 ± 3	17 ± 3	40	80

The statistical differences were obtained by comparing different samples to C for each time point (\*\*\*p<0.001, \*\*p<0.01, \*p<0.05).

The value of maximum stress of the control cement (C) increased as a function of time due to the hardening reaction. Direct addition of GS powder had a strong effect on both mechanical and setting properties of the cements (Table 23), as expected from the literature<sup>25</sup>. In fact, just the introduction of a 2% of GS provoked a reduction of the values of maximum stress in

comparison to those obtained for C cements, at every experimental time. Moreover, the compressive strength of the materials decreased as the amount of GS increased, along with a lengthening of both initial and final setting times. On the other hand, the addition of barium sulphate seemed to reduce the negative influence of GS on the mechanical properties without influencing the setting times.

Figure 69 reports as an example the XRD patterns recorded on C\_Ba cements after different soaking times, compared to BaSO<sub>4</sub> pattern. The presence of BaSO<sub>4</sub>, added in order to obtain a radiopaque material<sup>31,32</sup>, seems to elicit a negligible delay in the conversion reaction: after 21 days the most intense reflection of  $\alpha$ -TCP is barely appreciable. A quantitative evaluation of the extent of conversion of  $\alpha$ -TCP into hydroxyapatite, shown in Table 23, indicates that the cements loaded with 2% w/w of GS were almost totally converted after 7 days, suggesting that this amount of antibiotic does not greatly interfere with the hardening reaction. However, greater GS contents delayed the hardening reaction, thus justifying the worsening of the mechanical properties observed on increasing GS content<sup>25</sup> and led to a lengthening of both initial and final setting times. Concurrent addition of BaSO<sub>4</sub> limited this negative trend: however, it is evident that direct addition of GS to the powders must be limited to a value of 2% w/w, in order to maintain cement properties. On this basis, further investigations were carried out using only one percentage of GS (2% w/w), both when loaded into MPs and when directly added to the cement powders.

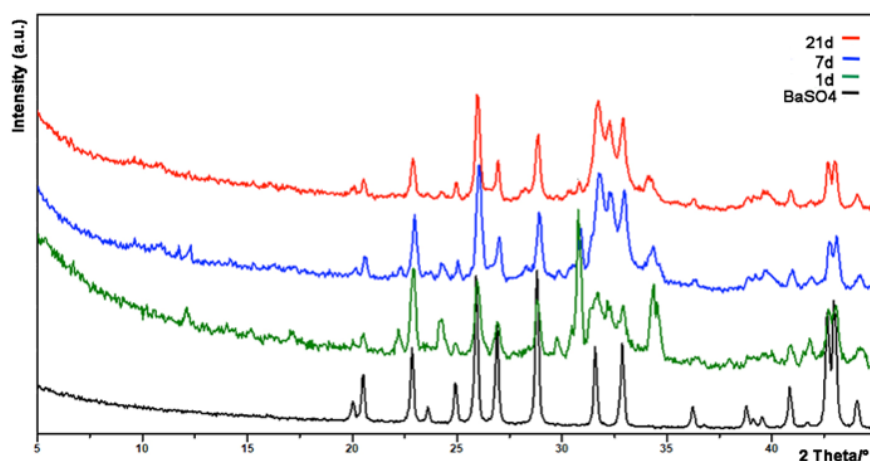


Figure 69. XRD patterns of C\_Ba cements after different periods of soaking, compared to that of BaSO<sub>4</sub>.

### Cement pastes containing MPs and MPsGS

Inclusion of MPs is an effective method to incorporate drugs or bioactive molecules into cement pastes without affecting cement properties<sup>8,28</sup>. Values of maximum stress under compression and initial and final setting times of MPs-containing cements are reported in Table 24, together with those of C samples for comparison. As desirable, the compressive strength of C\_MPs and of C\_MPsGS was not significantly different ( $p>0.05$ ), confirming that loading GS into the

microspheres did not modify the mechanical properties of the resulting cements (2way-ANOVA with Bonferroni post-tests). Only the cements containing both free GS and drug-loaded MPs displayed a significant worsening of the compressive strength at 7 days compared with C\_MPs, even though initial and final setting times were not significantly influenced by the presence of the additives.

Table 24 also reports the extent of hydroxyapatite obtained from  $\alpha$ -TCP conversion after different soaking times: the complete conversion of C cements took place after 7 days of soaking in PB, while in presence of both MPs and MPsGS, the hardening reaction slowed down, and the conversion was obtained after 21 days. Furthermore, with the aim to enhance the total amount of GS without worsening the cement properties, 2% w/w of GS powder was added to the formulation containing MPsGS and barium sulphate (sample C\_Ba\_GS2\_MPsGS). This addition did not affect the setting times and provoked just a slight reduction of the mechanical properties at 7 days, probably due to the lengthening of the hardening reaction (\*\*p < 0.01 C\_MPs vs C\_Ba\_GS2\_MPsGS), but no significant differences were observed at 21 days (Table 24).

*Table 24. Maximum stress values, initial and final setting times, and relative content (%) of Hydroxyapatite in cements containing different additives after different soaking times. Values are the mean  $\pm$ SD of at least 6 samples.*

Sample	s <sub>max</sub> (MPa)		t <sub>i</sub> (min)	t <sub>r</sub> (min)	HA content (%)	
	7 d	21 d			7 d	21 d
C	10.1 $\pm$ 0.6	15 $\pm$ 1	6 $\pm$ 1	13 $\pm$ 3	100	100
C_MPs	12 $\pm$ 2**§	10.2 $\pm$ 0.1	5 $\pm$ 1	11 $\pm$ 3	90	100
C_MPsGS	10 $\pm$ 1	10 $\pm$ 1	4 $\pm$ 1	7 $\pm$ 2	89	97
C_Ba_MPs	15 $\pm$ 5	13 $\pm$ 1	4 $\pm$ 2	6 $\pm$ 3	65	80
C_Ba_MPsGS	10 $\pm$ 1 <sup>§</sup>	10 $\pm$ 2	4 $\pm$ 2	6 $\pm$ 3	60	80
C_Ba_GS2_MPsGS	5.0 $\pm$ 0.5**	8 $\pm$ 2	4 $\pm$ 2	6 $\pm$ 3	40	70

\*\*p < 0.01 C\_MPs vs C\_Ba\_GS2\_MPsGS; §p > 0.05.

### Micro-CT characterization

To get some insights on the cement's texture influenced by the additives, micro-CT analysis was carried out on the samples C\_Ba, C\_GS2, C\_MPsGS and C\_Ba\_GS2\_MPsGS. 3D models of representative samples analyzed by micro-CT are reported in Figure 70.

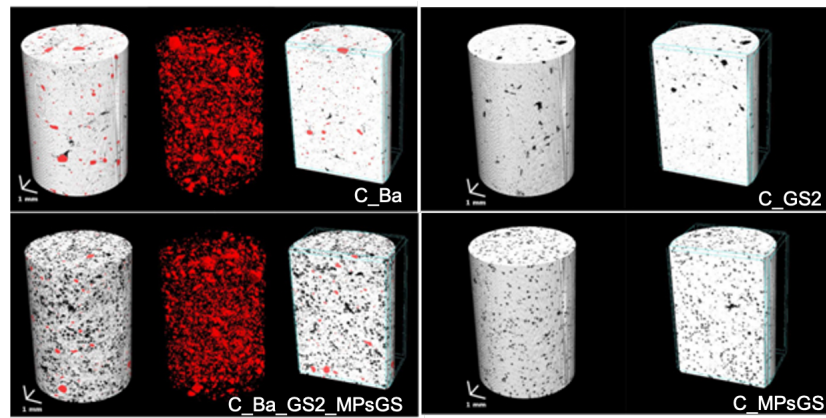


*Figure 70. 3D models of representative samples analyzed by micro-CT. In every box the whole sample inside the VOI is shown on the left, the agglomerates of BaSO<sub>4</sub> are, when present, in the center colored in red, and the sample 3D model cut virtually along.*

Due to the voltage set of micro-CT used for data acquisition of the composite cements, MPs and MP<sub>s</sub>GS resulted radiotransparent: this implies that part of the porosity detected in the samples may be constituted also by microparticles. In fact, together with a microporosity due to the cement structure, 2D distribution of pores size highlights a higher percentage of “porosity” of size between 0.1 and 0.2 mm in MP<sub>s</sub>- and MP<sub>s</sub>GS- containing cements (the main size of added microparticles). The values of total porosity (%) of C\_MP<sub>s</sub>GS (10.6%) and C\_Ba\_GS2\_MP<sub>s</sub>GS (22.6%) are indeed higher than those found for C\_Ba (3.4%) and C\_GS2 (3.9%), thus confirming this hypothesis.

### **Cytotoxicity assessment**

The influence of each additive on the biological and antibacterial properties of the cements was evaluated on samples C\_Ba, C\_Ba\_GS2, C\_Ba\_MP<sub>s</sub>GS and C\_Ba\_GS2\_MP<sub>s</sub>GS. A demonstration of the absence of any cytotoxic effect (a reduction of viability by more than 30% is considered a cytotoxic effect) relies in the values of proliferation (expressed as percentage relative to CTR-). LDH dosage is an indirect parameter of cytotoxicity because its release in culture medium is due to a damage of cell membranes. All values were significantly lower when compared to CTR+ ( $p < 0.0005$ ).

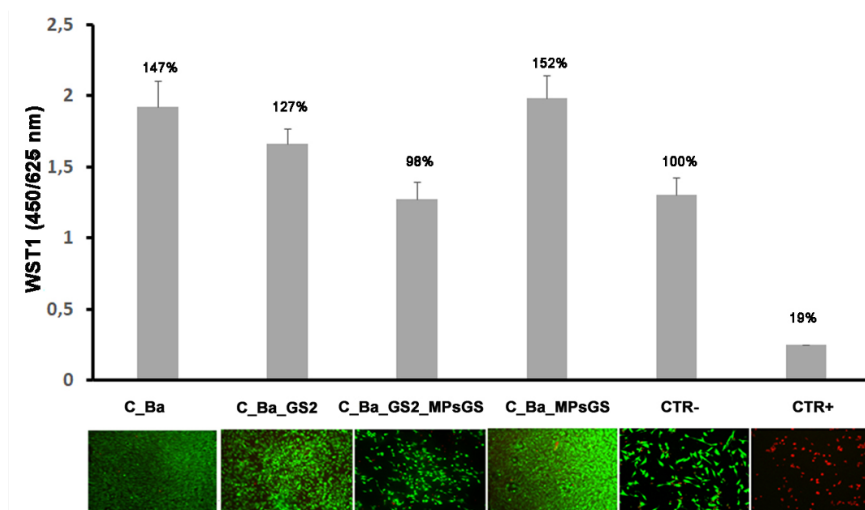


Figure 71. Viability test (top) by WST1 test and Live & Dead staining (10x, bottom).

Cell viability was performed after 72 h of culture (Figure 71): no signs of cytotoxicity were shown, as demonstrated by values of WST1 test, which did not differ (C\_Ba\_GS2\_MPsGS) or were even significantly higher (C\_Ba, C\_Ba\_MPsGS, C\_Ba\_GS2,  $p < 0.005$ ) than CTR-. Moreover, cells were stained with Live&Dead fluorescent staining for qualitative evaluation of cell morphology: all the samples showed good colonization of surface with cells displaying a normal morphology (green staining). As expected, CTR+ showed a significant reduction in viability and images confirmed the presence of numerous dead cells (red staining).

### Antibacterial activity

The antibacterial properties of the cements C\_Ba, C\_Ba\_GS2, C\_Ba\_MPsGS and C\_Ba\_GS2\_MPsGS were evaluated by a Kirby Bauer diffusion assay towards a set of control strains and a panel of clinical isolates characterized for their susceptibility profile by standard procedures (EUCAST testing guidelines). C\_Ba\_MPs was added as a further control.

Table 25. Antibacterial activity of the cements. Median values and range of inhibition zone diameters (mm) against ATCC control strain are reported.

Sample	<i>S. aureus</i> (ATCC 25923)	<i>S. epidermidis</i> (ATCC 12228)	<i>E. faecalis</i> (ATCC 29212)	<i>E. coli</i> (ATCC 25922)	<i>K. pneumoniae</i> (ATCC 9591)	<i>P. aeruginosa</i> (ATCC 27853)
C_Ba	NA*	NA	NA	NA	NA	NA
C_Ba_GS2	21 (20-22)	26.5 (26-27)	14 (13-15)	19.5 (19-20)	22 (21-23)	23.5 (23-24)
C_Ba_MPs	NA	NA	NA	NA	NA	NA
C_Ba_MPsGS	22.5 (22-23)	28.5 (27-30)	15	19.5 (19-20)	21.5 (21-22)	23.5 (23-24)
C_Ba_GS2_MPsGS	25.5 (25-26)	29 (28-30)	17 (16-18)	21 (20-22)	24 (23-24)	25 (24-26)
GMN <sup>§</sup>	18.5 (18-19)	24 (23-25)	9	18	18 (17-19)	17

\*NA= Not appearing; <sup>§</sup> GMN disk containing 10 ug of gentamicin and used as positive control.

As reported in Table 25, all disk-shaped biomaterials containing GS inhibited bacterial growth as a clear bacterial free zone was measured around disks following incubation. On the contrary,

C\_Ba and C\_Ba\_MPs did not determine inhibition, confirming the reliability of the sample preparation and testing procedure. Although no significant differences were appreciated in Gram-negative bacteria, the median values of the inhibition zone diameters obtained for Gram-positive strains on cements containing MP<sub>s</sub>GS were higher than those measured for samples containing GS loaded directly into cement composition. Considering that C\_Ba\_GS and C\_Ba\_MP<sub>s</sub>GS contain the same drug amount, it is possible to speculate that lipid microparticles enhanced GS uptake through the bacterial membrane.

For a fully characterization of the antibacterial potential, C\_Ba\_GS2, C\_Ba\_MP<sub>s</sub>GS and C\_Ba\_GS2\_MP<sub>s</sub>GS were assayed against 20 clinical isolates of *S. aureus* and *S. epidermidis*, including multidrug-resistant *Staphylococci*, and the results are reported in Table 26.

Table 26. Antibacterial activity of the cements against clinical strain. Median values and ranges of inhibition zone diameters (mm) are reported.

Sample	MSSA <sup>a</sup> (n = 5)	MRSA <sup>b</sup> (n = 5)	MSSE <sup>c</sup> (n = 5)	MRSE <sup>d</sup> (n = 5)
C_Ba_GS 2	29.5 (28-32)	26 (26)	34 (33-35)	31 (26-31)
C_Ba_MP <sub>s</sub> GS	29.5 (29-32)	26.5 (26-28)	34 (33-35)	31.5 (28-34)
C_Ba_GS2_MP <sub>s</sub> GS	32 (31-34)	28 (27-29)	36.5 (36-37)	34 (30-36)
GMN <sup>e</sup>	22.5 (22-23)	21 (19-22)	29 (28-30)	26.5 (22-28)

<sup>a</sup>methicillin-sensitive *S. aureus* strains; <sup>b</sup>methicillin-resistant *S. aureus* strains; <sup>c</sup>methicillin-sensitive *S. epidermidis* strains; <sup>d</sup>methicillin-resistant *S. epidermidis* strains; <sup>e</sup>GMN, disk containing 10µg of gentamicin and used as positive control.

The biomaterials displayed strong antibacterial properties against all tested clinical isolates and, comparing the diameters of the inhibition zones, a significantly greater activity of C\_Ba\_GS2\_MP<sub>s</sub>GS respect to C\_Ba\_GS2 and C\_Ba\_MP<sub>s</sub>GS was observed for methicillin-sensitive *S. aureus* strains (C\_Ba\_GS2 vs C\_Ba\_GS2\_MP<sub>s</sub>GS \*\*p<0.001; C\_Ba\_MP<sub>s</sub>GS vs C\_Ba\_GS2\_MP<sub>s</sub>GS \*p<0.05). These bacterial strains were chosen to represent a spectrum of pathogens associated with joint and bone infections, as resistance to antibiotics is one of the mayor concerns in antimicrobial therapy. The antibiotic-resistance profile of each clinical strain is reported in Appendix II.

### Antibacterial activity over time

In order to correlate the antibacterial activity over time to the cement's composition, GS containing cements (C\_Ba\_GS2, C\_Ba\_MP<sub>s</sub>GS and C\_Ba\_GS2\_MP<sub>s</sub>GS) were put in PB solution and withdrawals assessed towards *S. aureus* control strain. Up to the fourth recovery of PB solution, the GS released from the materials inhibited *S. aureus* growth at the same extent, while at later sampling the antibacterial activity of GS from C\_Ba\_MP<sub>s</sub>GS and C\_Ba\_GS2\_MP<sub>s</sub>GS was significantly higher compared to C\_Ba\_GS2. The effectiveness of GS

loaded as powder from C\_Ba\_GS2 samples gradually decreased with time, down to negligible levels (6.5%) at 21 days. On the contrary, GS from MPs displayed a strong and long-term inhibitory activity in both formulations (78.0% and 68.6% for C\_Ba\_MPsGS and C\_Ba\_GS2\_MPsGS, respectively). The excellent and prolonged activity of the biomaterials containing MPs was confirmed by KB diffusion assay performed with the cement disk recovered after 21 days of soaking. While the median value of the inhibition zone diameter obtained for C\_Ba\_GS2 was only 14 mm, for C\_Ba\_MPsGS and C\_Ba\_GS2\_MPsGS it was 18 mm, suggesting that these biomaterials maintained high inhibitory properties over a long period. These results suggest that both the composite biomaterials, C\_Ba\_MPsGS and C\_Ba\_GS2\_MPsGS could be really effective in the treatment of bacterial infections, combining a potent initial antibacterial action with a sustained release over time, which is an important feature to avoid the administration of insufficient doses of drug, which can lead to the arising of antibacterial resistances.

### **Injectable CPC formulation**

All the formulations could be employed to realize injectable cements by a proper adaptation of the liquid to powder ratio. Injectability of CPC is an important feature for minimally invasive surgical techniques, in applications involving defects with limited accessibility and narrow cavities and when there is the need to conform to a defect area of complex shape<sup>33</sup>. Injectable formulation of the previously described cements was easily obtained through a simple modification of the L/P ratio: the compositions and the added volumes of water are summarized in Table 27, which also reports the values of setting times measured at 37 °C.

*Table 27. Liquid to powder ratio and setting times of the injectable cements.*

Sample	Liquid/Powder (mL/g)	Setting times (min)	
		t <sub>i</sub>	t <sub>r</sub>
in_C_Ba	0,55	24± 3	38± 2
in_C_Ba_GS 2	0,60	22± 3	37± 2
in_C_Ba_MPsGS	0,65	18± 3	34± 2
in_C_Ba_GS 2_MPsGS	0,65	18± 3	33± 2
in_C_Ba_GS 2_MPsGS	0,75	19± 3	35± 2

The injectable cements presented good injectability<sup>34</sup>, as shown in Figure 72a, and an excellent cohesion: when injected into saline solution immediately after extrusion, the CPC paste maintained its wire-like shape until hardening, with no sign of disintegration during the process. The cement maintained a good cohesion even after 24 h and exhibited a highly homogeneous dispersion of MPs inside the extruded wire. In particular, there was no evidence of phase separation, which is a major issue inhibiting successful delivery of injectable CPC.

Furthermore, we collected the material at different times during the extrusion and performed an accurate morphological observation along the wire length by means of scanning electron microscopy (Figure 72b).

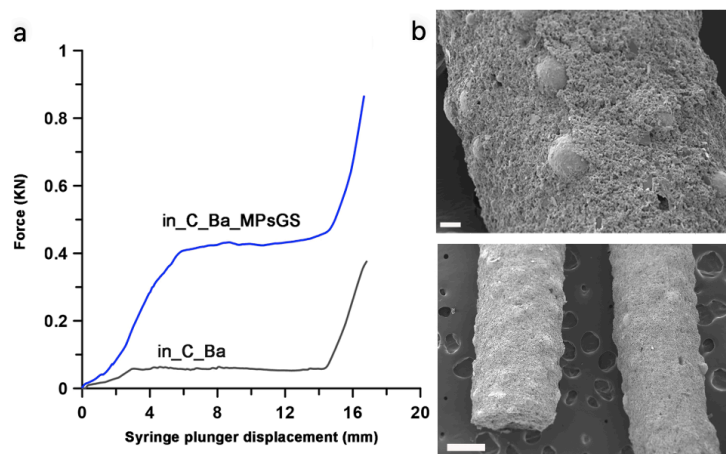


Figure 72. a) Injectability curves of *in\_C\_Ba* and *in\_C\_Ba\_MPsGS*; b) SEM images of the cement wire *in\_C\_Ba\_MPsGS* collected immediately after extrusion. Bar: 100  $\mu\text{m}$  (top), 50  $\mu\text{m}$  (bottom).

From the images recorded for sample *in\_C\_Ba\_MPs* and reported in Figure 72b, it can be inferred that the MPs are regularly distributed along the whole length of the wire, thus confirming their good dispersion and the absence of phase separation during injection. In the same Figure, injectability curves are reported, plotting the injection force as a function of the plunger displacement to assess the ease of injection. A very rapid increase of the load in the first millimeters of displacement is due to the critical force that must be applied to start the flow of the paste, while the subsequent plateau (in the absence of phase separation) is related to the load needed to maintain the flow. In the last portion of the curves, the load increases abruptly because of the mechanical contact between the plunger and the syringe's bottom when all the paste has been extruded: hence, the system was stopped<sup>35</sup>. The introduction of MPs into cement's formulation decreases the injectability, as expected: more pressure was needed to extrude the paste from the syringe (compare the blue curve with the black one in Figure 72a). Sample *in\_C\_Ba\_GS2\_MPsGS* was tested using two different liquid-to-powder ratios: the formulation at higher L/P ratio (0,75 mL/g) provided a good injectability of the cement since the required load during the extrusion is about 300 N. Radiopacity of *C\_Ba\_MPsGS* was demonstrated by the radiograph reported in Figure 73: the presence of barium sulphate allows easy detection of the cement.



*Figure 73. Radiographs of cement C\_Ba\_MPsGS.*

## **Conclusions**

The results of this study allowed to develop antibacterial and radiopaque calcium phosphate cements, which can be turned from non-injectable to fully injectable formulation by simple variation of liquid to powder ratio. Thanks to the use of spray congealed microparticles, gentamicin sulphate could be added to the cement composition without the lengthening of the setting times and the worsening of the compressive strength observed when the drug is loaded directly into the cement powder without the protection of the MPs. Human osteoblast-like cells displayed a good viability on all the examined cement formulations. Moreover, all the compositions exhibited a strong inhibitory activity towards Gram-positive and Gram-negative reference bacterial strains and clinical isolates. In particular, cements with gentamicin-loaded MPs showed an enhanced inhibition towards Gram-positive bacteria and a sustained release of the drug over time, which provides a long-term antibacterial activity, fundamental in the treatment of chronicle infections. Injectable formulations displayed good injectability, high cohesion and good dispersion of MPs into the extruded cements without any phase separation.

#### 4.4 CALCIUM PHOSPHATE BONE CEMENT ENRICHED WITH SELF-ASSEMBLING FIBRES

##### Introduction

An improvement in mechanical properties of calcium phosphate bone cements would considerably broaden their field of potential applications. In the last few decades, the incorporation of preformed fibres into a brittle cement matrix has been proven to increase the mechanical properties: in fact, it has been extensively explored even in the field of hydraulic cements and concretes for civil engineering and building applications<sup>36</sup>. Natural fibres (such as cellulose, sisal, jute, bamboo, rock-wool, etc.)<sup>37</sup> and man-made fibres (such as steel, titanium, glass, carbon, polymers, etc.) have been proposed as reinforcement for CPCs<sup>38</sup>, but, as far as found in literature, they have always been introduced inside the pasty material already in form of fibres. A prerequisite for an effective reinforcement relies on the mechanical properties of all the components and on the fiber-matrix adhesion, which is crucial for a successful load transfer. Unreinforced cements are characterized by a brittle behavior and an immediate fracture in two or more pieces, while in the case of fibre-reinforced CPCs (FRCPCs) a large amount of energy is absorbed during the fracture and the stress at break is higher<sup>39</sup>. The possibility to achieve a composite material reinforced with fibres grown directly inside the cement would represent a unique opportunity to obtain a better cohesion between fibres and cement paste, but it is not reported yet in literature. In this work, the self-assembling of fibres was achieved using a low-molecular-weight gelator (LMWG) derived from commercial L-Dopa. LMWGs are molecules with a molecular weight lower than 1000 Da and a specific stereochemistry, that can self-assemble into supramolecular structures, such as gels and fibres, by means of weak interactions, including hydrogen bonds,  $\pi$ - $\pi$  stacking and Van der Waals forces<sup>40</sup>. The process usually starts when a trigger is added to the gelator solution: the gelator molecules self-assemble in long structures which entangle together, forming a network able to trap the solvent. The ability to self-assemble into fibres in presence of calcium ions makes this gelator the perfect candidate to introduce inside CPCs. The main hurdle for the fibres growth in a cement matrix is the amount of liquid required for the formation of the networks. In fact, while hydrogels are mainly composed of a liquid phase (up to 99%), CPCs are made up of an inorganic powder mix that is necessary for the formation of the cement. The aim of this work was to demonstrate the feasibility to obtain self-assembling of fibres made of LMWG in CPCs thus improving mechanical properties and biocompatibility. Addition of barium sulphate as radiopacifying agent was also evaluated. Cements were fully characterized and their ability to ensure good cell

viability and to express the main gene markers that are necessary for bone formation was evaluated.

## **Results and discussion**

This study represents the first attempt to produce fibres-reinforced cements by self-assembling of fibres during cement hardening. The L-Dopa derivative gelator chosen as LMWG is biocompatible and presents the ability to form fibres in the presence of calcium.

### **Optimization of preparation steps**

Mixing the trigger first with the powder phase and then adding the liquid phase proved to be an inadequate method of preparation: the SEM analyses (Figure 74) highlighted the lack of fibers in all the prepared cements and the presence of small fragments of gel. Moreover, a poor porosity was found all over the samples.

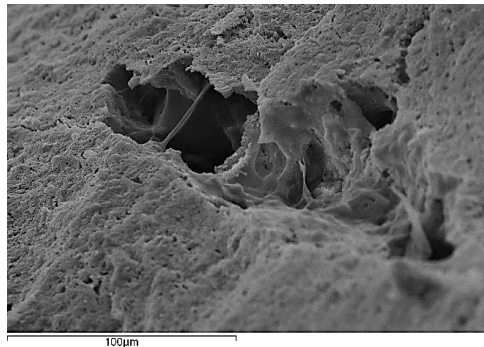


*Figure 74. SEM image of the cement obtained combining first the trigger with the powder phase.*

Therefore, it was hypothesized that the gelator, even in such conditions, is unable to come into contact with the trigger dispersed in the starting powders, thus making the formation of the fibers difficult. For this reason, a further test was performed carefully mixing the trigger with the gelator and then adding the obtained hydrogel to the cement powders, in order to favour a better dispersion of  $\text{CaCl}_2$  and hence a better interaction between calcium and the gelator.

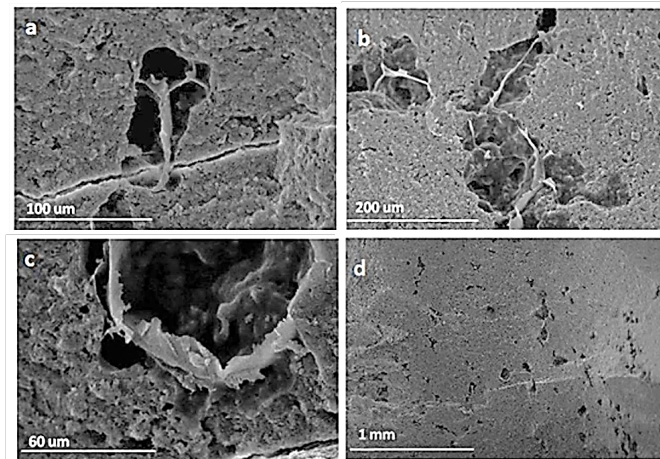


Figure 75. SEM images of the cement obtained combining the trigger, the phosphate powders and the gelator in a mortar.

From the SEM images shown in Figure 75a-d, the presence of fibres agglomerated in bundles can be clearly detected in different areas of the cement, proving that fibre formation is strongly dependent on the way the components are mixed. Based on these preliminary attempts, in the following tests the trigger will always be added to the gelator solution before mixing with powders.

### **Fibre- reinforced cements with different amount of trigger**

Mixing first the gelator solution with the trigger and then adding the cement powders, guaranteed the formation of fibres. Quantities of  $\text{CaCl}_2$  corresponding to 1, 1.3 and 1.6 gelator equivalents were used for the formation of cements. Both for cements formulation containing 1% and 2.6% w/w of fibres, the minimum trigger quantity corresponding to 1 equivalent proved to be insufficient to obtain an appropriate fibre formation. In fact, it is possible to note from Figure 76a,b that the fibres are not evenly distributed, and they are mainly located into the pores.

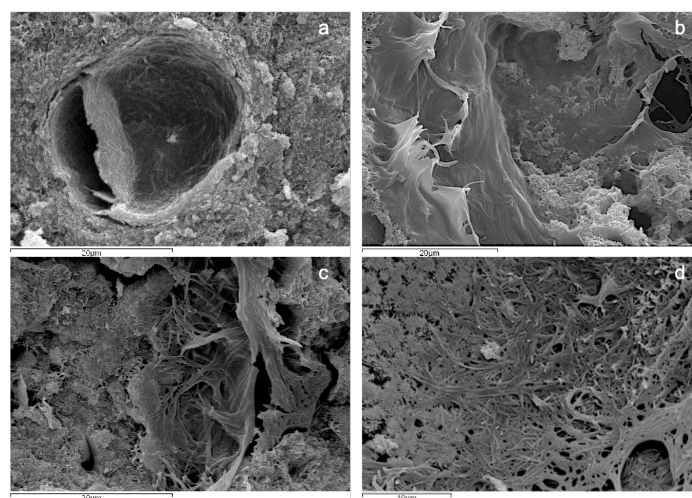


Figure 76. SEM images of samples obtained by using 1 (a,b), 1.3 (c) and 1.6 (d) equivalents of trigger.

Since significant differences were not found in the morphology and number of fibres formed by adding 1.3 or 1.6 trigger equivalents, the lowest amount was kept fixed in the subsequent preparations.

### Fibers mean diameters

The formation of fibres in aqueous solutions usually starts soon after the addition of the trigger ( $\text{CaCl}_2$ ) and up to 16 hours are required to obtain the final morphology: the obtained fibres are about 300 nm wide (Figure 77) and up to 1000 micron long and they form a well interconnected network.

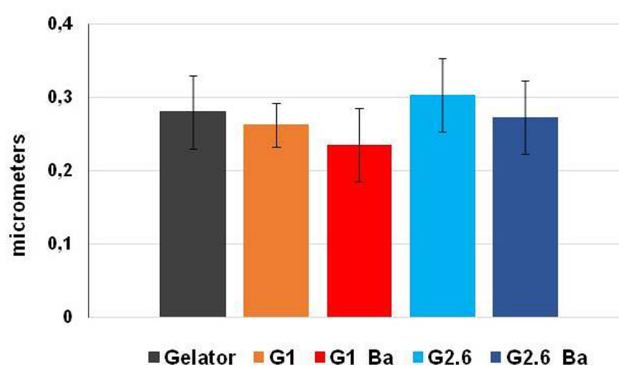


Figure 77. Mean diameters values of the fibres obtained by drying the gelator solution in air (black) and inside the different cement formulations.

No significant difference was found among the mean values of the fibre's diameters.

### Rheological tests

A time sweep analysis was carried out to evaluate the ability of the pure hydrogel to recover its shape and strength after fast spinning that transform the gel into sol.

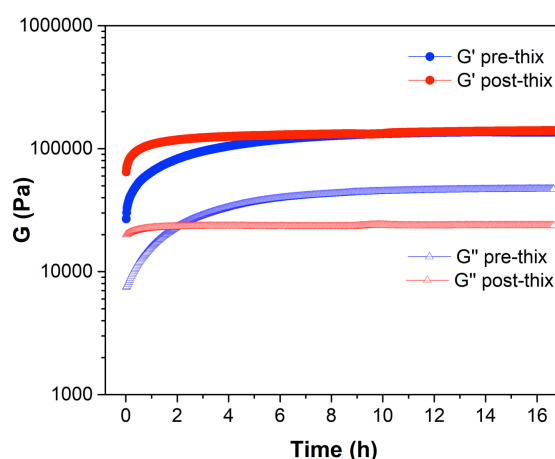


Figure 78. Time sweep analysis of the hydrogel before (blue) and after (red) shaking the vial.

In Figure 78 the blue line corresponding to  $G'$  (obtained by the hydrogel analysis before shaking) is superimposable to the red one (obtained after shaking), thus confirming the good

thixotropic properties of the hydrogel, a mandatory requirement for the fibres assembling inside the cement matrix.

The analysis was performed only on the hydrogel at 2% w/v, as this property is independent from the concentration.

### Fibre formation assessment

The LMWG used for cement's formulation can produce very long, thin and regular fibres (about 300 nm in diameter) forming a network in which they are strongly entangled (see Figure 79a), even when mixed with a huge amount of powders.

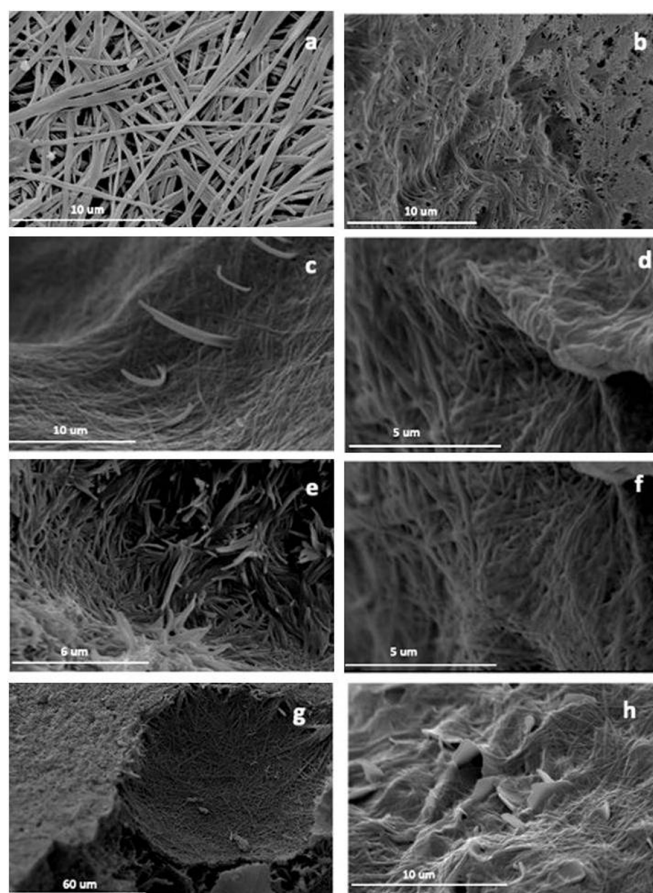


Figure 79. SEM images of the fibers obtained a) from the aqueous solution of the gelator used for the cement reinforcement at 1% w/w after air drying, and inside cement matrix of different compositions and after different hardening times: b) G1\_Ba after 20h of soaking in PB at 37°C; c,d) G1 after 7 days; e,f) G2.6 after 7 days; g,h) G1\_Ba and G2.6\_Ba, after 7 days, respectively.

Since a self-assembling of fibres in such a dense matrix had not been previously obtained, a morphological characterization was carried out to demonstrate their actual formation. The formation of fibres was monitored over time by immersing the cement sample in liquid nitrogen after set periods of soaking and collecting SEM images of the fractured surfaces. Like to what happens in water, where the formation of fibres takes about 16 hours to complete, inside the cement the hydrogel takes about the same time to acquire the final morphology. In fact,

the SEM analysis revealed that the fibres formation inside the dense matrix is quite completed after 20 hours, as shown in Figure 79b. For all the compositions enriched with the LMWG, the SEM images obtained from fractured surfaces after 7 days of soaking in PB at 37°C revealed a high number of fibres well distributed throughout the matrix, especially within the pores (Figure 79g). Moreover, fibres appear strongly entangled with each other and, most importantly, they show an excellent interaction with the apatite phase (Figure 79f,h), a crucial feature for the success of FRCPCs, as reported in literature <sup>41</sup>. However, on increasing hydrogel concentration a lower reproducibility was found: the presence of bushes of fibres, mainly located into pores, has been observed in cement G2.6 (Figure 79e) together with thin sheets of hydrogel.

### Structural Characterization

XRD patterns of the gelator and of selected cement samples after 7 days of soaking are reported in Figure 80.

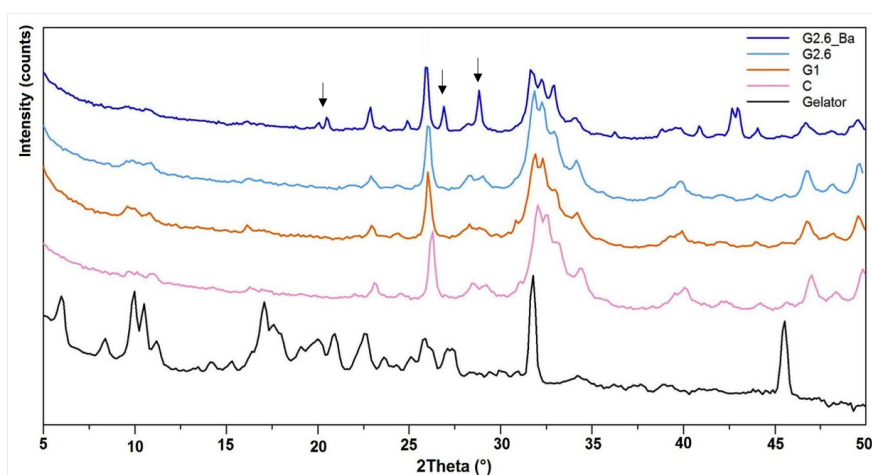


Figure 80. XRD diffraction pattern of the gelator and of some selected cements. Main  $BaSO_4$  reflections are evidenced in the pattern of G2.6\_Ba.

The presence of poorly crystalline hydroxyapatite as a result of cement's hardening is well evidenced, while the reflections belonging to  $\alpha$ -TCP and DCPD are no longer present, confirming that after 7 days the phase conversion was complete and not affected by the presence of the gelator. Due to the low concentration of the gelator compared to the cement powders (both 1% and 2.6%), its main reflections are not visible in the XRD of the composite materials. The presence of  $BaSO_4$ , added to obtain a radiopaque material <sup>42,43</sup>, did not interfere with the hardening reaction, as previously demonstrated by antibacterial CPC (Paragraph 4.3). The FT-IR spectra of the hardened pastes are reported in Figure 81: according to the X-rays patterns, infrared spectra are typical of a poorly crystalline hydroxyapatite.

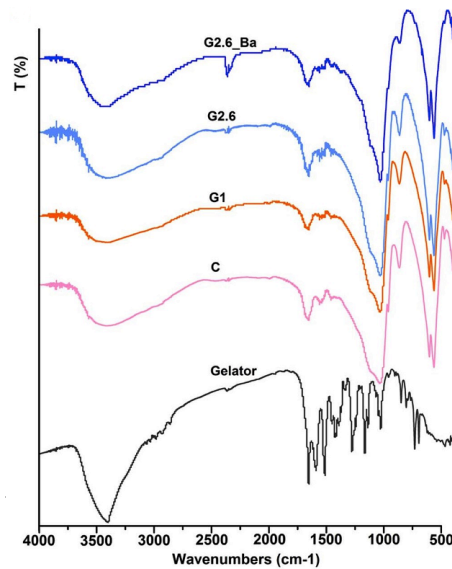


Figure 81. FT-IR spectra of the obtained samples and gelator.

In fact, the absorption band due to OH<sup>-</sup> stretching mode at 3572 cm<sup>-1</sup> is no longer appreciable. The main reflections found in the spectra are related to the phosphate's groups in the apatite matrix<sup>44</sup> with bands observed at 550, 600, and 1070 cm<sup>-1</sup>. Furthermore, the characteristic bands of carbonate ions associated with the symmetric stretching mode at 1450 cm<sup>-1</sup> and the out of plane bending mode at 870 cm<sup>-1</sup> are clearly detectable in all the formulations, thus evidencing the formation of a carbonated hydroxyapatite. Two more bands, belonging to Amide I and Amide II of gelatin are recognizable, while the presence of the hydrogel is not detectable, due to its low concentration.

### Mechanical properties

Figure 82 illustrates the effect of fibres addition on the mechanical properties of the reinforced CPCs, more pronounced when cements were tested in bending than in compression mode<sup>45</sup>.

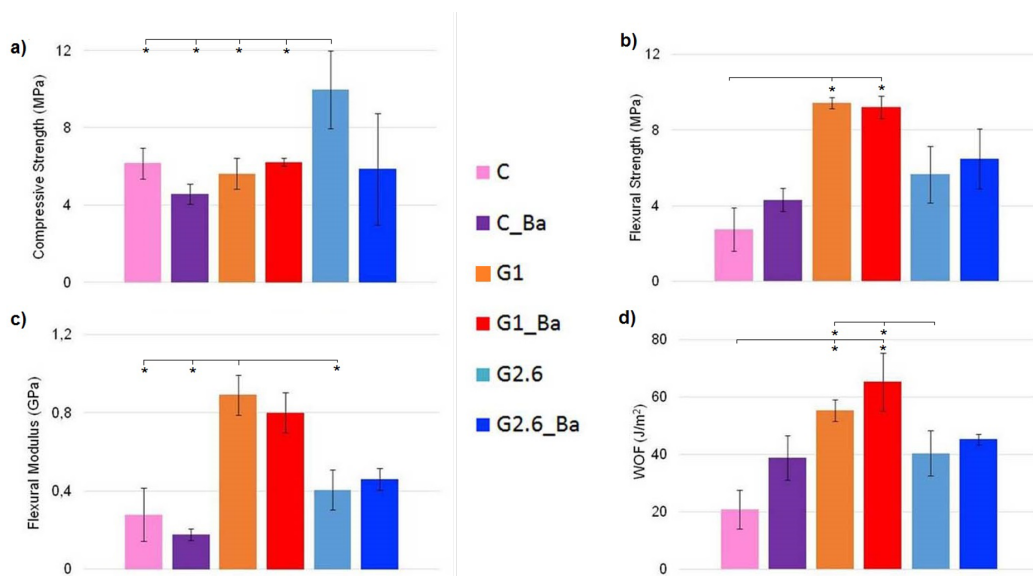


Figure 82. Mechanical properties of the obtained cements: a) Compressive Strength, b) Flexural Strength, c) Flexural Modulus and d) Work-Of-Fracture. Statistical analysis is reported in the figure (\*  $p < 0.05$ ):

- a. *Compressive strength: \*G2.6 vs C, C\_Ba, G1, G1\_Ba;*
- b. *Flexural strength: \*C vs G1, G1\_Ba;*
- c. *Flexural modulus: \*G1 vs C, C\_Ba, G2.6;*
- d. *Work Of Fracture: \*C vs G1, G1\_Ba; \*G2.6 vs G1, G1\_Ba.*

No significant difference in compressive strength between reinforced cements containing the lowest amount of gelator and their reference samples was found. In contrast, G2.6 cements showed higher stress values, significantly different when compared to all the formulations.

For the three-point bending tests the FRCPC sample bars were loaded to failure and the maximum flexural strength and modulus were calculated. The presence of fibres entangled with the inorganic phase strongly enhanced the flexural strength of G1 and G1\_Ba cements: recorded values are nearly doubled with respect to unreinforced cements C and C\_Ba. A similar trend is observed for flexural modulus, where the cements containing the lower amount of gel exhibited the greatest improvement of about three-fold compared to the corresponding fibres-free CPCs. Even if the reinforcement effect of the gelator fibres on the work-of-fracture is evident in all the formulations, a greater reinforcement was obtained from samples G1 and G1\_Ba compared to those containing 2.6% w/w of fibres. The toughness was improved of about three-fold, even if values are lower than those reported in literature, mostly due to the high L/P (liquid/powder) ratio used here to obtain an injectable cement and to the fibre's dimensions and composition. These results demonstrate the effective reinforcement of the fibres entangled within the cement matrix: in particular, it is important to emphasize that the three-fold increase of mechanical properties is obtained by a quite low amount (1% w/w) of short and thin fibres (about 1000 micron x 300 nm), with respect to the values reported in literature. For example, addition of PVA fibres of different length (ranging from 3 to 6 mm) and in different amount (2.5 and 5% w/w) to an  $\alpha$ -TCP-based cement, improved more than 2-fold the flexural strength, and highlighted the prominent effect of concentration with respect to the fibre length<sup>45</sup>. The observed reinforcement in our cements is due to the nature of self-assembled fibres, which demonstrated a high affinity for the apatite phase and a very high aspect/ratio, important features for a successful fibre-reinforcement<sup>46</sup>.

### **Injectability tests**

Injectability of CPCs is a key feature for minimally invasive surgical techniques, especially when defects have limited accessibility and when there is the need to conform to a defect area of complex shape. Since all the cements formulations showed a flowable consistency, injectability tests were carried out without any adjustment of the L/P ratio. Both Ba-containing formulations with 1% w/w and 2.6% w/w of fibres were tested and compared with their

reference cement C\_Ba. All cements presented a good injectability<sup>34</sup>, with load values required for the injection around 0,2- 0,3 kN.

Excellent cohesion has been demonstrated by all formulations: the paste extruded in PB solution immediately after the preparation remained intact after 24 h of immersion without any particle released to the surrounding medium. No evidence of phase separation, which is a major issue inhibiting successful delivery of injectable CPC, was found in the extruded samples.

### Micro-CT characterization

Generally, the presence and size of pores decrease strength and elastic modulus<sup>47-49</sup>. Micro-CT analysis showed that the presence of the fibres did not affect the overall porosity in G1 and G2.6 samples, with average values comparable to control sample (8.6% vs 8.1% porosity). The addition of barium appeared to reduce the porosity regardless of the presence of the fibres (4.3% averaging on C\_Ba, G1\_Ba and G2.6\_Ba).

Interestingly, differences between the pore's diameter distribution were found (Figure 83): in fact, while the most diffuse pore size in sample C is between 0-50  $\mu\text{m}$ , it increased up to 200  $\mu\text{m}$  in the other samples, highlighting that the presence of fibres and/or barium sulfate shifted the pore diameters towards higher values. In particular, a higher number of pores with diameters between 0-100  $\mu\text{m}$  was found in G1 sample.

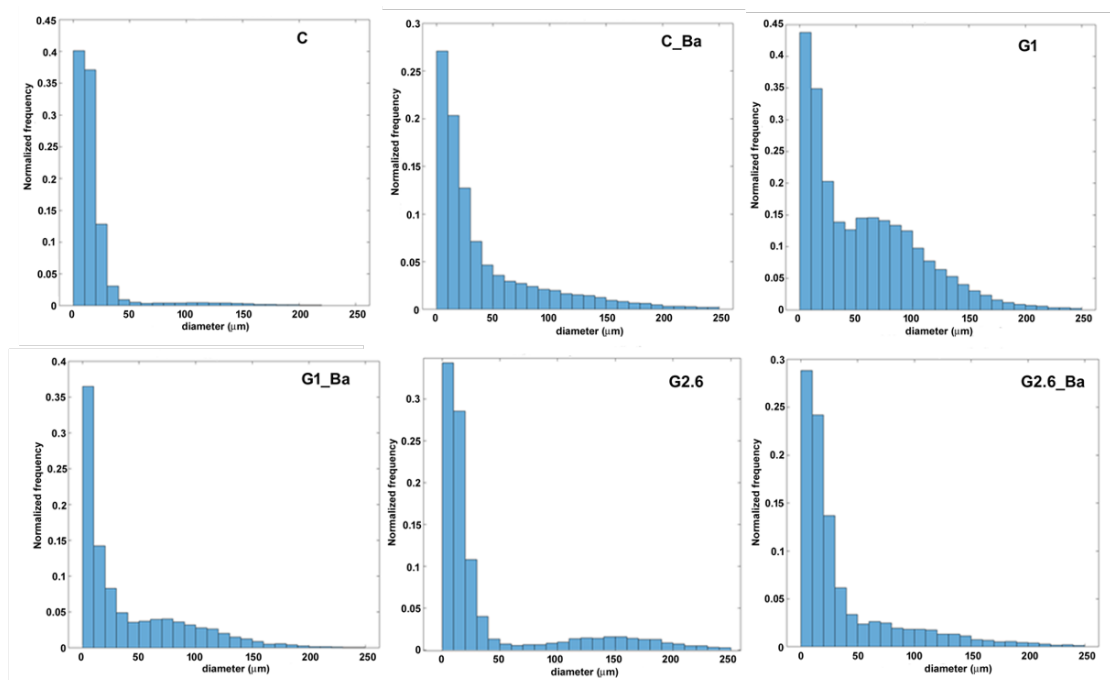


Figure 83. Distribution of average diameters in the different cement samples.

Despite the increasing of pores size around and beyond 100  $\mu\text{m}$ , fibres were able to enhance mechanical performances of composite cements. Pore size of at least 100  $\mu\text{m}$  is also beneficial for cell growth<sup>50-52</sup>.

### ***In vitro* biocompatibility**

To assess the biological safety of the materials, in accordance with their nature and duration of contact with human tissues, different biocompatibility tests must be performed (UNI EN ISO 10993-5:2009). First, the cell viability has been quantitatively assessed considering a reduction by more than 30% in comparison to CTR as a consequence of a cytotoxic effect, then the lactate dehydrogenase (LDH) in supernatant has been measured, since it is known that the release of this enzyme is a sign of cell membranes damage. The viability of MG63 was measured after 3 and 7 days of culture (Figure 84a).

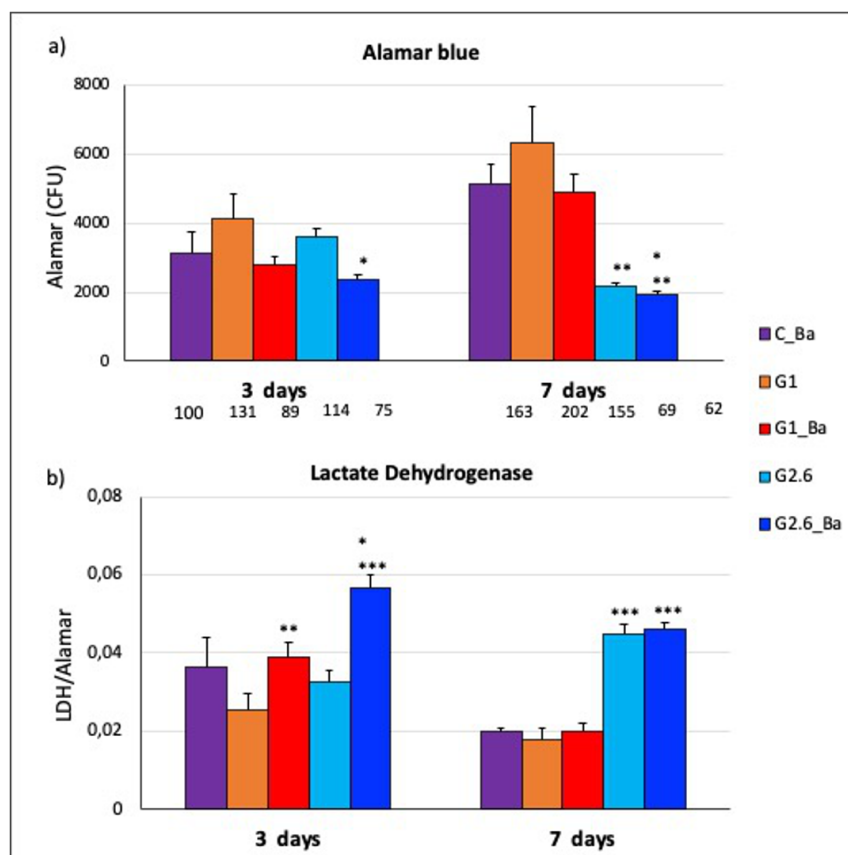


Figure 84. a) MG63 osteoblast viability (Alamar Blue test) and b) LDH release in supernatant (biochemical test) after 3 and 7 days of culture in standard conditions with experimental and reference samples. Percentages of viability are indicated under each column in graph a). Statistical analysis is reported in the figure (\* $p < 0.05$ , \*\* $p < 0.005$ , \*\*\* $p < 0.0005$ ):

a. Alamar Blue 3 days: \*G2.6\_Ba vs G1, G1\_Ba, G2.6; 7 days: \*\*G2.6, G2.6\_Ba vs C\_Ba, G1, G1\_Ba; \*G2.6\_Ba vs G2.6.

b. LDH 3 days: \*\*G1\_Ba vs G1; \*G2.6\_Ba vs C\_Ba; \*\*\*G2.6\_Ba vs G1, G1\_Ba, G2.6; 7 days: \*\*\*G2.6, G2.6\_Ba vs C\_Ba, G1, G1\_Ba.

At 3 days no differences were found among experimental samples and reference, apart from G2.6\_Ba, whose values were significantly lower than other materials. At 7 days viability

of C\_Ba, G1, and G1\_Ba was significantly improved when compared to 3 days values ( $p < 0.0005$ ,  $p < 0.005$ ,  $p < 0.0005$ , respectively). On the contrary, viability of both G2.6 and G2.6\_Ba was significantly lower when compared to C\_Ba, G1, G1\_Ba with values lower than 70% (69% and 63% for G2.6 and G2.6\_Ba, respectively), revealing cytotoxicity.

LDH results are shown in Figure 84b. The release of LDH in medium is due to damage of cell membrane and it reached significant higher values in G1\_Ba and G2.6\_Ba in comparison to other groups at 3 days. At 7 days C\_Ba, G1, and G1\_Ba values decreased; on the contrary, both G2.6 and G2.6\_Ba showed a significant higher release of LDH. The mechanical properties and pores size distribution matched very well to what observed by preliminary biological test and led to identify as most promising materials G1 and G1\_Ba. These results were strictly inversely correlated with viability data (Pearson  $-0,873$ ,  $p < 0,0005$ ).

### Gene expression

The analyses of representative markers of osteoblast activity and differentiation and of microenvironment inflammation were performed on MG63 after 7 days of culture on C\_Ba, G1, and G1\_Ba materials. G2.6 and G2.6\_Ba were excluded as the samples had previously showed typical signs of cytotoxicity. Furthermore, the poor amount of extracted RNA from G2.6 and G2.6\_Ba, not suitable to correctly carry out the subsequent analyses of gene expression, confirmed the scarcity of cells on these samples. Gene expression is reported in Figure 85a-f.

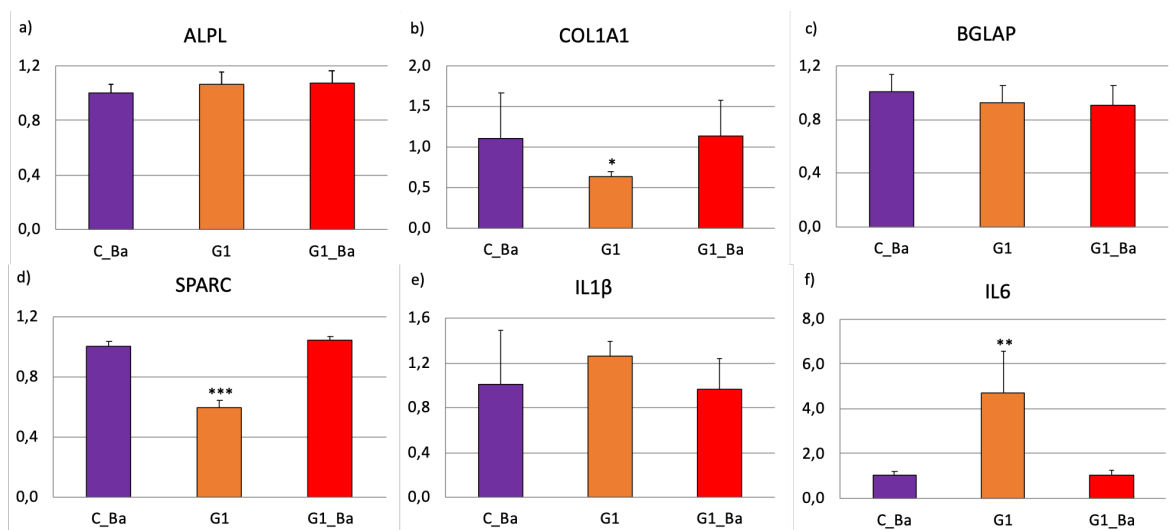


Figure 85. Gene expression of osteoblast after 7 days of culture by RT-PCR. Some representative markers of osteoblast differentiation and activity (a-d) and proinflammatory reaction (e-f) are shown. Results were normalized to GAPDH expression and data are given as fold change relative to the reference group (C\_Ba), considered as 1. Results are the main ( $\pm$  SD) of six replicates. Statistical analysis is reported in figure (\* $p < 0.05$ , \*\* $p < 0.005$ , \*\*\* $p < 0.0005$ ):

- b. COL1A1: \*G1 vs G1\_Ba;
- d. SPARC: \*\*\*G1 vs C\_Ba, G1\_Ba;
- f. IL6: \*\*G1 vs C\_Ba, G1\_Ba.

ALPL, COL1A1, SPARC and BGLAP, genes that encode for alkaline phosphatase, collagen type I, osteonectin and osteocalcin, respectively, are known to be expressed in different phases of the osteoblast's activity. No differences among groups were found for ALPL and BGALP (Figure 85a,c). Referring to these genes, G1\_Ba was similar to G1 and C\_Ba, demonstrating that these materials did not affect osteoblast differentiation and mineralization. COL1A1 and SPARC expression (Figure 85b,d) was significantly upregulated in G1\_Ba when compared to G1 sample gene expression and reached level similar to C\_Ba. By a further analysis (not shown) emerged a more abundant expression of SPARC and COL1A1 at this culture endpoint, thus revealing an intermediate stage of osteogenesis, already involving the mineralization phase. In fact, type I collagen represents the major component of the bone extracellular matrix, whose deposition is regulated also by osteonectin, which has high calcium affinity and contribute with collagen to form the matrix and to mineralize it<sup>53</sup>. IL1 $\beta$  and IL6 are pro-inflammatory cytokines involved in the process of bone formation, and they have a relevant role in osteoblast and osteoclast differentiation. Regarding IL1 $\beta$  expression, no differences were found among groups. IL6 was significantly over-expressed in G1, when compared to both C\_Ba and G1\_Ba. G1\_Ba was not different from C\_Ba (Figure 85e,f).

### Immunoenzymatic analysis

The protein quantification confirmed what observed by molecular biology: at 7 days of culture, similar amount of ALP, type I COLL and OSTC were detected in supernatants of all materials (Figure 86a-c).

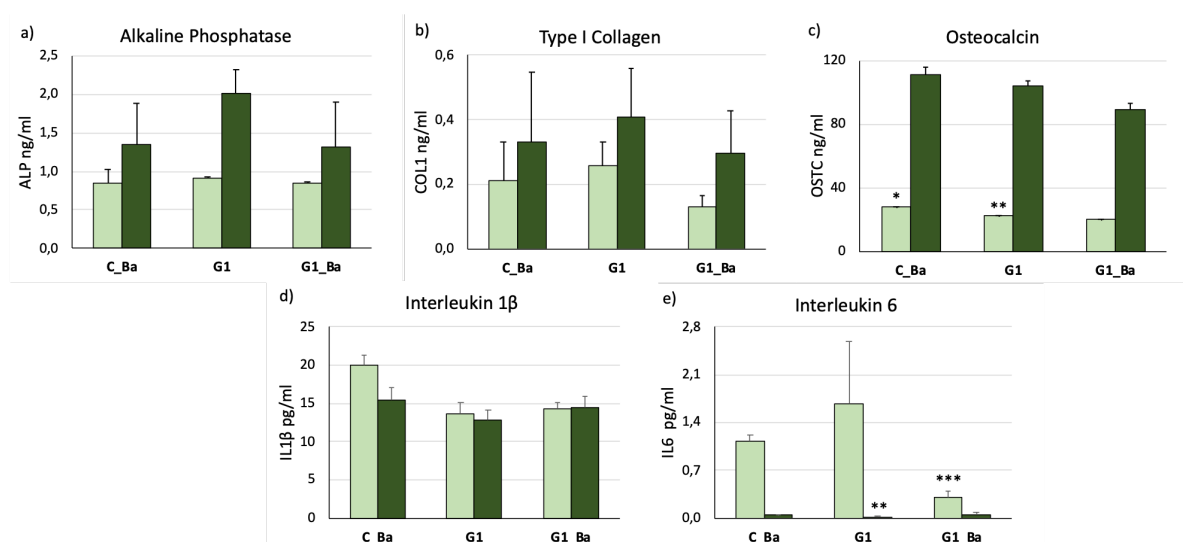


Figure 86. Protein release detected by ELISA assay after 3 (light green) and 7 (green) days of culture. Some representative markers of osteoblast differentiation and activity and proinflammatory reaction are shown. Results are the mean ( $\pm$  SD) of six replicates. Statistical analysis is reported in figure (\* $p < 0.05$ , \*\* $p < 0.005$ , \*\*\* $p < 0.0005$ ):

c. Osteocalcin 3 days: \*C\_Ba vs G1, G1\_Ba; \*\*G1 vs G1\_Ba;

e. IL6 3 days: \*\*\*G1\_Ba vs C\_Ba; 7 days: \*\*G1 vs C\_Ba.

Osteocalcin (OSTC) values were significantly higher in C\_Ba in comparison with G1 and G1\_Ba ( $p < 0.05$ ) and G1 was higher than G1\_Ba ( $p < 0.005$ ) at 3 days of culture, but at 7 days the differences were no longer significant. All markers showed much higher values at 7 days than at 3 days in all groups, demonstrating the growing activity of osteoblasts during the culture time and the maintenance of cell differentiation. Finally, IL1 $\beta$  and IL6 were quantified to exclude possible inflammatory effects elicited by the materials<sup>54</sup>. The measure of inflammatory cytokine IL1 $\beta$  revealed no differences of production among groups at both experimental times (Figure 86d). Conversely, the measurement of IL6 (Figure 86e) demonstrated a significant difference between G1\_Ba and C\_Ba at 3 days ( $p < 0.0005$ ) and between G1 and C\_Ba at 7 days ( $p < 0.005$ ), although the dosage of this interleukin in all groups was low at 3 days (below 3 pg/mL) and the values decreased again, being barely detected at 7 days (below 0.1 pg/mL).

## Conclusions

After several attempts, an efficient method for the preparation of an injectable FRCPC for bone regeneration was developed. Supramolecular fibres formed by LMWG self-assembling were grown for the first time inside a calcium phosphate bone cement using calcium ions as trigger and provided structural and mechanical support to the material. A 1% w/w ratio between the gelator and the cement powders and a L/P ratio of 0.52 mL/g ensured the formation of a great number of fibres, which were clearly visible from SEM images. The fibres were homogeneously dispersed all over the matrix, guaranteeing a reinforcement effect even if they promoted the formation of a higher number of pores larger than 100  $\mu\text{m}$  when compared with the reference cements.

The formulations containing 1% w/w of fibres were biocompatible and able to support a correct osteoblast activity in terms of main bone markers, without inducing inflammation. The increase of the anabolic markers and the decrease of ILs over time suggest osteoblasts growth in presence of bioactive molecules and drugs.

## 4.5 BIBLIOGRAPHY

- (1) Boyle, W. J.; Simonet, W. S.; Lacey, D. L. Osteoclast Differentiation and Activation. *Nature* **2003**, *423*, 337–342, DOI:10.1038/nature01658.
- (2) Smrke, D.; Roman, P.; Veselko, M.; Gubi, B. Treatment of Bone Defects — Allogenic Platelet Gel and Autologous Bone Technique. In *Regenerative Medicine and Tissue Engineering*; InTech, 2013; p 340, DOI:10.5772/55987.
- (3) Jiang, H.; Zuo, Y.; Zou, Q.; Wang, H.; Du, J.; Li, Y.; Yang, X. Biomimetic Spiral-Cylindrical Scaffold Based on Hybrid Chitosan/Cellulose/ Nano-Hydroxyapatite Membrane for Bone Regeneration. *ACS Appl. Mater. Interfaces* **2013**, *5* (22), 12036–12044, DOI:10.1021/am4038432.
- (4) Brown, W.E. and Chow, L. C. A New Calcium Phosphate Water-Setting Cement. In *Cements Research Progress*; Brown, W. E., Ed.; Westerville, 1986; pp 352–379.
- (5) O'Neill, R.; McCarthy, H. O.; Montufar, E. B.; Ginebra, M. P.; Wilson, D. I.; Lennon, A.; Dunne, N. Critical Review: Injectability of Calcium Phosphate Pastes and Cements. *Acta Biomater.* **2017**, *50*, 1–19, DOI:10.1016/j.actbio.2016.11.019.
- (6) Cabrejos-Azama, J.; Alkhraisat, M. H.; Rueda, C.; Torres, J.; Pintado, C.; Blanco, L.; López-Cabarcos, E. Magnesium Substitution in Brushite Cements: Efficacy of a New Biomaterial Loaded with Vancomycin for the Treatment of Staphylococcus Aureus Infections. *Mater. Sci. Eng. C* **2016**, *61*, 72–78, DOI:10.1016/j.msec.2015.10.092.
- (7) Ooms, E.; Wolke, J.; van der Waerden, J.; Jansen, J. Trabecular Bone Response to Injectable Calcium Phosphate (Ca-P) Cement. *J. Biomed. Mater. Res.* **2002**, *61* (1), 9–18, DOI:10.1002/JBM.10029.
- (8) Félix Lanao, R. P.; Leeuwenburgh, S. C. G.; Wolke, J. G. C.; Jansen, J. A. Bone Response to Fast-Degrading, Injectable Calcium Phosphate Cements Containing PLGA Microparticles. *Biomaterials* **2011**, *32* (34), 8839–8847, DOI:10.1016/j.biomaterials.2011.08.005.
- (9) Zhang, J.; Liu, W.; Schnitzler, V.; Tancret, F.; Bouler, J. M. Calcium Phosphate Cements for Bone Substitution: Chemistry, Handling and Mechanical Properties. *Acta Biomater.* **2014**, *10* (3), 1035–1049, DOI:10.1016/j.actbio.2013.11.001.
- (10) Torres, P. M. C.; Gouveia, S.; Olhero, S.; Kaushal, A.; Ferreira, J. M. F. Injectability of Calcium Phosphate Pastes: Effects of Particle Size and State of Aggregation of  $\beta$ -Tricalcium Phosphate Powders. *Acta Biomater.* **2015**, *21*, 204–216, DOI:10.1016/j.actbio.2015.04.006.
- (11) Ghosh, S.; Wu, V.; Pernal, S.; Uskoković, V. Self-Setting Calcium Phosphate Cements with Tunable Antibiotic Release Rates for Advanced Antimicrobial Applications. *ACS Appl. Mater. Interfaces* **2016**, *8* (12), 7691–7708, DOI:10.1021/acsami.6b01160.
- (12) Liu, X.; Wei, D.; Zhong, J.; Ma, M.; Zhou, J.; Peng, X.; Ye, Y.; Sun, G.; He, D. Electrospun Nanofibrous P(DLLA-CL) Balloons as Calcium Phosphate Cement Filled Containers for Bone Repair: In Vitro and in Vivo Studies. *ACS Appl. Mater. Interfaces* **2015**, *7* (33), 18540–18552, DOI:10.1021/acsami.5b04868.
- (13) Smith, B. T.; Santoro, M.; Grosfeld, E. C.; Shah, S. R.; van den Beucken, J. J. J. P.; Jansen, J. A.; Mikos, A. G. Incorporation of Fast Dissolving Glucose Porogens into an Injectable Calcium Phosphate Cement for Bone Tissue Engineering. *Acta Biomater.* **2017**, *50*, 68–77, DOI:10.1016/j.actbio.2016.12.024.
- (14) Habraken, W. J. E. M.; De Jonge, L. T.; Wolke, J. G. C.; Yubao, L.; Mikos, A. G.; Jansen, J. A. Introduction of Gelatin Microspheres into an Injectable Calcium Phosphate Cement. *J. Biomed. Mater. Res. - Part A* **2008**, *87* (3), 643–655, DOI:10.1002/jbm.a.31703.
- (15) Phillips, J.; Crane, T.; Noy, M.; Elliott, T.; Grimer, R. The Incidence of Deep Prosthetic Infections in a Specialist Orthopaedic Hospital: A 15-Year Prospective Survey. *J. Bone Joint Surg. Br.* **2006**, *88* (7), 943–948, DOI:10.1302/0301-620X.88B7.17150.

- (16) Di Filippo, M. F.; Dolci, L. S.; Albertini, B.; Passerini, N.; Torricelli, P.; Parrilli, A.; Fini, M.; Bonvicini, F.; Gentilomi, G. A.; Panzavolta, S.; Bigi, A. A Radiopaque Calcium Phosphate Bone Cement with Long-Lasting Antibacterial Effect: From Paste to Injectable Formulation. *Ceram. Int.* **2020**, DOI:10.1016/j.ceramint.2019.12.272.
- (17) Zanna, N.; Iaculli, D.; Tomasini, C. Organic & Biomolecular Chemistry The Effect of L-DOPA Hydroxyl Groups on the Formation of Supramolecular Hydrogels †. *Org. Biomol. Chem.* **2017**, *15*, 5797, DOI:10.1039/c7ob01026e.
- (18) Gaucher, A.; Dutot, L.; Barbeau, O.; Hamchaoui, W.; Wakselman, M.; Mazaleyrat, J. P. Synthesis of Terminally Protected (S)-B3-H-DOPA by Arndt-Eistert Homologation: An Approach to Crowned  $\beta$ -Peptides. *Tetrahedron Asymmetry* **2005**, *16* (4), 857–864, DOI:10.1016/j.tetasy.2004.11.089.
- (19) Giuri, D.; Jurković, L.; Fermani, S.; Kralj, D.; Falini, G.; Tomasini, C. Supramolecular Hydrogels with Properties Tunable by Calcium Ions: A Bio-Inspired Chemical System. *ACS Appl. Bio Mater.* **2019**, *2* (12), 5819–5828, DOI:10.1021/acsabm.9b00828.
- (20) Vallo, C. I. Influence of Load Type on Flexural Strength of a Bone Cement Based on PMMA. *Polym. Test.* **2002**, *21* (7), 793–800, DOI:10.1016/S0142-9418(02)00013-2.
- (21) Dunne, N. J.; Orr, J. F. Influence of Mixing Techniques on the Physical Properties of Acrylic Bone Cement. *Biomaterials* **2001**, *22* (13), 1819–1826, DOI:10.1016/S0142-9612(00)00363-X.
- (22) Kaufman, M. G.; Meaie, J. D.; Izaddoost, S. A. Orthopedic Prosthetic Infections: Diagnosis and Orthopedic Salvage. *Plast Surg* **2016**, *30*, 66–72, DOI:10.1055/s-0036-1580730.
- (23) Ginebra, M. P.; Espanol, M.; Montufar, E. B.; Perez, R. A.; Mestres, G. New Processing Approaches in Calcium Phosphate Cements and Their Applications in Regenerative Medicine. *Acta Biomater.* **2010**, *6*, 2863–2873, DOI:10.1016/j.actbio.2010.01.036.
- (24) Pastorino, D.; Canal, C.; Ginebra, M. P. Drug Delivery from Injectable Calcium Phosphate Foams by Tailoring the Macroporosity-Drug Interaction. *Acta Biomater.* **2014**, *12* (1), 250–259, DOI:10.1016/j.actbio.2014.10.031.
- (25) Ginebra, M. P.; Canal, C.; Espanol, M.; Pastorino, D.; Montufar, E. B. Calcium Phosphate Cements as Drug Delivery Materials. *Adv. Drug Deliv. Rev.* **2012**, *64* (12), 1090–1110, DOI:10.1016/j.addr.2012.01.008.
- (26) Schnieders, J.; Gbureck, U.; Thull, R.; Kissel, T. Controlled Release of Gentamicin from Calcium Phosphate—Poly(Lactic Acid-Co-Glycolic Acid) Composite Bone Cement. *Biomaterials* **2006**, *27* (23), 4239–4249, DOI:10.1016/J.BIOMATERIALS.2006.03.032.
- (27) Loca, D.; Sokolova, M.; Locs, J.; Smirnova, A.; Irbe, Z. Calcium Phosphate Bone Cements for Local Vancomycin Delivery. *Mater. Sci. Eng. C* **2015**, *49* (1), 106–113, DOI:10.1016/J.MSEC.2014.12.075.
- (28) Dolci, L. S.; Panzavolta, S.; Torricelli, P.; Albertini, B.; Sicuro, L.; Fini, M.; Bigi, A.; Passerini, N. Modulation of Alendronate Release from a Calcium Phosphate Bone Cement: An in Vitro Osteoblast-Osteoclast Co-Culture Study. *Int. J. Pharm.* **2019**, *554* (November 2018), 245–255, DOI:10.1016/j.ijpharm.2018.11.023.
- (29) Panzavolta, S.; Torricelli, P.; Bracci, B.; Fini, M.; Bigi, A. Alendronate and Pamidronate Calcium Phosphate Bone Cements: Setting Properties and in Vitro Response of Osteoblast and Osteoclast Cells. *J. Inorg. Biochem.* **2009**, *103* (1), 101–106, DOI:10.1016/j.jinorgbio.2008.09.012.
- (30) Panzavolta, S.; Torricelli, P.; Bracci, B.; Fini, M.; Bigi, A. Functionalization of Biomimetic Calcium Phosphate Bone Cements with Alendronate. *J. Inorg. Biochem.* **2010**, *104* (10), 1099–1106, DOI:10.1016/j.jinorgbio.2010.06.008.
- (31) Ginebra, M. P.; Albuixech, L.; Fernández-Barragán, E.; Aparicio, C.; Gil, F. J.; San Román, J.; Vázquez, B.; Planell, J. A. Mechanical Performance of Acrylic Bone Cements Containing Different Radiopacifying Agents. *Biomaterials* **2002**, *23* (8), 1873–1882, DOI:10.1016/S0142-9612(01)00314-3.

- (32) Fang, C.; Hou, R.; Zhou, K.; Hua, F.; Cong, Y.; Zhang, J.; Fu, J.; Cheng, Y. J. Surface Functionalized Barium Sulfate Nanoparticles: Controlled in Situ Synthesis and Application in Bone Cement. *J. Mater. Chem. B* **2014**, *2* (9), 1264–1274, DOI:10.1039/c3tb21544j.
- (33) Jansen, J.; Ooms, E.; Verdonschot, N.; Wolke, J. Injectable Calcium Phosphate Cement for Bone Repair and Implant Fixation. *Orthop. Clin. North Am.* **2005**, *36* (1), 89–95, DOI:10.1016/j.ocl.2004.06.014.
- (34) E.F. Burguera, H.K. Hockin, L. S. Injectable Calcium Phosphate Cement: Effects of Powder-to-Liquid Ratio and Needle Size. *J. Biomed. Mater. Res. Part B Appl. Biomater.* **2009**, *84* (2), 493–502, DOI:10.1002/jbm.b.30896.Injectable.
- (35) Liu, W.; Zhang, J.; Rethore, G.; Khairoun, K.; Pilet, P.; Tancret, F.; Bouler, J. M.; Weiss, P. A Novel Injectable, Cohesive and Toughened Si-HPMC (Silanized-Hydroxypropyl Methylcellulose) Composite Calcium Phosphate Cement for Bone Substitution. *Acta Biomater.* **2014**, *10* (7), 3335–3345, DOI:10.1016/j.actbio.2014.03.009.
- (36) Beaudoin, J. J. *Handbook of Fiber-Reinforced Concrete: Principles, Properties, Developments and Applications*; Noyes Publications: Park Ridge, N.J., 1990.
- (37) Nabi Saheb, D.; Jog, J. P. Natural Fiber Polymer Composites: A Review. *Adv. Polym. Technol.* **1999**, *18* (4), 351–363, DOI:10.1002/(SICI)1098-2329(199924)18:4<351::AID-ADV6>3.0.CO;2-X.
- (38) Canal, C.; Ginebra, M. P. Fibre-Reinforced Calcium Phosphate Cements: A Review. *J. Mech. Behav. Biomed. Mater.* **2011**, *4* (8), 1658–1671, DOI:10.1016/j.jmbbm.2011.06.023.
- (39) Krüger, R.; Groll, J. Fiber Reinforced Calcium Phosphate Cements - On the Way to Degradable Load Bearing Bone Substitutes? *Biomaterials* **2012**, *33* (25), 5887–5900, DOI:10.1016/j.biomaterials.2012.04.053.
- (40) Draper, E. R.; Adams, D. J. Low-Molecular-Weight Gels: The State of the Art. *Chem* **2017**, *3* (3), 390–410, DOI:10.1016/j.chempr.2017.07.012.
- (41) Gallinetti, S.; Mestres, G.; Canal, C.; Persson, C.; Ginebra, M. P. A Novel Strategy to Enhance Interfacial Adhesion in Fiber-Reinforced Calcium Phosphate Cement. *J. Mech. Behav. Biomed. Mater.* **2017**, *75* (August), 495–503, DOI:10.1016/j.jmbbm.2017.08.017.
- (42) Ginebra, M. P.; Albuixech, L.; Fernández-Barragán, E.; Aparicio, C.; Gil, F. J.; San Román, J.; Vázquez, B.; Planell, J. A. Mechanical Performance of Acrylic Bone Cements Containing Different Radiopacifying Agents. *Biomaterials* **2002**, *23* (8), 1873–1882, DOI:10.1016/S0142-9612(01)00314-3.
- (43) Fang, C.; Hou, R.; Zhou, K.; Hua, F.; Cong, Y.; Zhang, J.; Fu, J.; Cheng, Y.-J. Surface Functionalized Barium Sulfate Nanoparticles: Controlled in Situ Synthesis and Application in Bone Cement †. **2014** DOI:10.1039/c3tb21544j.
- (44) Hesarakı, S.; Alizadeh, M.; Borhan, S.; Pourbaghi-Masouleh, M. Polymerizable Nanoparticulate Silica-Reinforced Calcium Phosphate Bone Cement. *J. Biomed. Mater. Res. - Part B Appl. Biomater.* **2012**, *100 B* (6), 1627–1635, DOI:10.1002/jbm.b.32731.
- (45) Kucko, N. W.; De Lacerda Schickert, S.; Sobral Marques, T.; Herber, R. P.; Van Den Beuken, J. J. J. P.; Zuo, Y.; Leeuwenburgh, S. C. G. Tough and Osteocompatible Calcium Phosphate Cements Reinforced with Poly(Vinyl Alcohol) Fibers. *ACS Biomater. Sci. Eng.* **2019**, *5* (5), 2491–2505, DOI:10.1021/acsbomaterials.9b00226.
- (46) Castro, A. G. B.; Polini, A.; Azami, Z.; Leeuwenburgh, S. C. G.; Jansen, J. A.; Yang, F.; van den Beuken, J. J. J. P. Incorporation of PLLA Micro-Fillers for Mechanical Reinforcement of Calcium-Phosphate Cement. *J. Mech. Behav. Biomed. Mater.* **2017**, *71* (March), 286–294, DOI:10.1016/j.jmbbm.2017.03.027.
- (47) Marchiori, G.; Berni, M.; Boi, M.; Petretta, M.; Grigolo, B.; Bellucci, D.; Cannillo, V.; Garavelli, C.; Bianchi, M. Design of a Novel Procedure for the Optimization of the Mechanical Performances of 3D Printed Scaffolds for Bone Tissue Engineering Combining CAD, Taguchi Method and FEA. *Med. Eng. Phys.* **2019**, *69*, 92–99, DOI:10.1016/j.medengphy.2019.04.009.

- (48) Liu, D. M. Influence of Porosity and Pore Size on the Compressive Strength of Porous Hydroxyapatite Ceramic. *Ceram. Int.* **1997**, *23* (2), 135–139, DOI:10.1016/S0272-8842(96)00009-0.
- (49) Liu, D.; Šavija, B.; Smith, G. E.; J Flewitt, P. E.; Lowe, T.; Schlangen, E.; Liu, D.; Smith, G. E.; J Flewitt, P. E.; Šavija, B.; Schlangen Microlab, E.; Lowe, T. Towards Understanding the Influence of Porosity on Mechanical and Fracture Behaviour of Quasi-Brittle Materials: Experiments and Modelling. **2017**, *205*, 57–72, DOI:10.1007/s10704-017-0181-7.
- (50) Mandal, B. B.; Kundu, S. C. Cell Proliferation and Migration in Silk Fibroin 3D Scaffolds. *Biomaterials* **2009**, *30* (15), 2956–2965, DOI:10.1016/j.biomaterials.2009.02.006.
- (51) Lee, H.; Hwang, H.; Kim, Y. S.; Jeon, H.; Kim, G. H. Physical and Bioactive Properties of Multi-Layered PCL/Silica Composite Scaffolds for Bone Tissue Regeneration. *Chem. Eng. J.* **2014**, *250*, 399–408, DOI:10.1016/j.cej.2014.04.009.
- (52) Bružauskait, I.; Bironait, D.; Bagdonas Eiva Bernotien, E. Scaffolds and Cells for Tissue Regeneration: Different Scaffold Pore Sizes-Different Cell Effects. DOI:10.1007/s10616-015-9895-4.
- (53) Busch, E.; Hohenester, E.; Timpl, R.; Paulsson, M.; Maurer, P. Calcium Affinity, Cooperativity, and Domain Interactions of Extracellular EF-Hands Present in BM-40. *J. Biol. Chem.* **2000**, *275* (33), 25508–25515, DOI:10.1074/jbc.M001770200.
- (54) Varoni, E.; Canciani, E.; Palazzo, B.; Varasano, V.; Chevallier, P.; Petrizzi, L.; Dellavia, C.; Mantovani, D.; Rimondini, L. Effect of Poly-l-Lysine Coating on Titanium Osseointegration: From Characterization to in Vivo Studies. *J. Oral Implantol.* **2015**, *41* (6), 626–631, DOI:10.1563/AAID-JOI-D-13-00036.

## Chapter 5. CONCLUSIONS

I carried out my PhD with the research group of Prof. Panzavolta at the laboratory of Materials Chemistry and Biomimetics of the 'G. Ciamician' Chemistry Department of the University of Bologna.

For years, the team has focused on the study of biomaterials, materials able to safely interface with biological systems for a medical purpose. Biomaterials intended for tissue regeneration are able to support and/or replace the damaged functions, allowing the growth of new tissue. Biopolymers, known for many decades but ignored mainly because of the low cost of synthetic polymers, have the potential to replace them in many applications, thus reducing the problems of traditional plastics disposability and the dependence on petroleum. Natural biopolymers are in fact characterized by a high biocompatibility and biodegradability and have already prompted research in the field of regenerative medicine, which to date is one of the most popular scientific fields and represents the future of life sciences, where today's new technologies and public health challenges converge.

During these three years of my PhD, the purpose of my research was to use sustainable and largely available biopolymers or biodegradable polymers to produce biomaterials of different types. From a circular economy point of view, I have employed several sustainable materials, giving priority to those deriving from waste sources: I selected chitosan, cellulose derivatives, sodium hyaluronate, keratin and gelatin (both of mammal and fish). With these raw materials I have developed different biomaterials, in the form of films, scaffolds or bone cements, aimed at the regeneration of hard and soft tissues, such as bone, cartilage and skin.

In the previous Chapters, a separate treatment for each type of biomaterials has been reported. In particular, Chapter 2 deals with the production of flexible and versatile films: the materials I obtained have a wide range of applications, from cosmetics and food packaging to the biomedical field, where can be proposed as drug delivery platforms or for the treatment of wounds or burns. The peculiarity of these materials, inherently biodegradable and biocompatible, relies in the content of snail slime from *Helix Aspersa* snails in their formulation, which modulated their final properties. Varying the amount of slime contained in the film has indeed proven to be an effective method of modulating specific properties, according to the need.

Snail slime obtained from different suppliers and extracted by different methods have been introduced into the formulations of these materials, highlighting a certain variability of its properties, mainly due to the feeding and breeding of snails, as well as the extraction methods.

Therefore, in future it would be very important to perform a complete characterization of the composition of different snail slimes: a better understanding of the slime composition could be useful to obtain information on the interactions that occur between the components of the mixture. In addition, correlating the properties of the material to the presence of certain substances in specific concentrations, could significantly broaden the understanding of the composition of this natural extract and therefore its use.

As reported in Chapter 3, snail slime has also been used in the formulation of scaffolds based on chitosan and gelatin for the regeneration of cartilage, but its role in the scaffold's composition and its contribution to the scaffolds' properties must be studied deeper.

In the context of biomimetics, the science of imitating nature, in Chapter 3 I also report the development of a cylindrical scaffold obtained by rolling on itself one or more gelatin foamed strips to simulate the arrangement of the osteons in bone. Thanks to this method, the obtained scaffolds showed anisotropic properties, proving to be good candidates for bone tissue engineering. Moreover, by overlapping layers with different crosslinking degree, I was able to tune the stability of the biomaterial in physiological conditions.

Finally, I dedicated Chapter 4 to the development of bone cements based on calcium phosphates, biocompatible ceramic scaffolds that have the potential to mimic the mineral phase of bone.

My commitment has focused primarily on the possibility of obtaining drug delivery systems that can locally release an antibacterial drug, avoiding the risk of bacterial contamination after surgery. To do so, I encapsulated a broad-spectrum antibiotic inside degradable microparticles, which dissolve over time releasing the drug and promoting the formation of pores. The composition of the cement was further improved to obtain a radiopaque and injectable material. The last project concerned a feasibility study: in order to reinforce the CPC, a peptidic gelator capable of forming supramolecular networks was inserted into the liquid phase of the cement's composition. The effective and surprising ability of gelator molecules to self-assemble even in the presence of a large amount of powders, has allowed to obtain a huge amount of fibers, located mainly inside cement's pores, and a consequent effective mechanical reinforcement.

In all projects, I have dealt with both the synthesis of biomaterials and their characterization, as well as the interpretation of data and the drafting of scientific journal articles. I carried on my work using the equipment of the University and by employing procedures found through a careful bibliographical research, along with those developed by the research group over the years.

Biological tests with bacteria, fungi and cells, as well as porosity tests with the micro-CT technique were carried out thanks to external collaborations with other Departments and Structures, such as the group of Prof. Passerini and Albertini of the Department of Pharmacy and Biotechnology, Unibo, the group of Prof. Gentilomi at Microbiology Unit of S. Orsola-Malpighi University Hospital of Bologna, the IRCCS Rizzoli Orthopedic Institute of Bologna and the group of Dott. Aluigi at Isof-CNR of Bologna.

Overall, I am satisfied with the work I have done, full of collaborations with other research groups and distinguished by the multidisciplinary nature of this sector.

## APPENDIX I

*Table AI. Characterization of snail mucus obtained from Helix Aspersa Muller by means of MullerOne technology. Analyses were obtained by the supplier. The chemical and microbiological parameters evaluated are among those suggested for snail mucus characterization, as reported in <http://www.mullerone.com/it/en/our-slime-helix>.*

Specification	Values	Measure Units	Method
Aspect	Clear		
smell	Odorless		
Color	Pale yellow		
pH	2.9		
Density	1.0-1.04	g/ml	
Dry residual	5 %	M/V	M.I.M 180305/L Rev. 0:2005
Minerals (K, Ca, Na)	538	mg/L	M.I.M 110315/C Rev. 0:2005
Heavy metals	absent		
Proteins	80 - 120	mg/L	Bradford proteins assay method
Glycolic acid	60-80	mg/L	J. Chrom. A. 1322, pp 49-53, 2013
Allantoin	100-130	mg/L	J. Chrom. A. 1322, pp 49-53, 2013
Iron	3	mg/L	M.I.M 111010/C Rev. 0:2010
Citric acid	<0.1	mg/L	M.I.M 150212/A Rev. 0:2012
Ascorbic acid	<0.1	mg/L	M.I.M 150212/A Rev. 0:2012
Antiprotease	1.3	mg/L	M.I.M 0112016/A Rev. 0:2016
D-lactic Acid	<10	mg/L	M.I.M 0112016/A Rev. 0
L-lactic Acid	<10	mg/L	M.I.M 0112016/A Rev. 0
Sodium benzoate	<0.002%	m/m	M.I.M 150212/A Rev 0:2012
Collagen	2-60	mg/L	M.I.M 0112016/H Rev. 0:2016
Gram +	<10	UFC/g	UNI-EN ISO6888-1:2004
Gram -	<10	UFC/g	ISO 16649-2:2001
Fungi	<10	UFC/g	NFV08-059:2002

## APPENDIX II

*Table AII. Antibiotic resistance profile of the 20 clinical isolates assayed with C\_Ba\_GS 2, C\_Ba\_MPsGS and C\_Ba\_GS 2\_MPsGS*

<b><i>S. aureus</i></b>	<b>Antibiotic-resistance profile</b>
<i>MSSA 1</i>	CM <sup>S</sup> , E <sup>S</sup> , GMN <sup>S</sup> , LVX <sup>S</sup> , OX <sup>S</sup> , P <sup>R</sup> , TE <sup>S</sup> , SXT <sup>S</sup>
<i>MSSA 2</i>	<b>CM<sup>R</sup>, E<sup>R</sup></b> , GMN <sup>S</sup> , LVX <sup>S</sup> , OX <sup>S</sup> , P <sup>S</sup> , TE <sup>S</sup> , SXT <sup>S</sup>
<i>MSSA 3</i>	CM <sup>S</sup> , E <sup>S</sup> , GMN <sup>S</sup> , LVX <sup>S</sup> , OX <sup>S</sup> , P <sup>R</sup> , TE <sup>S</sup> , SXT <sup>S</sup>
<i>MSSA 4</i>	<b>CM<sup>R</sup>, E<sup>R</sup></b> , GMN <sup>S</sup> , LVX <sup>S</sup> , OX <sup>S</sup> , P <sup>S</sup> , TE <sup>S</sup> , SXT <sup>S</sup>
<i>MSSA 5</i>	CM <sup>S</sup> , E <sup>S</sup> , GMN <sup>S</sup> , LVX <sup>S</sup> , OX <sup>S</sup> , P <sup>R</sup> , TE <sup>S</sup> , SXT <sup>S</sup>
<i>MRSA 1</i> <sup>§</sup>	GMN <sup>S</sup> , LVX <sup>R</sup> , OX <sup>R</sup> , P <sup>R</sup> , TE <sup>S</sup> , TEC <sup>S</sup> , SXT <sup>S</sup> , VA <sup>S</sup>
<i>MRSA 2</i> <sup>§</sup>	GMN <sup>S</sup> , LVX <sup>R</sup> , OX <sup>R</sup> , P <sup>R</sup> , TE <sup>S</sup> , TEC <sup>S</sup> , SXT <sup>S</sup> , VA <sup>S</sup>
<i>MRSA 3</i> <sup>§</sup>	<b>CM<sup>R</sup>, E<sup>R</sup></b> , GMN <sup>S</sup> , LVX <sup>R</sup> , OX <sup>R</sup> , P <sup>R</sup> , TEC <sup>S</sup> , TE <sup>S</sup> , SXT <sup>S</sup> , VA <sup>S</sup>
<i>MRSA 4</i> <sup>§</sup>	CM <sup>S</sup> , E <sup>S</sup> , GMN <sup>S</sup> , LVX <sup>R</sup> , OX <sup>R</sup> , P <sup>R</sup> , TE <sup>S</sup> , TEC <sup>S</sup> , SXT <sup>S</sup> , VA <sup>S</sup>
<i>MRSA 5</i> <sup>§</sup>	CM <sup>S</sup> , E <sup>S</sup> , GMN <sup>S</sup> , LVX <sup>R</sup> , OX <sup>R</sup> , P <sup>R</sup> , TE <sup>S</sup> , TEC <sup>S</sup> , SXT <sup>S</sup> , VA <sup>S</sup>
<b><i>S. epidermidis</i></b>	<b>Antibiotic-resistance profile</b>
<i>MSSE 1</i>	CM <sup>S</sup> , E <sup>R</sup> , GMN <sup>S</sup> , LVX <sup>S</sup> , OX <sup>S</sup> , TE <sup>S</sup> , SXT <sup>S</sup>
<i>MSSE 2</i>	CM <sup>S</sup> , E <sup>S</sup> , GMN <sup>S</sup> , LVX <sup>S</sup> , OX <sup>S</sup> , P <sup>R</sup> , TE <sup>S</sup> , SXT <sup>S</sup>
<i>MSSE 3</i>	CM <sup>S</sup> , E <sup>S</sup> , GMN <sup>S</sup> , LVX <sup>S</sup> , OX <sup>S</sup> , P <sup>R</sup> , TE <sup>S</sup> , SXT <sup>S</sup>
<i>MSSE 4</i>	<b>CM<sup>R</sup>, E<sup>R</sup></b> , GMN <sup>S</sup> , LVX <sup>S</sup> , OX <sup>S</sup> , P <sup>S</sup> , TE <sup>S</sup> , SXT <sup>S</sup>
<i>MSSE 5</i>	CM <sup>S</sup> , E <sup>S</sup> , GMN <sup>S</sup> , LVX <sup>S</sup> , OX <sup>S</sup> , P <sup>R</sup> , TE <sup>S</sup> , SXT <sup>S</sup>
<i>MRSE 1</i> <sup>§</sup>	CM <sup>S</sup> , E <sup>R</sup> , GMN <sup>S</sup> , LVX <sup>S</sup> , OX <sup>R</sup> , P <sup>R</sup> , TE <sup>S</sup> , TEC <sup>S</sup> , SXT <sup>R</sup>
<i>MRSE 2</i> <sup>§</sup>	CM <sup>S</sup> , E <sup>S</sup> , GMN <sup>S</sup> , LVX <sup>S</sup> , OX <sup>R</sup> , TE <sup>S</sup> , SXT <sup>R</sup> , VA <sup>S</sup> , TEC <sup>S</sup>
<i>MRSE 3</i> <sup>§</sup>	CM <sup>S</sup> , DA <sup>S</sup> , E <sup>I</sup> , GMN <sup>S</sup> , LVX <sup>R</sup> , OX <sup>R</sup> , TE <sup>S</sup> , SXT <sup>S</sup> , VA <sup>S</sup> , TEC <sup>S</sup>
<i>MRSE 4</i> <sup>§</sup>	<b>CM<sup>R</sup>, E<sup>R</sup></b> , GMN <sup>S</sup> , LVX <sup>R</sup> , OX <sup>R</sup> , TE <sup>R</sup> , SXT <sup>S</sup> , VA <sup>S</sup> , TEC <sup>S</sup>
<i>MRSE 5</i> <sup>§</sup>	<b>CM<sup>R</sup>, DA<sup>S</sup>, E<sup>R</sup></b> , GMN <sup>S</sup> , LVX <sup>S</sup> , OX <sup>R</sup> , P <sup>R</sup> , TE <sup>R</sup> , SXT <sup>S</sup> , VA <sup>S</sup> , TEC <sup>S</sup>

CM=Clindamicyn; E=Erythromycin; GMN=Gentamicin; LVX=Levofloxacin; OX=Oxacillin; P=Penicillin; TE=Tetracycline; TEC=Teicoplanin; SXT=Trimethoprim/Sulfamethoxazole; VA =Vancomycin.

R=Resistant; S=Susceptible; I=Intermediate, as defined following the EUCAST guidelines  
<sup>§</sup>*Staphylococcus* species resistant to oxacillin were declared, by convention, methicillin resistant.